Virally induced salivary gland hypofunction and inflammation

Shaalan, Abeer Mohamed Kamaleldin Ahmed

Awarding institution:
King's College London

VIRALLY INDUCED SALIVARY GLAND HYPOFUNCTION AND INFLAMMATION

Thesis submitted for degree of

DOCTOR OF PHILOSOPHY

By

ABEER SHAALAN

SALIVARY AND MUCOSAL BIOLOGY

DEPARTMENT, DENTAL INSTITUTE,

KING'S COLLEGE LONDON, 2017

SUPERVISORS: PROF. GORDON PROCTOR & DR GUY CARPENTER

Abstract

A long association has been established between infectious inflammation and diseases of the salivary glands (SGs). However, the prompt responses of the exocrine tissues to these types of injuries remain unclear. Accordingly, an acute inflammation model was developed by the retrograde intraductal injection of a double-stranded (ds) RNA analogue; polyinosinic:polycytidylic acid (poly(I:C)), into the submandibular glands (SMGs), through Wharton's duct. The main aim of this study was to investigate the early functional and immune events downstream of exposure to this viral-like inflammagen. The first part of the current study highlighted that the SMGs responded to the locally injected poly (I:C) by a rapid decline in saliva secretion, which stopped completely after 24 hours of infection. The early loss of function perceived, paralleled the upregulated expression of Toll-like receptor-3 (TLR3) and that incited blocking of the receptor *in vivo* to assess its role in the loss of function. The outcome of these experiments confirmed that dysfunction of the acutely inflamed glands resulted from ligation of TLR3 and initiation and propagation of downstream cytokines. The current study revealed for the first time the possibility of using a protease inhibitor to restrict TLR3 neo-synthesis, dampen inflammation, fine-tune anti-viral innate immune responses and retrieve TLR3-induced loss of SMG function.

Next, the role played by the acute inflammatory cells which infiltrated the SMGs following poly (I:C) infection was examined. Despite successful depletion of these cells, the glands' secretory functions were not retrieved, verifying that TLR3 has induced dysfunction independent of the invasive acute cell infiltration.

In the last part of this study, it was demonstrated that the TLR3-inhibited, functionally-protected SMGs revealed loss of the pro-inflammatory cytokine, inducible nitric oxide synthase (iNOS), which displayed extensive acinar upregulation in response to poly (I:C) infection. Selective blocking of iNOS by aminoguanidine protected the secretory function of the poly (I:C) treated glands and specified iNOS as the earliest signal which disrupts the secretory machinery after innate immune activation.

To assess the injurious contributions of iNOS and its rapidly derived cytotoxic oxidant peroxynitrite, in the acute SG model, the gland homogenates were immunoblotted with the peroxynitrite marker, 3-nitrotyrosine, which revealed extensive nitration of a plethora of the gland proteins, including proteins at the electrophoretic mobility of the endoplasmic reticulum (ER) SERCA2 channel. Immunohistochemistry further revealed the physical co-localization of peroxynitrite and the critical regulator of calcium homeostasis, SERCA2. To comprehensively investigate the impact of this finding on the cellular calcium levels of the infected glands, a novel protocol which allowed assaying of $[Ca^{2+}]_i$ changes ex vivo was developed, optimized and applied to the aminoguanidine treated and non-treated mice. Through this protocol, iNOS-mediated dysregulations in resting and stimulated calcium were recorded. The set of experiments which followed these findings revealed upregulation of the unfolded protein response, global transcriptional downregulation of key water driving molecules and altered subcellular localization of these critical membranous receptors, water channels and ion transporters. All these changes in response to a single poly (I:C) dose, were remarkably reversed when the SMGs were treated with the iNOS inhibitor; aminoguanidine.

Acknowledgements

I would like to thank my first supervisor Prof. Gordon Proctor for guiding me throughout my studies. He has supported me and rendered this whole PhD experience possible. As well, I would like to acknowledge my second supervisor; Dr Guy Carpenter for his suggestions.

Also, I would like to acknowledge Rashida Pramanik for teaching me the qRT-PCR, Maria Jose for guiding me through the flow cytometry experiments, David Andersson for showing me the key settings of the Flexstation and Steven Gilbert for his continuous help and support. Additionally, I would like to thank all my colleagues, especially Polliane Carvalho who rendered the lab experience a friendly and supportive one.

Finally, all my gratitude goes to my husband. Words will never be enough to describe my sincere appreciation to his unlimited sacrifices and patience. To my mum, kids and sisters, I am the most fortunate person because of your unconditional love and support.

List of Presentations

Poster Presentation, 62nd annual meeting, June 22-28, 2007, American Academy of Oral and Maxillofacial Pathology (AAOMP), San Francisco, USA. Immunohistochemical expression of MUC1 and MUC2 in benign and malignant salivary gland tumours.

Poster Presentation, 101st annual world dental congress FDI, August 28-31, 2013,

Istanbul, Turkey. Longitudinal assessment of biocompatibility and healing response of MTA Fillapex.

Poster presentation, 10th European Symposium on Saliva, May 14-17, 2014, Egmond aan Zee, the Netherlands. Virally Induced Salivary Gland Hypofunction and Inflammation.

Poster presentation, International Association of Dental research (IADR) meeting, September 9-13, 2014, Dubrovnik Croatia. Salivary Gland Hypofunction and Inflammation induced by a Viral Mimic.

Poster presentation, Salivary Glands & Exocrine Biology, Gordon Research Conference,

February 15-20, 2015, Galveston, TX, USA. Virally Mediated Salivary Gland

Hypofunction Reduced the Expression of Aquaporin 5 and Sodium Potassium Chloride Cotransporter (NKCC1). Best poster Award.

Oral Presentation, 17th Annual Postgraduate Research Day King's College London, March 18, 2015, London, UK. Cellular and Innate Immune Responses of The Submandibular Glands in Response to synthetic dsRNA (Poly I:C).

Oral and poster Presentations, Salivary Glands & Exocrine Biology - Gordon Research Conference, February 17-24, 2017, Galveston, TX, USA. Virally-Mediated Submandibular Gland Injury & Dysfunction: Role of Inducible Nitric Oxide Synthase.

List of Abbreviations

SG: salivary gland

PG: parotid gland

SMG: submandibular gland

SLG: sublingual gland

ID: intercalated ducts

SD: striated ducts

ED: excretory ducts

H&E: haematoxylin & eosin

GCD: granular convoluted ducts

$[Ca^{2+}]_i$: intracellular calcium

NKCC1: Na-K-Cl cotransporter 1

TMEM16A: Transmembrane Protein 16A

PLCβ: phospholipase Cβ

PIP2: phosphatidylinositol 1,4, bisphosphate

DAG: diacylglycerol

IP3: inositol 1,4,5, trisphosphate

IP3Rs: IP3 receptors

RyR2: Ryanodine receptor 2

$[Ca^{2+}]_{ER}$: endoplasmic reticulum calcium

STIM1: Stromal interaction molecule 1

SOC: store-operated calcium channels

M3R: M3 muscarinic receptors

AQPs: aquaporins

NA: noradrenaline

cAMP: adenosine 30,50-cyclic monophosphate

PMCA: plasma-membrane Ca^{2+}-ATPASE

NCX: Na+/Ca^{2+} exchanger

SERCA: sarco(endo)plasmic Ca^{2+}-ATPase

BiP: Immunoglobulin Binding Protein

ATF6: Activating Transcription Factor 6

IRE1: serine/threonine-protein kinase/endoribonuclease inositol-requiring enzyme 1

PERK: PKR-like ER-localized eIF2α kinase

CHOP: C/EBP homologous protein

ATF4: Activating transcription factor 4

UPR: unfolded protein response

ROS: reactive oxygen species

TRPM2: Transient receptor potential cation channel, subfamily M, member 2

TRP6: The transient receptor potential protein homologue

SS: Sjögren’s syndrome

iNOS: inducible nitric oxide synthase

eNOS: endothelial nitric oxide synthase

nNOS: neuronal nitric oxide synthase

NO: nitric oxide

IFN: interferon

PAMPs: pathogen-associated molecular patterns

Poly (I:C): polyinosinic:polycytidylic acid

DC: dendritic cells

PRR: pattern recognition receptor

ECD: ectodomain

LRRs: leucine-rich repeats

TIR: Toll/IL-1 receptor domain

IRF3: Interferon regulatory factor 3

NF-κB: nuclear factor kappa-light-chain-enhancer of activated B cells

TICAM-1: Toll Like Receptor Adaptor Molecule 1

TLR: toll-like receptor

MDA5: Melanoma Differentiation-Associated protein 5

RLR: RIG-I-like receptor

OAS1: 2-5-Oligoadenylate Synthetase 1

PKR: protein kinase R

TRIF: TIR domain-containing adapter protein inducing IFNβ

ssRNA: single stranded RNA

miRNA: micro RNA

siRNA: Small interfering RNA

DAMP: death associated molecular pattern

TBK-1: serine/threonine tank binding kinase-1

STAT: signal transducer and activator of transcription

ISGs: type I IFN stimulated genes

RHIM: receptor-interacting protein homotypic interaction motif

RIPK: serine/threonine kinase receptor-interacting protein kinase

TRAF: TNF receptor associated factor

TAK1: transforming growth factor β activated kinase 1

IKK: IκB kinase-related kinase

TAB: TAK1 binding proteins

FADD: Fas-associated death domain

Caspase: cysteine-dependent aspartate-directed proteases

My-D88: Myeloid differentiation primary response gene 88

CARD: Caspase activation and recruitment domain

Table of Contents

Table of Figures

Table of Tables

Chapter 1

Introduction

1.1 Salivary Glands

1.1.1 Types and Anatomy of Salivary Glands

Human and murine SGs can be classified according to size into: (i) three paired **major** glands; parotid (PG), submandibular (SMG) and sublingual (SLG), and (ii) numerous glands forming **minor** packages located in the labial, palatine, buccal, lingual and sublingual submucosae (Denny et al., 1997, Amano et al., 2012). Based on secretion: saliva from the PG is entirely serous. While the SLGs are mucous; the SMGs produce mixed serous and mucous saliva. Major SGs of both humans and rodents are essentially similar in their anatomical architecture which comprises secretory end pieces (acini) and arborized ductal structures that open into the oral cavity. Table 1-1 and Figure 1.1 compare the prominent anatomic features of mice and human SGs.

Table 1-1 Comparison of anatomical features of major SGs in mice and human (Piper M. Treuting, 2012).

Feature	Mouse	Human
Submandibular	• Largest; located in ventral cervical region. • Duct opens caudal to lower incisors (Amano et al., 2012).	• In digastric triangle, anterior to digastric and posterior to stylohyoid ligament. • SMG Wharton's duct opens with SLG Bartholin's in the sublingual caruncle (Holmberg and Hoffman, 2014).
Sublingual	• Located in ventral cervical subcutaneous region. • Small single lobe. • Close association with submandibular; duct opens caudal to lower incisors.	• Smallest major gland. • located above the mylohyoid below the mucosa of the middle to anterior mouth floor.
Parotid	• Located in ventral cervical subcutaneous region. • Diffuse multi-lobed. • Duct opens near lower molars	• Largest gland. • Triangular base at zygomatic arch and apex just inferior to the angle of the mandible. • Extends posterior to the ear and anterior to cover masseter. • Stensen's duct opens in the mouth by second maxillary molar.

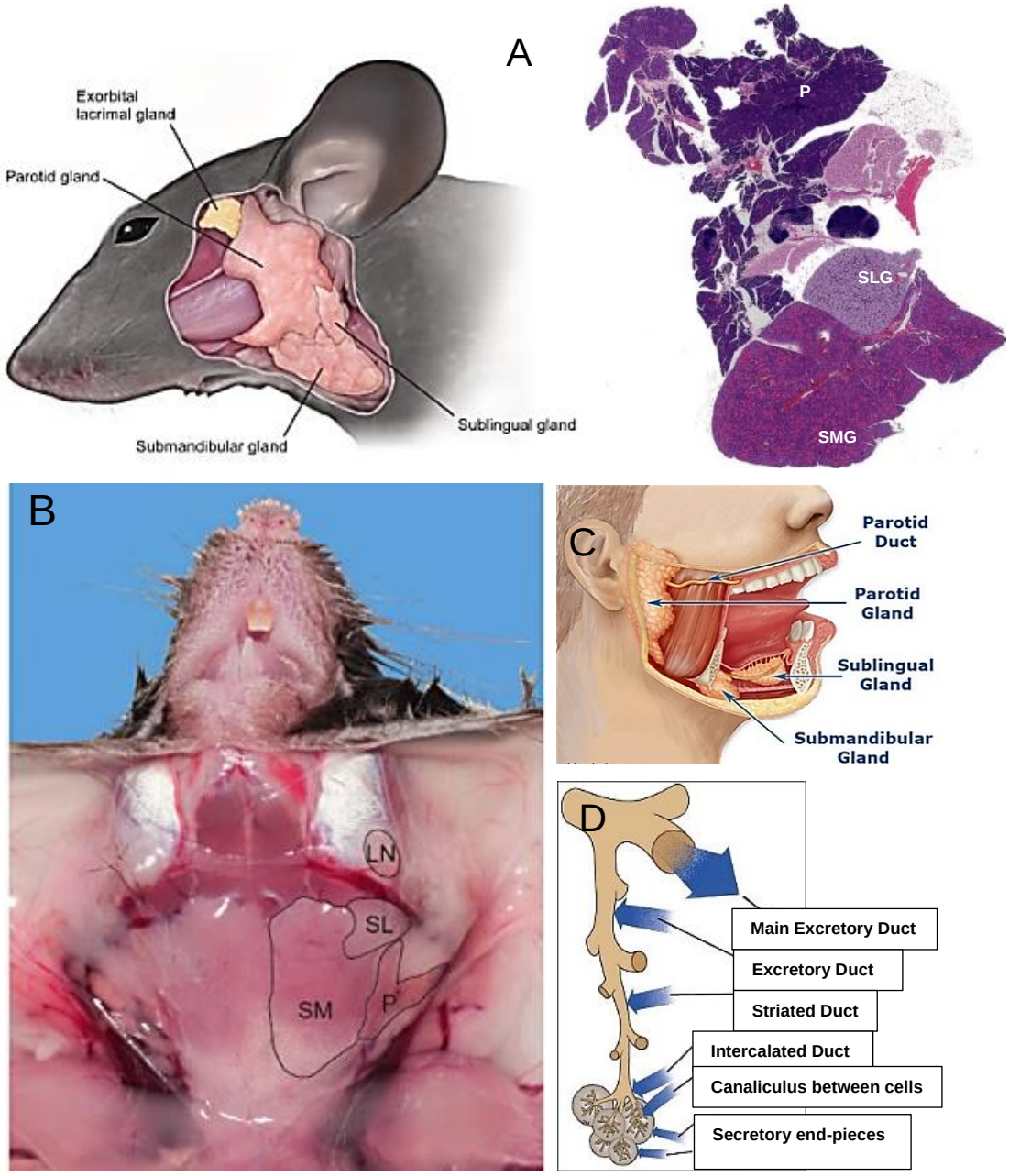

Figure 1.1 **Mouse and human salivary glands.**
A: Mouse regional cervical anatomy and sub-gross histologic section of cervical soft tissues from a male mouse. The SMG is the largest in the mouse, whereas the PG is relatively diffuse. **B:** Gross dissection of mouse ventral cervical region. Paired salivary glands are bilaterally located and outlined in black. The submandibular (SMG) and sublingual (SLG) glands are encapsulated with common fascia (Piper M. Treuting, 2012). **C:** Human regional cervical anatomy. D: Acini and arborized anatomy of salivary glands. Lymph nodes (LN).

1.1.2 Histomorphology of The Acinar and Duct Systems of SGs

A typical SG is surrounded by a fibrous connective tissue capsule, which sends remote septae to divide the gland into lobes and lobules. Salivary glands are made of three epithelial cell types: acinar, ductal and myoepithelial. The pattern of arrangement of these cells is similar in both mice and humans: glandular acini connect to intercalated ducts (ID) which drain to intralobular striated ducts (SD) and then interlobular ducts that finally merge into excretory ducts (ED) to empty into the oral cavity. In addition, the myoepithelial cells usually associate with both acini as well as intercalated ducts (Amano et al., 2012), figure 1.2.

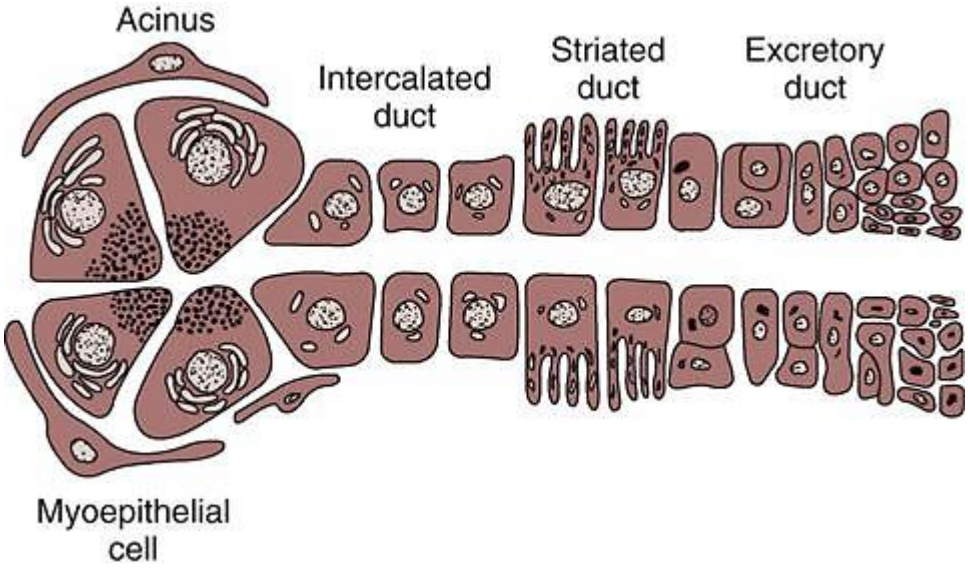

Figure 1.2 **Basic SG unit.**
Salivary glands are made of three epithelial cell types: acinar, ductal and myoepithelial cells. Acinar cells organized into pyramidal acini are connected to a network of ducts classified into: intercalated, striated and excretory ducts.

The acinus, the secretory end piece of salivary glands; produces and secretes the primitive saliva into the central lumen. Parotid acini have small pyramidal cells with regular nuclei, apical pink staining due to zymogen granules, and basal basophilia, when stained with haematoxylin & eosin (H&E).

Similarly, the SMG acini stain basophilic in histologic sections, with basal nuclei and may contain apical cytoplasmic mucin droplets. The sublingual acini are large pyramidal mucous-producing cells with abundant pale blue vacuolated cytoplasm (Piper M. Treuting, 2012). Figure 1.3 reveals the histologic features and variances between mice and human SGs.

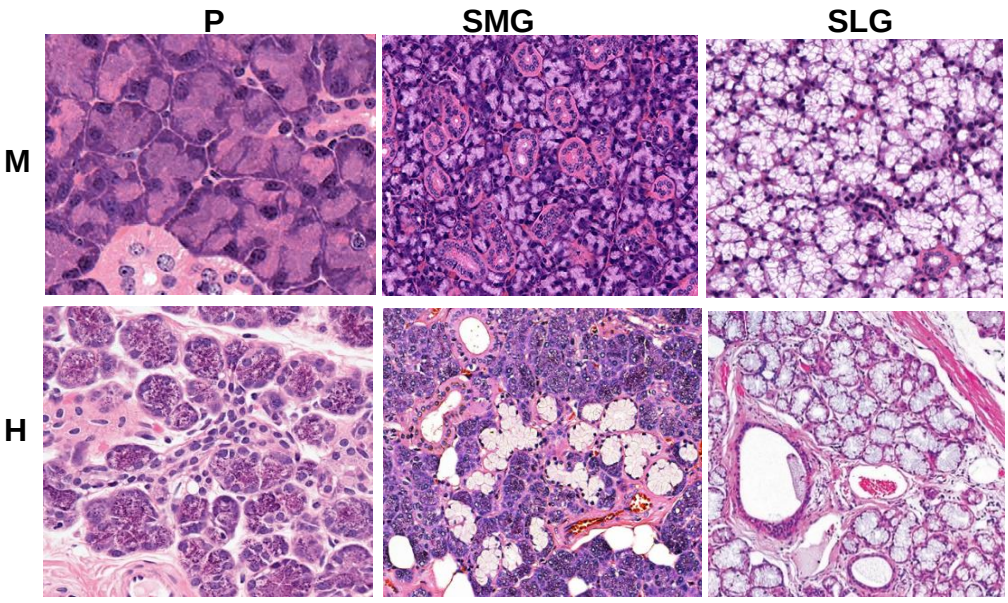

Figure 1.3 **Comparative histology of salivary glands in human and mice.** Parotid acini **(P)** in mice **(M)** and humans **(H)** are serous-secreting with apical cytoplasmic zymogen granules that stain pink with H&E. In both species, the **SMG** serous acini and ducts are numerous and clearly identified. In humans, seromucinous and mucous cells are lighter pale-blue staining and more prominent than in mice. In both species, mucinous acini predominate in the **SLGs**.

Like the human SGs, the duct system of rodents is composed of the ID, SD, ED and main excretory ducts. The IDs are lined by cuboidal to flattened epithelium in mice and cuboidal epithelium in humans. Intralobular SDs are lined by cuboidal to low-columnar cells in mice and tall columnar cells with large, apically located nuclei in humans. Both species have characteristic eosinophilic striations in the basal cytoplasm of the striated ducts.

These striations are caused by enfolding of the basal plasma membrane. Interlobar EDs have cuboidal epithelium. The main excretory ducts in the mouse are lined by cuboidal cells that transform to stratified squamous (oral mucosa) at the duct opening (Piper M. Treuting, 2012). In addition, mice have a unique ductal arrangement in the SMGs, which contain granular convoluted ducts (GCD) connecting the intercalated ducts to the striated ducts. This segment of ducts within the SMGs has sexual dimorphism in mice, since it is testosterone dependent (Chai et al., 1993). In males, cells lining the GCD are large and columnar containing bright pink granules. In females, cells are smaller with less distinct granules (Jayasinghe et al., 1990), figure 1.4.

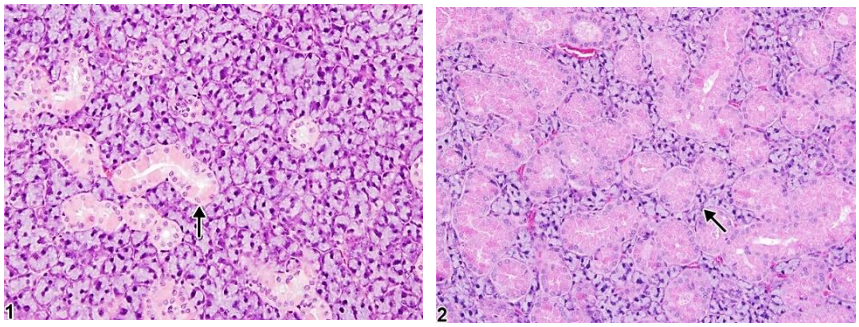

Figure 1.4 **Sexual dimorphism in mouse SMGs.**
Tissue sections from female (1) and male (2) SMGs showing the histologic dimorphism between each sex. Note the excess GCDs (arrow) in male SMGs as well as the intense eosinophilia reflecting abundance of secretory granules (Linda H. Kooistra and Abraham Nyska).

The GCD produces and secretes a variety of bioactive polypeptides, hormones, and cell growth factors including epidermal growth factor (EGF), nerve growth factor (NGF) (Gresik, 1994), brain-derived neurotrophic factor (BDNF) (Kondo et al., 2010, Tsukinoki et al., 2006), hepatocyte growth factor (HGF) (Amano et al., 1994, Amano and Iseki, 2001), insulin-like growth factor 1 (IGF-I) (Amano and Iseki, 1993, Amano and Iseki, 2001), transforming growth factor (TGF) -α (Wu et al., 1993) and -β (Amano et al., 1991, Amano and Iseki, 2001).

1.1.3 Functional and Secretory Pathway Variations in Mouse SG Acinar Cells

In mice, the PG, SMG, and SLG glands secrete 90% of the whole mouth saliva. Although all 3 major SGs appear to secrete fluid by a similar molecular mechanism, each gland contributes differently to this percentage, which denotes that the secretory machinery is functionally inequivalent for each gland. The PG secretes approximately 30% more saliva than does the SMG and 6-fold more than does the SLG, suggesting that the PG has a more robust secretory mechanism. These differences in flow rate are neither entirely dependent on the gland weight nor on the acinar volume of each SG (Kondo et al., 2015). To appreciate why the PG acini secrete significantly more saliva than do the SMG and SLG, the complex process of salivary fluid secretion must be briefly demonstrated. In short, Cl^- uptake by the basolateral Na-K-Cl cotransporter 1 (NKCC1) (Haas, 1989, Haas and Forbush, 1998, Haas, 1994) elevates the intracellular Cl^- concentration above its electrochemical equilibrium. This will promote the Ca^{2+}-activated Cl^- efflux by the apical channel; Transmembrane Protein 16A (TMEM16A) (Yang et al., 2008, Romanenko et al., 2010), once the acinar cells are stimulated by the cholinergic agonist; acetylcholine and intracellular calcium $[Ca^{2+}]_i$ mobilization takes place (Nauntofte, 1992, Ambudkar, 2014). Consequently, these events comprise the driving force for Na^+ and water movement through the tight junction complex and apical water channels, respectively (Melvin et al., 2005), figure 1.5.

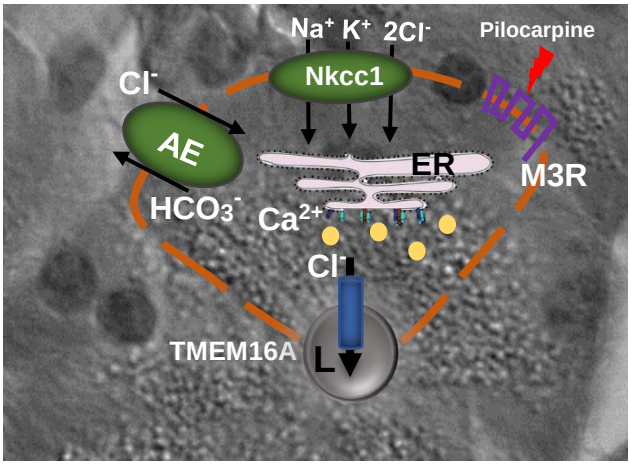

Figure 1.5 **Illustration summary of the saliva secretion mechanism in mouse acinar cells.** Muscarinic agonist-stimulated Ca^{2+} release, and Cl^- efflux into the lumen via the apically located TMEM16A channel. Towards osmotic balance, Na^+ will follow Cl^- into the lumen and NaCl will drive transcellular water movement.

According to (Kondo et al., 2015), both TMEM16A protein expression and the muscarinic agonist-induced Cl^- efflux mediated by this channel were greater in the PG acinar cells than in SMG and SLG, which highlighted the essential role played by this channel in the mouse salivary acinar cells. In addition to the TMEM16A Cl^- enhanced expression and activity, they demonstrated that the PG and SMG likely secrete greater volumes of fluid than do the SLG because they display a larger increase in the $[Ca^{2+}]_i$-stimulated response and more NKCC1 activity. Interestingly, they showed that the SLG, which exhibits relative deficiency in these functional determiners, rely on the basolateral Cl^-/HCO_3^- anion exchanger (Novak and Young, 1986, Melvin and Turner, 1992, Nguyen et al., 2004) in Cl^- uptake to compensate for the absence of NKCC1 activity (Catalan et al., 2015).

1.2 Salivary Gland Secretion, Calcium Homeostasis & Dysfunction

1.2.1 Control of Salivary Secretion

Parasympathetic and sympathetic arms of the autonomic nervous system interact simultaneously on secretory acinar cells to generate a reflex secretion of saliva (Proctor and Carpenter, 2007). While the parasympathetic stimulation functions to evoke a large volume of saliva, the sympathetic nerves will induce a protein-rich secretion (Anderson et al., 1995, Asking and Gjorstrup, 1987, Carpenter et al., 2000, Matsuo et al., 2000).

1.2.1.1 Parasympathetic Control: Fluid Secretion and Modification of Electrolytes

Parasympathetic nerves are secretomotor and their stimulation will cause the SGs to secrete a large volume of watery fluid that is high in electrolytes and low in proteins (Proctor, 1998, Proctor, 2016). In addition, parasympathetic activity causes blood vessels to dilate, thereby providing the gland with a source of water for secretion (Villa et al., 2016). The parasympathetic nerve supply to the major SGs (Khurana, 2009, Hall, 2011) is best summarized as in table 1-2 and figure 1.6.

Table 1-2 Summary of parasympathetic nerve supply to the SGs.

	PG	**SMG/SLG**
Preganglionic nerve supply	Arise from inferior salivary nucleus (dorsal nucleus of IXth nerve) of medulla.	Arise from superior salivary nucleus (dorsal of the VIIth nerve).
Preganglionic nerve fibres	Run via the tympanic nerve and small superficial petrosal nerve to the otic ganglion	Run in nervous intermedius (sensory division of VII nerve), join the facial nerve and leave by its chorda tympani branch to join the lingual nerve.
Ganglion	Otic	Submandibular
Postganglionic nerve fibres	From the Otic ganglion join the auriculotemporal nerve to the parotid gland	Arise from the submandibular ganglion and supply the glands along with the blood vessels.

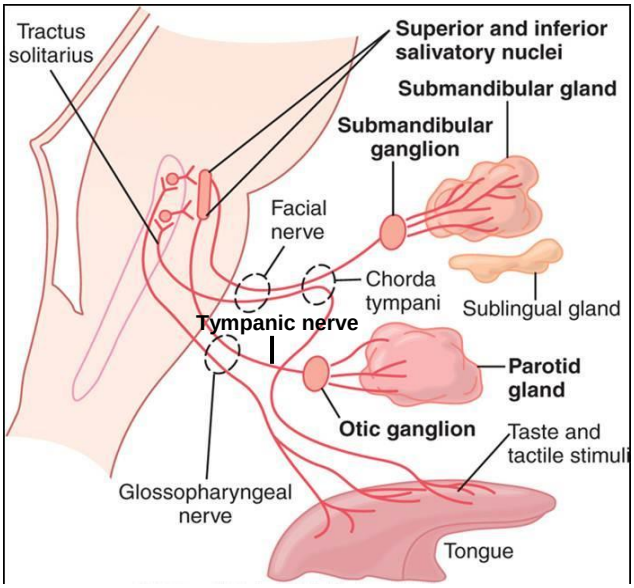

Figure 1.6 Diagram illustrating the parasympathetic nerve supply to the SGs. (Hall, 2011).

The SG fluid secretion in response to parasympathetic stimulation occurs in two phases; **acinar** secretion of isotonic saliva; which has the same Na^+, Cl^-, K^+ and HCO_3^- concentrations as plasma (Khurana, 2009), followed by **duct** modification phase, which results in the final hypotonic saliva secreted into the mouth. As previously illustrated, fluid secretion following the action of the parasympathetic postganglionic transmitter; acetylcholine on the acinar M3 muscarinic receptors (M3R) (Proctor and Carpenter, 2014), involves increase $[Ca^{2+}]_i$ and ion transport. The first phase comprises activation of phospholipase Cβ (PLCβ) which cleaves phosphatidylinositol 1,4, bisphosphate (PIP2) to produce diacylglycerol (DAG) and the soluble signalling molecule inositol 1,4,5, trisphosphate (IP3) (Berridge, 1993, Melvin et al., 2005). IP3, then activates the endoplasmic reticulum (ER)-Ca^{2+} release channels; IP3 receptors (IP3Rs), which induce Ca^{2+} release from the ER stores (Mikoshiba, 2007).

Ryanodine receptor 2 (RyR2) is another main intracellular Ca^{2+} release channel, abundantly localized in the basal region of acinar cells (Zhang et al., 1999). Positioned as such, it is presumed to play a role in globalization of the Ca^{2+} signal in acinar cells following stimulation, by spreading Ca^{2+} to sites of the ER where IP3Rs are sparse or those at a distance from the site of IP3 generation (Ambudkar, 2014). IP3-mediated Ca^{2+} release via IP3R, and the resultant depletion of endoplasmic reticulum calcium $[Ca^{2+}]_{ER}$, will then be detected by the ER-binding protein sensor STIM1 (Liou et al., 2005, Zhang et al., 2005, Zeng et al., 2008, Yuan et al., 2009, Hogan et al., 2010, Cheng et al., 2013, Prakriya, 2013), which will trigger further influx of extracellular calcium across the membranous store-operated calcium channels (SOC) of acinar cells (Putney, 1990) and will ensure sustained salivary secretion (Melvin et al., 2005, Ambudkar, 2014), figure 1.7.

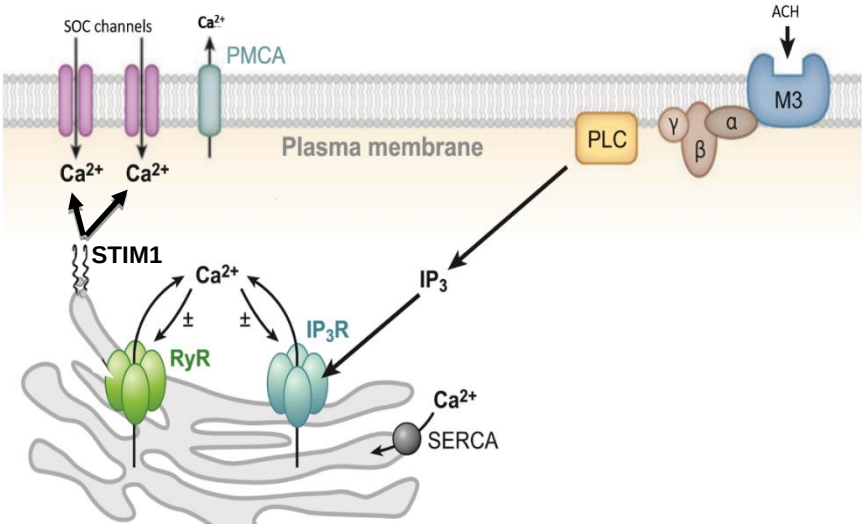

Figure 1.7 **Intracellular mechanisms of calcium release in salivary acinar cells.** The illustrated model describes 2 principal intracellular pathways of calcium mobilization. Acetylcholine binding to its cognate M3R (G protein-coupled receptor) results in production of inositol 1,4,5-trisphosphate (IP3), which causes ER calcium release. Calcium-induced calcium release (CICR) is brought about by calcium activation of the RyR2 channels. Adapted from (Petersen and Tepikin, 2008).

In the resting acinar cells: NKCC1, Na^+/H^+ and $Cl^-/ HCO3^-$ exchanger mediate Cl^- influx across the basolateral membrane of acinar cells to accumulate chloride ions (Cl^-), 4–5-fold above electrochemical equilibrium (Foskett, 1990, Zeng et al., 1997). The use of NKCC inhibitors showed that NKCC activity mediates about 70% of the Cl^- uptake that is secreted across the luminal membrane to drive secretory glands fluid secretion (Melvin et al., 2005). The central role of NKCC1 in salivary glands fluid and electrolyte secretion was further established by deletion of the Nkcc1 gene in mice, which resulted in about 70% inhibition of salivary secretion (Evans et al., 2000).

The second phase in stimulated saliva secretion follows the increase in $[Ca^{2+}]_i$ and starts with activation of the apical Cl^- channel; TMEM16A (Arreola et al., 1996, Hayashi et al., 1996). TMEM16A activation will release Cl^- into the central acinar lumen, which will be followed by sodium movement by a paracellular course through the tight junctions (Zhang et al., 2013). It is important to note that the muscarinic Ca^{2+}-dependent fluid secretion was completely abolished in the salivary glands of TMEM16A null ($Tmem16A^{-/-}$) mice, concluding the essential role played by this channel in fluid secretion in the adult salivary glands (Catalán et al., 2015).

Typically, the transcellular accumulation of NaCl ions in the acinar lumen will result in the obligatory osmotic water flow (Lee et al., 2012b). Although water can cross the membrane bilayer, water flow in secretory cells is facilitated by the water channels; aquaporins (AQPs). The luminal membrane of acinar cells express AQP5, which plays an indispensable role in exocrine glands' fluid secretion by providing highly permeable water channels (Krane et al., 2001).

This was confirmed by the: (i) 60% reduction in secretion observed in the AQP5 knockout mice (Alper, 2009, Melvin et al., 1988), (ii) aberrant trafficking of AQP5 in Sjögren's syndrome patients (Evans et al., 1999, Roussa et al., 1999), (iii) markedly decreased labelling intensity of AQP5 in severely damaged irradiated SGs (Takagi et al., 2003) and (iv) disrupted trafficking of the water channel in Streptozotocin-induced diabetic mice, featuring xerostomia (Ishikawa et al., 2004). In addition, since AQP5 appears to regulate the water permeability of the paracellular pathway, its deletion disrupted integrity of the tight junction and reduced the paracellular water permeability (Evans et al., 1999).

After acinar fluid secretion, saliva enters the **duct modification phase,** whereby salivary ducts secrete K^+ and HCO_3^- and reabsorb Na^+ and Cl^- (Cook DI, 1994). The hypotonicity of secreted saliva indicates that ducts are relatively impermeant to water (Melvin et al., 2005). The prevailing model for fluid and electrolyte transport in salivary ducts accounts for Na^+ and Cl^- influx into the duct cell luminally, through electroneutral pathways, i.e. a Na^+/H^+ exchanger (Luo et al., 2001) a Cl^-/HCO_3^- exchanger (Lee et al., 1998) and through Na^+ (Cook et al., 1998) and Cl^- (Zeng et al., 1997) channels. Large amounts of sodium and chloride will be transported out of the ductal cell and into the glandular interstitium via the basolateral sodium/potassium ATPase (sodium pump) and Cl^- channels, respectively (Proctor, 2016). Moreover, the HCO_3^- accumulated in the cytosol via the basolateral Na^+/H^+ exchanger (NHE1) will enter the lumen in exchange for Cl^- at the apical Cl^-/HCO_3^- exchanger (Cook DI, 1994). Figure 1.8 summarizes the acinar secretion and duct modification phases of secreted saliva.

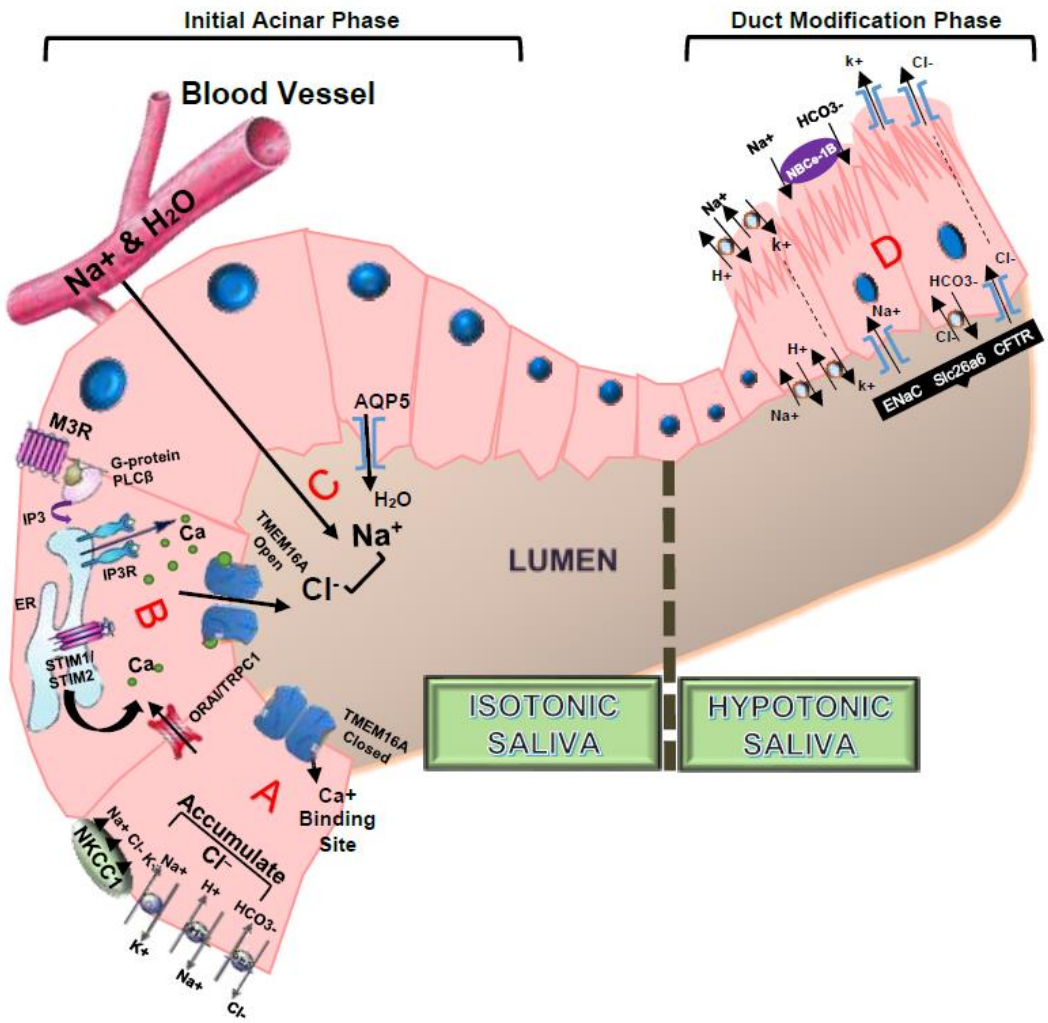

Figure 1.8 **Model depicting the mechanism of fluid and electrolyte secretion**.
A: Shows the major transporters in the basolateral and luminal membranes of acinar cells. The major Cl^- loading transporter at the basolateral membrane is NKCC1. TMEM16a/Ano1 is the major Ca^{2+}-activated Cl^- channel at the luminal membrane. **B:** Fluid and electrolyte secretion by acinar cells is regulated by Ca^{2+} mobilizing receptors and is a Cl^- secretion-driven process. The receptor-evoked $[Ca^{2+}]i$ increase is initiated at the apical pole where the Ca^{2+} signaling complexes are located and activates TMEM16a/ Ano1. The Ca^{2+}-mediated channel activation results in luminal Cl^- efflux. **C:** Na^+ then follows the Cl- into the acinar lumen through the tight junction. **D:** Model for the modification of primary saliva by ductal secretion. Salivary duct cells secrete K^+ and $HCO3^-$ and reabsorb Na^+ and Cl^- to produce the final saliva. The salivary duct epithelium is tight allowing no water movement, thus resulting in hypotonic saliva (NBCe1-A/B electrogenic $Na^+/HCO3^-$ cotransporters A/B, ENaC epithelial Na^+ channel, CFTR cystic fibrosis transmembrane conductance regulator).

1.2.1.2 Sympathetic Control and Protein Secretion

The preganglionic sympathetic nerve fibres originate from the lateral horn cells of T_1 and T_2 segments of the spinal cord and enter the paravertebral sympathetic chain via ventral roots to synapse with cells in the superior cervical ganglion. Subsequently, the postganglionic fibres run along the carotid artery branches and supply the major and minor salivary glands by travelling along the blood vessels (*Ekström J* 2012), figure 1.9.

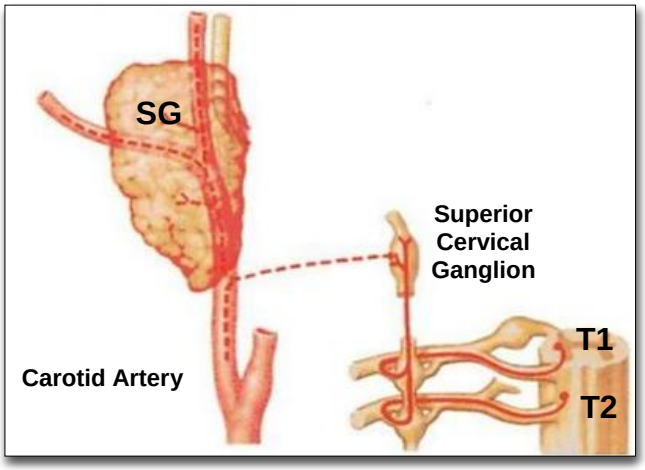

Figure 1.9 **Sympathetic nerve supply to the salivary glands** (BJ Baum, 1999).

The main sympathetic neurotransmitter is noradrenaline (NA) (BJ Baum, 1999). NA released from sympathetic nerve endings binds to β1 adrenoceptors on acinar cells and increases G protein-coupled adenylate cyclase activity with the generation of increased levels of intracellular messenger; adenosine 30,50-cyclic monophosphate (cAMP) (BJ Baum, 1999). Exocytosis of salivary proteins in parotid and submandibular acini is triggered mainly by cAMP and is potentiated by elevated Ca^{2+} (Quissell et al., 1992, Scott and Baum, 1985).

1.2.2 Calcium Signalling Homeostasis and Disruption

1.2.2.1 Key Molecular Determinants of $[Ca^{2+}]_i$ Homeostasis

$[Ca^{2+}]_i$ is a critical factor in the regulation of a plethora of physiological functions, including muscle contraction, secretion, metabolism, gene expression, cell survival and cell death. The key regulator of $[Ca^{2+}]_i$ homeostasis is determined by a balance between the 'initiating' responses that introduce $[Ca^{2+}]_i$ into the cytoplasm and the 'terminating' responses through which $[Ca^{2+}]_i$ is removed by the combined action of buffers, pumps and exchangers.

As previously mentioned in the current chapter, introduction of cytosolic Ca^{2+} follows activation of plasma membrane M3R and generation of IP3, which will bind to the ER receptor; IP3R, to release $[Ca^{2+}]_{ER}$ (Yule, 2001, Mikoshiba, 2007). On the other hand, removal of Ca^{2+} from the cytoplasm following termination of the secretion stimulus, maintains the resting level of Ca^{2+} at approximately 100 nM and ensures that the internal stores are kept loaded (Berridge et al., 2003). Different pumping mechanisms are activated via the increased $[Ca^{2+}]_i$ and are responsible for elimination of cytosolic Ca^{2+}: the plasma-membrane Ca^{2+}-ATPASE (PMCA), the Na^+/Ca^{2+} exchanger (NCX) and the sarco(endo)plasmic Ca^{2+}-ATPase (SERCA). Both SERCA and NCX contribute equally to Ca^{2+} clearance, which accounts for approximately 80% of the removal (Schwaller, 2012). SERCA uses the energy of ATP to drive Ca^{2+} across the membrane against the ion gradient, by forming a high-energy intermediate acyl-phosphate (Toyoshima, 2009). Moreover, SERCA plays a major role in Ca^{2+} homeostasis in the cells by controlling the SOCE activity (Bolotina, 2004) and reloading Ca^{2+} stores at the end of cell stimulation.

Alternatively, NCX is an ion transporter that can rapidly expel calcium ions from the cell by utilizing the energy stored in the transmembrane sodium gradient to allow influx of three sodium ions and extrusion of one calcium ion (Hilge, 2012, Ottolia and Philipson, 2013). Similar to SERCA, PMCA is responsible for fine tuning of Ca^{2+} level in the cell by pumping out Ca^{2+}across the PM at the expense of ATP, against a Ca^{2+} gradient (Niggli et al., 1982).

Although the ER is accepted as the major organellar Ca^{2+} buffer, several other subcellular organelles are known to eliminate cytosolic Ca^{2+} and maintain it at significantly higher levels than in the cytoplasm, figure 1.10. Golgi apparatus secretory-pathway Ca^{2+}ATPases (SPCAs), the mitochondrial uniporter (MCU), peroxisomes, and endosomes/lysosomes are all examples of organelles responsible for Ca^{2+} sequestration into their compartments (Prins and Michalak, 2011).

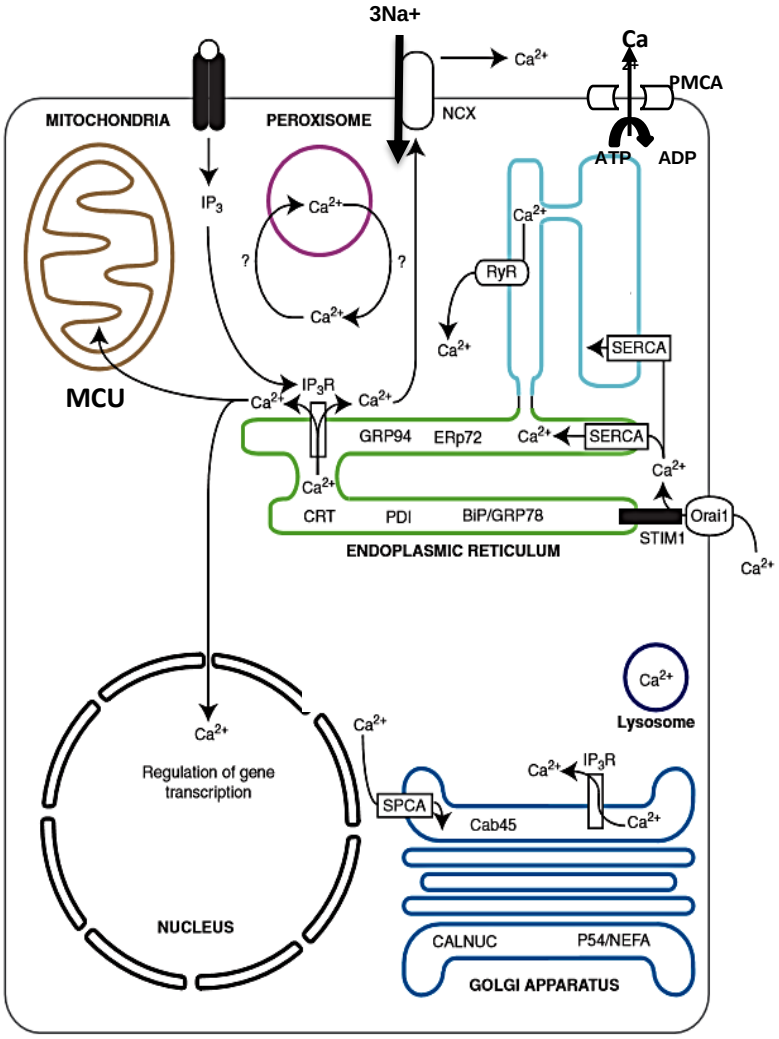

Figure 1.10 **[Ca^{2+}]$_i$ Elimination Portals.**
Ca^{2+} is stored within several different organelles: ER, Golgi apparatus, mitochondria, and peroxisomes. A typical Ca^{2+} release pathway ultimately stimulates releasing of Ca^{2+} from the ER lumen. Note that the Golgi apparatus also contains IP3R molecules and thus may contribute to Ca^{2+} release from stores. Golgi Ca^{2+} uptake occurs via SPCA pumps. Ca^{2+} released from the ER has several different fates, including: uptake by mitochondrial MCU, or extrusion from the cell via PMCA and Na^{+}/Ca^{2+} exchanger plasma membrane proteins. Orai1 functions as a plasma membrane Ca^{2+} channel that allows for Ca^{2+} entry from the extracellular milieu into the cytoplasm, where it is taken up by SERCA into the ER lumen. Peroxisomes are known to maintain Ca^{2+} at higher levels than in the cytoplasm. Elevated Ca^{2+} levels in the ER and in the Golgi apparatus, will mostly be bound to buffering proteins, as shown within these organelles. BiP/GRP78 binding protein/glucose-regulated protein of 78-kDa; CRT, calreticulin; GRP94, glucose-regulated protein of 94-kDa; IP3, inositol trisphosphate; IP3R, inositol trisphosphate receptor; NCX, Na+/Ca2+ exchanger; P54/NEFA, DNA binding/EF hand/acidic amino acid rich region protein; PDI, protein disulfide isomerase; SPCA, secretory pathway Ca2+-transport ATPase. Adapted from (Prins and Michalak, 2011).

1.2.2.2 Calcium and endoplasmic reticulum stress

Within the ER lumen, Ca^{2+} is present either in free-form or buffered via ER resident chaperones (Michalak and Opas, 2009), namely: Calreticulin, Immunoglobulin Binding Protein BiP/GRP78, GRP94, Protein Disulfide Isomerase (PDI). One characteristic uniting the ER Ca^{2+} buffers is their multifunctionality. Instead of being limited to serving as a passive sponge for Ca^{2+} within the organelle, Ca^{2+}-buffering proteins are responsible for a variety of processes, including chaperoning for post-translational protein modification and folding, regulation of apoptosis, and regulating Ca^{2+} release pathways (Bravo et al., 2013).

The multi-functional nature of the ER enables it to sense and integrate many of the incoming cell signals, in particular, the changes in free and bound Ca^{2+} concentrations in and outside of the ER compartment (Krebs et al., 2015). To fulfil this critical function, GRP78/BiP; an ER Ca^{2+}-binding protein associates with other ER transmembrane proteins; ATF6, IRE1 and PERK. The recruitment of Bip to these proteins is stabilized only by high Ca^{2+} concentrations (Suzuki et al., 1991). Thus, depleted and un-replenished Ca^{2+} stores which can lead to compromised action of calcium-activated chaperones will result in: (i) rapid accumulation of mis-folded proteins, (ii) dissociation of BiP from IRE1, PERK and ATF6 and (iii) activation of what's known by the unfolded protein response (UPR) pathway (Krebs et al., 2011), figure 1.11.

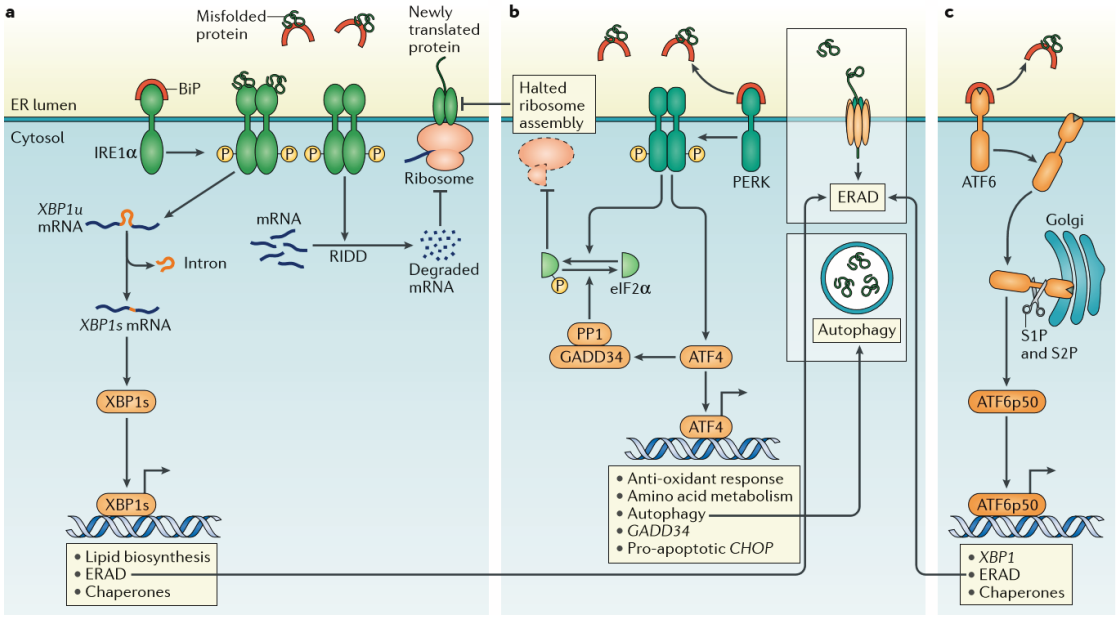

Figure 1.11 **The Unfolded Protein Response pathway**.
At a normal $[Ca^{2+}]_{ER}$: the ER-stress sensors are scaffolded and inactivated by GRP78/BiP. ER-resident chaperones facilitate the proper folding of the nascent protein and prevent its aggregation. Protein trafficking and quality-control mechanisms work normally. **In contrast, when the $[Ca^{2+}]_{ER}$ is remarkably decreased and not replenished**: the function of chaperones becomes disturbed and unfolded proteins accumulate and act as a sponge for luminal GRP78/BiP. As a consequence, ER-stress sensors are devoid of GRP78/BiP and become activated. **a-** Dissociation of binding immunoglobulin protein (BiP) from inositol-requiring enzyme 1α (***IRE1α***), or direct binding of misfolded proteins to IRE1α, activates the endoribonuclease domain of IRE1α, which non-conventionally splices an intron from unspliced X-box binding protein 1 (XBP1u) mRNA to produce XBP1s mRNA that encodes a potent transcriptional activator, XBP1s. Among the target genes of XBP1s are genes encoding proteins that increase the protein-folding capacity of the endoplasmic reticulum (ER) and that assist in the degradation of misfolded proteins by ER-associated degradation (ERAD). In addition, the entry of newly synthesized proteins into the ER is limited by the degradation of mRNA through regulated IRE1α-dependent decay of mRNA (RIDD). **b-** PKR-like ER kinase (***PERK***)- dependent phosphorylation of eukaryotic translation initiation factor 2α (eIF2α) inhibits ribosome assembly, which causes a translational block and allows the cell to manage temporary ER stress. Activating transcription factor 4 (ATF4) escapes translation inhibition under ER stress conditions and induces the transcription of genes that promote survival, including those involved in compensatory autophagy (see inset box). Once ER stress is resolved, eIF2α is dephosphorylated by the GADD34–protein phosphatase 1 (PP1) complex to restore protein translation. In addition, the unfolded protein response can activate apoptosis, mainly through C/EBP homologous protein (CHOP). **c-** Upon BiP dissociation from ***ATF6α*** during ER stress, ATF6α travels to the Golgi compartment where it is processed by the Golgi enzymes site 1 protease (S1P) and S2P to produce a cytosolic p50 fragment. ATF6p50 functions as a transcription factor that activates transcriptional programmes that increase ER capacity and protein folding, and that remove misfolded proteins from the ER for degradation (ERAD) (Grootjans et al., 2016).

An outstanding key task of acinar cells in the exocrine glands is the synthesis and packaging of proteins for transport. Accordingly, the ER of these cells is highly developed to accommodate the Ca^{2+} as well as the protein overload that can be experienced throughout their secretory role. As a consequence, secretory acinar cells may be highly sensitive to environmental conditions that impose ER stress like exposure to pathogenic inflammatory stimuli (Bettigole and Glimcher, 2015), particularly viral infections (Isler et al., 2005, Pavio et al., 2003, Tardif et al., 2002).

1.2.2.3 Disrupted Ca^{2+} Signalling in Dysfunctional Salivary Glands

Interestingly, due to the complexity of the signal which induces salivation, the integral acinar cell response to muscarinic receptor activation, with temporal and spatial $[Ca^{2+}]_i$ increase, can be prone to disruption. In fact, both physiologic and pathologic conditions can target acinar Ca^{2+} homeostasis.

Ageing has always been associated with the depletion of acinar tissue, hyperplasia of ducts and fibrosis of connective tissues in the salivary glands (Meisel et al., 1988). It is possible that these structural changes result in salivary insufficiency and xerostomia in the elderly (Niedermeier et al., 2000). Importantly, ageing is associated with signs of damage to many proteins including the Ca^{2+} handling proteins (Puzianowska-Kuznicka and Kuznicki, 2009). Of specific interest, studies have clearly demonstrated age-related cytosolic Ca^{2+} signal modulation in the aging parotid glands (Mahay et al., 2004, Salih et al., 1997, Maki et al., 1989). These studies suggested impaired or altered IP3-induced Ca^{2+} release from the ER in the aging parotid acinar cells, which in turn declined calcium influx machineries (Mahay et al., 2004).

Drugs are reported to induce dry mouth (Sreebny and Schwartz, 1997, Guggenheimer and Moore, 2003). Furthermore, xerostomia has been considered as a side effect of different classes of antihypertensive therapies (Nonzee et al., 2012). In particular, Hattori et al., suggested that the calcium channel blockers which are clinically administered for hypertension, can cause dry mouth by inhibiting the non-selective cation and voltage-dependent Ca^{2+} channels that are involved in resting salivation (Hattori and Wang, 2007).

Reactive oxygen species (ROS) are critical intracellular signalling factors that control cellular metabolism. However, high ROS levels exceeding the cellular antioxidant capacity cause detrimental effects with pathological consequences (Gorlach et al., 2015). ROS can be generated in irradiated salivary glands, that can lead to long-term irreversible dysfunction (Ambudkar and Muallem, 2016). In response to irradiation, the transient receptor potential melastatin-like 2 (TRPM2); a Ca^{2+}-permeable non-selective cation channel, is activated by ROS metabolites (Di et al., 2012) and contributes to irreversible salivary gland dysfunction by enhancing Ca^{2+} entry in salivary gland cells (Liu et al., 2013). In a variety of cell types, Ca^{2+} entry via TRPM2 has been associated with increased cell death and apoptosis (Ambudkar and Muallem, 2016).

Diabetes: xerostomia and pathological thirst (polydipsia) are two closely related complaints among diabetic patients which have been associated with impaired functions of the salivary glands (Fedirko et al., 2006). Due to the substantial $[Ca^{2+}]_i$ changes recorded in different cell types (Biessels et al., 2002, Kruglikov et al., 2004, Lagadic-Gossmann et al., 1996) and the altered Ca^{2+}-ATPase activity and expression in other tissues (Balasubramanyam et al., 2001, Evcimen et al., 1999, Vetter et al., 2002, Kim et al., 2001), Ca^{2+} dysregulation is currently

considered a basic pathology associated with diabetes complications. Importantly, experimental studies on diabetic rats revealed a marked decrease in saliva flow, protein content and amylase activity in response to pilocarpine stimulation, which paralleled abnormalities in acinar cell Ca^{2+} signalling (Fedirko et al., 2006, Murai et al., 1996, Watanabe et al., 2001). Furthermore, Fedirko, Kruglikov et al. 2006, described dramatic changes in Ca^{2+} homeostasis and signaling in acinar cells of rat submandibular salivary gland after 6–7 weeks of Streptozotocin-induced diabetes (Fedirko et al., 2006). Ca^{2+} alterations in the diabetic model comprised: (i) increased sensitivity and Ca^{2+}-mobilizing ability of muscarinic receptors, (ii) increased Ca^{2+} influx across the PM through the G-protein coupled Ca^{2+} channel; TRP6 and (iii) elevated resting $[Ca^{2+}]_i$ levels. Moreover salivary gland acinar cells from the diabetic rats exhibited delayed clearance of IP3-induced Ca^{2+} signals, slower replenishment of $[Ca^{2+}]_{ER}$ and diminished endoplasmic reticulum calcium $[Ca^{2+}]_{ER}$ content. These later findings were all substantiated to be related to dramatic reduction in the Ca^{2+} transporting abilities of both PMCA and SERCA pumps.

Sjögren's syndrome (SS) is a chronic autoimmune disease that results in lymphocytic infiltration and loss of secretory function in salivary and lacrimal glands (Nikolov and Illei, 2009). However, dysfunctional SGs of SS patients poorly correlate with inflammation (Shen et al., 2013, Xuan et al., 2013). Early studies have shown the upregulated expression of inducible nitric oxide synthase (iNOS) in the labial salivary glands of patients with SS when compared to healthy controls (Konttinen et al., 1997). Nitric oxide (NO) production from iNOS is known to be long-lasting and at relatively high concentrations when compared to the other two isotypes; endothelial (eNOS) and nNOS (Nathan and Xie, 1994).

Experiments which investigated the outcome of prolonged exposure of acinar cells to nitric oxide reported declined responsiveness of these cells to acetylcholine (Dawson et al., 2006), by desensitizing their receptors to stimulation (Caulfield et al., 2009). Furthermore, high levels of NO in SS patients (Caulfield et al., 2009, Konttinen et al., 1997, Ludviksdottir et al., 1999, Wanchu et al., 2000, Pertovaara et al., 2007) have been implicated in NO-mediated s-nitrosylation of receptors or other proteins involved in the Ca^{2+} evoked secretion signal (Caulfield et al., 2009). S-nitrosylation is the coupling of NO moiety to a reactive cysteine thiol to form an S-nitrosothiol; SNO, which ultimately alters the protein structure and function (Stamler et al., 1992a, Stamler et al., 1992b).

More recently, an important advancement in understanding the signal alteration underlying functional loss in SS patients, emerged from data which provided definitive evidence that IP3R deficits in acinar cells and subsequent decrease in neurotransmitter-stimulated Ca^{2+} signalling trigger the secretory dysfunction in those patients (Teos et al., 2015).

1.3 SG Infections (Sialadenitis)

1.3.1 General Risk Factors

Primary mechanisms predisposing to acute infections of the salivary glands involve: (i) stasis of flow and (ii) retrograde contamination by bacterial flora from the oral cavity (McQuone, 1999). The most prevalent inciting factor in stasis of flow is dehydration which is commonly seen: in postoperative patients, in those taking particular medications with xerostomia side effects like antihistamines and in post-irradiated patients or with certain medical conditions like hepatic and renal failures and diabetes mellitus (McQuone, 1999). Interestingly, the reduced secretion rate may also be initiated by an autoimmune mechanism (SS) or some other process, which is probably either developmental or related to a previous virus infection (Banks, 1968). Mechanical obstruction (sialoliths) is another factor which precipitates stasis of flow. Sialoliths are more commonly seen in the submandibular ductal system (McQuone, 1999), because of the more viscous (worsened in a dehydrated state) glycoprotein consistency, upward course of the duct, and higher concentrations of calcium carbonate and calcium phosphate than are found in the parotid glands (Knepil and Fabbroni, 2008).

Even with 85% to 90% of sialoliths being found in the submandibular glands, sialadenitis remains more prevalent in the parotid glands. This preferential predominance is due to the parotid gland fulfilling both risk factors mentioned beforehand. First, the relatively long, narrow parotid duct which is adapted to thin serous secretions is readily obstructed by small calculi or even by mucus plugs formed as a result of change in the content of the saliva, which is known to occur in certain circumstances (Patey, 1966).

This in addition to the secretory composition variances in both glands; the parotid glands secretion which is mostly serous, contain a higher concentration of fibronectin, which promotes the adherence of Streptococcus and S aureus around the ductal orifice (Mandel and Surattanont, 2002). Alternatively, the greater proportion of mucinoid substance in the sublingual and submandibular glands contains lysosomes, immunoglobulin A antibodies, and glycoproteins that bind epithelial cells and competitively inhibit bacterial attachments (McQuone, 1999).

1.3.2 Viral SG Infections

A long association has been established between viral infections and diseases of the salivary gland, which respond by reduced saliva production and/or swelling (Jeffers and Webster-Cyriaque, 2011). Although all salivary glands are susceptible to viral infection, the parotid and the submandibular glands are most prone (Chandak et al., 2012). Furthermore, murine models of viral infection have demonstrated that the SG is a unique site in regards to virus–cell interactions. Assisted by the abundant capillary supply and extraordinary high rate of blood flow (Lu and Jacobson, 2007), viruses can reach the SGs as a consequence of secondary viremia, with blood monocytes playing a major role in dissemination (Stoddart et al., 1994). Furthermore, in these viral models, the SGs maintained a chronic infection, with the infectious virus replicating for months after viral clearance from all other organs. Interestingly, the persistent virus was selectively sequestered in vacuoles of glandular acinar epithelial cells (Jonjic et al., 1989), suggesting that the host immune response to viruses at mucosal sites, like the SGs, may be different from systemic immunity; in that clearance is protracted and the incidence of reactivation is high (Lu and Jacobson, 2007).

1.3.3 Viruses Implicated in SG Pathology

Mumps is the most common viral SG infection, and the profound xerostomia produced by mumps is well recognized (Banks, 1968). It is caused by a single stranded RNA virus belonging to the genus Rubula virus and the family Paramyxoviridae. In humans, mumps is the most common cause of non-suppurative acute sialadenitis; 85% of cases occur in children younger than 15 years (McQuone, 1999).

It has no animal reservoir and is therefore purely a human disease (Senanayake, 2008). The disease is highly contagious and spreads by airborne droplets from salivary, nasal, and urinary secretions. There is a primary viral infection of the oral cavity, after which the virus replicates within the upper respiratory tract and local reticuloendothelial and lymphoid systems. Subsequently, there is a period of 7–10 days of viremia, during which other organs can become infected (Singh et al., 2006). Symptoms include acute onset of unilateral or bilateral tender, self-limited swelling of the parotid gland, lasting two or more days without other apparent cause. In 10% of cases, other salivary glands may also be involved (Senanayake, 2008).

Discovered in cultured Burkitt's lymphoma cells (Epstein et al., 1964), **Epstein-Barr virus (EBV)** is an enveloped DNA herpesvirus that is transmitted by saliva and is shed even in apparently healthy subjects (Gerber et al., 1972). Identification of EBV in chronic nonspecific sialadenitis, Warthin's tumour and lymphoepithelial carcinoma, is highly suggestive of its role in these lesions (Kim et al., 1999). EBV infects the oropharyngeal epithelium and replicates there. Then it infects the surrounding B lymphocytes in a form of latent infection. The infected

B lymphocytes then re-infect the epithelial cells of other tissues via circulation in the blood (Hatton et al., 2014).

In addition to the large percentage of **Human Immunodeficiency Virus** (HIV)-infected patients which have been reported with SS-like conditions and dry mouth (Ulirsch and Jaffe, 1987), **Human immunodeficiency virus**-associated salivary gland disease (HIV/SGD) is another oral manifestation of HIV infection (Schiodt et al., 1989). A low, unstimulated, whole-saliva flow rate has been associated with HIV/SGD (Grimoud et al., 1998, Flaitz et al., 1998). In addition, quantitative changes have been detected in saliva of HIV/SGD patients; such as lower secretory rates of sodium, calcium chloride, cystatin, lysozyme, and total anti-oxidant capacity, which affect the homeostasis of the oral cavity and account for significant morbidity during the progression of HIV disease (Lin et al., 2003). Histologically, HIV/SGD is characterized by hyperplastic, intra-parotid lymph nodes and/ or predominant CD8+ T-cells peri-ductal lymphatic infiltrates. Histochemical analysis has revealed acinar atrophy, ductal dilation, and mild to moderate fibrosis with collagen deposition (McArthur et al., 2003).

Several **DNA, RNA and retroviruses** have been considered important co-factors in the development of SS. In fact, two mechanisms have been reported to correlate viral infections to development of SG autoimmunity. Viral proteins exhibiting structural or functional molecular mimicry with host components can result in production of autoantibodies in SS patients (Navone et al., 2005). Moreover, activation of the innate immune responses upon viral recognition, results in a prolonged inflammatory response that may lead to chronic inflammation with activation of adaptive immune responses (Francis and Perl, 2010). Whereas the DNA viruses that have been studied in association with SS

are cytomegalovirus (CMV) and EBV (Saito et al., 1989, Mariette et al., 1991, Maitland et al., 1995), the RNA viruses detected within the salivary glands of SS patients are hepatitis C (HCV) and Coxsackie virus (Triantafyllopoulou et al., 2004, Carrozzo, 2008). Table 1-3 lists the viruses which are related to salivary gland diseases (Jeffers and Webster-Cyriaque, 2011).

Table 1-3 Viruses Detected in SGs (Jeffers and Webster-Cyriaque, 2011)

Virus	Associated Disease(s)
BK virus (polyomavirus family)	HIV-SGD
Paramyxovirus	Mumps
Human immunodeficiency virus (HIV)	HIV-SGD, SS
Epstein-Barr virus (EBV)	Benign Lymphoepithelial Cysts (BLC), salivary gland tumors, SS
Cytomegalovirus (CMV)	Sialadenitis
Coxsackie virus	SS
Human T-lymphotropic virus (HTLV)	SS
Human herpes virus 6 (HHV-6)	Parotitis
Human herpes virus 7 (HHV-7)	Parotitis
Kaposi sarcoma virus (KSHV)	Warthin's tumor, SS-associated parotid MALT lymphomas
Influenza	Parotitis
Parainfluenza virus (PIV)	Parotitis
Guinea pig CMV	Guinea pig CMV infection
Hepatitis C	SS
Mouse CMV (MCMV)	Acute and chronic SGD
Mouse polyomavirus (PyV)	Mouse parotid tumor
Encephalomyocarditis (EMC)	Sialodacryoadenitis

1.3.4 Double Stranded (ds) RNA

Invading pathogens are recognized by several innate receptors, termed pattern recognition receptors (PRRs), which are located both at the cell surface and intra-cytosolic. These sensors function to generate immune responses against conserved structures on microorganisms, known as pathogen-associated molecular patterns (PAMPs) (Melchjorsen, 2013). Albeit the diversity of viral PAMPs; which include: surface structures, genomic material, and capsids, the intermediates generated during the replication cycle can also constitute PAMPs. In fact, the dsRNA produced during the replication of many RNA and DNA viruses (Kawai and Akira, 2007) is considered a hallmark PAMP and the most potent viral trigger of innate immune signalling (Nellimarla and Mossman, 2014).

1.3.4.1 Origin of dsRNA

It has been commonly assumed that the major source of cellular *dsRNA is* ***viral*** infections (Wang and Carmichael, 2004). Viruses possess unique long stretches of dsRNA (Brencicova and Diebold, 2013), the origin of which is diverse. RNA viruses with double-stranded genomes induce the innate immune response through their genome itself. This property, however, is not exclusive to these viruses, and as mentioned beforehand, it is generally accepted that most viruses also produce dsRNAs when replicating (Jacobs and Langland, 1996). While it was suggested that the electronegative properties of dsRNA would limit its ability to disseminate (Majde, 2000), studies reported travel of dsRNA between cells and tissues in plants and nematodes (Obbard et al., 2009). Similarly, in Drosophila, studies have reported that viral dsRNA travels from the site of infection and induces antiviral responses in neighbouring or uninfected cells (Saleh et al., 2009).

As opposed to viral dsRNAs, which are often much longer, ***endogenous (self) dsRNAs*** are commonly found in short stretches (<20bp) (Kato et al., 2008). Self dsRNA can arise from microRNAs (miRNAs) which are constantly synthesized by the cell (Gantier and Williams, 2007). Micro-RNAs represent an abundant and important class of noncoding RNA species, which can enter the sequence-specific RNA interference (RNAi) pathway, where they mediate the destruction of targeted mRNAs (Rana, 2007). In addition to microRNA, necrosis in the absence of infection also releases self dsRNA, leading to inflammatory and autoimmune responses (Nellimarla and Mossman, 2014).

In the laboratory, most studies utilize ***dsRNA substitutes*** to look at the dsRNA-mediated-IFN antiviral response in a reproducible manner (DeWitte-Orr and Mossman, 2010). Synthetic poly(I:C), which consists of stretches of inosine and cytidine forming dsRNA-like motifs (Michelson et al., 1967), has been extensively used since its discovery, half a century ago, to mimic viral dsRNA. Both animals and humans develop an acute phase response characteristic of viral infections following treatment with poly (I:C) (Caskey et al., 2011). Moreover, studies have demonstrated that a single local administration of poly (I:C) induces inflammatory responses in the lungs of mice similar to that observed in the lungs of patients with chronic obstructive pulmonary disease (Harris et al., 2013). Also, poly (I:C) was shown to play a significant role in disruption of self-tolerance and establishment of an autoimmune response as seen in poly (I:C) induced autoimmune uveitis (Ren et al., 2011) and myasthenia gravis (Cufi et al., 2013).

1.3.4.2 Uptake of dsRNA

Poly (I:C) internalization is the best studied model of dsRNA uptake in both *in vitro* and *in vivo* studies. Poly (I:C) is internalized into cells through clathrin-mediated endocytosis and delivered to endosomal TLR3 and to cytoplasmic MDA5 (melanoma differentiation-associated gene 5) (Kato et al., 2008). Previous studies confirmed that the cytoplasmic lipid raft protein; raftlin, is essential for poly (I:C) cellular uptake in human myeloid DCs and epithelial cells. In raftlin knockdown cells, poly (I:C) neither enters the cell nor activates TLR3 and MDA5, further indicating that cellular uptake is a prerequisite for dsRNA-induced cellular responses. Upon poly (I:C) stimulation, raftlin migrates from the cytoplasm to the cell surface, where it associates with the clathrin–AP-2 (clathrin associated adaptor protein-2) complex and induces cargo delivery (Watanabe et al., 2011), figure 1.12.

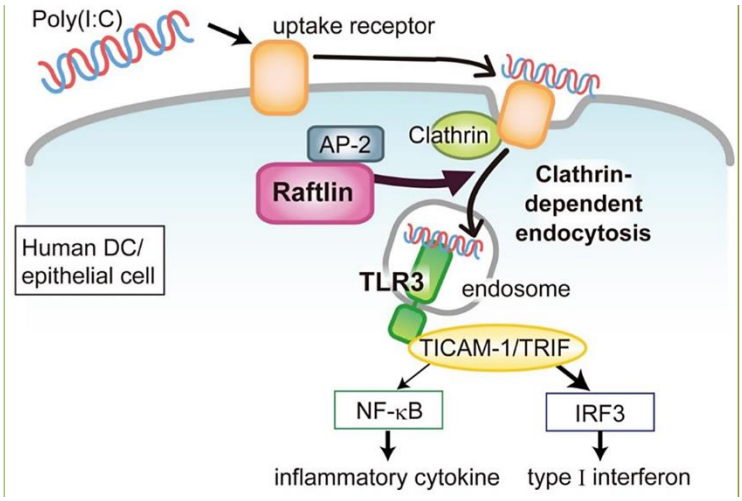

Figure 1.12 **Extracellular poly (I:C) uptake.**
Poly (I:C) is recognized by cell surface uptake receptor and delivered to the TLR3-resident endosomes through Rarftlin- and clathrin-dependent endocytosis. Upon ligand recognition, TLR3 activates IRF3 and NF-κB via TICAM-1, leading to production of type I IFN and inflammatory cytokines, respectively. Adapted from (Misako Matsumoto, 2016)

Furthermore, studies have shown that class A scavenger receptor (SR-As); a cell surface pattern recognition receptor (PRR), is critical for poly (I:C) induction of inflammatory responses (Limmon et al., 2008). In fact, the ubiquitously expressed SR-As mediate dsRNA entry via clathrin-mediated endocytosis, delivering them to intracellular dsRNA-binding proteins and inducing antiviral responses both *in vitro* and *in vivo* (DeWitte-Orr et al., 2010). The role played by scavenger receptors was further confirmed by studies which showed that downregulation of these critical sensors inhibited dsRNA uptake (Rocha et al., 2011).

Other different mechanisms of dsRNA uptake have been reported: while uptake by B cells is mediated through their B-cell receptor (BCR) (Leadbetter et al., 2002), bone marrow derived macrophages (BMDMs) depend on CD14 for dsRNA internalization (Lee et al., 2006). Finally, CD11b has also been found to essentially facilitate the internalization of poly (I:C) in peritoneal macrophages and RAW 264.7 cells (Zhou et al., 2013).

1.3.4.3 Innate Sensing of dsRNA

It has been known for many years that introduction of synthetic or naturally occurring dsRNAs into the cytoplasm can trigger nonspecific and global immune responses in animals (Cunnington and Naysmith, 1975). Since dsRNA is the most potent trigger of the innate immune system, it is not surprising that cells possess several receptors for its recognition (figure 1.13).

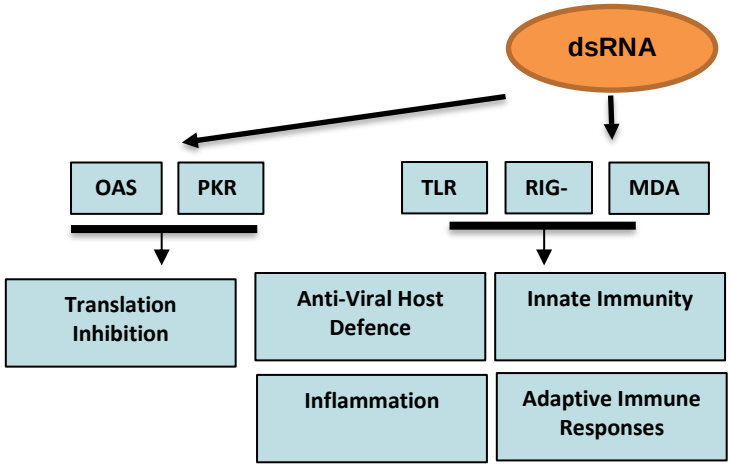

Figure 1.13 Recognition and biological effects of dsRNA signalling pathways

1.3.4.3.1 Toll-like receptor (TLR)

TLRs were the first PRRs to be identified and have been most thoroughly studied (Lester and Li, 2014). First acknowledged in Drosophila, the Toll receptor was shown to be important for host defence against fungal infection (Lemaitre et al., 1996). Subsequently, 15 subfamilies of TLRs have been identified in vertebrates (Takeda et al., 2003b). These transmembrane receptors, which localize to both the PM and endolysosomal compartments (figure 1.14), play key roles in development, homeostasis and injury repair (Ramnath et al., 2016).

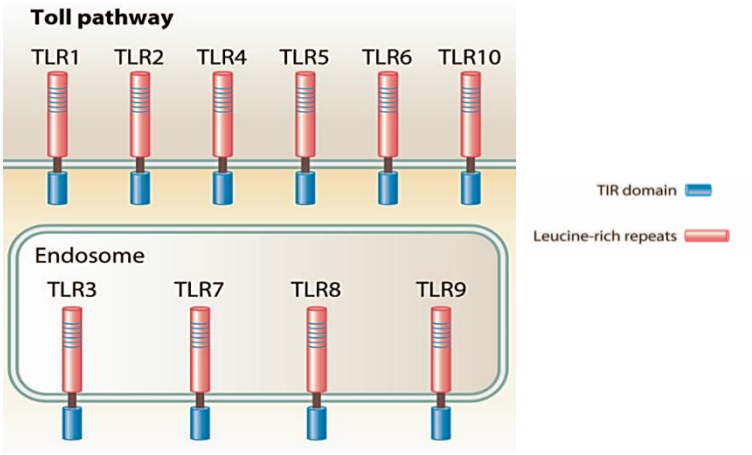

Figure 1.14 **TLRs**
TLRs are membrane-bound receptors localized at the cellular or endosomal membranes, recognizing PAMPs via the leucine-rich repeats (LRR) domain and transducing signals to the intracellular environment through the Toll–IL-1 receptor (TIR) domain (Mogensen, 2009).

Each TLR is specialized in recognition of distinct PAMPs among which TLR3, 7, 8 and 9 recognize foreign nucleic acids (Blasius and Beutler, 2010). TLR7 and TLR8 recognize virus-derived ssRNA (Diebold et al., 2004, Heil et al., 2004, Lund et al., 2004), while TLR9 recognizes microbial non-methylated CpG-containing DNA (Hemmi et al., 2000). TLR3 is the only TLR that recognizes virus-derived dsRNA and its synthetic analogue, poly (I:C) (Alexopoulou et al., 2001), as well as self RNAs derived from damaged cells via its ectodomain (Takemura et al., 2014).

1.3.4.3.1.1 TLR3 Structure and Ligand Binding

TLR3 is a type I integral transmembrane glycoprotein. Similar to all TLRs, TLR3 possess an extracellular domain or ectodomain (ECD) comprising 19–25 tandem copies of leucine-rich repeats (LRRs), a transmembrane domain, and an intracellular Toll/IL-1 receptor (TIR) domain (Akira and Takeda, 2004) (figure 1.17). The crystal structure of the TLR3 ectodomain resembles a long solenoid bent into the shape of a horseshoe, of which one face is largely masked by carbohydrate, whereas the other is unglycosylated. Each turn of the solenoid corresponds to a single LRR sequence from a total of 23 leucine-rich repeats (Bell et al., 2005). Binding of dsRNA to TLR3 induces the receptor to homodimerize (Liu et al., 2008), causing a structural rearrangement where the TIR domains come into close contact and provide a “platform” for the adaptor protein TIR domain-containing adapter protein inducing IFNβ (TRIF) (O'Neill and Bowie, 2007), figure 1.15. This structural re-organization is essential for ligand binding of both viral dsRNA and poly (I:C) (Wang et al., 2010).

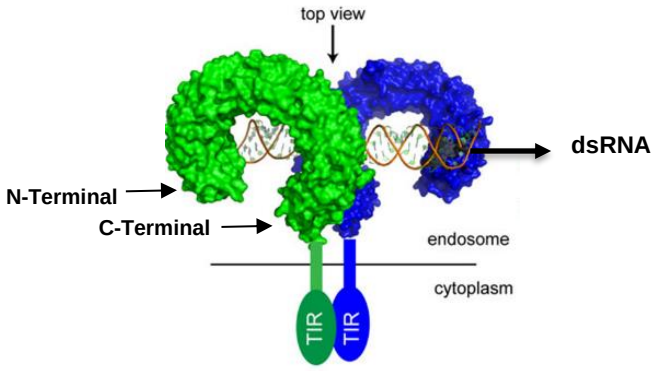

Figure 1.15 **TLR3 Structure and Dimerization**.
TLR3 consists of an ECD containing: 23 LRRs and the N (N-terminal) and C (C-terminal) regions, the transmembrane domain, the cytoplasmic linker region and the TIR (Toll–IL-1 receptor) domain. The TIR domain is critical in signalling of TLR3 through interaction with downstream signal adaptor molecules. dsRNA interacts with both an N- and a C-terminal-binding site of each TLR3 ECD (Liu et al., 2008). The two LRR-CT regions come together, which is essential for stable receptor–ligand complex formation and facilitates the dimerization of the cytoplasmic TIR domain (Wang et al., 2010).

Several studies using different lengths of the preferential TLR3 ligand; poly(I:C), indicated that longer duplexes of at least 40-50 bp are prerequisites to induce TLR3 signalling (de Bouteiller et al., 2005, Okahira et al., 2005). This length requirement would help avoid inappropriate recognition of cellular ssRNAs with short hairpin structures or mature siRNAs or miRNAs (Peisley and Hur, 2013).

1.3.4.3.1.2 TLR3 Intracellular Trafficking and Maturation

Endosomal TLR maturation is tightly regulated through a combination of receptor-specific intracellular trafficking and proteolysis. The concept of TLR signalling being functionally intertwined with the cellular membrane trafficking machinery has received much attention in recent years (Barton and Kagan, 2009). However, despite great progress in the identification of the molecular components of TLR signalling pathways, still little is known about whether and how regulators of the endosomal/phagosomal trafficking system affect TLR signalling and function, particularly under inflammatory in vivo conditions. TLR9 resides predominantly in the ER in resting cells (Leifer et al., 2004) and reaches the acidic endolysosomal compartments after stimulation by dsDNA (Barton et al., 2006, Tabeta et al., 2006). In contrast, TLR3 is continuously exported to the Golgi and accumulates in the endolysosomal compartments, where it undergoes a single cleavage by cathepsins and the two fragments remain associated without disruption even after ligand binding (Toscano et al., 2013) (figure 1.16).

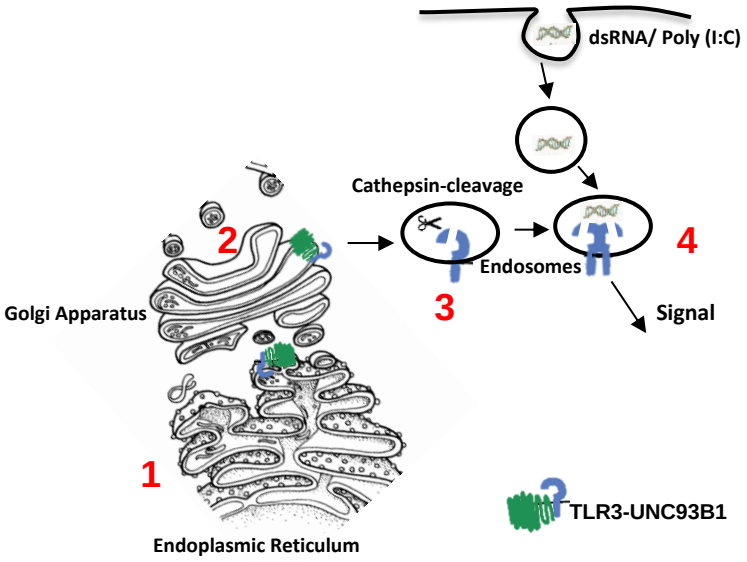

Figure 1.16 **Proposed model of TLR3 trafficking and maturation**.
(1) TLR3 is neosynthesized and N-glycosylated in the ER. (2) it crosses the Golgi apparatus where it is fully glycosylated to become EndoH resistant. TLR3 exits the Golgi to enter the endosome membrane where it is cleaved by cathepsins (3). The two proteolytic fragments remain associated to fully signal (4) (Toscano et al., 2013). Interestingly, acidified endosomes are required not only for cleavage of TLR3 but also for activation of cleaved TLR3, likely by inducing a conformational change required for signalling. The strongest response to dsRNA is achieved between pH 5.7 and 6.7 (de Bouteiller et al., 2005), which corresponds to endosomal pH range (Cain et al., 1989). As with other endosomal TLRs, TLR3 trafficking and subsequent cleavage and signalling, depend on the transporter protein UNC93B1 (an ER chaperone with 12 membrane-spanning domains). It interacts with transmembrane segments of TLR3 (Tabeta et al., 2006). Beside its role in TLR3 trafficking, Unc93b1 is also important for TLR3 cleavage and stability by protection from ubiquitination and degradation (Qi et al., 2012).

Monoclonal antibodies generated against the TLR3 ectodomain revealed that at steady state, there exists three forms of TLR3: a full length, 130 kDa highly glycosylated TLR3, a C-terminal fragment observed after cathepsin cleavage and another isoform which is predicted to represent the N-terminal fragment of cleaved TLR3 (Garcia-Cattaneo et al., 2012, Toscano et al., 2013, Murakami et al., 2014). Furthermore, immunoblotting analysis revealed the increased expression levels of the cleaved C-terminal fragment of TLR3 following exposure to poly (I:C).

Importantly, it is the cleaved form of TLR3 that signals from endosomes upon ligand recognition in nonimmune (epithelial) and immune (MDDC) cells (Garcia-Cattaneo et al., 2012). Based on the TLR3 3D structure, the predicted TLR3 cleavage site has been localized within the region which encompasses the LRR12 flexible loop that protrudes from the lateral face of the ectodomain, hence it is potentially well exposed to proteases (Choe et al., 2005, Park et al., 2008) (figure 1.17).

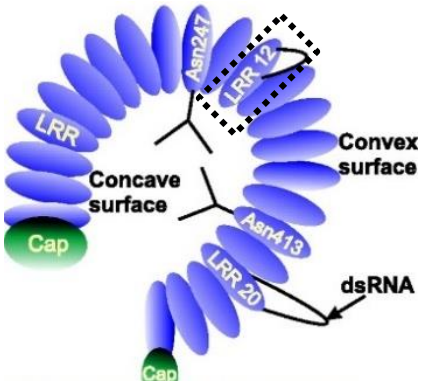

Figure 1.17 **TLR3 cleavage.**
It occurs at the LRR 12 loop facilitated by its structural protrusion from the helix and exposure to the endolysosomal cysteine proteases.

In epithelial cells, TLR3 cleavage depends on cysteine protease cathepsins B and H, as poly (I:C)-dependent TLR3 signalling is inhibited and cleavage is reduced in cells exposed to the cathepsin inhibitor; z-FA-fmk or silenced for both cathepsins using siRNA (Garcia-Cattaneo et al., 2012).

1.3.4.3.1.3TLR3-Mediated Innate Immune Responses

As formerly mentioned, TLR3 is assembled in the endoplasmic reticulum, from where it is recruited to endosomes by the transmembrane protein UNC93B1 (Kim et al., 2008). Although TLR3 signals exclusively via the TRIF pathway, all other TLRs use the adaptor MyD88. The alanine residue present in the TLR3 TIR domain plays a major role in this uniqueness, as evidenced by mutation of TLR3 Ala795 into a proline; present in other TLR TIR domains, which resulted in MyD88-biased signalling (Verstak et al., 2013). The cascade of events triggered upon TLR3 engagement by its ligands; example poly (I:C), commences by the receptor homodimerization and recruitment of TRIF (Kaisho and Akira, 2006, O'Neill and Bowie, 2007), after which TLR3 signalling diverges into several distinct arms, figure 1.18.

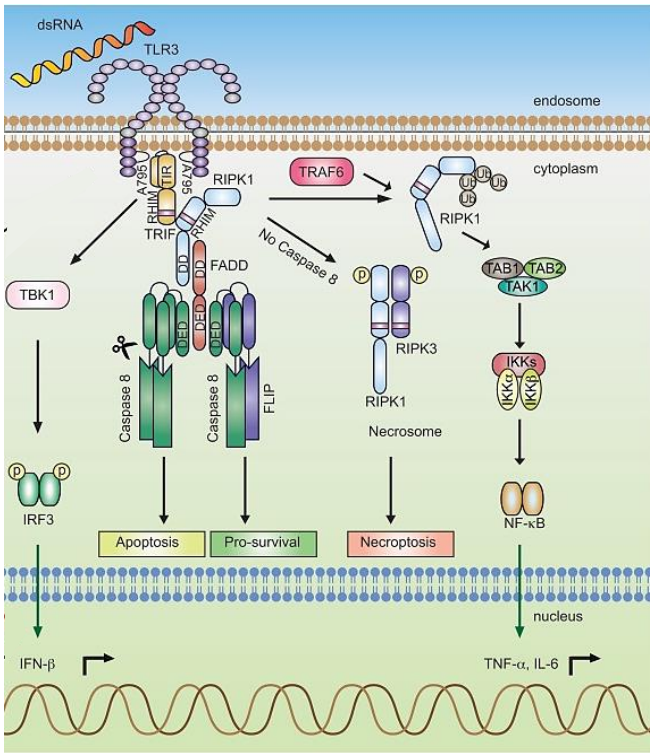

Figure 1.18 **TLR3 Signalling Pathway**
(Ramnath et al., 2017)

TRIF activates the serine/threonine tank binding kinase-1 (TBK-1), which directly binds to and phosphorylates IRF3 (Sato et al., 2003). Phosphorylated IRF3 (pIRF3) dimerizes and translocates to the nucleus and leads to the transcription of IFN-β (Honda and Taniguchi, 2006, O'Neill and Bowie, 2007). IFN-β signals in an autocrine fashion to activate the transcription factors signal transducer and activator of transcription (STAT) 1 and 2, resulting in the activation of type I IFN stimulated genes (ISGs) and subsequent anti-viral responses (Platanias, 2005).

In addition, the transcription factor NF-κB is induced through TLR3 stimulation (Kaisho and Akira, 2006, Gauzzi et al., 2010, Sen and Sarkar, 2005, O'Neill and Bowie, 2007, Matsumoto et al., 2011). The C-terminal region of TRIF contains a receptor-interacting protein homotypic interaction motif (RHIM), which is essential for its interaction with the serine/threonine kinase receptor-interacting protein kinase (RIPK)1 (Meylan et al., 2004). RIPK1 interacts with TRAF6 which polyubiquitinates transforming growth factor β activated kinase 1 (TAK1) and IκB kinase-related kinase γ (IKKγ) (Jensen and Thomsen, 2012). IKKγ directly associates with IKKα and IKKβ, while TAK1 forms a complex with TAK1 binding proteins 1, 2, and 3 (TAB1, 2, and 3) and then phosphorylates IKKβ (Brown et al., 2011). The activated IKK complex then phosphorylates IκBα facilitating its ubiquitination and degradation, and the release and activation of NF-κB (Jensen and Thomsen, 2012, Gauzzi et al., 2010, Mathes et al., 2008). The TRIF-RIPK1 axis is a central control point in cell survival/death pathways, since RIPK1 also associates with Fas-associated death domain (FADD), via a death domain interaction (Kaiser and Offermann, 2005). This subsequently leads to the assembly of a death-inducing signalling complex that contains caspase-8.

Homodimerized caspase-8 undergoes autocatalytic processing and activation, leading to RIPK1 cleavage and inactivation, followed by apoptotic cell death. However, if caspase-8 heterodimerizes with a non-catalytically active homologue of caspase-8, FLICE-like inhibitory protein, it is partially activated. This complex is not able to cleave RIPK1 adequately to cause apoptosis, and therefore mediates cell survival (Kaiser and Offermann, 2005). Furthermore, if caspase-8 activity is compromised, RIPK1 cleavage is completely prevented, thereby allowing it to interact with RIPK3 to form a necrosome, leading to necroptotic cell death (Kaiser et al., 2011, Oberst et al., 2011). Thus, RIPK1 acts as a central signalling hub in dictating whether TLR3 signalling promotes survival, apoptotic cell death or necroptotic cell death. Importantly, TLR-3 induced apoptotic cells discharged into the extracellular space, will release endogenous death associated molecular patterns (DAMPs), exposing molecular hydrophobic portions that were normally hidden in a healthy living cell. DAMPs are a rapidly growing class of potent inflammatory stimuli. They act in an autocrine manner, alerting the host of damage, but can also amplify inflammation leading to further tissue damage (Prince et al., 2011).

1.3.4.3.2 RIG-I-Like Receptors, RLRs

The RLR family is another cytosolic dsRNA sensor comprising 3 closely related members of RNA helicases, RIG-I, MDA-5, and LGP2, which can detect cytoplasmic dsRNA, generated during replication of RNA viruses (Kawai and Akira, 2008, Loo and Gale, 2011, Dixit and Kagan, 2013). All 3 members contain centrally located RNA helicase domains, whereas RIG-I and MDA5, but not LGP2, have 2 N-terminal caspase-recruitment domains (CARDs) (figure 1.19).

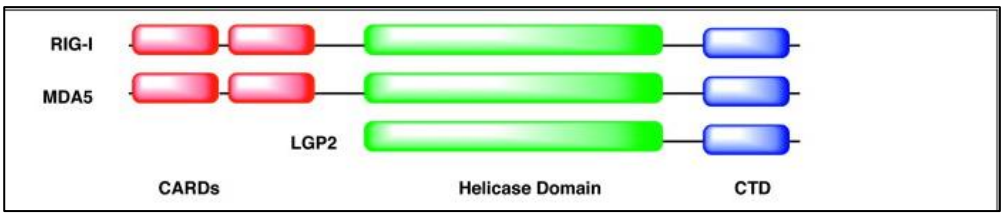

Figure 1.19 **RLR structural domains**
((Bowzard et al., 2011).

The helicase domain is responsible for the recognition of RNA, whereas the CARD domains are required for downstream signalling. LGP2, which lacks the CARD domains, cooperates with RIG-I and MDA-5 and enhances their functions (Moresco and Beutler, 2010, Satoh et al., 2010, Childs et al., 2013). Studies have shown that the length of dsRNA is a determinant for the recognition by specific RLRs; RIG-I and MDA-5 can preferentially detect short and long dsRNA species, respectively (Kato et al., 2008). Since poly (I:C) is a mixture of various lengths of RNA species, it can be recognized by both RIG-I and MDA-5 (Chattopadhyay and Sen, 2014). Upon activation by cytoplasmic dsRNA, RIG-I and MDA-5 activate downstream signalling via the CARD containing adaptor protein IPS-1, which binds to them through CARD–CARD interaction (Bruno Miguel Neves, 2012) (figure 1.20).

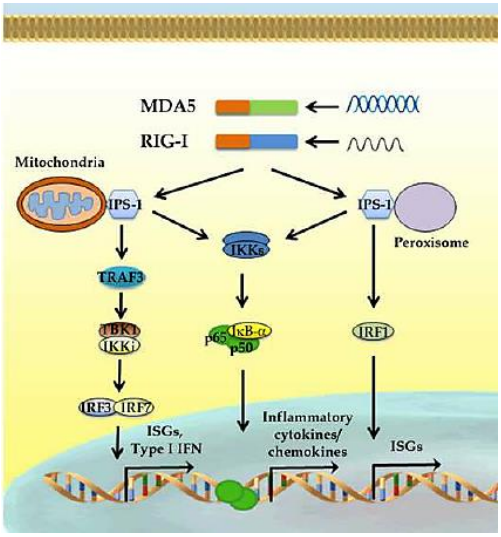

Figure 1.20 **RLR signalling**.
RIG-I and MDA5 function as cytosolic sensors of short and long dsRNAs, respectively. Binding of dsRNAs to these receptors activates signalling through the adaptor protein IPS-1, located in the outer mitochondrial membrane or on peroxisomes. Mitochondrial IPS-1 leads to activation of NF-κB and IRF3/IRF7 through the IKK complex and TBK1/IKKi, respectively, which results in the production of inflammatory cytokines, type I interferons and interferon-stimulating genes (ISGs). In turn, peroxisomal IPS-1 induces early expression of ISGs via transcription factor IRF1 (Bruno Miguel Neves, 2012).

1.3.4.3.3 dsRNA-activated protein kinase (PKR)

PKR is a central player in the cytoplasmic response to dsRNA. PKR is an interferon-inducible, dsRNA-activated Ser/Thr protein kinase (Clemens, 1997, Proud, 1995). This enzyme is normally present only at low levels in cells and exists in an unphosphorylated, inactive form (Hovanessian, 1989, Samuel, 1991). When dsRNA binds to PKR, this induces its dimerization, auto-phosphorylation and activation (Wang and Carmichael, 2004). Consequently, pPKR phosphorylates a number of substrates, the most important of which is the eukaryotic initiation factor 2 (eIF-2α) (Samuel, 1979), which results in global cellular inhibition of protein synthesis (Samuel, 1993).

The activation of PKR is independent of the sequence of dsRNAs but depends on both their concentration and on their length. PKR is activated by low concentrations of dsRNAs but inhibited by higher concentrations (Samuel 1993). Activated PKR can mediate signal transduction in response to dsRNAs (Proud, 1995), figure 1.21. In addition, there is evidence that dsRNAs can trigger apoptosis through PKR (Gil and Esteban, 2000) by activation of the Fas-associated death domain/caspase 8 pathways (Balachandran et al., 1998) or of caspase 9 (Gil et al., 2002).

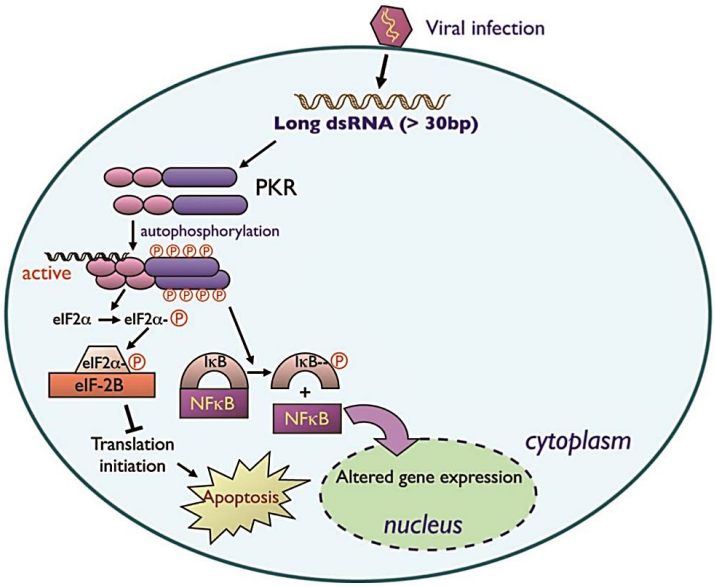

Figure 1.21 **dsRNAs can bind to and activate PKR**.
Activated PKR phosphorylates a number of targets, including the translation factor eIF2, leading to translation inhibition. It can phosphorylate IκB, releasing it from the transcription factor NF-κB, which can now be translocated to the nucleus, where it activates the expression of genes having NF-κB binding sites. These genes include beta interferon (Thanos and Maniatis, 1995), Fas (Donze et al., 1999), p53 (Cuddihy et al., 1999), Bax (Gil and Esteban, 2000), and others (Williams, 2001).

1.3.4.3.4 2’,5’-AS/RNase L.

In addition to the PKR pathway, the 2’,5’-oligoadenylate synthetase (2’,5’-AS)/RNase L pathway responds to dsRNA. IFN signalling leads to the induction of oligoadenylate synthetases (OAS1), which following activation by long double stranded RNA (dsRNA), generates 2’-5’-linked oligoadenylates (2-5A) (Hovanessian, 2007). 2-5A then binds to RNase-L, leading to its dimerization and enabling its nuclease activity (Tanaka et al., 2004). RNase L, which is a widely expressed cytoplasmic endoribonuclease, catalyses the degradation of viral and cellular RNAs (Li et al., 1998), including mRNAs, thus inhibiting protein synthesis (Iordanov et al., 2000) (figure 1.22).

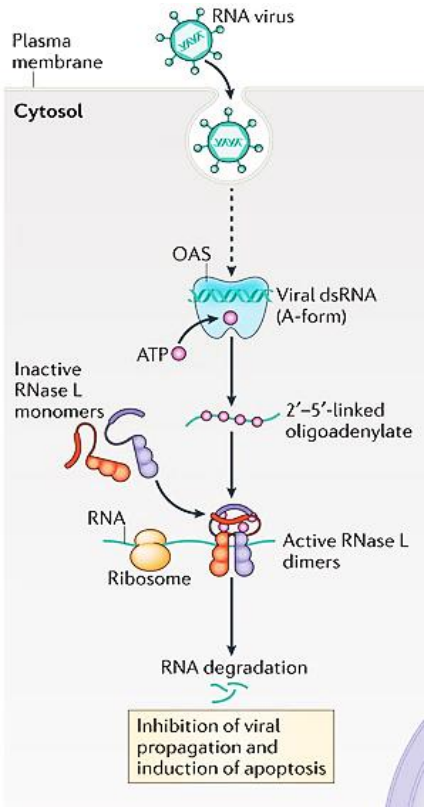

Figure 1.22 **2',5'-oligoadenylate synthetase 1 (OAS1)**
OAS1 is expressed at low constitutive levels and is upregulated by type I interferons (IFNs). OAS1 protein accumulates in the cell cytoplasm as an inactive monomer. Following activation by dsRNA, the enzyme oligomerizes to form a tetramer that synthesizes 2',5'-oligoadenylates (using ATP as a substrate) that, in turn, activates the constitutively expressed inactive ribonuclease L (RNaseL). RNase L then forms a crossed dimer and degrades RNA that is of both cellular and viral origin, leading to the inhibition of viral propagation (Hornung et al., 2014).

1.4 Aims of The Study

A long association has been established between viral infections and diseases of the salivary gland. However, the mechanism(s) by which primary viral infections can induce glandular injury and compromise the secretory machinery are not well understood. Previous studies demonstrated that multiple systemic injections of poly (I:C) in *SS prone* NZB/WF1 mice, resulted in loss of glandular function (Nandula et al., 2013, Deshmukh et al., 2009). These studies hypothesized the involvement of cumulative effects of type I IFN production and other inflammatory cytokines in the perceived glandular hypofunction (Deshmukh et al., 2009).

The aims of this study were:

1-To develop a viral mimic model based on direct injection of poly (I:C) into the SMGs and activation of local exocrine innate immunity, ruling out any possible extraneous impacts arising either from systemic delivery responses or autoimmune susceptibility of mice.

2- To utilize the SG model to verify the initial impact of these types of infections on the functional responses of the glands.

3- To comprehensively characterize the early molecular events and innate immune signalling pathways that can be triggered by viruses and potentially contribute to acute exocrine injury and dysfunction.

Chapter 2

Materials And Methods

2.1 Viral Mimic Model Development

Female C57BL/6 mice, weighing 18-21 grams (Harlan Labs Ltd., Loughborough, UK), were aged between 10-12 weeks at the start of the experiments. They were housed in a temperature-controlled environment under a 12 h light–dark cycle with free access to food and water. All procedures were approved by the local ethics committee, and performed in accordance with the Home Office license.

Female mice were chosen due to studies suggesting that they possess the combined capacity of: (1) heightened sensitivity to infectious and injurious stimuli (in the form of increased number of tissue macrophage with a greater density of pathogen/injury-sensing TLRs), (2) more efficient phagocytosis and NADPH oxidase-mediated killing by resident macrophage that eliminate pathogens faster than in males and (3) increased population of resident anti-inflammatory T-lymphocytes that selectively prevent excessive macrophage-derived cytokine production without affecting phagocytosis. Based on these findings, the mechanisms that regulate leukocyte function in females are more efficient to that in males as rapid detection and elimination of pathogens increases the threshold for pathogen-induced tissue injury in females (Scotland et al., 2011). In addition, relative rarity of the granular convoluted tubules in the female submandibular glands, which were used in this study, render them histologically and functionally more comparable to the human glands.

To develop the mouse model, we cannulated the mouse SMGs as previously performed in rats (Correia et al., 2010) and mice (Bombardieri et al., 2012). Submandibular glands were used in this study for ease of cannulation, in addition to the gland encapsulation, lacking in the mouse parotid glands, which makes it much easier to identify and excise all infiltrated and inflamed tissues.

Initially, a glass cannula (Supelco, 25715, PA- USA) was stretched over a flame (figure 2.1 A) and fitted into a polyethylene tube with 0.28 mm inner diammeter. Polyinosinic–polycytidylic acid sodium salt (P1530-25MG, Sigma-Aldrich) was then diluted in 0.9% saline solution to a final concentration of 4mg/ml. Towards consistent, visualised and flawless submandibular gland (SMG) injection, poly I:C was pre-mixed with Trypan blue (T8154-100ML-Sigma- Aldrich) prior to injection. Eighty micrograms of poly (I:C) in 20 µls were loaded in a 0.3 ml syringe (613-4900, VWR International). Finally, the glass cannula, polyethylene tube and syringe were mounted on a fixed holder as the setting in figure 2.1 B exemplifies.

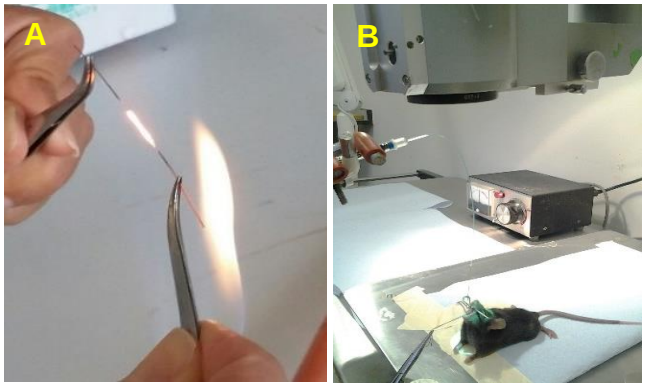

Figure 2.1 **Pre-injection Set-up**.
A: Stretching of glass cannula over a flame. **B:** Final Injection Setup

For recovery experiments, mice were anaesthetised intraperitoneally (i.p) with 0.1 ml of combined 5 mg Ketamine/1 mg Xylazine. Under a stereomicroscope, the glass cannula was inserted into Wharton's duct and poly (I:C) was injected slowly and constantly into the left SMG (Correia et al., 2010) (figures 2.3 A, B and C). The same volume of the vehicle (0.9% saline and Trypan blue) was delivered to the right SMG as a contralateral negative control.

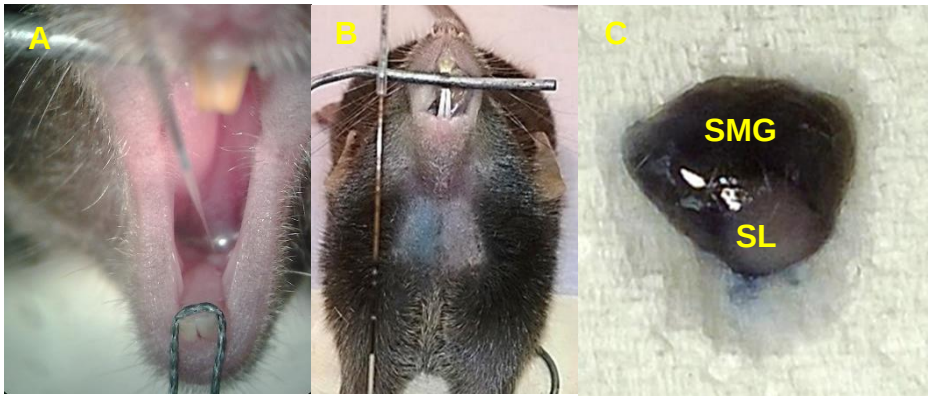

Figure 2.2 **SMG Retrograde Ductal Injection**.
A: Microscopic depiction of pre-fabricated glass cannula inserted into Wharton Duct for poly (I:C) delivery **B:** Left SMG with clear Trypan blue-poly (I:C) injection. **C:** Excised SMG showing specific retrograde SMG injection.

Prior to tracheal exposure and endotracheal intubation, the animal was i.p anaesthetized with 150 µl of Pentobarbital Sodium (Euthatal, Merial) 1 mg/ml. A minor tracheal cut was performed and a polyethylene tube was inserted gently into the trachea to avoid asphyxia caused by accumulation of lung fluids during pilocarpine induced functional assessment. Skin incision over the mylohyhoid muscle was made and followed by gentle maceration of the posterior and medial fibres to form an oval shaped tissue slit over the submandibular and sublingual ducts. Through these surgical breaches, the submandibular ducts on both sides were medially and partially cut to avoid cutting of the laterally adjacent sublingual gland (SLG) ducts.

Polyethylene tubes were fitted into the needles of two insulin syringes and a pilocarpine stock solution (Sigma Ltd) of 10 mg/ml was diluted in saline to 0.1 mg/ml from which 0.1 ml was injected i.p. to stimulate salivation. The tissue slits were flushed briefly with saline and local anaesthetic to avoid contamination of the streamed saliva with any blood or tissue fluids.

After approximately 5-7 min post pilocarpine injection, saliva started flowing from the duct incisions and accumulating into the primed myelohoid cavities. Pooled saliva was drawn with the insulin syringes for 5 minutes and collected into pre-weighed Eppendorf tubes (figures 2.3 A and B). The volume of collected saliva calculated (1mg = 1µl saliva) was used to assess the flow rate expressed as µl saliva/min. for different experiments in the present research, saliva was collected and mice were culled at: 6hrs, 9hrs, 24 hrs days- post poly I:C delivery.

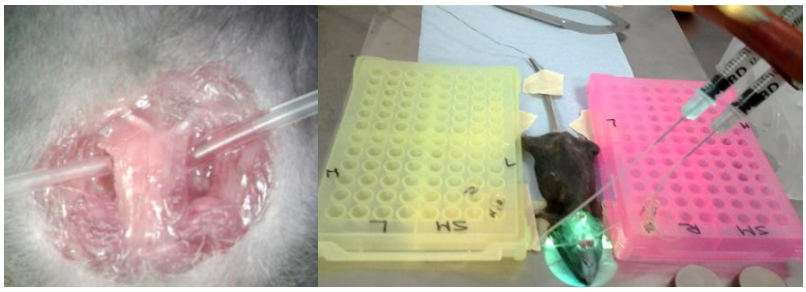

Figure 2.3 **Extraoral saliva collection**.
A: Myelohoid muscle slits enclosing the accumulated saliva. **B:** Saliva collection overall setup

The SMGs were carefully excised and dissected from the SLGs, then weighed on a sensitive balance and sectioned. Tissues for histopathologic examination and immunohistochemistry were fixed in 10% neutral buffered formalin [50 ml 37% formaldehyde, 450 ml distilled water, 3.25 gm sodium phosphate, dibasic (Na_2HPO_4), 2 gm sodium phosphate, monobasic (NaH_2PO_4)]. Other tissue pieces were stored in RNAlater® (R0901-100ml, Sigma-Aldrich) in -20°C freezer for future analyses (RTqPCR and protein analysis). For calcium signalling and flow cytometry experiments, tissues were flushed with Dulbecco's phosphate buffered saline (PBS) (D8537-100ml, Sigma-Aldrich) to eliminate hair and blood then preserved in Hanks' Balanced Salt solution (H9394-100ML, Sigma-Aldrich) until reaching the appropriate facility where the experiments were conducted on the same day.

2.2 Histopathologic Examination

Following formalin fixation, salivary gland tissues were briefly washed in distilled water, enclosed in uniquely numbered/labelled cassettes, rinsed in distilled water, drained and held in 70% alcohol while setting up the processing machine (Leica TP1020). Once the tissue processing was completed, cassettes were transferred into the embedding station (Leica TP1020) and salivary gland tissues were embedded and allowed to cool on the cold plate. After 30 mins, the blocks were removed from their base moulds and 5 µm sections cut with a microtome, mounted on glass slides and placed on a hot plate for a minimum of 1 hour. Paraffin is hydrophobic and impervious to aqueous solutions, so removal of the wax was done by immersing tissue sections in three changes of xylene (a hydrocarbon solvent), then hydrating them in three changes of absolute alcohol followed by thorough rinsing in water. Sections were stained in Mayer hematoxylin for 1 minute, blued in a weakly alkaline ammonia solution and submerged in aqueous eosin. Following eosin staining, slides were rinsed and passed through several changes of alcohol to remove all traces of water, then dipped in several baths of xylene to clear the tissues and render them completely transparent. A thin layer of DPX mounting medium was applied on each tissue section followed by a glass cover slip. Mounted tissue sections were ready to examine under light microscope attached to a digital camera, to capture significant histopathologic and morphologic changes following poly (I:C) and vehicle injections into the SMGs.

2.3 Immunohistochemistry

Three µm tissue sections were microtome cut and mounted on Superfrost™ Plus adhesive glass slides (10149870-Fisher Scientific Ltd) and placed on a hot plate for 1 hour. In order to standardize immunohistochemistry, increase staining intensity and reduce non-specific background staining, Trilogy™ (Cell Marque, Rocklin, CA-920P-06) was used for deparaffinization, rehydration, and unmasking (Chang et al., 2013) . Slides were placed in a plastic rack and in a staining pot filled with approx. 800 ml of Trilogy™. Since this product performs its purpose only when boiled under pressure, the pot with slide rack was placed in an autoclave adjusted to boil at 121°C and chamber pressure approximately 15 psi for 10 minutes. After the autoclave run came to an end, slides were retrieved from the Trilogy™ solution and washed thoroughly for 5 minutes with 1X TBS immunobuffer wash. Then slides were drained very briefly on absorbent tissue (all efforts should be made hence after to avoid tissue dryness and later on false positive results). To block endogenous peroxidase activity and avoid non-specific background reactions, sections were incubated in 3% hydrogen peroxide solution for 20-30 minutes. Slides were washed for 5 minutes in 1X TBS buffer and ringed using a delimiting 'PAP' pen (S2002-dako). To block non-specific epitopes on the tissue samples, sections were incubated with 1% BSA in 1X TBS and azide, pH7.6 for 5 minutes. The blocking buffer was flicked off and the primary antibody (see each relevant chapter) was applied at the appropriate working dilution overnight at 4°C. On the following day, slides were rinsed in 1X TBS and washed for 10 mins in 500ml 1X TBS. Excess solution was flicked off and sections were incubated for 60 mins at room temperature with a secondary antibody raised against the appropriate primary antibody host. Slides were then rinsed in 1X TBS and washed once for 10 mins in the 500ml 1X TBS.

Colour was developed for 5-10 mins in DAB solution (34002-Pierce™) and slides were washed under running tap water for 5 mins. Counterstaining was performed by dipping slides for 2 mins in Mayer haematoxylin and washing under a running tap until clear. Blue colour was developed with ammonia solution, and optimal intensity of nuclear staining under was checked light microscope. Slides were dehydrated by rinsing thoroughly in three changes of absolute alcohol, and cleared by dipping in 2 changes of xylene, 5 mins each. Slides were DPX-mounted and left to set before thorough examination under the light microscope.

2.4 Gland homogenization, Protein extraction and Western Blotting

Tissues stored in RNAlater® were retrieved and weighed on a sensitive balance and placed in 2 ml lysing matrix tubes (Lysing Matrix D, 6913-100-MP Biomedicals) with cell lysis buffer (AA-LYS-10 ml- RayBiotech, Inc., Norcross, GA) and protease inhibitor cocktail (1:10 dilution, Calbiochem, UK). Tubes were fitted in FastPrep™ tissue homogenizer (MP Biomedicals Santa Ana, CA) carousel which was adjusted to allow sample disruption with the lysing beads in 60 seconds (20 seconds X 3 intervals). Samples were briefly centrifuged at 4°C, this was followed by incubation on ice on a gentle rocker for 30 mins. Subsequently, protein homogenates were retrieved from the lysing matrix tubes and transferred to labelled Eppendorf tubes which were then sonicated on ice for 5 minutes. Homogenized samples were centrifuged at 10,000 g for 20 mins at 4°C and supernatants were collected without disrupting the pellet, aliquoted and stored at -80°C for later use. For accurate measurement of the extracted protein concentration, Qubit® 3.0 Fluorometer (Q33216, Invitrogen™, UK) was used. Three assay tubes for the standards and one for each sample were setup. 200

µL of Qubit® working solution was prepared by diluting the Qubit® reagent 1:200 in Qubit® buffer for each standard and experimental sample (figure 2.4).

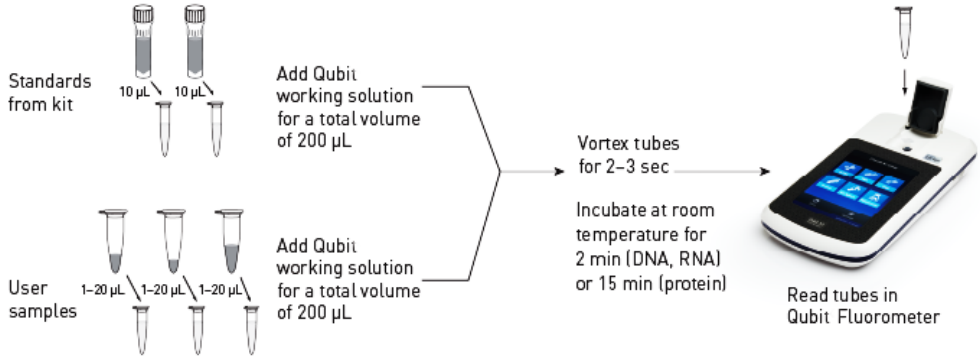

Figure 2.4 Outline for protein concentration measurement using Qubit® kit.

Homogenates were diluted 1:5 with distilled water and prepared for SDS-PAGE by mixing with DTT 1:10 and LDS 1:4. Tubes were centrifuged, vortexed and boiled at 100°C for 3 mins, during which running buffer (NP0002, Novex™) was prepared at 1:20. Samples were then electrophoresed on precast 4-2% SDS-PAGE gel (NuPAGE® Novex™ Bis-Tris Gels, Invitrogen™ UK) at 200V and 200mA for 35 mins. During this period, 0.2 µm pore–size nitrocellulose membrane (1620112, Bio-Rad, UK) were cut and soaked in buffer: 25 ml transfer buffer (BT00061, Novex™), 50 ml methanol and 375 ml distilled water, together with sponge pads and filter papers. Electro-transfer of proteins was done for 1 hour according to standard protocol (Invitrogen, UK, Paisley) at 30V and 200mA.

Following protein transfer, membranes were blocked with 5% bovine serum albumin (BSA) in TBS-T (20 mM TRIS, 150 mM NaCl, 0.1% Tween-20, PH 7.6), washed three times (5 minutes each) in TBS-T and incubated at 4°C overnight with the appropriate working dilutions of primary antibodies (will be mentioned in each relatable chapter) in blocking buffer. On the next day, the membrane was incubated with the recommended dilution of conjugated secondary antibody in blocking buffer at room temperature for 1 h followed by three washes of TBS-T, 5 min each. For signal development, an Enhanced Chemioluminescence substrate (ECL, GE Healthcare, UK) was prepared following the kit manufacturer's recommendations and applied over the membranes. Excess reagent was flicked and positive and negative protein expression was assessed and captured using ChemiDoc™ MP System (Bio-Rad, UK).

2.5 RTqPCR Analysis

RNAlater® -stored SMGs were weighed and 5-15 mg of tissues were placed in 2 ml lysing matrix tubes with 20X RNA-Bee™ and homogenized with FastPrep™ tissue homogenizer (MP Biomedicals Santa Ana, CA) for 60 seconds (20 seconds X 3 intervals). RNeasy® Micro Kit (74004, Qiagen) was used for total RNA extraction according to the manufacturer's protocol. RNA concentration as well as the $A_{260/280}$ and $A_{260/230}$ ratios were then measured with the NanoDrop ND-1000 Spectrophotometer (Thermo Fischer Scientific, Nottingham UK). iScript™ cDNA Synthesis kit (170-8890, Bio-Rad) was used to reverse transcribe 100 ng of extracted RNA. 20 µl of reverse transcription (RT) reaction was incubated as follows: 5 minutes at 25°C, 30 minutes at 42 °C, 5 minutes at 85 °C and the reaction was terminated by transferring the tubes to ice (4 °C).

qPCR reactions (10 µl) were prepared by adding all required components according to table 2-1 and scaled according to the number of samples.

Table 2-1 RTqPCR Reaction Mix

Component	Volume per 10 µl reaction	Final Conentration
SsoAdvanced ™ Universal SYBR Green Supermix (172-5271, Bio-Rad)	5	1X
Primers (PrimerDesign™, Ltd.) (will be mentioned in each relevant chapter)	2	600 nM
cDNA template	3	—

The main steps of RTqPCR is depicted in figure 2.5. the three main steps comprising the RTqPCR protocol are repeated 40 times or cycles. In first cycle, the double stranded template DNA strand is first **denatured** into 2 single strands by heating to above 90°C, so that the region to be specifically amplified can be made accessible. The temperature is then cooled to between 40-60°C and the **annealing** step starts by primers bind to the complementary sequence, and serve to “prime” the DNA synthesis reaction. The third step, DNA synthesis or **extension** is carried out by a thermo stable DNA polymerase which catalyzes the synthesis of a new strand from the primed single strand template (Aldape et al., 2002).

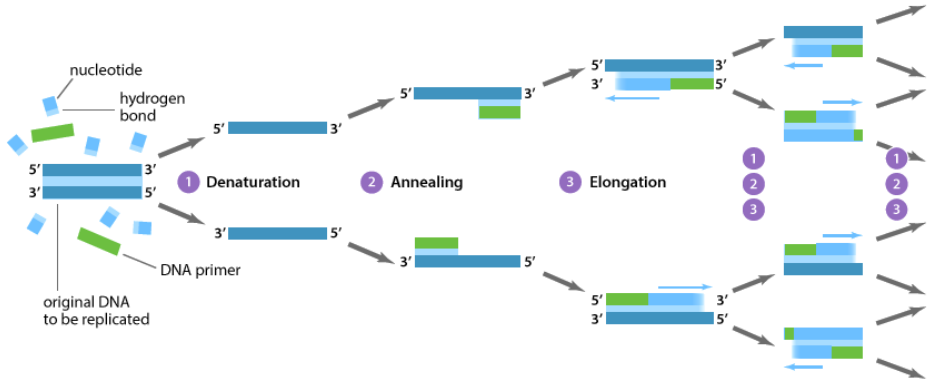

Figure 2.5 **Stages of PCR**: denaturation, annealing and elongation.

Thermal cycling was performed using Corbett RotorGene 6000 System (Qiagen, UK) following the protocol in table 2-2.

Table 2-2 Corbett RotorGene Setting

Setting/Mode	Polymerase Activation and DNA Denaturation	Amplification			Melt Curve Analysis
		Denaturation	Annealing	Cycles	
Fast	2 mins at 98°C	15 secs	30 secs	40	65-95 °C 0.5 °C increment 2-5 sec /step

In all RTqPCR experiments, relative gene quantification was assessed according to the "Delta Delta CT" (ΔΔCT) (Winer et al., 1999), where ΔΔCT= [C_t GOI $_{Exp}$ – C_t HKG $_{Exp}$]-[C_t GOI $_{Cal}$ – C_t HKG $_{Cal}$]: **C_t**: cycle threshold, **GOI**: gene of interest, **Exp**: poly (I:C)-injected glands, **HKG**: housekeeping gene showing the highest stability within each experiment condition, **Cal**: control glands injected by the vehicle.

2.6 Statistical Analysis

Results were shown as mean ± SEM (standard error of means). Statistical significance between individual comparisons was determined using Student t-test. For multiple comparisons, one-way ANOVA with Sidak's (selected pairs) pairwise test were used. The calculations were performed with the statistical software package GraphPad Prism (version 7). P values ≤ 0.05 were considered statistically significant.

Chapter 3

TLR3 Mediated SMG Dysfunction Independent of Acute Cellular Infiltrate

3.1 Introduction

The dsRNA is the most potent viral stimulant of the innate arm of the immune system, and is largely believed to be an intermediate replication by-product generated by most viruses (Jacobs and Langland, 1996). The synthetic dsRNA; poly (I:C) has been extensively studied for its capability to induce the characteristic innate immune responses, closely mimicking those associated with viral infections; such as: loss of epithelial integrity, inflammatory cytokine production and declined functions (Lever et al., 2015).

TLR3 is a dsRNA sensor found in mammals and is activated by viral dsRNA or poly (I:C). Traditionally, newly synthesized endogenous TLR3 is transported through the ER and Golgi apparatus to endosomes, aided by the multi-pass transmembrane protein UNC93B1 (Kim et al., 2008). Within the endosomes, TLR3 is rapidly processed by cathepsins to generate a short fragment which corresponds to the C-terminal, functional form of the receptor. Once ligated by poly (I:C), TLR3 protein expression is up-regulated, leading to the accumulation of this cleaved terminus (Garcia-Cattaneo et al., 2012).

At the signalling level, poly (I:C) binding to TLR3 will be followed by recruitment of the adaptor molecule; TRIF, and initiation of a signalling cascade, leading to upregulation of type I IFN and inflammatory cytokines, via activation of IRF3 and NF-κB, respectively (Kawasaki and Kawai, 2014). Previous data demonstrated the combined contribution of type I IFNs and IL-6 in inducing salivary gland hypofunction (Nandula et al., 2013). Moreover, in various viral models, poly (I:C) prompted an acute inflammatory response, featuring the migration and activation of innate immune cells, principally neutrophils and monocytes (Clarke et al., 2014, Kanaya et al., 2014, De Alba et al., 2015).

Beside efficiency of these cells in combating viral infections (Gabriel et al., 2013), tissue damage can be collaterally mediated by: ROS, superoxides, inflammatory cytokines and NETs (Hemmers et al., 2011, Drescher and Bai, 2013). This, in addition to their destructive potential via a number of inherent proteases; namely: neutrophil elastase (NE), cathepsin G and myeloperoxidase (MPO) (Kanaya et al., 2014). In particular, MPO which is predominantly stored in lysosomes of monocytes as well as azurophilic granules of PMNs (Klebanoff, 2005), is one of the most abundant enzymes released on neutrophil activation and predominantly involved in tissue damage (Nagra et al., 1997, Eiserich et al., 2002, Malle et al., 2003). It has been implicated in downregulation of aquaporins at the gene level (Sakai et al., 2014), in addition to disruption of plasma membrane ion transport channels (N.S. MacCallum, 2007) and epithelial tight junction proteins (Kucharzik et al., 2001).

Despite the thoroughly documented injurious consequences of all the formerly mentioned molecular events, the sequelae of acute exposure of the SGs to viral infections have never been comprehensively investigated. In this chapter, we developed a novel acute SG model via intraductal retrograde infusion of the synthetic viral analogue; poly (I:C), into the C57/B6 mouse SMGs. The developed model is unique in rapidly and reliably demonstrating the functional and immune consequences prompted by the exocrine SGs, upon local exposure to the potent viral mimetic.

3.2 Materials and Methods

3.2.1 Surgical Procedure and Saliva Collection

Chapter 2, paragraph 2.1 details the surgical procedures, the method of saliva collection and calculation of flow rates.

3.2.2 TLR3 Inhibition and LY6G/LY6C Depletion Models

Table 3-1 summarizes the drugs and doses used in the experiments of the current chapter.

Table 3-1 Drugs used in in vivo injections

Drug	Mechanism	Source	Catalogue Number	Dose	Administration Protocol
TLR3/dsRNA Complex Inhibitor	Competitively inhibits dsRNA binding to TLR3.	Calbiochem Merck Millipore	614310	*i.p.* 1 mg/mouse (Takemura et al., 2014) + 50 ng combined to poly (I:C) local injection(Chintala et al., 2015)	*i.*p injection at the same time of combined TLR3 /dsRNA+poly (I:C) local injection
Ly-6G (Gr-1) Clone: RB6-8C5	Reacts with mouse Ly6G	eBioscience	16-5931	*i.p.* 200 µg/mouse (Daley et al., 2008)	24 hrs prior to poly (I:C) local injection

In the TLR3-inhibitor model, the contralateral SMGs received the vehicle (saline and trypan blue) in addition to the TLR3/dsRNA inhibitor drug dose given in combination with the poly (I:C).

3.2.3 Immunohistochemical Analysis

Paraffin-embedded SMG sections were deparaffinised, rehydrated and antigen retrieved by autoclaving with Trilogy™ as detailed in chapter 2, paragraph 2.3. Subsequently, slides were incubated in hydrogen peroxide to block endogenous peroxidase activity and protein block to inhibit non-specific background reaction. After incubation with the specific primary antibodies (table 3-2), the detection was completed using the compatible host HRP-conjugated secondary antibodies. Nuclear and counterstaining was done with Mayer's haematoxylin or VECTASHIELD Antifade Mounting Medium with DAPI (vector laboratories, H-1200) in case of fluorescence imaging.

Table 3-2 Primary Antibodies Used in Immunohistochemical Analysis

Antibody	Source & Catalogue Number	Host	Working Dilution
J2 anti-dsRNA	SCICONS Budapest, Hungary, J2-1511	Mouse	1:1500
TLR-3	Abcam, Ltd, ab62566	Rabbit	1:10000
MDA 5	Abcam, Ltd, ab69983	Rabbit	1:450
RIG I	Bioss Inc., bs-0993R	Rabbit	1:700
Cox2	Abcam, Ltd, ab133466	Rabbit	1:400
iNOS	Novus Biologicals, USA, NB300-605	Rabbit	1:650
Interferon-gamma (IFN-γ)	Proteintech Europe,15365-1-AP	Rabbit	1:2500
Phospho-NF-κB (p50)	Santa Cruz Biotechnology, sc-271908	Mouse	1:900
Cleaved caspase 3	R&D Systems, MAB835	Rabbit	1:280
Myeloperoxidase	BosterBio, USA, PB9057	Rabbit	1:1000
Goat anti-Mouse IgG (H+L) Secondary Antibody, Alexa Fluor® 594 conjugate	Thermo Fisher Scientific, A-11005	Goat	1:1000
Polyclonal Goat Anti-Rabbit Immunoglobulins-HRP	Dako, P0448	Goat	1:200

3.2.4 Western Blotting

SMG protein extracts were electrophoresed on precast 4-2% SDS-PAGE gel and transferred to nitrocellulose membrane as detailed in chapter 2, Paragraph 2.4. Membranes were incubated with primary antibody, followed by 1 hr incubation with the appropriate secondary antibody (table 3-3). Subsequently, signal development and exposure with Enhanced Chemioluminescence and ChemiDoc™ MP System were performed.

Table 3-3 List of Antibodies Used in Western Blots

Antibody	Source & Catalogue Number	Host	Working Dilution
TLR-3	Abcam, Ltd, ab62566	Rabbit	1:10000
Myeloperoxidase	BosterBio, USA, PB9057	Rabbit	1:1000
B-actin	Sigma, A2228	Mouse	1 µg/mL
Polyclonal Goat Anti-Rabbit Immunoglobulins-HRP	Dako, P0448	Goat	1:2000
Polyclonal Goat Anti-Mouse Immunoglobulins- HRP	Dako, P0447	Goat	1:1000

3.2.5 RTqPCR

Total RNAs isolated from SMG tissues (stored in RNAlater®) were extracted using RNeasy® Micro Kit (Qiagen) and 100 ng of extracted RNAs were reverse-transcribed in a 20 µL reaction using the iScript™ cDNA Synthesis kit. Quantitative real time PCR (qRT-PCR) was carried out as detailed in chapter 2, Paragraph 2.5. All mouse primers were synthesized by PrimerDesign™, Ltd and are listed in Table 3-4. All experiments were performed in triplicate.

Table 3-4 *List of Primers used*

Gene	**Accession N^{O}**
MX-1 (MX dynamin-like GTPase 1)	NM_010846
ISG-15 (ISG15 ubiquitin-like modifier)	NM_015783
OAS1a (2'-5' oligoadenylate synthetase 1A (Oas1a)	NM_145211
PKR	NM_011163
IL 6	NM_031168
IL 1β	NM_008361
TNF	NM_013693
TLR3 (Toll-like receptor 3)	NM_126166
MDA5 (Interferon induced with helicase C domain 1 (Ifih1),	NM_027835
RIG1 (DEAD (Asp-Glu-Ala-Asp) box polypeptide 58 (Ddx58)	NM_172689
Chemokine (C-X-C motif) ligand 1 (Cxcl1), KC	NM_008176
Chemokine (C-X-C motif) ligand 2 (Cxcl2), MIP2-a	NM_009140
Chemokine (C-X-C motif) ligand 5 (Cxcl5), LIX	NM_009141
Chemokine (C-X-C motif) ligand 15 (Cxcl15), IL-8	NM_011339
Chemokine (C-C motif) ligand 2 (Ccl2), MCP-1	NM_011333
HPRT (Hypoxanthine guanine phosphoribosyl transferase)	NM_013556
GAPDH (glyceraldehyde-3-phosphate dehydrogenase)	NM_008084

3.2.6 Histologic Examination

As described in chapter 2, paragraph 2.2, following gland excision and formalin fixation of tissues, samples were processed, embedded in paraffin, microtome sectioned, stained with H&E and examined under a light microscope.

3.2.7 Flow Cytometric Analysis

Excised glands were rinsed with PBS, minced and transferred through a 100 µm cell strainer mesh (352369, Corning Life Sciences, DL) using a syringe plunger into a 50 ml Falcon tube. The mesh was washed 3 times with Dulbecco's phosphate buffered saline and the tube was centrifuged at 600 g for 10 minutes. The supernatant was discarded and 3 ml fresh PBS was pipetted up and down several times to further dissociate any cell clumps.

The tube was centrifuged again at 600 g for another 10 minutes after which the supernatant was discarded. 3 ml cell staining buffer (420201, Biolegend, UK) was applied on top of the cells and pipetted up and down before the whole volume was passed through a 35µm nylon mesh of a cell strainer cap fitted to 5mL Falcon® tube with round bottom (352235, Corning). Twenty microliters of this preparation were pipetted in a 0.5 ml tube for cell counting, whereas the whole cell suspension was transferred to a 15 ml Falcon tube and centrifuged at 600 g for 10 minutes. According to the number of cells in the cell suspension, the volume of the blocking antibody; TruStain fcX™ anti-mouse CD16/32 (101319, Biolegend) was calculated and cells were incubated at 1.0 µg per 10^6 cells for 5-10 minutes on ice prior to immunostaining. After 10 minutes, the Falcon tube with TruStain fcX™-blocked cells was centrifuged at 600 g for 10 minutes and the supernatant was discarded. Immunostaining with the fluorochrome-conjugated antibodies followed directly without an intermediate washing step. The anti-mouse antibodies used and their isotype controls (Biolegend, UK) are shown in table 3-5.

Table 3-5: Antibodies and Isotype Controls Used in Flow Cytometry Experiments

Cells: Neutrophils, Macrophages, Monocytes					
Fluorochromes	**FITC**	**PE**	**PE/CY7**	**APC**	**APC/CY7**
Antibody Panel	F4/80	CD45	CD11b	LY6G	LY6C
Catalogue Number	123107	103207	101215	127613	128025
Isotype Control	Rat I_gG 2a	Rat I_gG 2b	Rat I_gG 2b	Rat I_gG 2a	Rat I_gG 2c
Catalogue Number	400505	400607	400617	400511	400719

Supernatant over centrifuged cells was discarded and cells were re-suspended in 300 µl cell staining buffer. All antibodies were diluted 1:100 in the cell staining buffer and in a 96-well plate with rounded bottom, 50 µl of the cell suspension was mixed with 50 µl of each panel and incubated for 2 hrs in the dark at 4 °C. Compensations for spillover and spectral overlap were established by labelling 6 tubes for each of the 5 fluorochromes used and 1 for a fluorochrome-free tube as an unstained sample.

Twenty microliters of OneComp eBeads® (01-1111-41, eBioscience, Ltd, UK) was mixed with 0.5 µl of each fluorochrome and 80 µl of the cell staining buffer and incubated in the same 96-well plate holding the cell suspensions, antibodies and isotype controls. An automated compensation algorithm in BD™ FACSDiva 6.1 software (BD Biosciences) was used to read the spectral overlap values from single-color compensation controls in sequential acquisitions. Spectral overlap values were automatically calculated by the software and applied to the experiment.

After 2 hrs, the 96-well plate was retrieved from the fridge and 100 µl cell staining buffer was dispensed on each stained sample and pipetted up and down several times. The plate was then centrifuged at 600 g at 4°C for 10 minutes. After plate centrifugation, cells were seen precipitated at the well bottoms, vigorous propelling of the supernatants was done and 150 µl cell staining buffer was applied to each well. Precipitated cells were thoroughly mixed with the dispensed cell staining buffer and the content of each well was re-transferred through a 35µm nylon mesh of a cell strainer cap fitted to a 5mL Falcon® tube to finally and completely dissociate any cell that may have clustered and to prevent clogging of the machine fluidic system.

All samples were analysed using a 3-laser (405, 488 and 630 nm) 5-color BD FACS Canto II flowcytometer (BD Bioscience). Thresholds on Forward Scatter (FSC) and Side Scatter (SSC) were set to: 505 V for FSC and 571 V for SSC and the positive population was gated and recorded. The flow rate of the cytometer was set to medium while acquiring and recording 100,000 events for each sample. Data for each sample was stored as an FCS 3.0 file and subsequently analysed by Flowing Software 2.5.1. Mean fluorescence intensity (MFI) of isotype controls was subtracted from the MFI measured for specific markers to control for background auto-fluorescence and non-specific fluorescence. The gating strategy employed in the analysis was designed to detect and discriminate $LY6G^+/LY6C^+$ cells.

3.3 Results

3.3.1 Establishment of the acute viral mimic model: Poly (I:C) Internalization and Induction of an Antiviral State in the SMGs

Despite the extensive use of poly(I:C) in diverse experimental models, very little is known about its uptake and intracellular fate. Accordingly, it was mandatory to validate internalization of the poly (I:C), since the well-characterized dsRNA-binding proteins are intracellular (Saunders and Barber, 2003). To achieve this objective, dsRNA monoclonal antibody was used to immunolabel poly (I:C) and track its fate, 6hrs and 24 hrs post retrograde duct injection. The vehicle-injected SMGs did not show any dsRNA-positive signal. Conversely, the ducts and acini of the poly (I:C)-injected SMGs showed retention of poly (I:C) up till 24 hrs following its injection, figure 3.1.

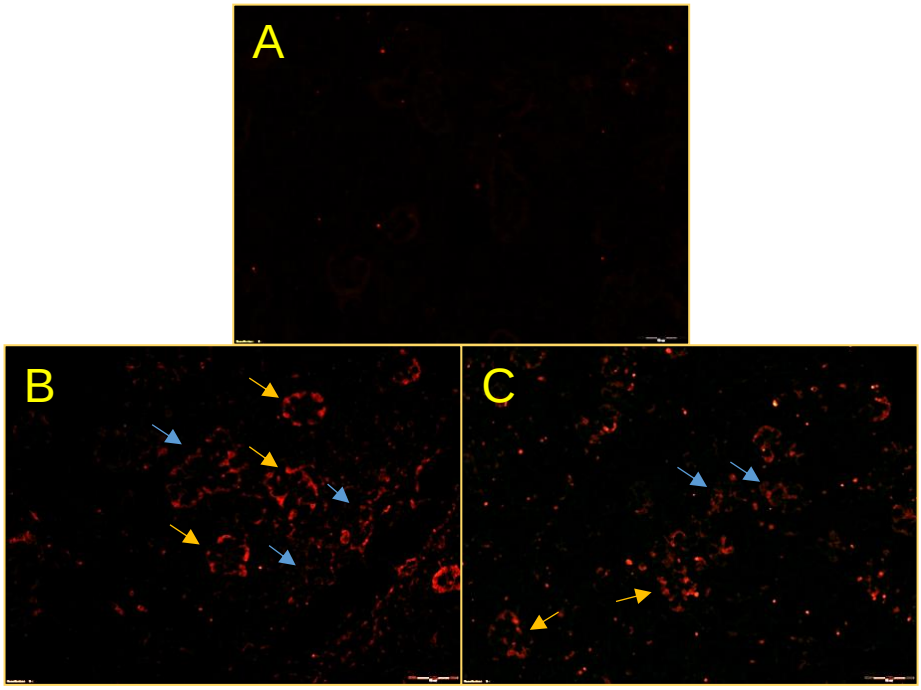

Figure 3.1 **Immunolabelling of poly (I:C) with the monoclonal dsRNA J2 antibody.** **A**: Control vehicle-injected SMG. **B**: 6hrs post poly (I:C) injection, dsRNA was immunolocalized in duct cells (yellow arrows) as well as acinar cells (blue arrows). **C**: 24 hrs post poly (I:C) injection, more dispersed and less immunostaining intensity of poly (I:C) in duct cells (yellow arrows) as well as acinar cells (blue arrows). Original magnification= 40x.

To ensure the reliability of a single local poly (I:C) dose in the induction of an antiviral condition in the SMGs, we examined the expression of the best characterized antiviral genes including MX1, ISG15, OAS1 and PKR. Real-time qRT-PCR results showed that poly (I:C) prompted a significant upregulation in these gene, 6hrs post its local introduction (Figure 3.2). The interferon-inducible MX1 antiviral gene showed the highest expression relative to HPRT housekeeping gene and the vehicle injected control glands, followed by ISG15, OAS1 and finally; PKR.

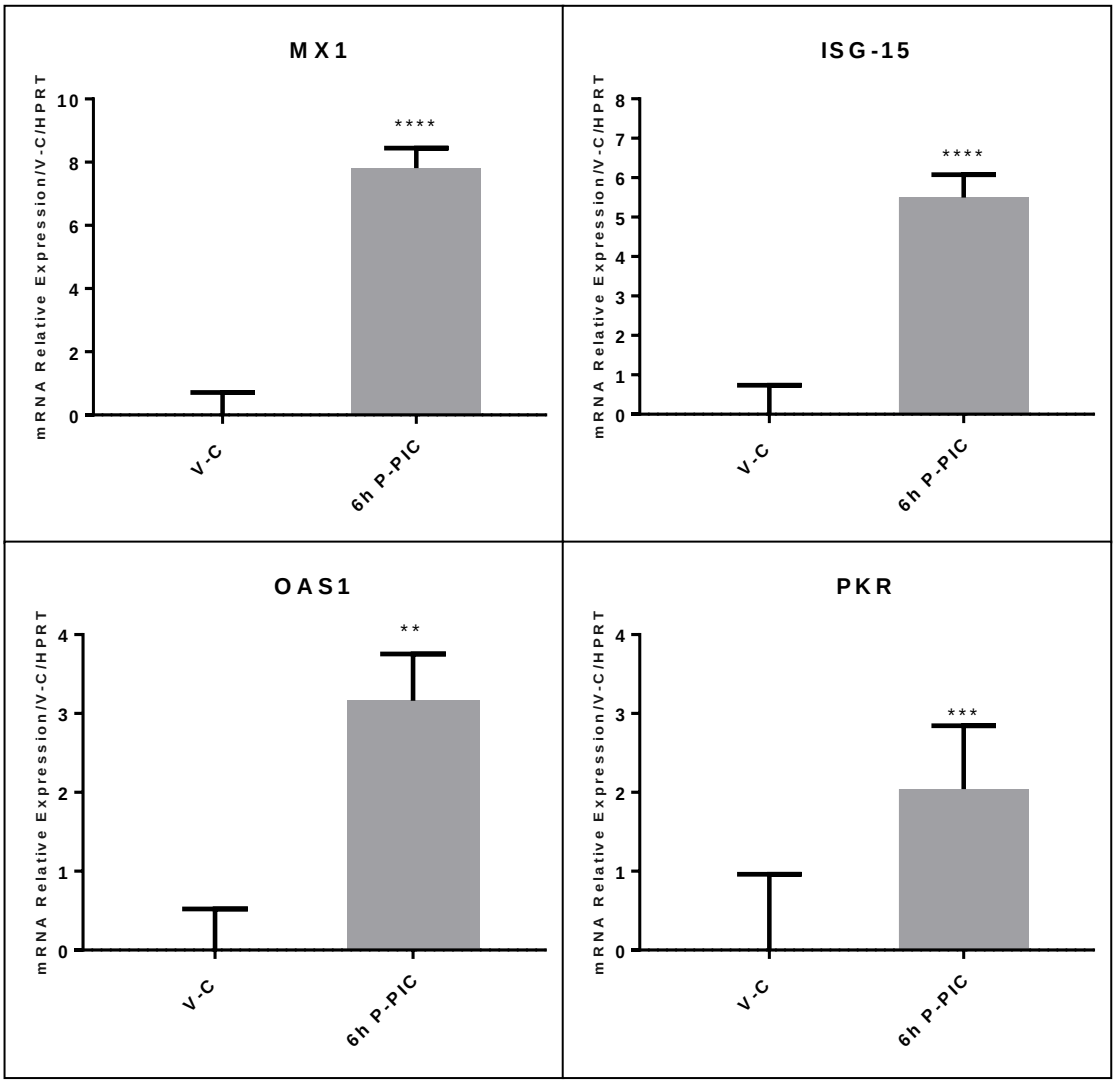

Unpaired Two Tailed t test

	MX1	ISG15	OAS1	PKR
P value	<0.0001	<0.0001	0.001	0.0002
P value summary	****	****	**	***

Figure 3.2 **mRNA expression of MX1, ISG15, OAS1 and PKR antiviral genes.** Upregulation of all antiviral genes in the SMGs, 6 hrs post poly (I:C) injection (6h P-PIC) compared to the vehicle injected control glands (V-C). Data represent means ± SEM (n=3). **p≤0.01 ***P≤0.001 and ****p≤0.0001.

3.3.2 Poly (I:C) Induced SMG Hypofunction

To explore the functional response of the SMGs to poly (I:C), the mean flow rates of pilocarpine-stimulated saliva was measured from control and infected glands for 5 minutes: 6hrs, 9hrs and 24 hrs following poly (I:C) retrograde injection. For simplicity of analysis, all vehicle-injected control SMGs showing approximately equal flow rates at different time points were assembled in one group, to which the experimental flow rates following poly (I:C) injection were compared. The poly (I:C) injected glands exhibited progressive and rapid loss of function, which started 6 hrs post its retrograde injection and was further deteriorated by 9 hrs, until the glands ceased secretion completely after 24 hrs of poly (I:C) innoculation. No difference in mean flow rates was recorded between the vehicle injected glands and un-injected normal SMGs, figure 3.3.

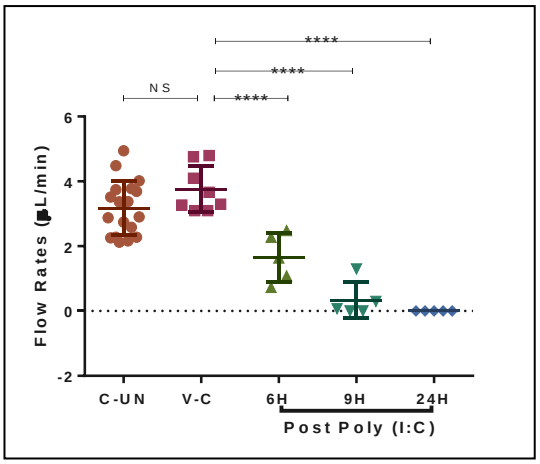

One Way ANOVA	
P value	<0.0001
P value summary	****

Dunnett's test	Summary	P Value
V-C vs. C-UN	ns	0.1927
V-C vs. 6H	****	0.0001
V-C vs. 9H	****	0.0001
V-C vs. 24H	****	0.0001

Figure 3.3 **Salivary Flow rates in Control and Poly (I:C)-Injected SMGs.** Scatter plot analysis of the mean ± SD SMG flow rates after 6h, 9h and 24h of poly (I:C) intraductal injection, all compared to the vehicle injected glands (V-C). Non-injected SMGs (C-UN) were compared to the vehicle injected ones to assess the impact of retrograde injection on the gland functional capabilities, and a non-significant change was seen between the two groups. Conversely, poly (I:C) induced an extremely significant reduction in mean flow rates as early as 6 hrs of its infusion and ultimately lead to complete impairment of the SMG function after 24 hrs. ****: P<0.0001, ns: non-significant.

3.3.3 Loss of SMG Secretion in Response to The Viral Mimic is TLR3 Mediated

3.3.3.1 Characterization of the dsRNA Sensors in the SMG.

To assess receptors that sense dsRNA in the SMGs, we examined the expression of TLR3 and the cytoplasmic RLR receptors; MDA5 and RIG-I at the mRNA as well as their subcellular protein expression pattern. qRT-PCR revealed that poly (I:C) significantly upregulated all dsRNA sensors in the SMGs, after 6 hrs of poly (I:C) intraductal infusion, figure 3.4. Since these results indicated that SMGs are equipped to upregulate functional endosomal and cytoplasmic dsRNA sensors, immunohistochemical staining was performed consequently to identify cell phenotypes expressing these receptors.

Basal expression level was first determined for the three dsRNA receptors, TLR3 showed intense membranous and cytoplasmic immunostaining in intercalated ducts. Conversely, the cytosolic dsRNA receptors; MDA5 and RIG-I were immunolocalized almost exclusively in resident peri-ductal immune cells. Following poly (I:C) introduction, TLR3 showed immunopositivity in the basolateral membranes of acinar and duct cells with increased numbers of intensely stained intercalated ducts. On the other hand, the glands which received poly (I:C) revealed intense MDA5 and moderate RIG-I immunostaining, exclusively limited to infiltrating immune cells which embraced ducts and acini. Frequently, MDA5 and RIG-I positive immune cells were seen extruded into duct lumena, figure 3.4.

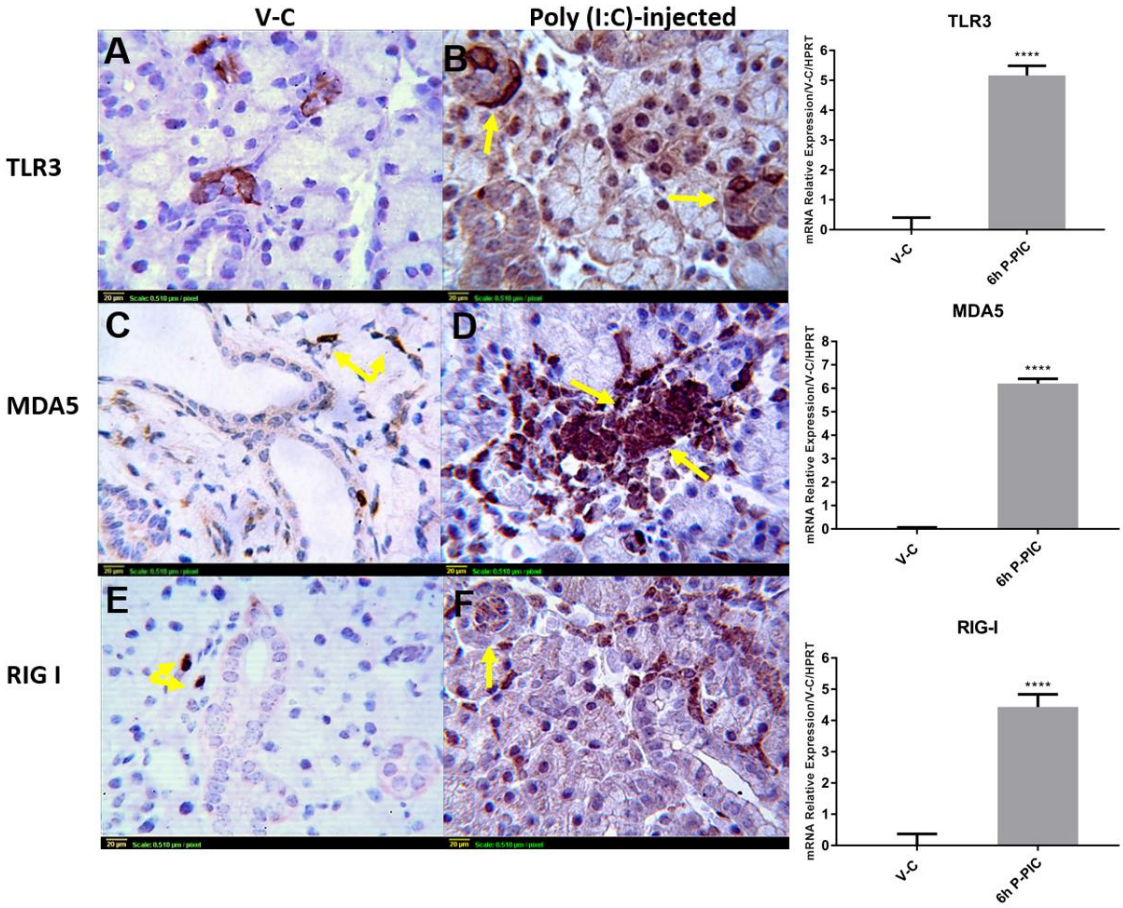

Unpaired Two Tailed t test

	TLR3	MDA5	RIG1
P value	<0.0001	<0.0001	<0.0001
P value summary	****	****	****

Figure 3.3.4 **Expression of dsRNA sensors; TLR3, MDA5 and RIG-I.**
Right: Transcriptional upregulation of all dsRNA sensors in the SMGs, 6 hrs post poly (I:C) injection (6h P-PIC). Data represent means ± SEM (n=3). ****p≤0.0001. V-C: vehicle injected control, HPRT: Hypoxanthine guanine phosphoribosyl transferase (housekeeping gene). **Left:** Immunoexpression of the dsRNA sensors. A- basal TLR3 expression in intercalated duct cells B- poly (I:C) injection induced intense membranous and cytoplasmic positivity of intercalated ducts (arrow) as well as moderate basolateral staining of the acinar and duct cells. C- MDA5 expression in resident immune cells of the saline injected control SMGs. D- MDA5 positive immunostaining following poly (I:C) injection was exclusively detected in peri-ductal and peri-acinar infiltrating immune cells, MDA5 positive cells was commonly seen extruded in duct lumen (arrows). E- RIG-I labelling the resident immune cells in the control SMG (arrow). F- poly (I:C) injected glands showing moderate immunostaining of infiltrating inflammatory cells. Note the extrusion of RIG-I positive cells into the duct lumen (arrow). Original magnification =40x

3.3.3.2 TLR3/dsRNA complex inhibition

Expression of TLR3 in the ducts of the control SMGs, as well as its intense epithelial immunolocalization post poly (I:C) injection, incited the priority to assess its role in the perceived SMG injury. A TLR3/dsRNA competitive inhibitor was used to competitively disrupt poly (I:C) binding to TLR3. Previous studies documented that poly (I:C) exposure increased the expression of the cathepsin-cleaved C-terminus form of TLR3 which directly correlates to its signalling capacity (Garcia-Cattaneo et al., 2012). The outcome of TLR3 blocking was investigated initially by analysing the expression levels of neo-generated, TLR3 C-terminal, using a polyclonal antibody raised against 15 amino acids near the carboxy terminus of TLR3. Immunohistochemistry and western blotting were conducted on the control as well as the poly (I:C)-injected glands, treated and non-treated with the TLR3/dsRNA complex inhibitor. Results revealed that the TLR3/dsRNA inhibitor, caused an extremely significant downregulation of the TLR3 C-terminus in the poly (I:C)-injected glands, compared to its widely-upregulated expression, 9 hrs post poly (I:C) injection, figure 3.5.

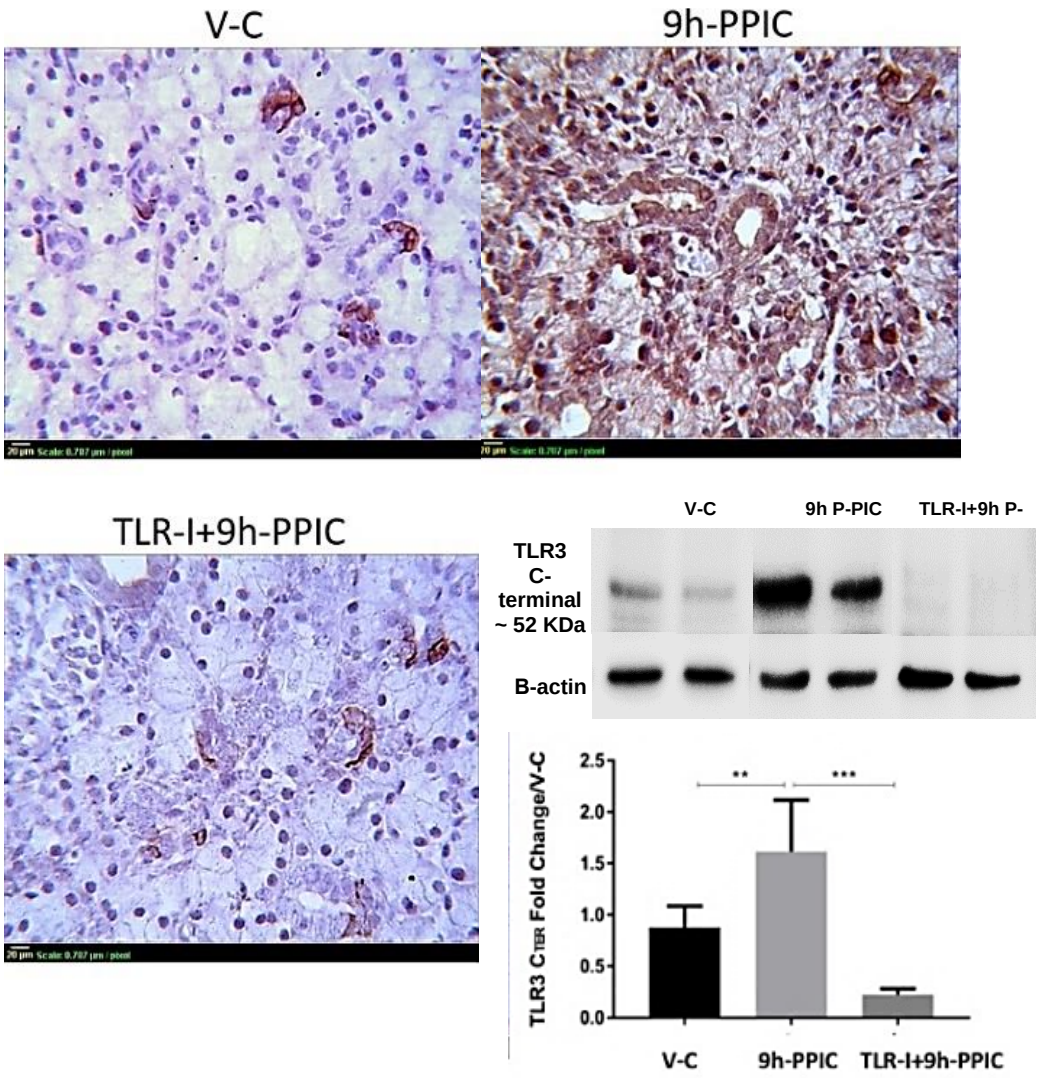

ANOVA summary		Sidak's multiple comparisons test	Summary	P Value
P value	<0.0001	**V-C vs. TLR-I+PIC**	**	0.0015
P value summary	****	**PIC vs. TLR-I+PIC**	****	<0.0001

Figure 3.5 **TLR3 C-terminal expression in the SMGs following competitive inhibition by dsRNA/TLR3 complex molecule.**
LEFT: The basal intercalated duct-positive immunoexpression of TLR3 C-terminal (arrows) was extensively upregulated 9 hrs post poly (I:C) injection (9h-PPIC), TLR3 was seen immunolabelling all ducts and acinar cells. Following administration of the dsRNA/TLR3 complex (TLR-I) which competes with poly (I:C) over TLR3 binding, the TLR3 C-terminal was remarkably downregulated and positive TLR3 immunostain was exclusively seen in intercalated ducts (arrows) in a pattern comparable to the vehicle injected control glands (V-C). Original magnification=25x. **RIGHT:** Similar results were seen in the representative western blots of the tested groups, TLR3 expression was calculated as TLR3/β-actin ratio fold change from control saline injected glands. ANOVA showed an extremely significant reduction in the receptor in dsRNA/TLR3-treated glands, 9 hrs post poly (I:C) exposure. Additionally, the level of TLR3 C-terminus even revealed a very significant decrease below the basal level seen in the vehicle injected control glands. Data represent mean ± SD of three independent experiments for each tested group. **p≤0.01, **** p<0.0001

To detect the TLR3 signal which prompted the perceived loss of function, mRNA and protein levels of cytokines and inflammatory mediators downstream TLR3 inhibition were investigated using qRT-PCR and immunohistochemistry, respectively. Figure 3.6 reveals the extremely significant transcriptional reduction of pro-inflammatory cytokines in the glands which received the TLR3 inhibitor in conjunction with the poly (I:C), versus those which didn't receive it, normalized to the relevant, vehicle injected control glands and GAPDH housekeeping gene (in the TLR-inhibited glands) and HPRT (in the glands which received poly (I:C) only without the inhibitor).

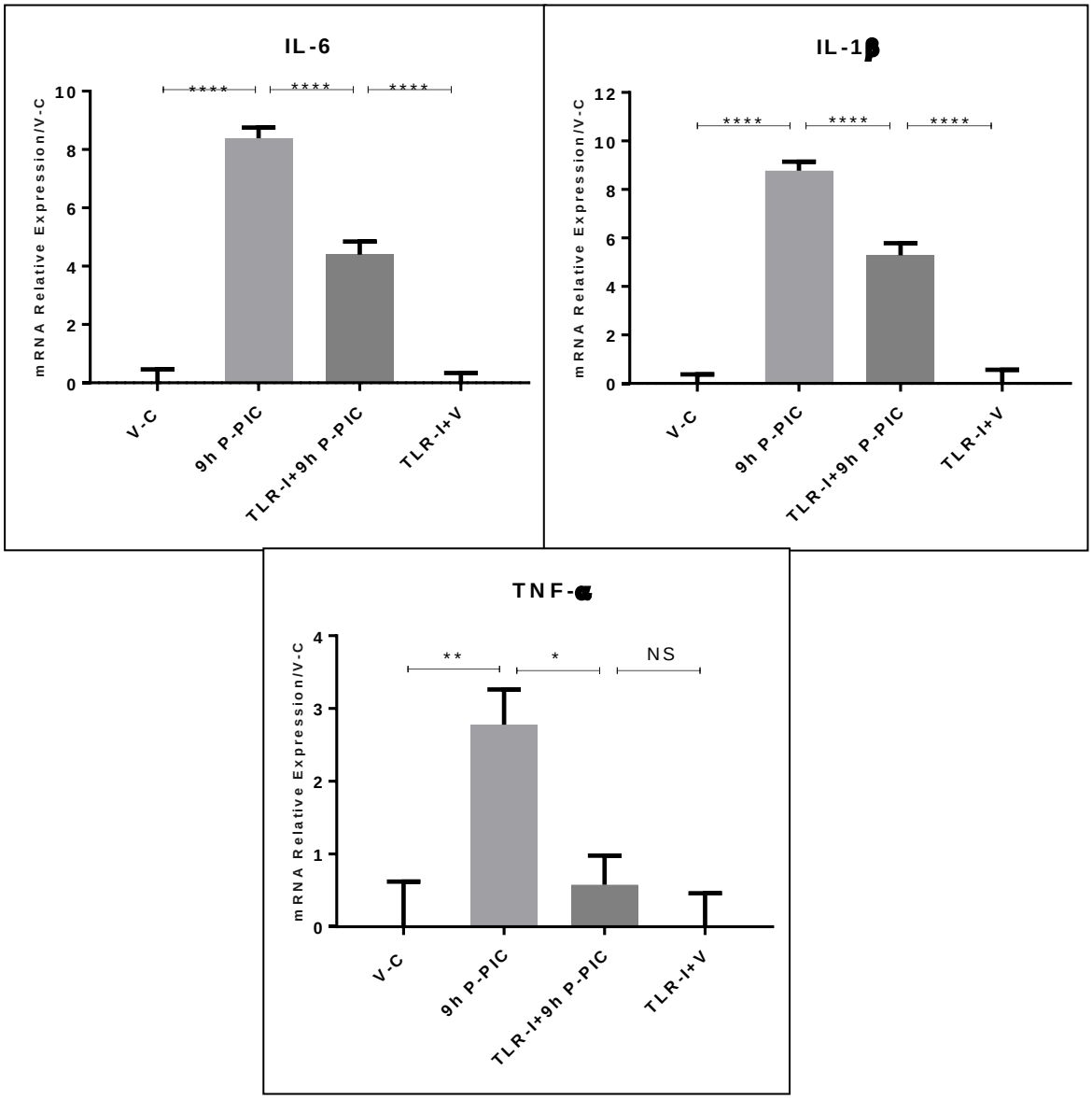

ANOVA	IL-6	IL-1β	TNF-α
P-value	<0.0001	<0.0001	0.0009
	****	****	***

Sidak's multiple comparisons test

	IL-6		IL-1β		TNF-α	
V-C vs. 9h P-PIC	****	<0.0001	****	<0.0001	**	0.0012
9h P-PIC vs. TLR-I+9h P-PIC	****	<0.0001	****	<0.0001	*	0.0112
TLR-I+V vs. TLR-I+9h P-PIC	****	<0.0001	****	<0.0001	ns	0.8039

Figure 3.6 **mRNA Expression of pro-inflammatory cytokines; IL6, IL1β and TNF-α.**
The TLR3/dsRNA complex inhibitor significantly reduced the transcriptionally upregulated pro-inflammatory cytokines, 9 hrs post poly (I:C) injection (9h P-PIC). Data represents means ± SEM (n=3). *P≤0.05, **p<0.01 ****p<0.0001, NS: non-significant, TLR-I: TLR3/dsRNA inhibitor complex, V: vehicle (trypan blue, saline and TLR3/dsRNA inhibition drug).

Next, immunohistochemistry was performed to explore the: (i) expression of other pro-inflammatory cytokines, (ii) induction of apoptosis and the (iii) acute inflammatory cellular infiltrate, downstream TLR3 ligation and following its inhibition. Histologic sections from mouse SMGs treated with the vehicle, poly (I:C) or poly (I:C) along with TLR3-inhibitor were stained with H&E and immunolabelled with antibodies against IFN-γ, Cox2, NF-κB, iNOS and cleaved caspase-3 (csp-3). Figure 3.7 reveals that the TLR3/dsRNA inhibitor has successfully interfered with NF-κB nuclear translocation in response to poly (I:C) stimulation and declined the parenchymal expression of the assessed antibodies. Moreover, H&E staining of these tissue sections revealed efficient elimination of the acute inflammatory cells which infiltrated the tissues in response to poly (I:C) injection, figure 3.7.

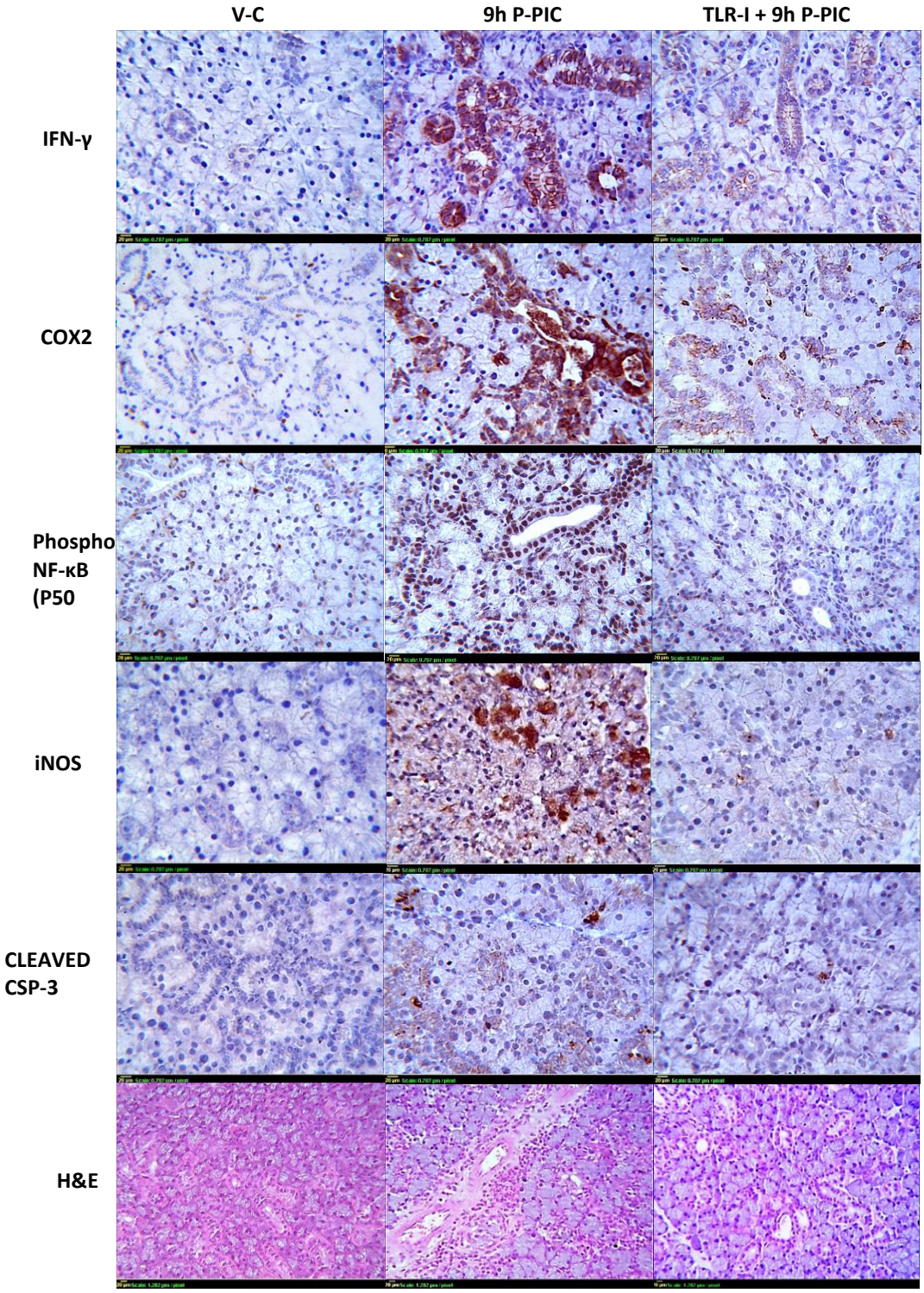

Figure 3.7 **Immunohistochemical representation of IFN-γ, Cox2, NF-κB, iNOS and cleaved csp-3 markers as well as H&E histology.**
Analysis of the vehicle injected control (V-C) glands and 9 hrs post poly (I:C) local administration in glands treated and non-treated with the TLR3/dsRNA inhibitor (TLR-I) revealed the remarkable reduction in expression of the tested proteins in response toTLR3 inhibition. H&E sections of TLR3/dsRNA blocker treated and non-treated SMGs showed the efficient depletion of the infiltrating immune cells in response to TLR3 competitive inhibition Original magnification of immunohistochemistry photomicrographs= 25x. H&E=16x.

3.3.3.3 TLR3 Inhibition Protected the SMG from Secretory Dysfunction.

At the functional level, inhibition of: (i) poly (I:C) binding to TLR3, (ii) TLR3 C-terminal neo-synthesis and (iii) subsequent downstream immune signals, protected the SMG secretory functions. The mean flow rates of the glands which received the TLR3 inhibitor in conjunction with poly (I:C) was similar to the contralateral glands which received the vehicle, Figure 3.8.

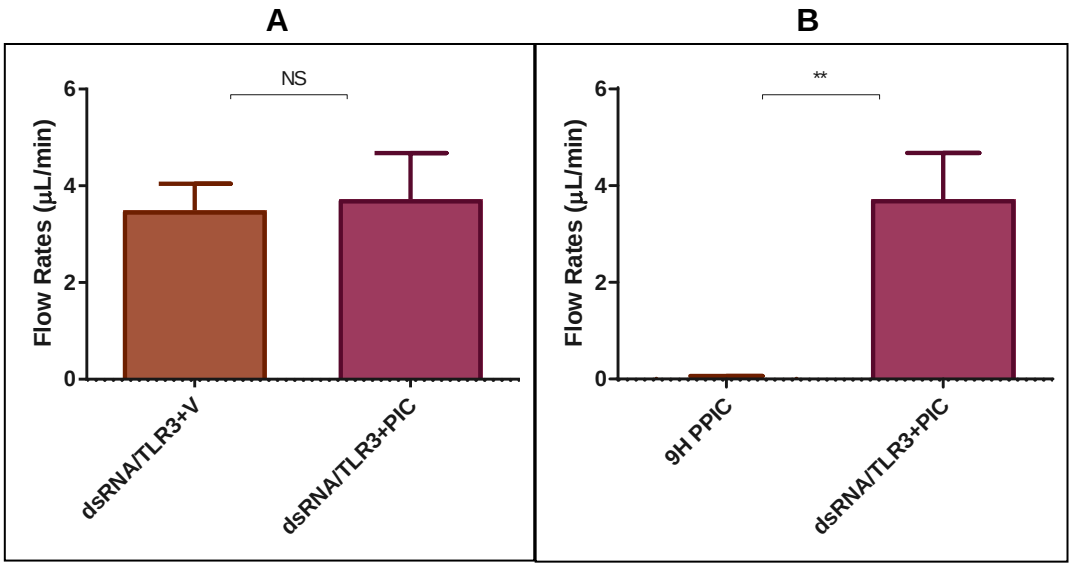

Two-tailed Paired t test	
P value	0.8169
P value summary	ns

Two-tailed Unpaired t test	
P value	0.0026
P value summary	**

Figure 3.8 **Functional analysis of the SMGs in response to TLR3 inhibition**. Data represent mean ± SD of the TLR3 inhibited glands (TLR3/dsRNA inhibitor + poly (I:C) & TLR3/dsRNA inhibitor + Vehicle). **A**: Inhibition of TLR3 in the current model sustained a constant salivary flow rate even after 9hrs of poly (I:C) exposure. **B**: The lost saliva secretion, 9 hrs post poly (I:C) injection was very significantly preserved upon combining the TLR3 competitive inhibitor to the viral mimic. N=3 for each tested group. **: P ≤ 0.01, NS: Non-significant.

3.3.4 TLR3 Mediated SMG Dysfunction Independent of Acute Inflammatory Infiltrate

3.3.4.1 Poly (I:C)-Mediated Transcriptional Upregulation of Neutrophil and Monocyte Chemo-attractants

In various viral models, poly (I:C) induced migration and activation of acute inflammatory cells, principally neutrophils and monocytes. qRT-PCR was performed to explore the mRNA expression of chemokines that organize trafficking of these acute inflammatory leukocytes. Results showed that retrograde duct injection of a single poly (I:C) dose induced an extremely significant up-regulation of four genes encoding neutrophil chemoattractants: keratinocyte-derived chemokine (KC)/CXCL1, macrophage-inflammatory protein-2 (MIP-2)/CXCL2, lipopolysaccharide-induced chemokine (LIX)/CXCL5, and CXCL15/lungkine (mouse IL-8) which exhibited the highest mRNA expression. In addition, the monocyte chemoattractant protein-1 (MCP-1)/CCL2 revealed very significant upregulation in response to poly (I:C). mRNA expression of the tested chemokines was calculated relative to HPRT internal control and the vehicle injected glands, figure 3.9.

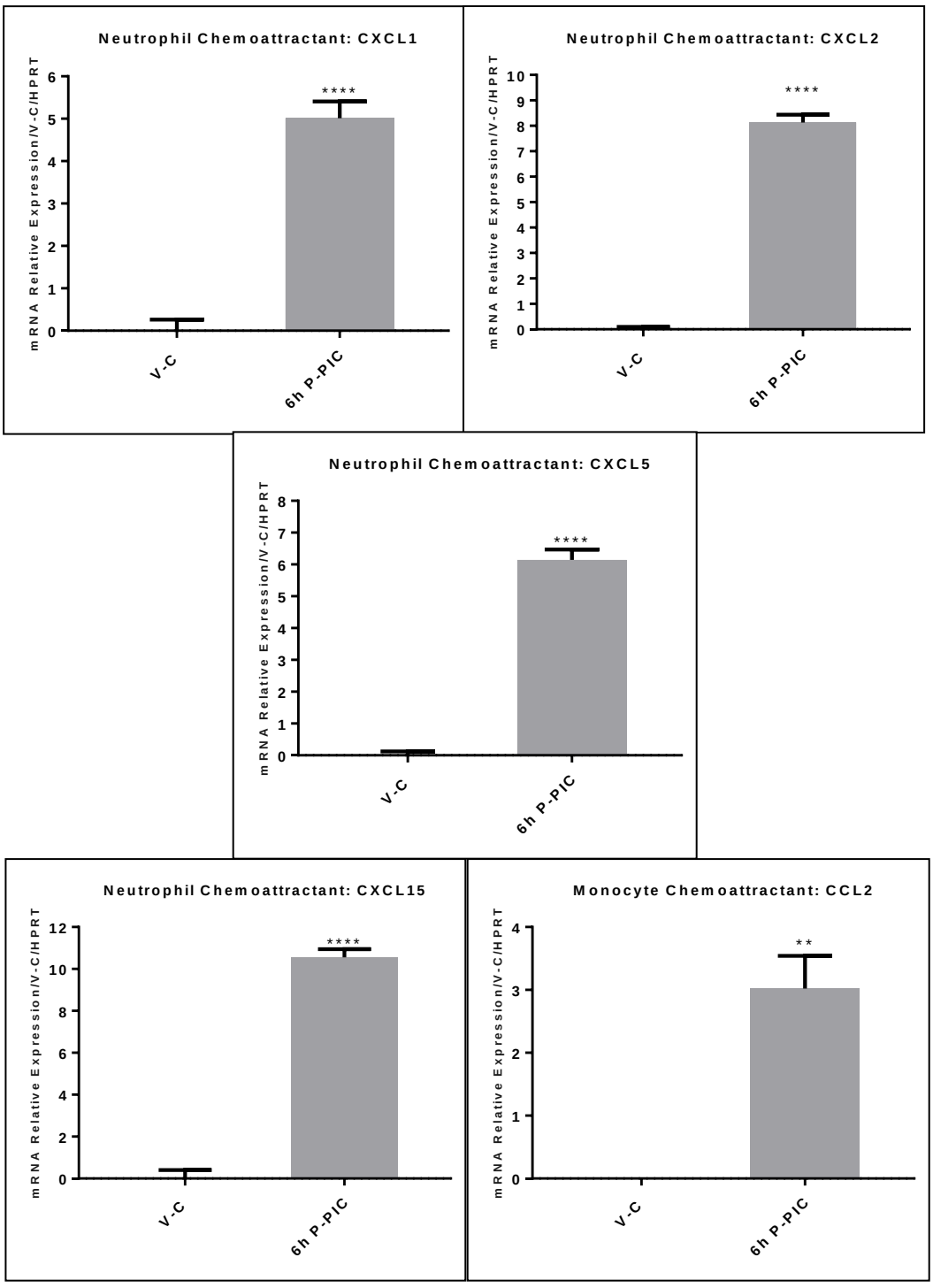

Unpaired t test

	CXCL1	CXCL2	CXCL5	CXCL15	CCL2
P value	<0.0001	<0.0001	<0.0001	<0.0001	0.0016
P value summary	****	****	****	****	**

Figure 3.9 **mRNA Expression of pro-inflammatory chemokines; CXCL1, CXCL2, CXCL5, CXCL15 and CCL2.**
Extremely significant upregulation of all neutrophil chemo-attractants and very significant increase in the monocyte chemokine; CCL2, 6hrs post poly (I:C) introduction (6h P-PIC). Data represents means ± SEM (n=3). **p<0.01 ****p<0.0001.

3.3.4.2 Invasive Infiltration of Immune Cells Showing High MPO-Positivity

The former PCR findings, in addition to the results seen in figure 3.7 which indicated a highly positive, TLR-3-driven inflammatory signal, incited us to explore the intensity and pattern of immune cell distribution in the SMGs. Accordingly, sections from the control and poly (I:C)-injected glands, at various experimental time points, were stained with H&E. Besides, based on the transcriptional overexpression of the neutrophil and monocyte chemo-attractants, we verified the predominance of these immune cell subsets in the SMG tissues using MPO, which is expressed in lysosomes of monocytes as well as azurophilic granules of neutrophils.

The H&E stained sections revealed that the SMGs which were injected and non-injected with the vehicle showed normal histology in the form a compact lobular structure with packed acini having pale basophilic cytoplasm and basal nuclei. The ductal system was patent and included intercalated, striated and secretory ducts with supporting connective tissues, all exhibiting normal appearance. Six hours post poly (I:C) inoculation, the SMG vasculature exhibited margination and transmigration of acute inflammatory cells. The infected glands displayed an apparently normal histomorphologic feature with oedema and pervasive inflammatory cells that were sometimes seen extruded into duct lumens. Surprisingly, the inflammatory cells were seen invading the duct lining from the blood vessels direction, pushing and flattening the native duct epithelial cells. Similarly, inflammatory cells were frequently seen invading and occupying acinar cells adjacent to blood vessels. By 9hrs, widespread infiltration of immune cells was displayed in extended stromal spaces, obscuring interlobular ducts and invading inter-acinar tissues.

Likewise, SMG morphology was still well-maintained after 24 hours of poly (I:C) injection, some infrequent vacuolar degeneration and interlobular oedema transformed some parts of the gland into an island-like appearance. Diffuse inflammatory cell infiltrate was seen throughout the whole glandular tissues, with the predominant cells exhibiting the multilobulated, doughnut-shaped nucleus which characterizes active neutrophils. Immunolabelling the SMG tissues with MPO revealed that after 6 hrs of introducing the viral mimetic, MPO-positive cells were seen clustering perivascularly and peri-ductally. Nonetheless, obvious migration of these cells to more distant and widespread inter-acinar orientations was detected at this early time point.

By 9 hrs, more extensive MPO positivity was perceived and the immune cells were seen within the gland acini and ducts. 24 hrs post poly (I:C) infusion, MPO positive cells were ubiquitously detected in interlobular, inter-acinar and more interestingly intra-acinar locations, analogous to the H&E intrusive patterns. Remarkably, the peri-ductal infiltrating cells at 6hrs displayed a confined homogenous cytoplasmic MPO positivity, whereas a spattered-like immunostaining pattern was seen in the inter-acinar and more pronounced in the intra-acinar MPO positive cells at 9hrs and 24 hrs post poly (I:C) introduction, figure 3.10.

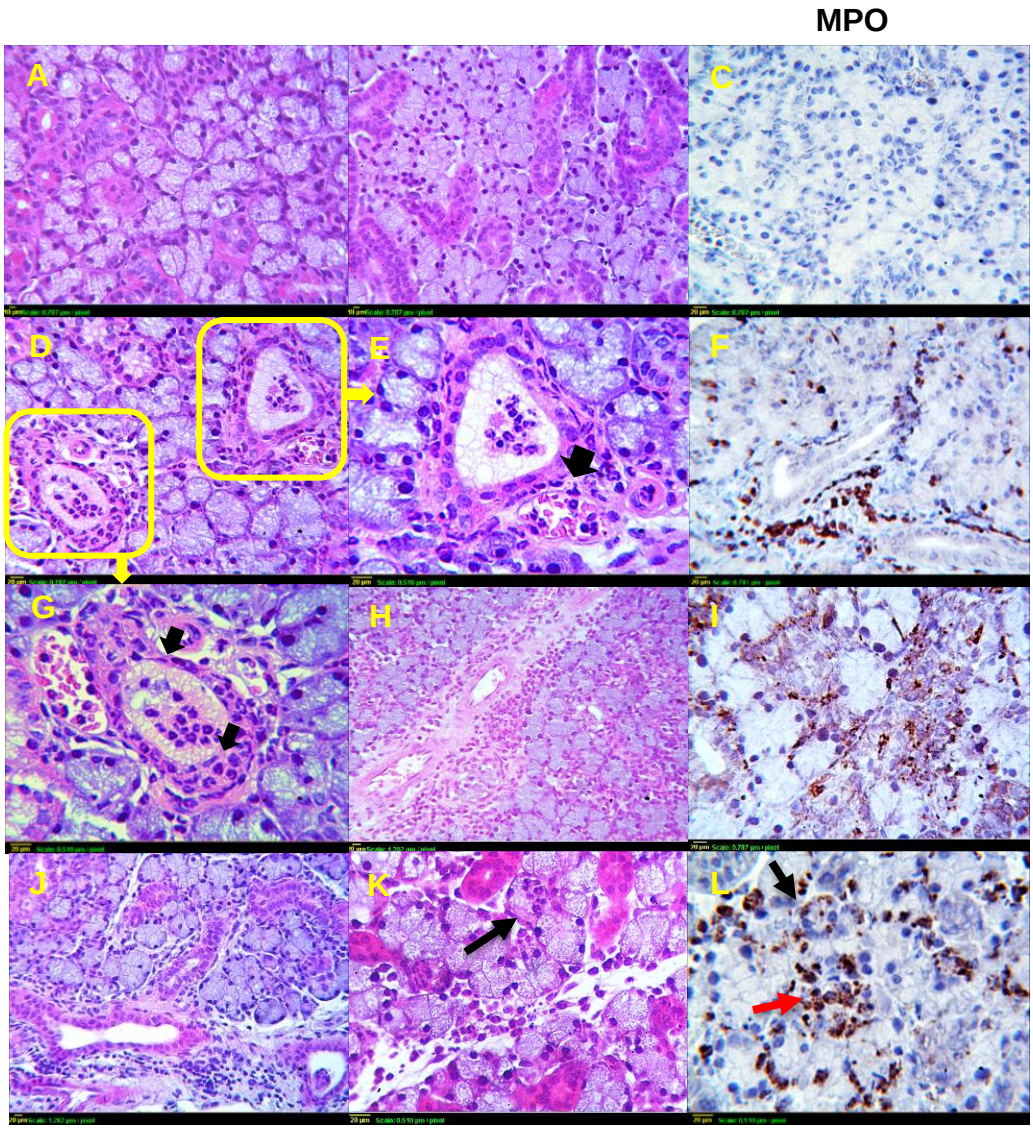

Figure 3.10 **H&E and MPO Immunostain of control and poly (I:C)-injected SMGs**. **A:** histomorphology of normal un-injected SMG and **B:** vehicle injected control SMG. **C:** Negative MPO expression in the vehicle injected control SMG. **D:** 6 hrs post poly (I:C) showing apparently preserved histomorphology, with inflammatory cells extruded into duct lumens. **E**: higher magnification of D revealing margination and transmigration (arrow) of inflammatory cells. **F:** the peri-ductal and sporadic inter-acinar cells are MPO-positive. **G:** Another higher magnification photomicrograph showing invasion of the infiltrating inflammatory cells into the SMG duct lining from all directions where blood vessels are sited, note the apparent replacement of native duct epithelial cells (now pushed and flattened, (arrows)) by the plethora of infiltrating cells. **H**: Extensive infiltration of stromal acute inflammatory cells, 9 hrs after poly (I:C) injection. **I:** MPO-positive cells invading ducts and interlobular spaces, 9 hrs after poly (I:C). **J:** 24 hrs following poly (I:C): edema and widening of the interlobular and inter-acinar spaces transforming the gland architecture into island-like morphology, with diffuse inflammatory cell infiltrate broadly occupying the expanded spaces. **K:** cells exhibiting the histologic features of neutrophils (doughnut-shaped /multilobulated nuclei) can be seen interlobular, inter-acinar and intra-cinar (arrow). **L:** intra-acinar (red arrow) and intra-ductal (black arrow) MPO-positive cells, 24 hrs after poly (I:C). Original Magnification A, B, J =16X. C, D, F, H, L=25X. E, G, I, K, =40X

3.3.4.3 Ly6G/Ly6C Depletion in the Acute SG Dysfunction Model Repressed MPO-Positive Cells

Immunohistochemistry substantiated abundant MPO-positive cellular infiltrate in response to the viral mimetic. Accordingly, we hypothesized that these cells may be major contributors in the poly (I:C)-mediated SMG injury and hypofunction. To validate our theory, we used the RB6-8C5 monoclonal antibody which binds to neutrophils (Hickey, 2012) and monocytes (Jutila et al., 1988). 200 µg of the depletion antibody; RB6-8C5 was administered intraperitoneally into the mice, 24 hrs before poly (I:C) local injection, and saliva was collected 24hrs after introduction of the viral mimic. Successful depletion of the acute inflammatory cell infiltrate was reflected in the flow cytometry results, which showed that the $CD45^+$ fraction was declined from 21.47% in the poly (I:C) injected SMGs, to 8.62% in the viral mimic-infected SMG from mice primed with the depletion antibody. Moreover, gating the $CD45^+$ cells within the $F4/80^-$ $CD11b^+$ channel, revealed that the Rb6-8C5 depletion drug efficiently reduced the $LY6G^+/LY6C^+$ populations, figure 3.11.

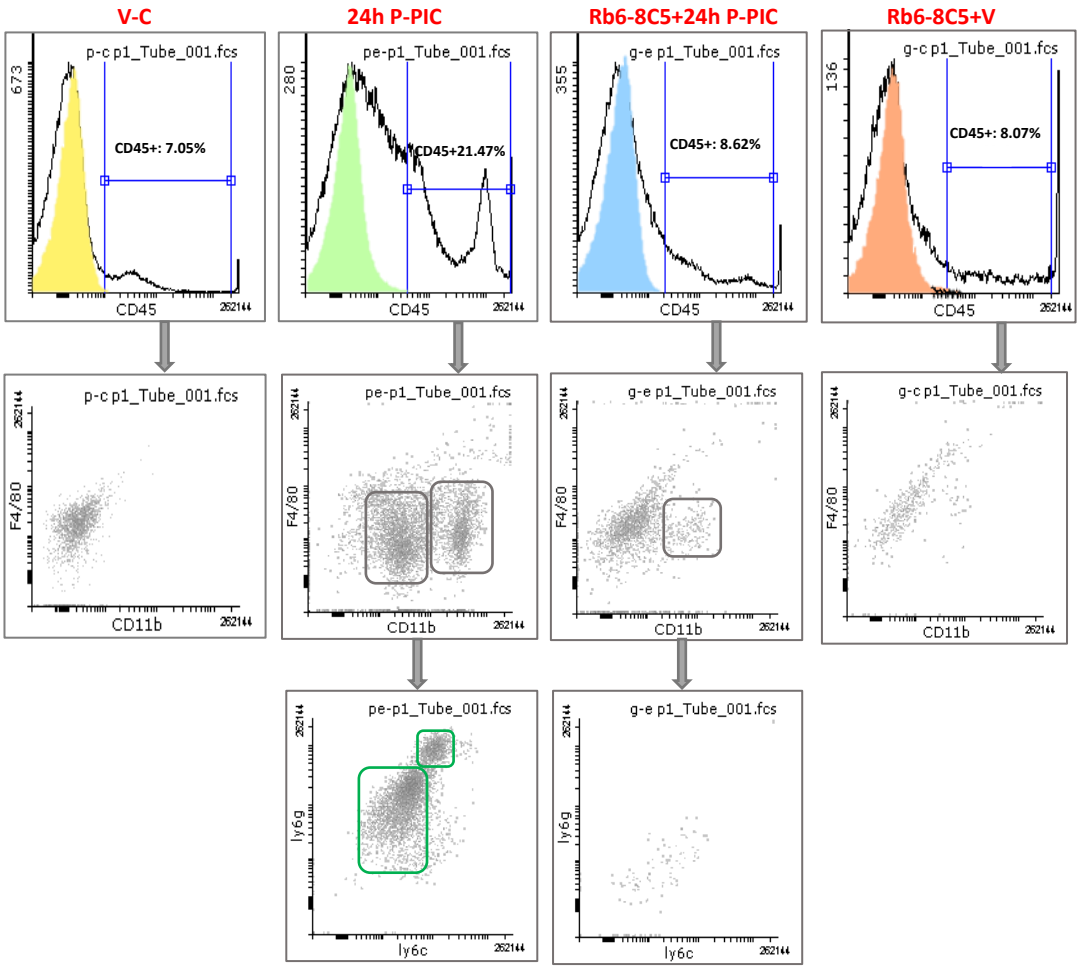

Figure 3.11 **Representative flow cytometry analysis images of RB6-8C5 treated and non-treated glands.**
Cell suspensions of SMGs from mice which received the viral mimic versus animals which were primed with the granulocyte depletion drug, 24hrs before receiving the poly (I:C). For neutrophil discrimination, cells were serially gated in the $CD45^{+}F4/80^{-}CD11b^{+}LY6C^{+}LY6G^{+}$ channels. Obvious decline in the percentage of $CD45^{+}$ cells was perceived in the depleted animals. Note the absence of distinct immune cell populations in the SMGs from mice which were exposed to the depletion drug in contrast to the very characteristic $CD45^{+}F4/80^{-}CD11b^{+}LY6C^{+}LY6G$ populations seen 24 hrs post poly (I:C) injection.

3.3.4.4 Depletion of LY6C/LY6G Eliminated the MPO Positive Cells.

To explore if RB6-8C5 had efficiently depleted the MPO-positive immune cell populations in the SMGs, immunohistochemistry and western blot analysis were conducted which showed that the Rb6-8C5 antibody successfully repressed MPO expression in the SMGs, figure 3.12.

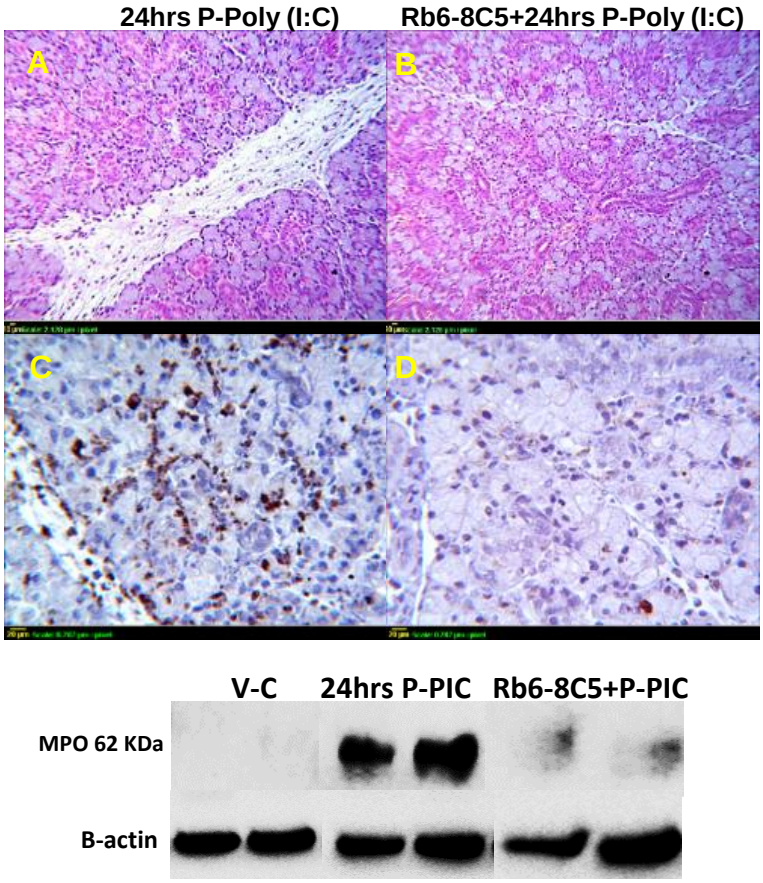

Figure 3.12 **RB6-8C5 depleted MPO positive cells.**
(A&C) Photomicrograph of SMG tissue sections injected only with poly (I:C) and **(B&D)** with the Rb6-8C5 depletion antibody followed by the viral mimic after 24 hrs. Original magnification: A, B=10X, C, D=25X. Representative western blot confirming reduction in MPO protein expression in response to Rb6-8C5 depletion drug, 24 hrs post poly (I:C) retrograde injection (P-PIC).

3.3.4.5 SMG Functional Capacity in Response to Immune Cell Depletion

Depletion of $LY6G^+/LY6C^+$ inflammatory cells, 24 hrs prior to poly (I:C) retrograde duct injection did not induce any recovery in the SMG function, 24 hrs following exposure to the viral mimic. A significant reduction in mean flow rates of the SMGs which received the viral mimic was perceived independent of immune cell depletion, figure 3.13.

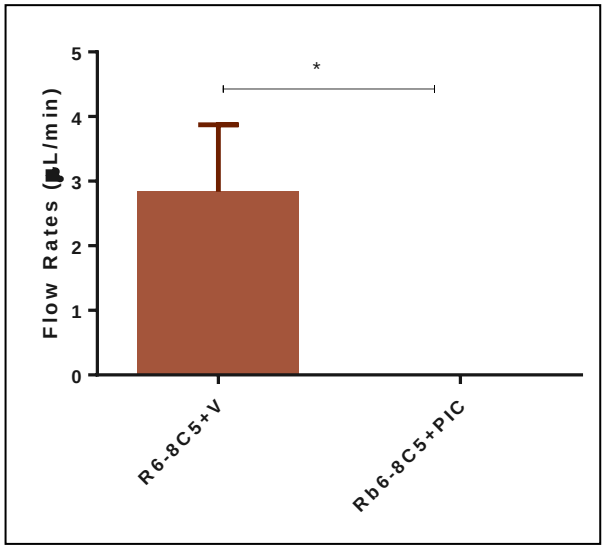

Two-tailed Paired t test	
P value	0.0422
P value summary	*

Figure 3.13 **SMG flow rates 48 hrs following the RB6-8C5 administration and 24 hrs post poly (I:C) retrograde injection.** Data represents mean ± SD from three independent mice experiments and shows persistent loss of secretion of the SMGs independent of immune cell depletion. *p≤0.05

3.4 Discussion

In the current study, we demonstrated the development of an acute viral SG dysfunction model based on the retrograde ductal injection of a synthetic dsRNA; poly (I:C), into the SMGs. By developing this model, we aimed at mimicking and characterizing the acute functional, tissue and signalling changes sequential to primary exposure of the SMGs to a viral mimetic.

Poly (I:C) is a viral analogue, it has been consistently used in vitro and in vivo to study IFN-based pathways in a reproducible manner (DeWitte-Orr and Mossman, 2010). Studies reported that poly (I:C) is internalized into cells via clathrin-and raftlin- mediated endocytosis where it co-localizes with endosomal TLR3 (Kato et al., 2008). However, despite of the extensive poly (I:C) use in diverse experimental models, its uptake and intracellular fate have been rarely demonstrated (Nellimarla and Mossman, 2014). Therefore, to verify the consistent and reliable parenchymal infectivity of poly (I:C) in the present model, initial experiments aimed at visualizing its internalization and retention in the SMG ducts and acini. The J2 monoclonal antibody is the gold standard in dsRNA detection and an extremely useful tool for the recognition of acute, and potentially persistent viral infection in formalin-fixed, paraffin-embedded tissue samples (Richardson et al., 2010). Vehicle injected control glands were negatively stained with the dsRNA monoclonal antibody, suggesting that it does not detect endogenous species of dsRNA that might be present in the cells (such as microRNAs or transferRNAs). This is in accordance with the fact that these endogenous dsRNA species are usually less than 50 bp in length and the antibody reportedly recognises only those dsRNA species which exceed 50 bp in length (Schonborn et al., 1991).

On the contrary, the dsRNA monoclonal J2 antibody positively stained acinar and duct cells which internalized the poly (I:C) as early as 6 hrs post its retrograde infusion. Immunofluorescent staining of the SMG tissues further disclosed the ability of the gland epithelial cells to hold the viral mimic for 24 hrs post its inoculation, which may be reflect the role played by the exocrine tissues in retaining viruses during infection periods. Given the role played by viruses in triggering SG disease and dysfunction, the detection of dsRNA immunohistochemically might provide a straightforward approach to substantiate infection or even tropism. In addition, this provides an efficient method for following up therapeutic interventions, prior to embarking on other time and money consuming methods example viral microarrays (Weller et al., 2016), or in-situ hybridization (Hilton et al., 1992).

Importantly, the SGs in the current model displayed a rapidly progressive functional decline, which started after 6 hrs of poly (I:C) infusion and nearly peeked after 9 hrs, until the SMGs ceased secretion completely after 24 hrs. Previous studies demonstrated that multiple, systemic injections of poly (I:C) in SS prone NZB/WF1 mice, resulted in loss of glandular function (Deshmukh et al., 2009, Nandula et al., 2013). The model represented herein is unique in demonstrating the direct influence of innate immune activation on the SG functional responses, ruling out possible extraneous impacts arising either from systemic delivery responses or autoimmune susceptibility of mice.

In the current model, loss of SMG functions upon local exposure to poly (I:C) paralleled upregulation of the dsRNA sensors; TLR3, MDA5 and RIG-I. Nonetheless, the parenchymal immunoexpression of TLR3 in the control and poly (I:C)-stimulated glands raised the postulation that TLR3 is the most likely receptor which may have responded to poly (I:C) by interfering with saliva secretion. In contrast, since MDA5 and RIG-I exclusively immunolabelled the infiltrating immune cells, these cytosolic receptors were theoretically considered as one of the TLR3 acute responses in the viral mimic model, rather than active contributors in the perceived loss of function. To verify our hypothesis, experiments were planned to selectively inhibit TLR3 *in vivo* and assess its exclusive role in the poly (I:C)-driven secretory dysfunction.

Previous studies have revealed that in the absence of stimuli; TLR3 is found as both a full-length 130 kDa protein corresponding to the highly-glycosylated receptor and a shorter form which corresponds to the C-terminal fragment that accumulates in the cells after cleavage by cathepsin (Garcia-Cattaneo et al., 2012). In addition, exposure to poly (I:C) has been shown to upregulate the TLR3 C-terminal, which was correlated to the signalling capacity of the receptor (Garcia-Cattaneo et al., 2012). Initially, we depicted the endogenous expression of the TLR3 C-terminus in the SMGs using an antibody against 15 amino acids in this fragment. Immunohistochemistry clearly demonstrated that the positive signal was exclusively seen in the intercalated ducts in the normal SMGs. This novel illustration may reflect the readily defensive property of these ducts in confronting viral infections via expressing the functional form of the receptor (Garcia-Cattaneo et al., 2012).

Furthermore, immunohistochemistry and western blot analysis revealed the significant increase in the TLR3 C-terminus, following poly (I:C) introduction, this phenomenon was previously illustrated and indicates a positive feedback loop that regulates the constant expression of TLR3 in epithelial cells, to maintain an antiviral response throughout the duration of infection (Garcia-Cattaneo et al., 2012).

To analyse the role played by the TLR3 C-terminal in the acute SMG dysfunction, we used a TLR3/dsRNA complex inhibitor to competitively interfere with poly (I:C) binding to TLR3. Expectedly, the SMGs which received a TLR3 inhibitor that competes with poly (I:C) over the receptor binding, did not show any upregulation of the C-terminus. Our results show for the first time the importance of ligand binding *in vivo* for the neo-synthesis of this fragment. More distinctively, these experiments revealed that the *in vivo* inhibition of TLR3 C-terminus accumulation, paralleled effective rescue of the poly (I:C)-mediated loss of secretion.

Interestingly, experiments conducted to validate the efficiency of the drug complex in inhibition of TLR3 showed **partial** mRNA downregulation of the poly (I:C)-induced pro-inflammatory cytokines; IL6, IL-1β and TNF-α as well as incomplete inhibition of IFN-γ and Cox2 protein expression, all of which, may be attributed to the signalling contribution of the cytoplasmic dsRNA sensors; MDA5 and RIG-I. Conversely, TLR3 blocking in the infected SMGs, proficiently inhibited: (i) acute inflammatory cell infiltration, (ii) cleaved caspase-3 positive acinar cells, (iii) nuclear translocation of NF-κB and (iv) upregulated expression of the pro-inflammatory mediator; iNOS. Based on these findings, the potential role played by each of the efficiently inhibited signals downstream TLR3/dsRNA blocking

were chosen for successive investigation to identify the early, acute, TLR-3-mediated event which interfered with saliva secretion.

TLR3 inhibition in the current model, interfered with infiltration of immune cells into the poly (I:C)-injected glands. These findings are in accordance with previous studies which revealed that in absence of TLR3, skin wounds displayed defective recruitment of neutrophils and macrophages, in association with decreased expression of the chemokines; MIP-2/CXCL2, MIP-1α/CCL3, and MCP-1/CCL2, (Lin et al., 2011). To investigate the role played by the infiltrating immune cells in the TLR3-mediated loss of function, we started by characterizing the immune cell chemo-attractants that were upregulated upon exposure to the viral mimic. qRT-PCR was conducted on the control and poly (I:C)-injected SMGs, which highlighted the immediate induction of the neutrophils' chemoattractants; CXC: KC/CXCL1, MIP-2/CXCL2, LIX/CXCL5 and CXCL15 (DeVries et al., 2003), in addition to expression of CC-chemokine (MCP-1/CCL2) encoding monocytes. These results initially indicated the phenotype of immune cells which may have infiltrated the SMGs sequential to poly (I:C) infection.

The former PCR results were followed up by microscopic examination of the SMG tissue sections, which revealed that poly (I:C) induced widespread infiltration of inflammatory cells having the histologic features of active neutrophils (bilobed nucleus). Surprisingly, a unique pattern of intra-acinar and intra-ductal invasive distribution was displayed by these cells. They were frequently seen dislocating and flattening the resident duct nuclei, in addition to being commonly extruded into the lumens. Interestingly, duct cells (Ogawa et al., 2002), as well as acinar cells (Dios, 2010) have demonstrated ability to respond to inflammatory signals by the production of chemokines.

Accordingly, the inherent ability of the salivary gland epithelial cells to produce these low molecular weight chemo-attractants may have guided the infiltrating immune cells to the perceived intra-epithelial invasive positions.

Next, immunolabelling the SMG tissues with a polyclonal antibody against MPO revealed that the robustly recruited immune cells, tethering, transmigrating and invading into ducts and acini were MPO positive, which emphasized their neutrophil/monocyte identity (Klebanoff, 2005), and directed towards using RB6-8C5 as the appropriate method for their specific depletion. The discovery that high doses of RB6-8C5 are very effective at removing neutrophils from the circulation, gave researchers a convenient and reproducible approach for assessing the contribution of neutrophils to experimental models of inflammation. RB6-8C5 binds to 2 members of the Ly6 family of leukocyte-expressed markers; Ly6C and Ly6G (Hickey, 2012). The mechanism by which RB6-8C5 can deplete immune cells is based on the demonstrated inability of neutrophils to respond to chemotactic stimuli, in the presence of this monoclonal antibody. Furthermore, the recruitment capabilities of neutrophils were significantly compromised upon Ly6G ligation, this is due to diminished surface levels and function of crucial adhesion molecules as the β2 integrins; CD11a and CD11b (Hickey, 2012), figure 3.14.

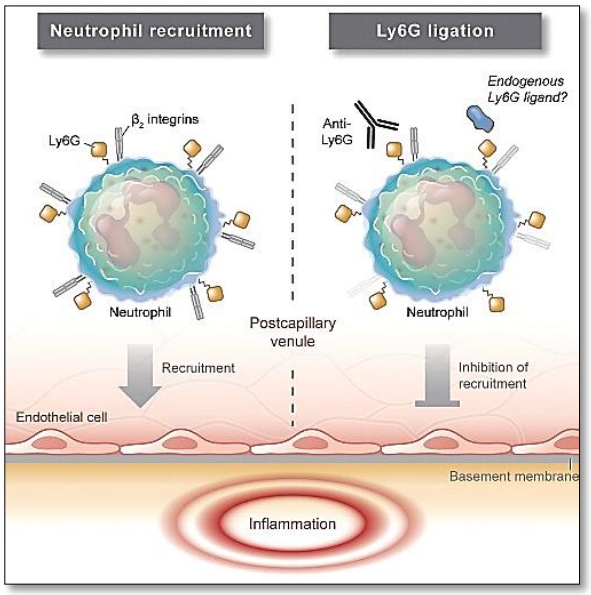

Figure 3.14 **Ly6G.**
A GPI-linked protein, is present at high levels on the neutrophil surface, although its function is unknown. Wang et al (Wang et al., 2012) showed that Ly6G is co-localized with β2 integrins, and that antibody ligation of Ly6G reduces β2 integrin expression and inhibits neutrophil recruitment. Professional illustration by Kenneth X. Probst., (Hickey, 2012).

In addition, RB6-8C5 was shown to bind to Ly6C which is not only expressed on neutrophils, but also on dendritic cells (DCs), and subsets of monocytes, macrophages, and lymphocytes (Jutila et al., 1988, Hestdal et al., 1991, Kung et al., 1991, Jutila et al., 1994). Thus, in the present study, RB6-8C5 antibody was used to dually deplete neutrophils and monocytes and investigate their injurious role in the acute virally-mediated loss of function. Histopathology, flow cytometry, immunohistochemistry and western blot showed that priming of the mice with RB6-8C5 markedly attenuated immune cell invasion into the SMGs, after 24hrs of poly (I:C) treatment.

Surprisingly, treatment of mice with the anti-Ly6G/Ly6C which efficiently restrained tissue inflammation and eliminated the MPO-positive immune cells, did not induce functional recovery. These experiments verified that TLR3 interfered with the secretory ability of the SMGs independent of the invasive immune cell signal. Findings from the current experiments, combined to other neutrophil-independent injury models (Raeburn et al., 2002, de Vries et al., 2003) and studies which frequently demonstrate irrelevance between secretory hypofunction and immune cellular infiltration (Shen et al., 2009, Shen et al., 2013), strongly implicate alternative impairment mechanisms by which the SG epithelial cells endogenously respond to injury and suggest a bystander role of the early acute and later lymphocytic infiltrations in exocrine dysfunction.

In conclusion, results presented in the current chapter identified the exclusive role played by TLR3, in the poly (I:C)-mediated loss of secretion. Our findings highlighted for the first time the basal and stimulated expression of the functional form of TLR3; the C-terminal fragment and suggested its blockade as a promising therapeutic strategy for the treatment of SG diseases with viral implications. Moreover, the results demonstrated herein undoubtedly excluded the invasively infiltrating neutrophils; one of the robustly induced and fundamentally damaging signals, from the contribution to the acute TLR3-mediated secretory dysfunction. Experiments in the upcoming chapters will verify alternative injurious signals downstream of TLR3 activation and correlate their induction to the loss of function in the mouse model.

Chapter 4

Pan Caspase Inhibitor; z-VAD-fmk Protected the SMG From the TLR3-Mediated Dysfunction

4.1 Introduction

Evidence has accumulated over the years that poly (I:C) can directly trigger apoptosis in many types of cells by activating TLR3. Moreover, studies have indicated that adaptor proteins involved in TLR3 signalling pathways play crucial roles in initiating apoptosis (Zhao et al., 2012). Specifically, the key adaptor of TLR3 signalling pathway; TRIF, was shown to be indispensable for apoptotic cell death (Yamamoto et al., 2002).

Apoptosis has been considered as one of the main factors which may be related to loss of SG secretory function (Hayashi, 2011). In fact, death of ductal and acinar cells are considered major mechanisms for salivary gland dysfunction of patients with SS (Horai et al., 2016) and following irradiation of salivary glands (Acauan et al., 2015).

We reported in the previous chapter that TLR3 has triggered an apoptotic signal in the poly (I:C)-infused glands, marked by the increased expression of cleaved caspase-3-positive cells. Caspase family members function as important signals in the last step of several apoptosis signalling pathways (Vaux and Strasser, 1996). The cell permeable pan- caspase inhibitor; z-Val-Ala-Asp (Ome) fluoro-methyl-ketone (z-VAD-fmk), was reported to have a strong antiapoptotic effect in vivo (Li et al., 2000), via irreversibly binding to the catalytic site of caspase proteases (Gregoli and Bondurant, 1999). Therefore, we hypothesized that by systemic administration of this caspase inhibitor, we can protect the SMG parenchymal cells from apoptosis, rescue the compromised secretory machinery and identify induction of apoptosis as the injury signal which induced dysfunction in the current model.

Unexpectedly, the conducted experiments unravelled novel, off-target properties of z-VAD-fmk which culminated in recovery of the TLR3-induced loss of function, independent of apoptosis inhibition.

4.2 Materials and Methods

4.2.1 z-VAD-fmk Mouse Model

Table 4-1 summarizes the z-VAD-fmk dose and administration protocol used in the current chapter.

Table 4-1 In vivo inhibition dose and protocol of the z-VAD-fmk model

Mechanism	Source	Catalogue Number	Dose	Administration Protocol
General Caspase Inhibitor	BD Pharmingen™	550377	10mg/kg (Equils et al., 2009)	i.p. 30 min prior to Poly (I:C) local injection

4.2.2 Immunohistochemical Analysis

Paraffin-embedded SMG sections were deparaffinised, rehydrated and antigen retrieved by autoclaving with Trilogy™ as detailed in chapter 2, paragraph 2.3. Subsequently, slides were incubated in hydrogen peroxide to block endogenous peroxidase activity and protein block to inhibit nonspecific background reaction. After incubation with the specific primary antibodies (table 4-2), the detection was completed using the compatible host HRP-conjugated secondary antibodies. Nuclear and counterstaining was done with Mayer's haematoxylin, then slides were examined for immunopositivity under the light microscope.

Table 4-2 Primary Antibodies Used

Antibody	Source & Catalogue Number	Host	Working Dilution
Cleaved caspase 3	R&D Systems, MAB835	Rabbit	1:280
TLR-3	Abcam, Ltd, ab62566	Rabbit	1:10000
Myeloperoxidase	BosterBio, USA, PB9057	Rabbit	1:1000
IFN-beta	Bioss USA, bs-0784R	Rabbit	1:1100
Cox2	Abcam, Ltd, ab133466	Rabbit	1:400
Interferon-gamma (IFN-γ)	Proteintech Europe,15365-1-AP	Rabbit	1:2500
Phospho-NF-κB (p50)	Santa Cruz Biotechnology, sc-271908	Mouse	1:450
iNOS	Novus Biologicals, USA, NB300-605	Rabbit	1:650
Polyclonal Goat Anti-Rabbit Immunoglobulins-HRP	Dako, P0448	Goat	1:200

4.2.3 Western Blotting

SMG protein extracts were electrophoresed on precast 4-2% SDS-PAGE gel and transferred to nitrocellulose membrane as detailed in chapter 2, Paragraph 2.4. Membranes were incubated with the primary antibody, followed by 1 hr incubation with the appropriate secondary antibody (table 4-3). Subsequently, signal development and exposure with enhanced chemiluminescence and ChemiDoc™ MP System were performed.

Table 4-3 List of Antibodies Used in Western Blots

Antibody	Source & Catalogue Number	Host	Working Dilution
Cleaved Caspase 3	Novus Bio, NB100-56113	Rabbit	1:5000
TLR-3	Abcam, Ltd, ab62566	Rabbit	1:10000
B-actin	Sigma, A2228	Mouse	1 µg/mL
Polyclonal Goat Anti-Rabbit Immunoglobulins-HRP	Dako, P0448	Goat	1:2000
Polyclonal Goat Anti-Mouse Immunoglobulins- HRP	Dako, P0447	Goat	1:1000

4.2.4 RTqPCR

Total RNAs isolated from SMG tissues (stored in RNAlater®) were extracted using RNeasy® Micro Kit (Qiagen) and 100 ng of extracted RNAs were reverse-transcribed in a 20 µL reaction using the iScript™ cDNA Synthesis kit. Quantitative real time PCR (qRT-PCR) was carried out as detailed in chapter 2, Paragraph 2.5. All mouse primers were synthesized by PrimerDesign™, Ltd and are listed in Table 4-4. All experiments were performed in triplicate.

Table 4-4 List of Primers used

Gene	Accession Number
MX-1 (MX dynamin-like GTPase 1)	NM_010846
ISG-15 (ISG15 ubiquitin-like modifier)	NM_015783
IL 6	NM_031168
IL 1β	NM_008361
Interferon gamma (Ifng)	NM_008337
TLR3 (Toll-like receptor 3)	NM_126166
MDA5 (Interferon induced with helicase C domain 1 (Ifih1), transcript variant 1)	NM_027835
HPRT (Hypoxanthine guanine phosphoribosyl transferase)	NM_013556
GAPDH (glyceraldehyde-3-phosphate dehydrogenase)	NM_008084

4.2.5 Histologic Examination

As described in chapter 2, paragraph 2.2, following gland excision and formalin fixation of tissues, samples were processed, embedded in paraffin, microtome sectioned, stained with H&E and examined under a light microscope.

4.2.6 PCR Array of Mouse Toll-Like Receptor Signaling Pathway

The Mouse RT² Profiler Toll-Like Receptor (TLR) signaling pathway array (Qiagen, PAMM-018Z) profiles the expression of 84 genes central to TLR-mediated signal transduction and innate immunity, including members of the TLR signaling family as well as adaptor and effector proteins, members of the NFκB, JNK/p38, IRF and JAK/STAT signaling pathways downstream of TLR activation. RNA for the control and poly (I:C) injected glands were extracted as detailed in chapter 2 Paragraph 2.6. Genomic DNA elimination and reverse transcription were performed on 800 ng of extracted RNA, using the RT² First Strand Kit (330401, Qiagen), according to the manufacturer's protocol. 20 µl of the PCR reaction mix (table 4-5) was added to individual wells of the RT² Profiler PCR array format R (PAMM-018ZR, Qiagen) and the thermal cycler was set according to http://www.SABiosciences.com/pcrarrayprotocolfiles.php.

Table 4-5 PCR Components Mix

2x RT2 SYBR Green ROX FAST Mastermix (330520, Qiagen)	1150 µl
cDNA synthesis reaction	102 µl
RNase-free water	1048 µl
Total Volume	2300 µl

A threshold value above the background signal was chosen and the CT values for the run samples were extracted to an excel sheet and analysed using the web-based PCR Array Data Analysis Software available at www.SABiosciences.com/pcrarraydataanalysis.php. Table 4-6 lists the TLR-related genes incorporated in the PCR array.

Table 4-6 Gene table: RT² Profiler PCR Array

Gene Table					
Position	**Unigene**	**GeneBank**	**Symbol**	**Description**	**Gene Name**
A01	Mm.4475	NM_013482	Btk	Bruton agammaglobulinemia tyrosine kinase	AI528679, xid
A02	Mm.336851	NM_009812	Casp8	Caspase 8	CASP-8, FLICE, MACH, Mch5
A03	Mm.290320	NM_011333	Ccl2	Chemokine (C-C motif) ligand 2	AI323594, HC11, JE, MCAF, MCP-1, MCP1, SMC-CF, Scya2, Sigje
A04	Mm.3460	NM_009841	Cd14	CD14 antigen	-
A05	Mm.89474	NM_009855	Cd80	CD80 antigen	B71, Cd28l, Ly-53, Ly53, MIC17, TSA1
A06	Mm.1452	NM_019388	Cd86	CD86 antigen	B7, B7-2, B7.2, B70, CLS1, Cd28l2, ETC-1, Ly-58, Ly58, MB7, MB7-2, TS, A-2
A07	Mm.439656	NM_009883	Cebpb	CCAAT/enhancer binding protein (C/EBP), beta	C, EBPbeta, CRP2, IL-6DBP, LAP, LIP, NF-IL6, NF-M, Nfil6
A08	Mm.3996	NM_007700	Chuk	Conserved helix-loop-helix ubiquitous kinase	AI256658, Chuk1, Fbx24, Fbxo24, IKBKA, IKK1, Ikka, NFKBIKA
A09	Mm.248327	NM_019948	Clec4e	C-type lectin domain family 4, member e	C86253, Clecsf9, Mincle
A10	Mm.4922	NM_009969	Csf2	Colony stimulating factor 2 (granulocyte-macrophage)	Csfgm, GMCSF, Gm-CSf, MGI-IGM
A11	Mm.1238	NM_009971	Csf3	Colony stimulating factor 3 (granulocyte)	Csfg, G-CSF, MGI-IG
A12	Mm.877	NM_021274	Cxcl10	Chemokine (C-X-C motif) ligand 10	C7, CRG-2, INP10, IP-10, IP10, Ifi10, Scyb10, gIP-10, mob-1
B01	Mm.490895	NM_007922	Elk1	ELK1, member of ETS oncogene family	Elk-1
B02	Mm.5126	NM_010175	Fadd	Fas (TNFRSF6)-associated via death domain	Mort1, FADD
B03	Mm.246513	NM_010234	Fos	FBJ osteosarcoma oncogene	D12Rfj1, c-fos, cFos
B04	Mm.207047	NM_010439	Hmgb1	High mobility group box 1	DEF, HMG-1, Hmg1, SBP-1, amphoterin, p30
B05	Mm.334313	NM_008284	Hras1	Harvey rat sarcoma virus oncogene 1	H-ras, Ha-ras, Harvey-ras, Hras-1, Kras2, c-H-ras, c-Ha-ras, c-rasHa, ras
B06	Mm.433409	NM_010472	Agfg1	ArfGAP with FG repeats 1	AU045498, C130049H11Rik, C85612, D730048C23Rik, Hrb, RAB, Rip
B07	Mm.6388	NM_010479	Hspa1a	Heat shock protein 1A	Hsp70-3, Hsp70.3, Hsp72, hsp68, hsp70A1
B08	Mm.1777	NM_010477	Hspd1	Heat shock protein 1 (chaperonin)	60kDa, Hsp60
B09	Mm.1245	NM_010510	Ifnb1	Interferon beta 1, fibroblast	IFN-beta, IFNB, Ifb
B10	Mm.240327	NM_008337	Ifng	Interferon gamma	IFN-g, Ifg

B11	Mm.277886	NM_010546	Ikbkb	Inhibitor of kappaB kinase beta	AI132552, IKK-2, IKK-beta, IKK2, IKK[b], IKKbeta
B12	Mm.874	NM_010548	Il10	Interleukin 10	CSIF, Il-10
C01	Mm.103783	NM_008351	Il12a	Interleukin 12A	IL-12p35, Il-12a, Il12a, p35
C02	Mm.15534	NM_010554	Il1a	Interleukin 1 alpha	Il-1a
C03	Mm.222830	NM_008361	Il1b	Interleukin 1 beta	IL-1beta, Il-1b
C04	Mm.896	NM_008362	Il1r1	Interleukin 1 receptor, type I	CD121a, CD121b, IL-iR, Il1r-1
C05	Mm.14190	NM_008366	Il2	Interleukin 2	Il-2
C06	Mm.1019	NM_031168	Il6	Interleukin 6	Il-6
C07	Mm.2856	NM_010559	Il6ra	Interleukin 6 receptor, alpha	CD126, IL-6R, Il6r
C08	Mm.38241	NM_008363	Irak1	Interleukin-1 receptor-associated kinase 1	AA408924, IRAK, IRAK-1, IRAK1-S, Il1rak, Plpk, mPLK
C09	Mm.152142	NM_172161	Irak2	Interleukin-1 receptor-associated kinase 2	6330415L08Rik, AI649099, IRAK-2
C10	Mm.105218	NM_008390	Irf1	Interferon regulatory factor 1	AU020929, Irf-1
C11	Mm.489648	NM_016849	Irf3	Interferon regulatory factor 3	C920001K05Rik, IRF-3
C12	Mm.275071	NM_010591	Jun	Jun oncogene	AP-1, Junc, c-jun
D01	Mm.87787	NM_010735	Lta	Lymphotoxin A	LT, LT-[a], LT-alpha, LT[a], LTalpha, Ltx, TNF-beta, TNFSF1, Tnfb, Tnfsf1b, hlb382
D02	Mm.3177	NM_010739	Muc13	Mucin 13, epithelial transmembrane	114, A10, 14, A10, AI159736, Lrrp, Ly64, NJ-1
D03	Mm.2639	NM_010745	Ly86	Lymphocyte antigen 86	MD-1, MD1
D04	Mm.116844	NM_016923	Ly96	Lymphocyte antigen 96	ESOP-1, MD-2, MD2
D05	Mm.18494	NM_008928	Map2k3	Mitogen-activated protein kinase kinase 3	AW212142, MEK3, MKK3, Prkmk3, mMKK3b
D06	Mm.412922	NM_009157	Map2k4	Mitogen-activated protein kinase kinase 4	JNKK1, MEK4, MKK4, PRKMK4, Sek1, Serk1
D07	Mm.15918	NM_011945	Map3k1	Mitogen-activated protein kinase kinase kinase 1	MAPKKK1, MEKK1, Mekk
D08	Mm.258589	NM_172688	Map3k7	Mitogen-activated protein kinase kinase kinase 7	B430101B05, C87327, Tak1
D09	Mm.21495	NM_016700	Mapk8	Mitogen-activated protein kinase 8	AI849689, JNK, JNK1, Prkm8, SAPK1
D10	Mm.43081	NM_013931	Mapk8ip3	Mitogen-activated protein kinase 8 interacting protein 3	BB120594, D17Wsu15e, JIP-3, JSAP1, JSAP1a, JSAP1b, JSAP1c, JSAP1d, Jip3, Syd2, mKIAA1066
D11	Mm.68933	NM_016961	Mapk9	Mitogen-activated protein kinase 9	AI851083, JNK2, Prkm9, p54aSAPK
D12	Mm.213003	NM_010851	Myd88	Myeloid differentiation-primary response gene 88	
E01	Mm.256765	NM_008689	Nfkb1	Nuclear factor of kappa light polypeptide gene enhancer in B-cells 1, p105	NF-KB1, NF-kappaB, NF-kappaB1, p105, p50, p50, p105

E02	Mm.102365	NM_019408	Nfkb2	Nuclear factor of kappa light polypeptide gene enhancer in B-cells 2, p49/p100	NF-kappaB2, lyt, p49, p49, p100, p50B, p52
E03	Mm.170515	NM_010907	Nfkbia	Nuclear factor of kappa light polypeptide gene enhancer in B-cells inhibitor, alpha	AI462015, Nfkbi
E04	Mm.220333	NM_010908	Nfkbib	Nuclear factor of kappa light polypeptide gene enhancer in B-cells inhibitor, beta	IKB-beta, IKappaBbeta, IkB, IkBb
E05	Mm.300795	NM_010909	Nfkbil1	Nuclear factor of kappa light polypeptide gene enhancer in B-cells inhibitor-like 1	Def-7, IKBL
E06	Mm.238146	NM_172766	Nfrkb	Nuclear factor related to kappa B binding protein	A530090G11Rik
E07	Mm.87062	NM_011630	Nr2c2	Nuclear receptor subfamily 2, group C, member 2	TAK1, Tr4, mKIAA4145
E08	Mm.28957	NM_023324	Peli1	Pellino 1	2810468L03Rik, A930031K15Rik, AA409794, AI586297, D11Ertd676e
E09	Mm.21855	NM_009402	Pglyrp1	Peptidoglycan recognition protein 1	PGRP, PGRP-S, Pglyrp, Tag7, Tasg7, Tnfsf3l
E10	Mm.212789	NM_011144	Ppara	Peroxisome proliferator activated receptor alpha	4933429D07Rik, AW742785, Nr1c1, PPAR-alpha, PPARalpha, Ppar
E11	Mm.378990	NM_011163	Eif2ak2	Eukaryotic translation initiation factor 2-alpha kinase 2	2310047A08Rik, 4732414G15Rik, AI467567, AI747578, Pkr, Prkr, Tik
E12	Mm.292547	NM_011198	Ptgs2	Prostaglandin-endoperoxide synthase 2	COX2, Cox-2, PGHS-2, PHS-2, Pghs2, TIS10
F01	Mm.4869	NM_009044	Rel	Reticuloendotheliosis oncogene	c-Rel
F02	Mm.249966	NM_009045	Rela	V-rel reticuloendotheliosis viral oncogene homolog A (avian)	p65
F03	Mm.112765	NM_138952	Ripk2	Receptor (TNFRSF)-interacting serine-threonine kinase 2	2210420D18Rik, CARD3, CARDIAK, CCK, D4Bwg0615e, RICK, RIP2
F04	Mm.34580	NM_019786	Tbk1	TANK-binding kinase 1	1200008B05Rik, AI462036, AW048562
F05	Mm.203952	NM_174989	Ticam1	Toll-like receptor adaptor molecule 1	AW046014, AW547018, TICAM-1, TRIF
F06	Mm.149280	NM_173394	Ticam2	Toll-like receptor adaptor molecule 2	B430113A10, TICAM-2, TRAM, Tirp, Trif
F07	Mm.23987	NM_054096	Tirap	Toll-interleukin 1 receptor (TIR) domain-containing adaptor protein	AA407980, C130027E04Rik, Mal, Tlr4ap, Wyatt
F08	Mm.273024	NM_030682	Tlr1	Toll-like receptor 1	-
F09	Mm.87596	NM_011905	Tlr2	Toll-like receptor 2	Ly105
F10	Mm.33874	NM_126166	Tlr3	Toll-like receptor 3	AI957183
F11	Mm.38049	NM_021297	Tlr4	Toll-like receptor 4	Lps, Ly87, Ran, M1, Rasl2-8

F12	Mm.116894	NM_016928	Tlr5	Toll-like receptor 5	-
G01	Mm.42146	NM_011604	Tlr6	Toll-like receptor 6	-
G02	Mm.489377	NM_133211	Tlr7	Toll-like receptor 7	-
G03	Mm.196676	NM_133212	Tlr8	Toll-like receptor 8	-
G04	Mm.44889	NM_031178	Tlr9	Toll-like receptor 9	-
G05	Mm.1293	NM_013693	Tnf	Tumor necrosis factor	DIF, TNF-a, TNF-alpha, TNFSF2, TNFalpha, Tnfa, Tnfsf1a
G06	Mm.116683	NM_009397	Tnfaip3	Tumor necrosis factor, alpha-induced protein 3	A20, Tnfip3
G07	Mm.474976	NM_011609	Tnfrsf1a	Tumor necrosis factor receptor superfamily, member 1a	CD120a, FPF, TNF-R, TNF-R-I, TNF-R1, TNF-R55, TNF-alphaR1, TNFAR, TNFR60, TNFRI, TNFRp55, TNFalpha-R1, Tnfr-2, Tnfr1, p55, p55-R
G08	Mm.103551	NM_023764	Tollip	Toll interacting protein	4930403G24Rik, 4931428G15Rik
G09	Mm.264255	NM_001033161	Tradd	TNFRSF1A-associated via death domain	9130005N23Rik, AA930854
G10	Mm.292729	NM_009424	Traf6	Tnf receptor-associated factor 6	2310003F17Rik, AI851288, C630032O20Rik
G11	Mm.440187	NM_080560	Ube2n	Ubiquitin-conjugating enzyme E2N	1500026J17Rik, AL022654, BB101821, UBC13
G12	Mm.360108	NM_023230	Ube2v1	Ubiquitin-conjugating enzyme E2 variant 1	0610011J09Rik, AI256840, CROC-1, CROC1, D7Bwg1382e, UEV-1
H01	Mm.3317	NM_010368	Gusb	Glucuronidase, beta	AI747421, Gur, Gus, Gus-r, Gus-s, Gus-t, Gus-u, Gut, asd, g
H02	Mm.299381	NM_013556	Hprt	Hypoxanthine guanine phosphoribosyl transferase	C81579, HPGRT, Hprt1
H03	Mm.2180	NM_008302	Hsp90ab1	Heat shock protein 90 alpha (cytosolic), class B member 1	90kDa, AL022974, C81438, Hsp84, Hsp84-1, Hsp90, Hspcb
H04	Mm.304088	NM_008084	Gapdh	Glyceraldehyde-3-phosphate dehydrogenase	Gapd
H05	Mm.391967	NM_007393	Actb	Actin, beta	Actx, E430023M04Rik, beta-actin
H06	N/A	SA_00106	MGDC	Mouse Genomic DNA Contamination	MIGX1B
H07	N/A	SA_00104	RTC	Reverse Transcription Control	RTC
H08	N/A	SA_00104	RTC	Reverse Transcription Control	RTC
H09	N/A	SA_00104	RTC	Reverse Transcription Control	RTC
H10	N/A	SA_00103	PPC	Positive PCR Control	PPC
H11	N/A	SA_00103	PPC	Positive PCR Control	PPC
H12	N/A	SA_00103	PPC	Positive PCR Control	PPC

4.3 Results

4.3.1 Investigating the Role of Apoptosis in TLR3-Mediated SMG Dysfunction

Intraperitoneal priming of mice with the pan caspase inhibitor; z-VAD-fmk was undertaken to inhibit apoptosis and assess the role of TLR-3 mediated cell death in the SMG hypofunction perceived. The SMG flow rates from the z-VAD-treated mice showed an extremely significant recovery compared to the approximate loss of secretion perceived in the non-treated animals, 9hrs post poly (I:C) introduction, figure 4.1.

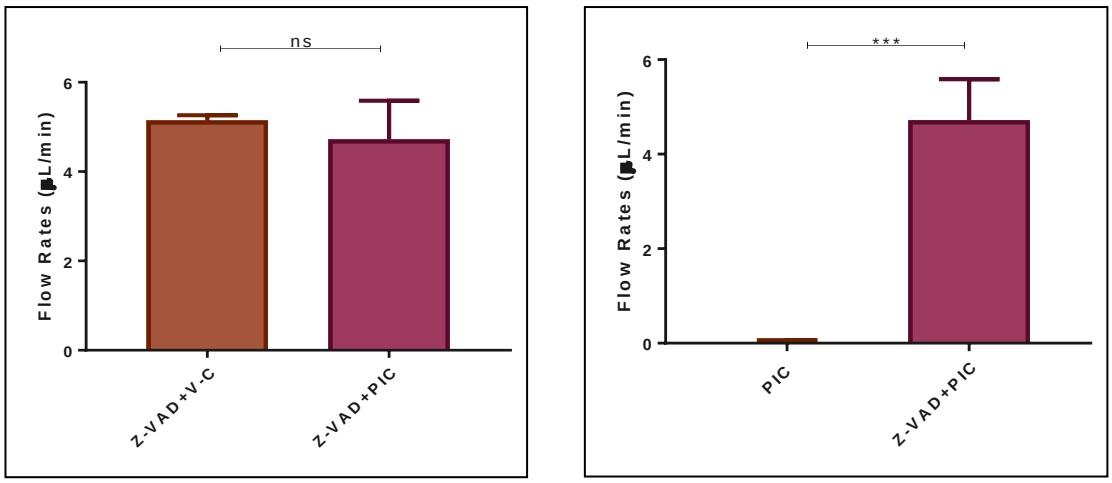

Paired t test	
P value	0.4587
P value summary	ns

Unpaired t test	
P value	0.0007
P value summary	***

Figure 4.1 **SMG flow rates in response to z-VAD-fmk treatment.**
Data represent the mean ± SD SMG flow rates of the control (V-C: trypan blue and saline) and poly (I:C) (PIC)-injected glands from mice treated and non-treated with z-VAD-fmk, 9 hrs post poly (I:C). An extremely significant recovery was perceived in the SMGs from mice which received a single i.p injection of z-VAD-fmk, 30 mins before the poly (I:C) retrograde injection. Ns: non-significant, ***p≤0.001

Western blot analysis and immunohistochemistry were performed to validate the efficient inhibition of apoptosis by z-VAD-fmk and correlate this to the preserved SMG functions. Surprisingly results obtained from these experiments revealed the incomplete elimination of the cleaved csp-3 immunolabelled apoptotic cells in the SMGs, despite priming the mice with the pan caspase inhibitor, figure 4.2.

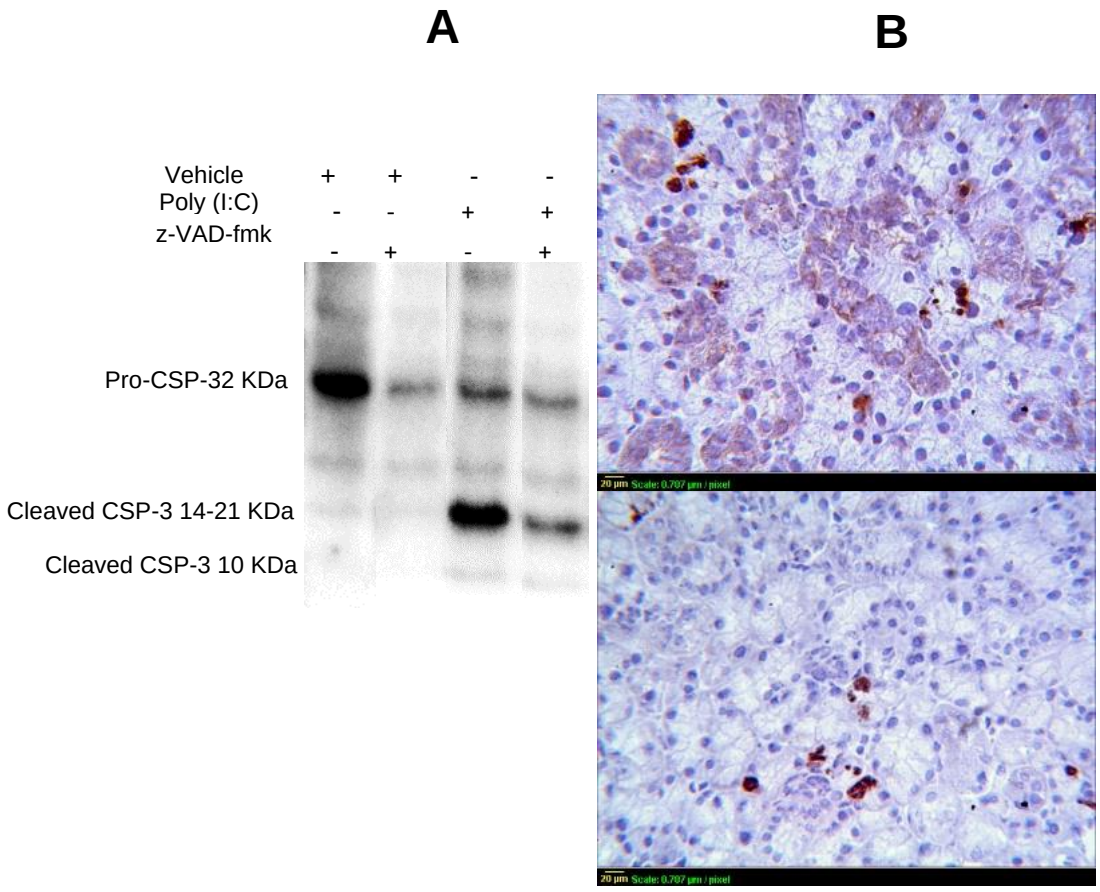

Figure 4.2 **Caspase-3 expression in the SMGs from z-VAD-fmk treated and non-treated mice**.
A: Western blot analysis demonstrated that the control vehicle-injected SMG tissue extracts revealed the 32 KD pro-caspase 3 only and lack of its proteolytic cleavage. Poly (I:C) injection induced apoptosis in the SMGs and the pro and cleaved bands were clearly seen. The glands from mice primed with z-VAD-fmk prior to poly (I:C) injection exhibited incomplete inhibition of apoptosis which was demonstrated by expression of the cleaved csp-3 positive band. **B:** Immunohistochemically, cleaved caspase-3 immunolabelled cells were still clearly depicted in the in acini of SMG tissue sections from z-VAD-primed mice. Original magnification= 25x.

4.3.2 Investigating Off-Target Effects of z-VAD-fmk

These unexpected results prompted us to broadly investigate the likely off-target therapeutic effect of the pan caspase inhibitor, z-VAD-fmk, which protected the viral mimic-infected SMGs. To provisionally assess the histomorphology of the tissues, H&E sections from SMGs of the z-VAD-treated and non-treated mice were microscopically examined. Surprisingly, the viral mimic-infected glands from the z-VAD treated mice were inflammation- and edema-free; two hallmark features which were widely observed in the poly (I:C) injected glands lacking priming with the caspase inhibitor, figure 4.3. Although we have previously shown that loss of function in the current model is independent of neutrophil infiltration, we aimed at confirming the unpredictable anti-inflammatory effect which z-VAD conferred on the viral mimic-infected glands by labelling these tissues with MPO and comparing the results to those perceived in the dsRNA/TLR3 inhibition model. Immunohistochemistry similarly confirmed the H&E results, whereby the SMGs from the z-VAD-treated mice displayed broad MPO negative immunoreactivity, parallel to that seen in the TLR3-inhibited glands, figure 4.3.

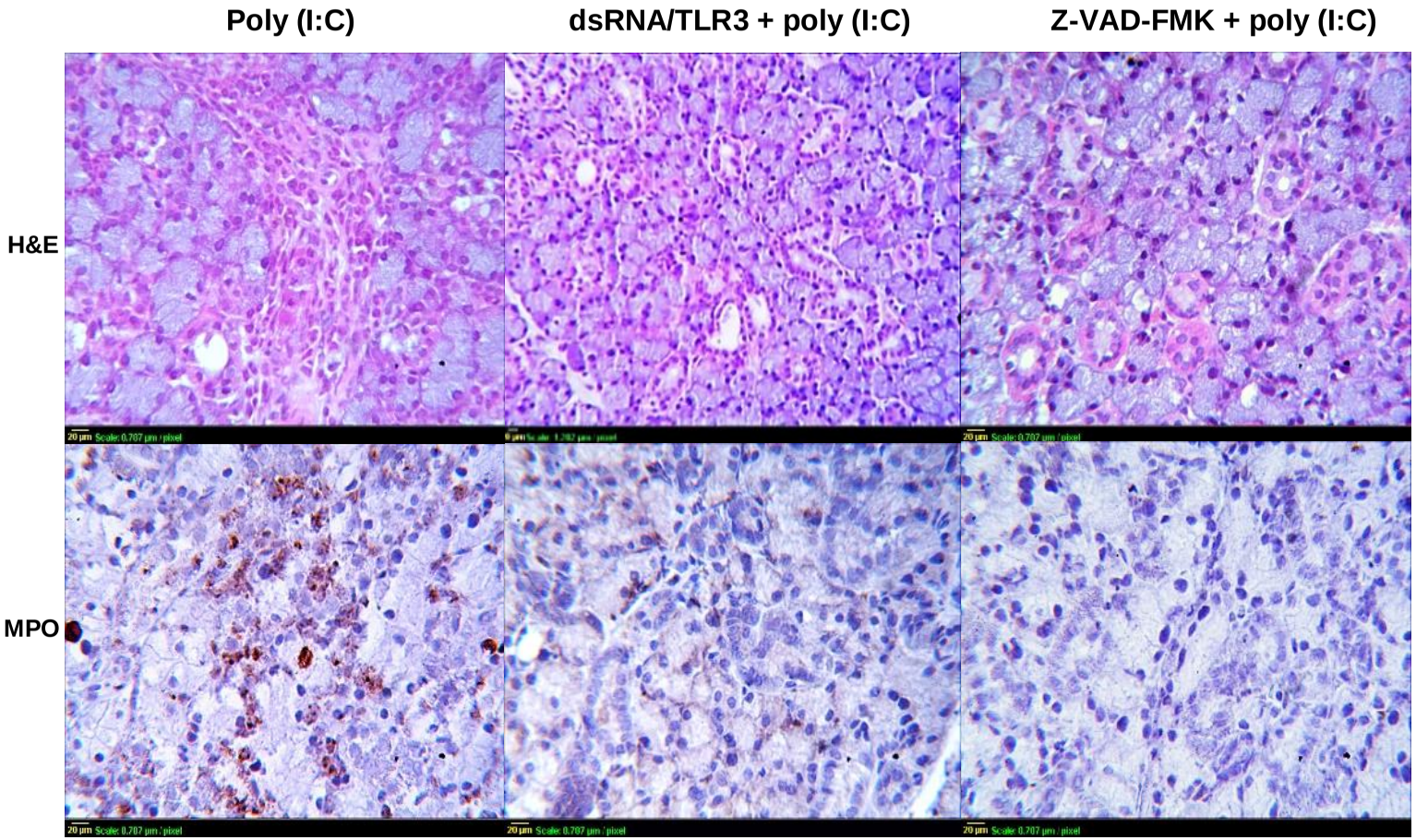

Figure 4.3 **H&E sections and MPO immunostaining of poly (I:C) injected SMGs.**
In the z-VAD-fmk group, absence of infiltrating inflammatory cells was clearly seen in vast areas of the tissue sections compared to the glands from mice which didn't receive the drug.

Based on these finding, we hypothesized that z-VAD which can efficiently inhibit cathepsin activity (Schotte et al., 1999, Rozman-Pungercar et al., 2003), might have protected the viral mimic induced SMG dysfunction via interfering with the cathepsin-mediated proteolytic processing of TLR3 (Garcia-Cattaneo et al., 2012) and subsequent generation of the C-terminal cleaved isoform.

A straightforward verification of our hypothesis came from probing gland homogenates from mice pre-treated with z-VAD with the TLR3 C-terminal antibody and comparing the results with the glands which received the viral mimic only. Figure 4.4 illustrates the extremely significant, declined expression of the cleaved form of the receptor in the glands of the z-VAD-treated group, in contrast to its upregulated expression in the non-treated mice which received poly (I:C) only.

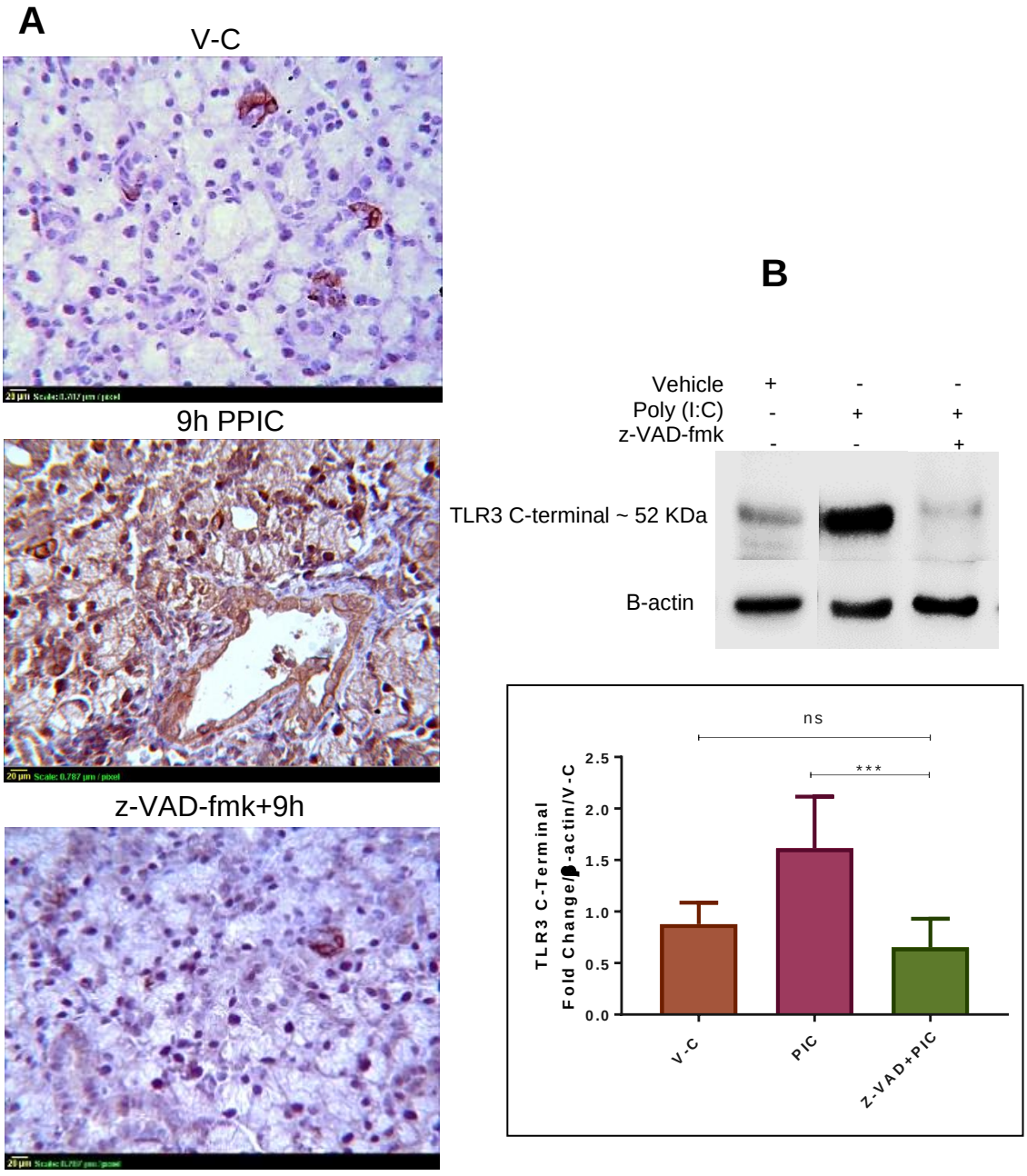

ANOVA summary	
P value	0.0002
P value summary	***

Sidak's multiple comparisons test	Summary	P Value
V-C vs. z-VAD+PIC	ns	0.4280
PIC vs. z-VAD+PIC	***	0.0002

Figure 4.4 **TLR3 C-terminal immunohistochemistry and western blots following z-VAD-fmk treatment.**
A: Excessive tissue upregulation of TLR3 C-terminal in the ducts and acini following poly (I:C) exposure, and its remarkable retraction when mice were pre-treated with z-VAD-fmk. **B**: TLR3 expression was calculated as TLR3/β-actin ratio fold change from control saline injected glands. ANOVA showed an extremely significant reduction of the receptor C-terminal isoform in the z-VAD treated group following poly (I:C) exposure, which was retracted to a level non-significant from that expressed in the control vehicle glands. Data are representative of three independent experiments for each tested group. ns: non-significant, ***p≤0.001.

4.3.3 Mapping Poly (I:C)-Induced Innate Immune Signals Following z-VAD-fmk

Mouse RT_2 Profiler™ TLR PCR array was used to provide wide-ranging analysis of TLR-related, innate immune adaptor and effector genes and downstream signalling pathways. We analysed a total of 84 genes in the SMGs, 6 hrs post vehicle and poly (I:C) injection, in the z-VAD-fmk treated and non-treated mice. Unpredictably, z-VAD-fmk damped the expression level of all TLR-related genes, compared to the extensive transcriptional upregulation seen in the SMGs which received the poly (I:C) only, figure 4.5

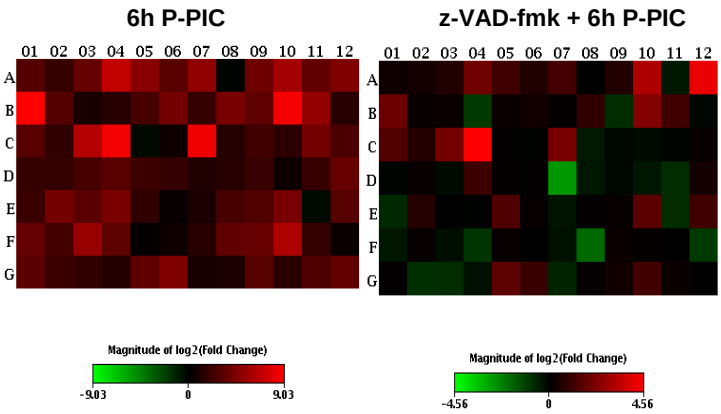

6 hrs P-PIC

Layout	1	2	3	4	5	6	7	8	9	10	11	12
A	Agfg1	Btk	Casp8	Ccl2	Cd14	Cd80	Cd86	Cebpb	Chuk	Clec4e	Csf2	Csf3
	7.75	3.59	11.84	119.02	28.94	8.78	33.59	-1.12	15.08	55.91	10.7	22.86
B	Cxcl10	Eif2ak2	Elk1	Fadd	Fos	Hmgb1	Hras	Hspa1a	Hspd1	Ifnb1	Ifng	Ikbkb
	522.76	8	1.84	2.6	5.46	16.51	3.57	19.16	9.85	445.72	37.01	2.53
C	Il10	Il12a	Il1a	Il1b	Il1r1	Il2	Il6	Il6ra	Irak1	Irak2	Irf1	Irf3
	8.2	3.05	82.71	396.18	-1.27	1.38	364.56	2.43	4.72	2.9	16.8	6.02
D	Jun	Lta	Ly86	Ly96	Map2k3	Map2k4	Map3k1	Map3k7	Mapk8	Mapk8ip3	Mapk9	Muc13
	3.56	3.67	5.66	8.78	4.45	3.59	2.22	2.57	3.88	1.38	3.84	12.04
E	Myd88	Nfkb1	Nfkb2	Nfkbia	Nfkbib	Nfkbil1	Nfrkb	Nr2c2	Peli1	Pglyrp1	Ppara	Ptgs2
	4.08	17.15	9.13	19.7	3.32	1.24	1.93	5.62	7.16	18.83	-1.27	8.43
F	Rel	Rela	Ripk2	Tbk1	Ticam1	Ticam2	Tirap	Tlr1	Tlr2	Tlr3	Tlr4	Tlr5
	11.55	4.99	41.36	9.71	1.09	1.39	2.52	10.37	12.34	75.06	3.61	1.27
G	Tlr6	Tlr7	Tlr8	Tlr9	Tnf	Tnfaip3	Tnfrsf1a	Tollip	Tradd	Traf6	Ube2n	Ube2v1
	9.32	4.07	3.29	2.32	10.2	23.43	1.82	1.9	8.31	2.69	6.77	11.27

z-VAD- + 6 hrs P-PIC

Layout	1	2	3	4	5	6	7	8	9	10	11	12
A	Agfg1	Btk	Casp8	Ccl2	Cd14	Cd80	Cd86	Cebpb	Chuk	Clec4e	Csf2	Csf3
	1.2	1.27	1.48	4.03	2.17	1.48	2.33	-1.01	1.54	8.94	-1.34	18.51
B	Cxcl10	Eif2ak2	Elk1	Fadd	Fos	Hmgb1	Hras	Hspa1a	Hspd1	Ifnb1	Ifng	Ikbkb
	3.78	1.1	1.12	-2.04	1.13	1.26	1.06	1.82	-1.71	5.19	2.2	-1.07
C	Il10	Il12a	Il1a	Il1b	Il1r1	Il2	Il6	Il6ra	Irak1	Irak2	Irf1	Irf3
	2.7	1.53	4.2	23.59	1.01	-1.02	4.58	-1.34	-1.08	-1.13	-1.05	1.11
D	Jun	Lta	Ly86	Ly96	Map2k3	Map2k4	Map3k1	Map3k7	Mapk8	Mapk8ip3	Mapk9	Muc13
	-1.05	1.12	-1.12	2.13	1.06	1.02	-6.63	-1.31	-1.07	-1.32	-1.72	1.29
E	Myd88	Nfkb1	Nfkb2	Nfkbia	Nfkbib	Nfkbil1	Nfrkb	Nr2c2	Peli1	Pglyrp1	Ppara	Ptgs2
	-1.62	1.55	1	-1.02	2.62	1.09	-1.24	1.02	1.06	3.05	-1.73	2.19
F	Rel	Rela	Ripk2	Tbk1	Ticam1	Ticam2	Tirap	Tlr1	Tlr2	Tlr3	Tlr4	Tlr5
	-1.3	1.08	-1.18	-1.9	1.12	1.01	-1.22	-3.72	1.13	1.04	1	-2.03
G	Tlr6	Tlr7	Tlr8	Tlr9	Tnf	Tnfaip3	Tnfrsf1a	Tollip	Tradd	Traf6	Ube2n	Ube2v1
	1.03	-1.76	-1.72	-1.22	3.13	2	-1.55	1.08	1.25	2.24	1.13	1.01

Figure 4.5 **Heat map of TLR PCR array.**
Differential expression of 84 genes in SMGs stimulated with poly (I:C), normalized to the control contralateral glands and GUSB housekeeping gene in case of z-VAD non-treated and β-actin in z-VAD treated mice. The fluorescence range from high (red) to low (green) is indicated by the coloured bar and reflects the degree of fluorescence intensity/gene expression. Note the overall decline in the SMG innate immune-related genes following priming the mice with z-VAD-fmk and interference with neo-generation of the TLR3 C-terminal.

Next, to confirm this novel, off-target role played by z-VAD-fmk in controlling innate immunity following SMG infection with a viral mimic, qRT-PCR was carried out to further analyse the mRNA expression levels of dsRNA-response genes and pro-inflammatory cytokines in the SMGs of z-VAD-fmk treated mice. Bar charts in figure 4.6 and 4.7 clearly demonstrate the overall significant decline in tested genes in the z-VAD-fmk group, compared to the poly (I:C)-upregulated responses seen in the glands from non-treated mice, all normalized to the 'relevant' vehicle injected control glands and GAPDH housekeeping gene (for the glands from z-VAD-fmk treated mice) and HPRT (in the glands which received poly (I:C) only).

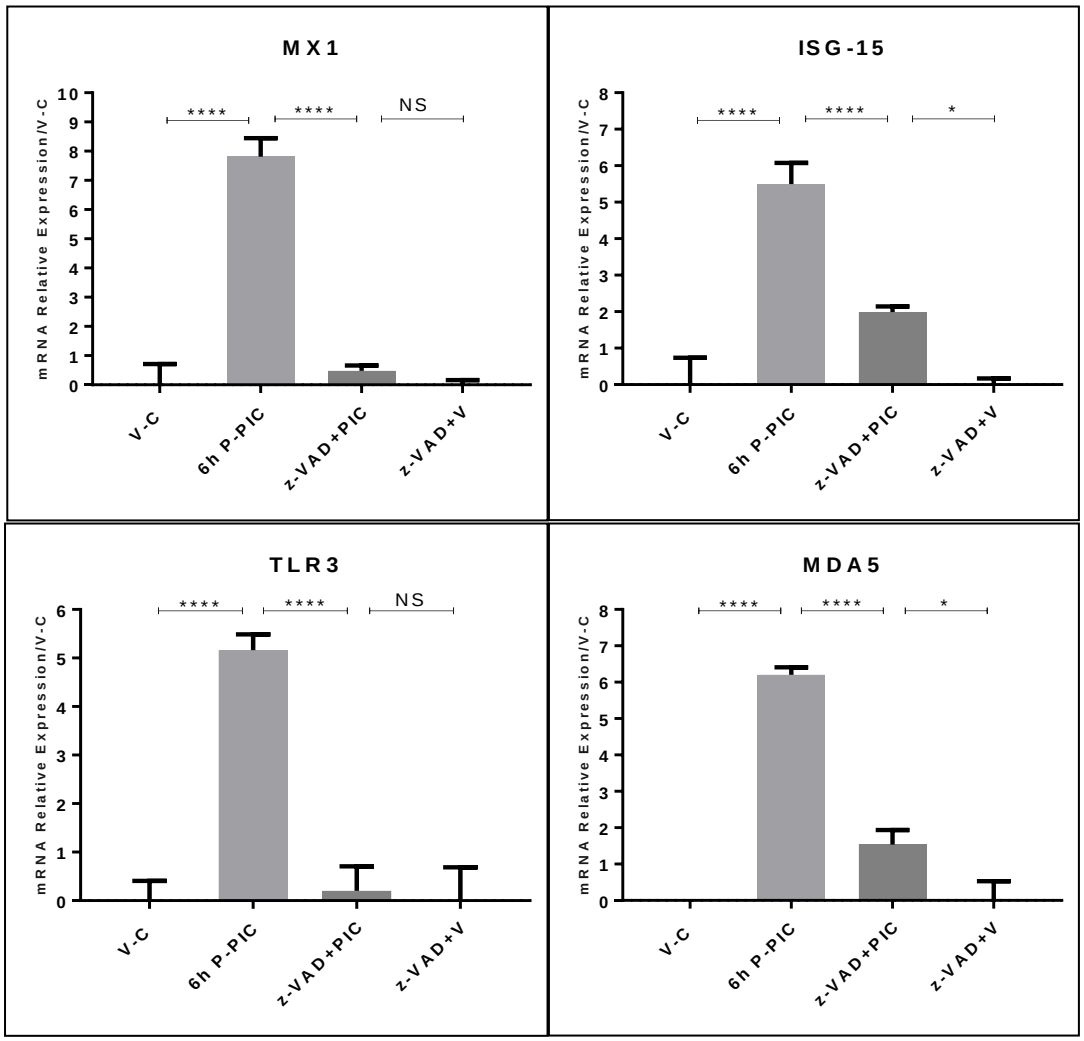

ANOVA	ISG15	MX1	TLR3	MDA5
P value	<0.0001	<0.0001	<0.0001	<0.0001
P value summary	****	****	****	****

Sidak's multiple comparisons test	MX1		ISG15		TLR3		MDA5	
V-C vs. 6h P-PIC	****	<0.0001	****	<0.0001	****	<0.0001	****	<0.0001
6h P-PIC vs. z-VAD+PIC	****	<0.0001	****	<0.0001	****	<0.0001	****	<0.0001
z-VAD+PIC vs. z-VAD+V	ns	0.8738	*	0.0191	ns	0.9886	*	0.0116

Figure 4.6 **mRNA Expression of dsRNA response genes: antiviral genes; MX1 and ISG15 as well as the dsRNA sensors; TLR3 and MDA5.**
SMGs from z-VAD-fmk-treated animals showed either non-significant (TLR3 and MX1) or mild activation (MDA5 and ISG15) of the dsRNA response genes compared to the extremely significant upregulation of these genes, 6hrs following poly (I:C) (6h P-PIC) in the glands from z-VAD-fmk non-treated animals. Data represents means ± SEM (n=3). ns: p>0.05, *P≤0.05, ****p≤0.0001.

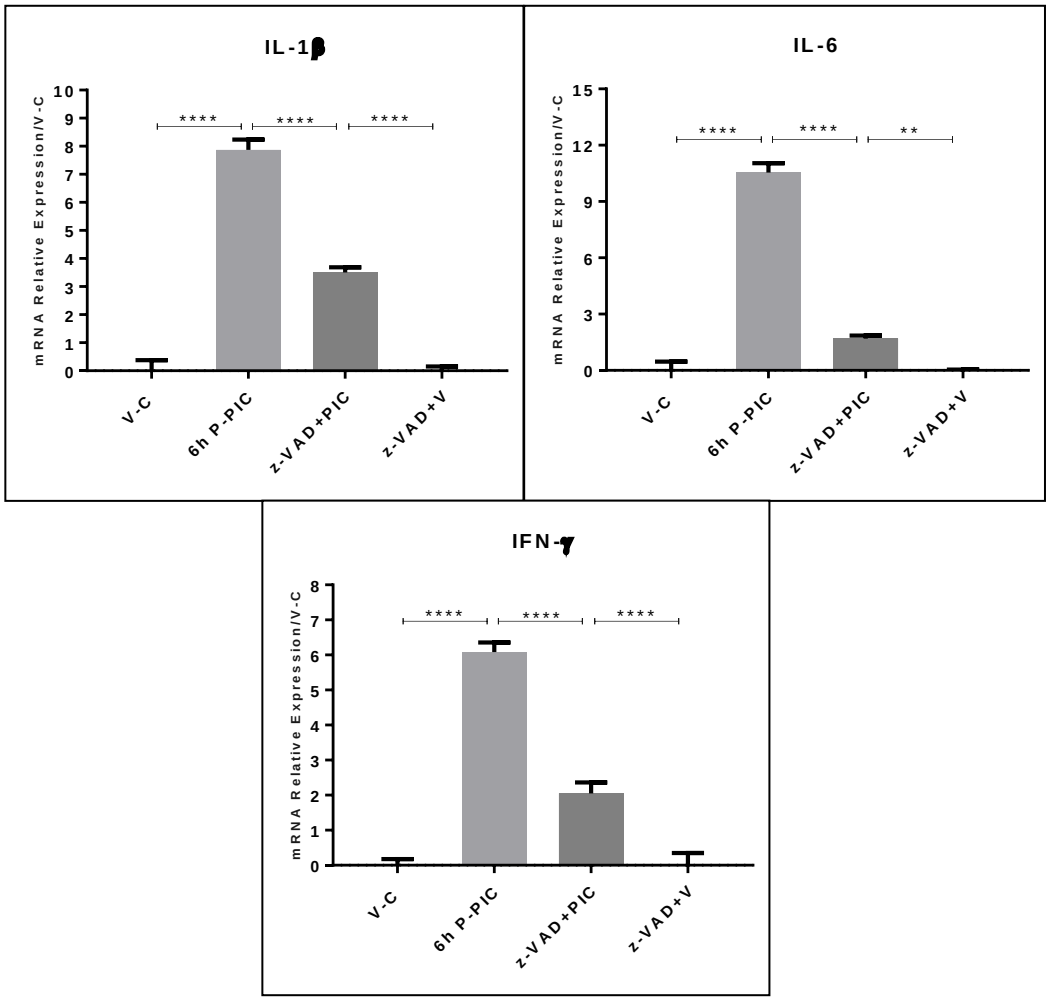

ANOVA	IL-1B	IL-6	IFN-G
P value	<0.0001	<0.0001	<0.0001
P value summary	****	****	****

Sidak's multiple comparisons test

	IL-1B		IL-6		IFN-G	
V-C vs. 6h P-PIC	****	<0.0001	****	<0.0001	****	<0.0001
6h P-PIC vs. z-VAD+PIC	****	<0.0001	****	<0.0001	****	<0.0001
z-VAD+PIC vs. z-VAD+V	****	<0.0001	**	0.0058	****	<0.0001

Figure 4.7 **mRNA Expression of genes encoding pro-inflammatory cytokines; IL-1β, IL-6 and IFN-γ.**
z-VAD-fmk remarkably downregulated the pro-inflammatory cytokine response perceived 6 hrs following poly (I:C) (6h-P-PIC) injection. Data represents means ± SEM (n=3). **P≤0.01, ****p≤0.0001

To confirm the PCR outcome which identified a novel non-specific immune regulatory role of the cysteine protease inhibitor; z-VAD-fmk, tissue sections were immunolabelled with cytokines, which have been prominently upregulated in response to local poly (I:C) injection. Figure 4.8 clearly demonstrates an overall reduction in the immunhohistochemical expression of tested cytokines in tissues from mice primed with z-VAD-fmk in contrast to the non-primed ones. Interestingly, in the SMGs from z-VAD-treated mice, traces of IFN-β, Cox2 and IFN-γ cytokines were perceived in the glandular parenchymal tissues, which parallels their minimal transcriptional activation recorded by the RT_2 profiler arrays (figure 4.5). Conversely, NF-κB nuclear translocation and iNOS immunoexpression were completely inhibited in the protected SMGs from mice primed with z-VAD-fmk.

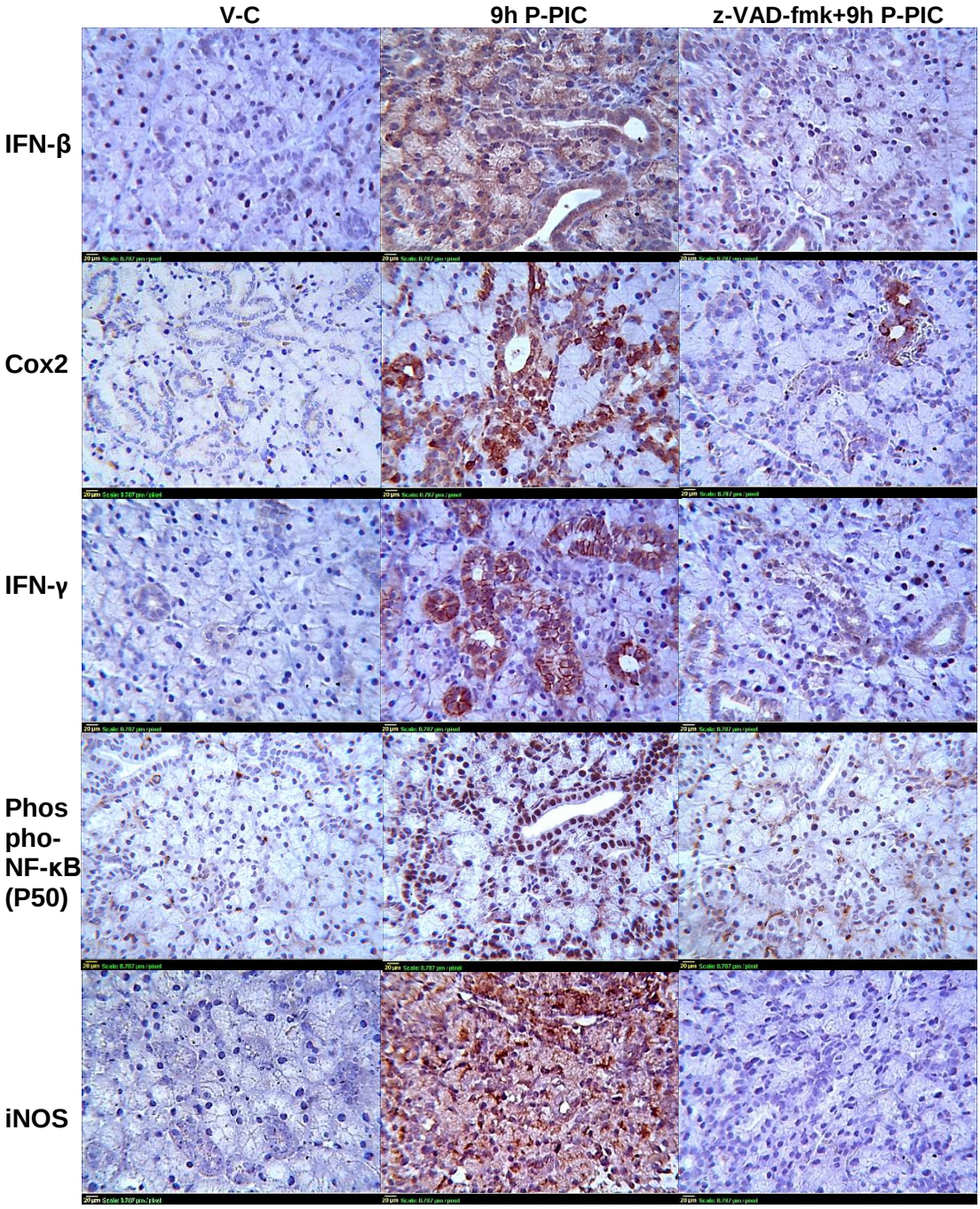

Figure 4.8 **Immunohistochemical analysis of pro-inflammatory cytokines expression in the control-vehicle and poly (I:C) injected SMGs of the z-VAD-fmk treated and non-treated mice.**
Note the remarkably reduced protein expression of IFN-β, Cox2 and IFN-γ in response to z-VAD priming. On the contrary, NF-κB nuclear translocation which was abundantly seen 9h post poly (I:C) (insets) and extensive iNOS immunoexpression, were completely inhibited to levels comparable to the control glands. Original magnification= 25x.

4.4 Discussion

In the current chapter, a novel mechanism was reported, whereby the pan caspase inhibitor z-VAD-fmk: (i) restricted TLR3 C-terminal neo-generation, (ii) limited the innate immune responses and (iii) guarded against the TLR3-induced loss of SMG function. Initial experiments to investigate the role of apoptosis in the current dysfunction model, revealed two contradictory results: priming mice with the pan caspase inhibitor efficiently preserved saliva secretion, despite of the incomplete elimination of cleaved caspase 3-positive signal.

Key players involved in apoptosis are the eight cysteine aspartyl proteases caspase- 2, -3, -6, -7, -8, -9, -10, -12 (Earnshaw et al., 1999). Typically, the extrinsic apoptotic signalling pathway mediated by caspase 8 (Donepudi et al., 2003) as well as the intrinsic pathway mediated by caspase 9 (Wang, 2001), converge into cleavage of caspase 3, which then triggers the appearance of the apoptotic morphology, particularly DNA/nuclear fragmentation (Krammer, 2000). In the current model, the persistent cleaved caspase 3 positive signal in the presence of z-VAD-fmk, can be attributed to the dose of the pan caspase inhibitor, which at many instances turn out to be highly unspecific at the concentrations widely used to test programmed cell death (Schotte et al., 1999). Also, previous studies have suggested non-caspase, serine proteases, which might be active under cellular stress conditions, as upstream prerequisites to caspase-3 processing as well as cytochrome c release and apoptosis, even in the presence of z-VAD-fmk (Egger et al., 2003). Finally, Marsden et al., proposed that a yet unknown z-VAD-fmk -insensitive caspase acting aside or upstream of mitochondria was responsible for intrinsic cell death, in the presence of z-VAD-fmk (Marsden et al., 2002).

Attempts to broadly investigate the unexpected rescuing effect of z-VAD-fmk, revealed depletion of MPO positive cells in the poly (I:C) injected glands, similar to what was demonstrated in the TLR3/dsRNA inhibition model. The overlapping of these findings, suggested that the pan caspase inhibitor has unexpectedly targeted TLR3 activation and inhibited its downstream inflammatory response. Cathepsin B has already been considered an essential component in TLR3 signalling, by proteolytically processing TLR3 to generate the functional C-terminal form of the receptor, crucial for signalling (Garcia-Cattaneo et al., 2012, Murakami et al., 2014, Toscano et al., 2013). Indeed, it has been shown that z-VAD-fmk concentrations that are commonly used to reveal a role of caspases, can potently bind and inhibit cysteine proteases of the cathepsin family, mainly Cathepsin B (Schotte et al., 1999). The reason for this non-specific binding is unclear, given that the structures and catalytic sites of caspases do not resemble those of cathepsin B (Chou et al., 1997, Podobnik et al., 1997). However, cathepsins possess broad substrate specificity that can explain its proposed inhibition by z-VAD-fmk (Turk et al., 2001). By considering the previously documented z-VAD-fmk 'off-target' effects (Satoh et al., 2013, Rozman-Pungercar et al., 2003, Wu et al., 2011, Schotte et al., 1999) and its non-specific inhibition of cathepsins (Schotte et al., 1999), we hypothesized that z-VAD-fmk may have inhibited TLR3-driven immune responses and subsequent SMG dysfunction by interfering with cathepsin-mediated TLR3 cleavage in acidic compartments, figure 4.9.

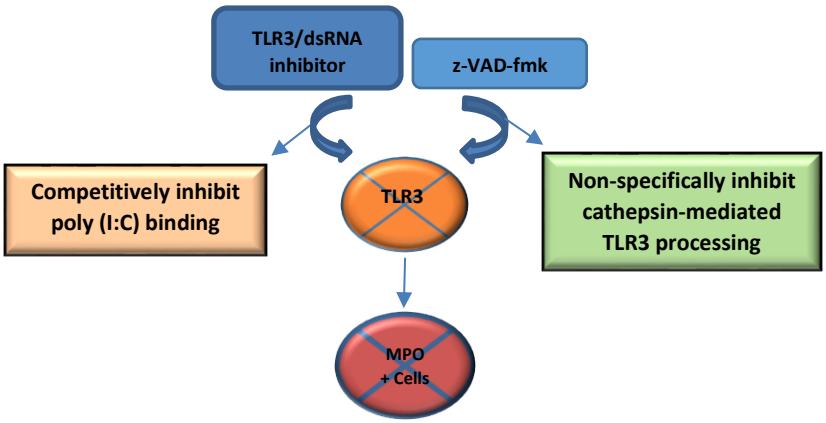

Figure 4.9 Hypothesis to explain z-VAD-fmk therapeutic and anti-inflammatory effects in the acute viral SMG dysfunction model.

Cysteine cathepsins constitute the largest cathepsin family, including 11 members; cathepsins B, C, F, H, K, L, O, S, W, V and X (Rawlings et al., 2012). They are synthesized as inactive precursors that are normally activated in the acidic environment of lysosomes. Although, cathepsin B inhibition by z-VAD-fmk has not been comprehensively verified in the current model, immunoblotting of the SMG homogenates from the z-VAD-fmk treated group revealed that the pan caspase inhibitor had efficiently inhibited the neo-synthesis of TLR3 C-terminal fragment and accounted for a novel anti-viral, regulatory role of this drug.

To overcome the constrains of large-scale experimental analysis of the complex innate immune responses to TLR3, and in the meantime broadly investigate the novel z-VAD-fmk immune regulatory role, we used an array of 84 genes encoding TLR-related adaptor and effector molecules. Six hrs post its infusion, poly (I:C) predictably upregulated TLR3 expression, as well as IFN-β and acute pro-inflammatory cytokine genes; IL-1α, IL-1β, IL-6, TNF-α and IFN-γ.

In addition, we identified CXCL10 (interferon gamma-induced protein 10, IP-10), a chemokine that promotes leukocyte trafficking (Muller et al., 2010) and directly contributes to the pathogenesis of excessive neutrophil-mediated inflammation (Ichikawa et al., 2013). Alongside its protective role during viral infections, CXCL10 may enhance the severity of these types of infections and cause apoptosis (Sui et al., 2004) as well as calcium dysregulation (Sui et al., 2006). Other several interesting groups of genes showed remarkable upregulation in the TLR array, example the CD14 which has been shown to bind poly (I:C) at the cell surface (Lee et al., 2006). In addition, HMGB1 and the Hspa1a genes were upregulated in the current model in response to poly (I:C), possibly due to DAMPs released subsequent to TLR-3 induced apoptosis and necroptosis (Cunningham et al., 2004, Wang and Carmichael, 2004, Leadbetter et al., 2002). Finally, previous studies reported that components of the TLR2 and NOD2 signalling cascade had been significantly upregulated upon monocytes recruitment into acutely inflamed tissues (Zigmond et al., 2012), which may justify the upregulation of the TLR2-MyD88-NOD2-RIPK2 signalling axis in the current acute viral mimic model.

The pattern of innate, TLR-related gene transcription in the SMGs following poly (I:C) injection shifted towards baseline and declined levels when mice were primed with z-VAD-fmk. Besides, the immunohistochemical analysis, revealed that the poly (I:C)-induced NF-κB nuclear translocation and extensive protein expression of IFN-β, IFN-G, Cox2 and iNOS, were retracted or completely inhibited in response to priming with z-VAD-fmk. These results clearly signify the inhibitory effect which the pan caspase inhibitor had on TLR3 downstream signalling.

In this regard, it is worth noting that that protease inhibitors have been used successfully to dampen inflammation during HIV and HCV infections (Equils et al., 2004). Their therapeutic ability was shown to rely on the interaction with the proteasome, which is important for degradation of inhibitor κB, restricting NF-κB nuclear translocation, hence, its activation.

Although much has been learned on the biochemical and cell biological characteristics of TLRs, the integration of their signalling pathways into the trafficking network, under inflammatory conditions, remains to be defined. Endosomal cathepsins have been documented to cleave TLR9, as a prerequisite to its activation (Ewald et al., 2008, Park et al., 2008, Sepulveda et al., 2009). However, newly synthesized TLR9 is retained in the ER at steady state until exposed to CpG DNA ligand, which promotes its trafficking to endosomes (Fukui et al., 2009), where it is subjected to cathepsin-mediated proteolytic processing to initiate signalling (Ewald et al., 2011, Park et al., 2008). In contrast, in vitro experiments have shown that: in the absence of ligand, TLR3 is transported to the endosome via a classical-secretion pathway, where cleavage occurs and a pool of cleaved C-terminal fragment accumulates there, ready to signal (Garcia-Cattaneo et al., 2012). Since the antibody against the TLR3 C-terminus has detected minimal expression of this fragment in the SMGs of the z-VAD treated group, this residual positivity may probably correspond to the control cellular pools of the basally-cleaved TLR3.

In the current study, incomplete inhibition of the innate immune signals has been observed in the SMGs from mice primed with z-VAD-fmk. These signals can be attributed either to the cytosolic RLRs or the initial innate immune signals which took place following ligation of basal TLR3.

Also, these detected signals may have been truncated by z-VAD-fmk, which interrupted TLR-3 neo-synthesis and propagation of its downstream responses. Our results undoubtedly highlight, the possibility of fine-tuning innate immune responses using z-VAD-fmk or similar protease inhibitor drugs in vivo, which can provide promising clues into developing therapeutic approaches against SG viral infections.

Finally, functional analysis of the z-VAD-fmk treated SMGs revealed the therapeutic effects that can be achieved by z-VAD-fmk in acute SG dysfunctions. Based on cytokine profiling of the protected glands following TLR3 inhibition and z-VAD-fmk treatment, we observed that functional rescue in both models paralleled complete blocking of the potent pro-inflammatory cytokine, iNOS. Given this recurrent finding and the injurious role played by iNOS in salivary gland injury and dysfunction (de la Cal et al., 2006, Takeda et al., 2003a, Hanaue et al., 2007, Konttinen et al., 1997), we hypothesized the potential involvement of this innate immune cytokine in the TLR-3 mediated loss of function. Therefore, in the next chapter, iNOS expression and its potential injurious effects in the acute viral SMG model will be comprehensively characterized.

Chapter 5

Injurious Contribution of Inducible Nitric Oxide Synthase in the Acute SMG Dysfunction Model

5.1 Introduction

In a previous chapter of this thesis, the synthetic dsRNA analogue has induced SMG injury and loss of function, in TLR3-dependent manner. In addition, it was demonstrated that the functionally-preserved, TLR3-inhibited SMGs (in the dsRNA/TLR3 and z-VAD-fmk models) revealed loss of the extensively upregulated pro-inflammatory cytokine; iNOS. Nitric oxide synthase (NOS) is the enzyme responsible for converting L-arginine into nitric oxide in the presence of O_2. Three isoforms of NOS are known in mammals: two constitutive isoforms (NOS1 or nNOS, produced by neurons; NOS3 or eNOS, produced by endothelial cells) and one inducible isoform (iNOS or NOS2) (Knowles and Moncada, 1994). In contrast to constitutive NOS isoforms which produce nitric oxide (NO) within seconds, with direct and short acting activities, inducible NOS produces very large, toxic amounts of NO in a sustained manner (Salvemini et al., 2003), which plays regulatory roles at nearly each phase of the inflammatory response (Guzik et al., 2003).

iNOS expression can be induced by a wide range of stimuli, such as microbial products and cytokines. Signal transduction via MyD88 or TRIF converge in the activation of the transcription factor NF-κB, which upregulates iNOS transcription. Cytokines such as IL-1β, which also activates the signalling pathway of MyD88 and IRAK and TNF-α also induces the production of iNOS by activating NF-κB (Uehara et al., 2015). Additional participating transcription factors include AP-1, STAT1a and IRF-1 (Tripathi et al., 2007) (figure 5.1).

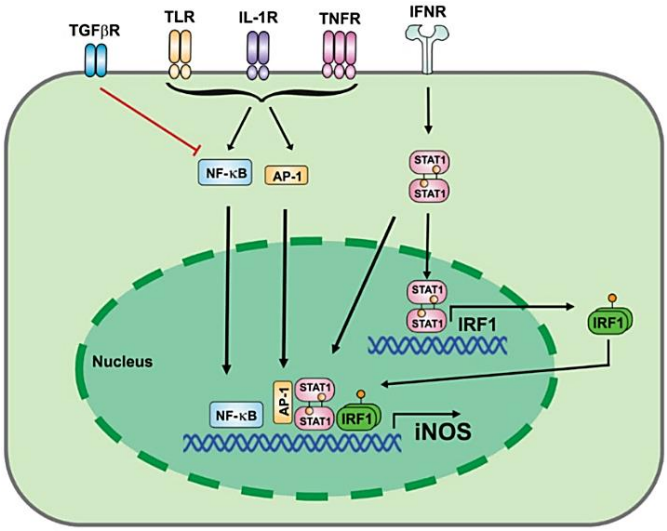

Figure 5.1 **Overview of iNOS induction by TLR agonists and cytokines**.
iNOS expression can be induced and/or potentiated by PAMPs, DAMPs, and cytokines. TLR, IL-1R, and TNFR signalling induce the activation of AP-1 and NF-kB, the main transcription factor involved in iNOS expression. Further, IFN-R activates STAT1, which in turn can directly promote iNOS transcription and alternatively promote the synthesis of interferon regulatory factor 1 (IRF1), another transcription factor that positively regulates iNOS transcription. In turn, TGF-β inhibits NF-κB activation thus suppressing iNOS expression (Uehara et al., 2015)

A very likely event during the inflammatory response is the side by side generation of large amounts of iNOS-driven NO and superoxide anion (O^{2-}), where the reaction of these unstable molecules will yield a more stable and more potent cytotoxic peroxynitrite (ONOO-) (Channon and Guzik, 2002, Guzik et al., 2002) (figure 5.2). No enzyme is required to form peroxynitrite because no enzyme can possibly catalyze any reaction as fast. Consequently, the kinetics of the reaction of superoxide with NO make the formation of peroxynitrite inevitable in vivo (Pacher et al., 2007).

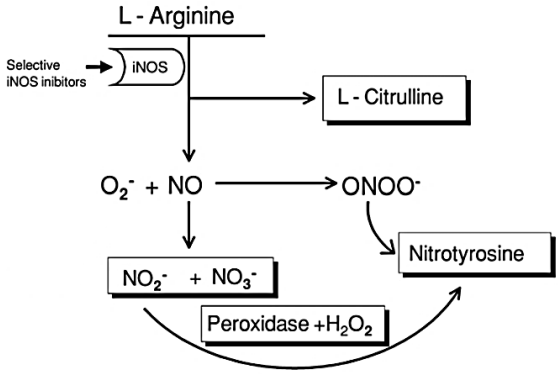

Figure 5.2 **Scheme of Nitric oxide, superoxide and the product of their reaction peroxynitrite formation.**
iNOS catalyses the oxidation of L-arginine to L-citrulline, producing NO, which combined with superoxides to yield peroxynitrite, nitrites and nitrates (Salvemini et al., 2003).

Peroxynitrite accompanies various inflammatory responses, and has been proposed to play an important role in mediating NO-related cellular injury (Szabo, 2003). Previous studies have suggested peroxynitrite-promoted modulations of cell signalling, induction of oxidative injury (Pacher et al., 2007), release of matrix metalloproteinases (MMPs) (Ichikawa et al., 2014) and nitration of tyrosine residues (Ischiropoulos, 1998). Alongside its contribution to multiple pathways of cytotoxicity (Szabo, 2003), peroxynitrite has been shown to inhibit a variety of ion pumps including calcium pumps (Klebl et al., 1998), calcium-activated potassium channels and also membrane Na+/K+ ATP-ase activity (Muriel and Sandoval, 2000). Another major aspect of peroxynitrite-dependent cytotoxicity relies on its ability to trigger lipid peroxidation in membranes (Radi et al., 1991), causing membrane permeability and fluidity changes with significant biological consequences (Richter, 1987).

The implication of iNOS (Konttinen et al., 1997) with accumulated damage from NO (Konttinen et al., 1997, Kimura-Shimmyo et al., 2002, Takeda et al., 2003a, Dawson et al., 2006) and peroxynitrite (Hanaue et al., 2007) in the loss of saliva production, have been previously reported. Experiments which investigated the effect of NO on the SG secretory function, validated desensitization of the SMG acinar cells after prolonged exposure to NO (Caulfield et al., 2009). In addition, NO has been shown to mediate Ca^{2+} disruption, either via ***tyrosine nitration*** of SERCA-ATPase (Xu et al., 1999, Viner et al., 1999) and inhibition of Ca^{2+} uptake from cytosol or ***S-nitrosylation*** of RyR (Xu et al., 1998) and excessive Ca^{2+} release to cytosol. Based on this, it has been reported that through its ability to disturb ER Ca^{2+} homeostasis (Oyadomari et al., 2002), NO can initiate the ER stress pathway (Oyadomari et al., 2001, Xu et al., 2004). Since the salivary glands' ER is involved in extensive folding, processing and trafficking of newly synthesised secretory and membrane proteins, these exocrine tissues are exceptionally sensitive to ER stress and its inhibitory impact on integral formation of key receptors, channels and transporters.

The aim of the present chapter was to determine the temporal expression and possible injurious contributions of the pro-inflammatory mediator; iNOS and its subsequent oxidant; peroxynitrite, in the SMG acute dysfunction model.

5.2 Materials & Methods

5.2.1 iNOS Inhibition Model

To investigate the possible injurious effect of iNOS on the SMG functions, we used the selective iNOS inhibitor, aminoguanidine (AG). Table 5.1 summarizes the AG doses used in the experiments of the current chapter.

Table 5-1 Aminoguanidine Hydrochloride used in in vivo injections

Mechanism	Source, Catalogue Number	Dose and Administration Protocol
Selective iNOS Inhibitor	Sigma, 396494	**For short term inhibition:** 100mg/kg i.p. AG (Tunctan et al., 1998) and 0.1 mg AG combined with poly (I:C): tissue and saliva collection after 9 hrs of poly (I:C). **For long term inhibition (MacFarlane et al., 1999)**: 2.5% AG in drinking water for 7 days. Poly (I:C) local injection in conjunction with 0.1 mg AG: tissue and saliva collection after 24 hrs of poly (I:C).

The vehicle injected control gland received: trypan blue, saline, and 0.1 mg aminoguanidine.

5.2.2 Immunohistochemistry

Paraffin-embedded SMG sections were deparaffinised, rehydrated and antigen retrieved by autoclaving with Trilogy™ as detailed in chapter 2, paragraph 2.3. After incubation with the specific primary antibodies (table 5-2), the detection was completed using the compatible host HRP-conjugated or fluorescent conjugated secondary antibodies. Nuclear and counterstaining was done with Mayer's haematoxylin or Vectashield Antifade DAPI Mounting Medium (Vector Laboratories, H-1200), respectively.

Table 5-2 Primary Antibodies Used

Antibody	Source & Catalogue Number	Host	Working Dilution
iNOS	Novus Biologicals, USA, NB300-605	Rabbit	1:1000
3-Nitrotyrosine	Millipore, 05-233	Mouse	1:1000
SERCA2 ATPase	Novus Biologicals, NBP2-20305	Rabbit	1:1000
Aquaporin 5 (AQP-5)	Santa Cruz Biotechnology, sc-9890	Goat	1:1000
Na-K- CL-Cotransporter 1 (NKCC1)	ABCAM, ab59791	Rabbit	1:6000
Muscarinic 3 Receptor (M3R)	Santa Cruz Biotechnology, sc-9108	Rabbit	1:1000
Transmembrane member 16A (TMEM16A)	ABCAM, ab53213	Rabbit	RTU 1:1
Cathepsin B (S-12)	Santa Cruz Biotechnology, sc-6493	Goat	1:1000
CD107a / LAMP-1 clone H4A3	Exbio, 10-671-C025	Mouse	1:1000
Polyclonal Goat Anti-Rabbit Immunoglobulins-HRP	Dako, P0448	Goat	1:200
Polyclonal Goat Anti-Mouse Immunoglobulins- HRP	Dako, P0447	Goat	1:100
Polyclonal Rabbit Anti-Goat Immunoglobulins/HRP	Dako, P0160	Rabbit	1:200
Goat anti-Mouse IgG (H+L) Secondary Antibody, Alexa Fluor® 594 conjugate	Thermo Fisher Scientific, A-11005	Goat	1:1000
Donkey anti-Rabbit IgG (H+L) Secondary Antibody, Alexa Fluor 488	Thermo Fisher Scientific, A-21206	Donkey	1:1000

5.2.3 Western Blotting

SMG protein extracts were electrophoresed on precast 4-2% SDS-PAGE gel and transferred to nitrocellulose membrane as detailed in chapter 2, Paragraph 2.4. Membranes were incubated with primary antibody (table 5-3), followed by application of anti-rabbit secondary antibody. Subsequently, signal development and exposure with Enhanced Chemioluminescence and ChemiDoc™ MP System were performed.

Table 5-3 List of Antibodies Used in Western Blots

Antibody	Source & Catalogue Number	Host	Working Dilution
3-Nitrotyrosine	Millipore, 05-233	Mouse	1:1000
Phospho-eIF2alpha (Ser51)	Cell Signaling Technology, 9721	Rabbit	1:1000
B-actin	Sigma, A2228	Mouse	1 µg/mL
Polyclonal Goat Anti-Rabbit Immunoglobulins-HRP	Dako, P0448	Goat	1:2000
Polyclonal Goat Anti-Mouse Immunoglobulins- HRP	Dako, P0447	Goat	1:1000

5.2.4 RTqPCR

Total RNAs isolated from SMG tissues (stored in RNAlater®) were extracted using RNeasy® Micro Kit (Qiagen) and 100 ng of extracted RNAs were reverse-transcribed in a 20 µL reaction using the iScript™ cDNA Synthesis kit. Quantitative real time PCR (qRT-PCR) was carried out as detailed in chapter 2, Paragraph 2.5. All mouse primers were synthesized by PrimerDesign™, Ltd and are listed in Table 5-4.

Table 5-4 List of Primers used

Gene	Accession Number
X-box binding protein 1 (Xbp1)	NM_013842
heat shock protein 5 (Hspa5) (BIP) (GRP 78)	NM_001163434
DNA-damage inducible transcript 3 (Ddit3) (CHOP)	NM_007837
actin, beta (Actb)	NM_007393
HPRT (Hypoxanthine guanine phosphoribosyl transferase)	NM_013556
Aquaporin 5 (AQP-5)	NM_009701.4
Na-K- CL-Cotransporter 1 (NKCC1) Solute carrier family 12, member 2 (Slc12a2)	NM_009194.3
Muscarinic 3 Receptor (M3R)	NM_033269.4
Transmembrane member 16A (TMEM16A)	NM_178642.5

5.2.5 Microplate Intracellular Calcium Assays

We developed a novel protocol for assessment of Ca^{2+} signalling in the acinar units of the control and poly (I:C)-injected SMGs after their isolation from the C57/B6 mice, using the benchtop, multi-mode, FlexStation 3. The main outline of the protocol is illustrated in figure 5.3

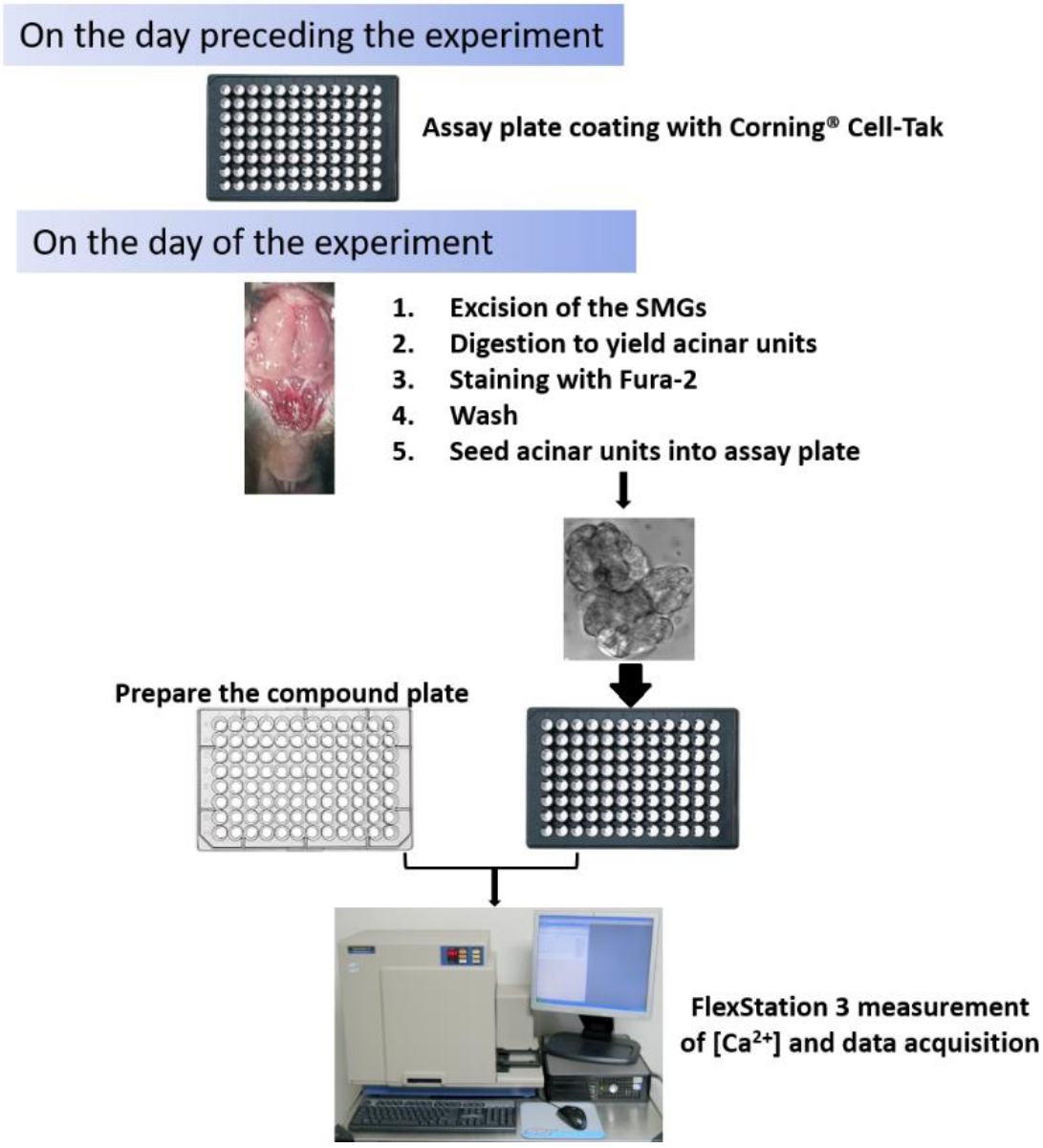

Figure 5.3 Illustrated summary of the novel protocol for measuring $[Ca^{2+}]_i$

- **Reagents**

1. HEPES (Sigma-Aldrich, Cat. # H3375).
2. NaCl (Sigma-Aldrich, Cat. # S7653).
3. KCl (BDH, AnalaR, Cat. # 101984L).
4. MgCl2 (Sigma-Aldrich, Cat. # M8266).
5. CaCl2 (Sigma-Aldrich, Cat. # C-4901).
6. Glucose (Sigma-Aldrich, Cat. # G8270).
7. Glutamine (Sigma-Aldrich, Cat. # G7513).
8. MEM Non-Essential Amino Acids Solution (100X) (Thermo Fisher Scientific (Life Technologies) Cat. # 11140050).
9. Bovine serum albumin (BSA) (Sigma-Aldrich, Cat. # A2153).
10. Collagenase from Clostridium histolyticum (Type-4 collagenase) (Sigma-Aldrich, Cat. # C5138).
11. Soybean Trypsin Inhibitor (Thermo Fisher Scientific (Life Technologies), Cat. # 17075029).
12. Corning® Cell-Tak (Fisher Scientific Ltd, Cat. # 354240).
13. $NaHCO_3$ (Sigma-Aldrich, Cat. # S6014).
14. Fura-2 AM (Molecular Probes™, Cat. # F-1201).
15. Probenecid (Sigma-Aldrich, Cat. # P8761).
16. Half-area, 96-well plates ((Fisher Scientific Ltd, Cat # 10717804).
17. Carbachol (CCh) (Santa Cruz Biotechnology, Cat. # sc-202092).
18. Ionomycin (IM) (Santa Cruz Biotechnology, Cat. # sc-3592).
19. Culture grade dimethyl sulfoxide (DMSO) (Sigma-Aldrich, Cat. # 276855).
20. Dulbecco phosphate buffered saline (DPBS) (Sigma-Aldrich, Cat. # D8662).

- **Recipes**

1. ***HEPES incubation buffer:*** **A- Ca^{2+}-containing buffer:** 20 mM HEPES, 95 mM NaCl, 4.7 mM KCl, 0.6 mM MgCl2, 1.3 mM CaCl2, 10 mM glucose, 2 mM glutamine, and 1 × minimum Eagle's medium non-essential amino acids, pH 7.4. The buffer was oxygenated for 20 minutes before use. **B: Ca^{2+}-free buffer:** prepared as previous, with the exception that 1M EGTA Ca^{2+} chelator was added and CaCl2 was omitted.
2. ***BSA incubation buffer:*** BSA, 1% w/v final added to 25 ml of the HEPES buffer.
3. ***Collagenase digestion buffer (CDB):*** 1.1 mg/ml type-4 collagenase and 1 mg/ml soybean trypsin inhibitor added to 6 ml of BSA incubation buffer.
4. ***Sodium bicarbonate (NaHCO3) neutral buffer solution:*** 0.1 M sodium bicarbonate, pH 8.0 was prepared by dissolving 420 mg $NaHCO_3$ in 50 ml ultrapure distilled water.
5. ***For coating of a half area 96-well plate:*** dilute 30 µl of Corning® Cell-Tak in 2 ml of the neutral bicarbonate buffer.
6. ***Fura-2 AM stock solution:*** Suspend 1 mg of lyophilized Fura-2 AM with DMSO to yield a 1 mM stock. Aliquot this stock and keep at all times in the dark at -20 ^{o}C.
7. ***1M probenecid:*** dissolve in 1 M NaOH (50 mg/ml), yielding a clear, colorless solution
8. ***Fura-2 working solution:*** 4 µl Fura-2 AM stock, 4µl probenecid 1M and 4 ml HEPES buffer. **Caution:** Buffer preparation and cell loading were performed in the dark to prevent degradation of the Fura-2.

- **Assay plate preparation:**

To maintain acinar units in place throughout the FlexStation 3 measurements, Corning® Cell-Tak adhesive was used to coat the half-area, 96-well assay plates which were used in these experiments. Corning® Cell-Tak adhesive is a formulation of the "polyphenolic proteins" (Waite and Tanzer, 1981) extracted from the marine mussel, Mytilus edulis. This family of related proteins is the key component of the glue secreted by the mussel to anchor itself to solid structures in its natural environment (Waite, 1983).

1. On the day preceding the experiment, the NaHCO3 neutral buffer solution was filter-sterilized.
2. The amount of Corning® Cell-Tak required for each well in the assay plate was calculated according to the manufacturer's recommendations: 0.56 µg Corning® Cell-Tak/well.
3. The correct amount of Corning® Cell-Tak was diluted into the neutral buffer, mixed thoroughly, and dispensed into the assay plate wells within 10 minutes.
4. The plate cover was placed and the coated assay plate was incubated overnight **at room temperature.**
5. On the next day (the day of the experiment), the unevaporated Cell-Tak was poured off and each well was washed with 200µl filter-sterile distilled water to remove the bicarbonate.

➢ **Hint:** it is of extreme importance not to place the Cell-Tak-coated assay plate in the CO_2 incubator while preparing the compound plate, otherwise Cell-Tak will lose its activity and acinar units will be detached from the plate bottom

when the secretagogues are added and severe inconsistency in fluorescence recording will occur.

- **Isolation and preparation of the SMGs**

1. The SMGs were dissected out and rinsed with Hanks balanced salt solution
2. Excised SMG was minced with scalpels or curved scissors in a labelled weighing boat, containing 1 ml of the CDB.
3. The gland homogenate was transfered to a 50ml falcon tube and incubated in 4ml CDB, in a 37 °C water bath for 30 min.
4. After the digestion was complete, the CDB was carefully pipetted-out and replaced with 6 ml of BSA incubation buffer.
5. The tube was shaken vigorously by hand for 10 secs, in order to disperse the cells into smaller acinar units, figure 5.4.
6. The physiologic units were allowed to settle, then the supernatant was discarded and replaced with HEPES buffer-containing Fura-2 AM.

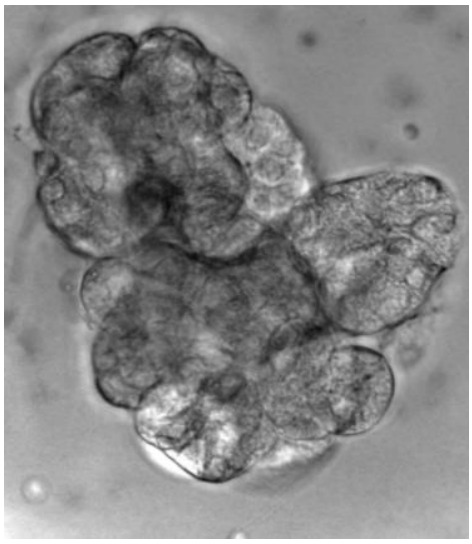

Figure 5.4 Representative example of the physiologic acinar units obtained in the present protocol following collagenase digestion.

- **Hint:** care should be taken to remove the BSA buffer completely, followed by replacement with HEPES incubation buffer.

- **Dye loading**

1. To prevent leakage of the dye from the cells, add 1 mM probenecid; an organic anion transport blocker, to the dye buffer.
2. The acinar units (in the falcon tube) were incubated in 4 ml Fura-2 working solution in a CO_2 incubator at 37°C for 1 hour.
3. During this period, the FlexStation 3 was switched on and the temperature was adjusted to 37°C.
4. After one hour, the acinar units were washed with HEPES buffer once.
5. The final HEPES buffer volume to be dispensed on the acinar units was calculated according to number of wells to be seeded, using the following formula: final HEPES buffer per gland= number of wells to be seeded x 75 (final volume/well in the assay plate).
6. After seeding the HEPES buffer/acinar units into the assay plate, it was covered and placed into its allocated position in the FlexStation, until preparation of the compound plate is complete. **Caution:** Do NOT do this step in the CO_2 incubator.

- **Hint:**

It is essential to take into consideration the importance of having relatively equal density of acinar units per well. To achieve this:

  - Pipette the digested acinar units gently up and down frequently between each transfer of HEPES buffer/acinar units into the wells of the assay plate.

- We recommend performing this critical step near an inverted microscope to frequently check uniform density of the seeded acinar units.

- **Compound plate preparation:**

1. The stock solutions of the cholinergic receptor agonist; CCh and the calcium ionophore; IM were prepared in DMSO
2. The intermediate and working solutions were prepare in DPBS, Table 5-5.

Table 5-5 Carbachol and ionomycin preparation

Carbachol stock solution (100mM): 100 mg CCh in 5.47 ml DMSO.			
Intermediate: **1:100 (in DPBS)**			
Final conc. (µM) in assay plate	Initial conc. (µM) in compound plate	CCh (µl)	Buffer (µl)
50	**200**	**40**	**160**
20	**80**	**16**	**184**
10	**40**	**8**	**192**
Ionomycin stock solution (3mM): 5 mg IM in 2.23 ml DMSO			
Intermediate: **No intermediate is required**			
Final conc. (µM) in assay plate	**Initial conc. (µM) in compound plate**	**IM (µl)**	**Buffer (µl)**
6	**30**	**2**	**198**

Caution 1: The FlexStation will be set-up to transfer 25 µl CCh followed by 25 µl IM, from the compound plate columns to the 75 µl buffer/acinar units' columns in the assay plate. Accordingly, it is very important to take into consideration that determination of the final concentrations in the compound plate, depends on the buffer volume in the corresponding well of the assay plate, before the compound addition, Figure 5.5.

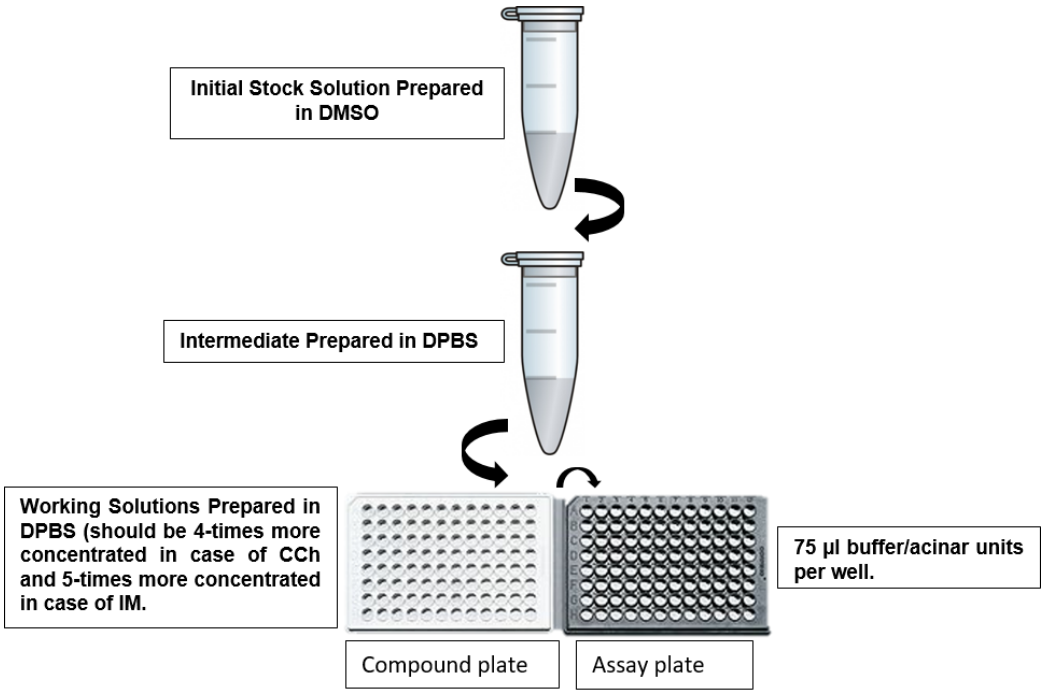

Figure 5.5 **Step-wise illustration of compound plate preparation**

Caution 2: It is very important to note that the compound concentration is subject to change after each compound addition (in experiments where multiple compounds are used).

- **Equipment**

FlexStation 3 (Molecular Devices, Inc.) benchtop scanning fluorometer is used to measure changes in fluorescence of the fura-2 stained acinar units upon agonists' transfer from the compound plate to the pre-designated set of wells in the assay plate.

1. The FlexStation 3 was set-up to record changes in calcium signals before (baseline) and after compound additions, as demonstrated in Table 5-6.

2. For baseline fluorescence reading, the settings were adjusted similar to that demonstrated in Table 2, except that:

(i) An endpoint read type was selected

(ii) The compound transfer option was not selected.

3. The emission ratios with excitation wavelengths of 340 and 380 nm were recorded every 6 seconds after compound applications, for 3 minutes.

4. Experimental data was processed directly using the SoftMax Pro software (otherwise it can be copied and pasted into any spreadsheet program, such as Microsoft Excel).

Table 5-6 Flexstation setting

- Read mode **FL**
- Read type **Flex**
- Category

1. Wavelength **[2 wave length pairs]**

- **Excitation: Lm1 340 nm** **Emission: Lm1 510**

Lm2 380 nm **Lm2 510**

Auto cut-off.

2. Plate type

- 96-well Corning half area flat clear bottom

3. Read area settings

- **Select all (read the whole plate)**

4. PMT and optics settings

- **PMT Gain: Medium**
- **Flashes per Read: 6**

5. Timing settings

- **Total run time: 3 mins**
- **Interval: 6 secs.**
- **Number of reads: 21**

6. Compound transfer

- Number of transfers: **2**

Parameter	**Compound 1 (CCh)**	**Compound 2 (IM)**
Initial volume (µl)	75	100
Pipette height *	90	100
Volume	25	25
Rate (µl/sec) *	2	2
Time point	20	120

* **The parameters for the integrated FlexStation pipettor require optimization for each assay. The dispensation height of the pipettor and the speed of dispensation should be adjusted to ensure optimal delivery of the compounds to the specific plates being used. Optimal delivery should not cause cell disruption but should allow adequate mixing of the compounds in the well. To assist adequate mixing of compounds, the volume of agonist added to the well is typically 25% of the final well volume. The optimal dispenser speed may vary according to how well cells adhere to the bottom of the well (Marshall et al., 2005).**

7. Compound plate type

- **Costar 96 opaque 3 ml**

8. Pipette tips and layout

- **Subject to experimental condition**

9. Compound and tips column

- **Subject to experimental condition**

10. No trituration.

5.3 Results

5.3.1 Temporal iNOS Upregulation in the Acute Viral Mimic Model

To examine the temporal acute induction of inducible nitric oxide synthase in response to SMG viral mimic inoculation, immunohistochemical analysis was performed on tissue sections from the poly (I:C) injected glands as early as 3 hrs post its retrograde infusion. It can be clearly seen from figure 5.6 the early intense acinar immunoexpression of the pro-inflammatory mediator in response to the viral mimic.

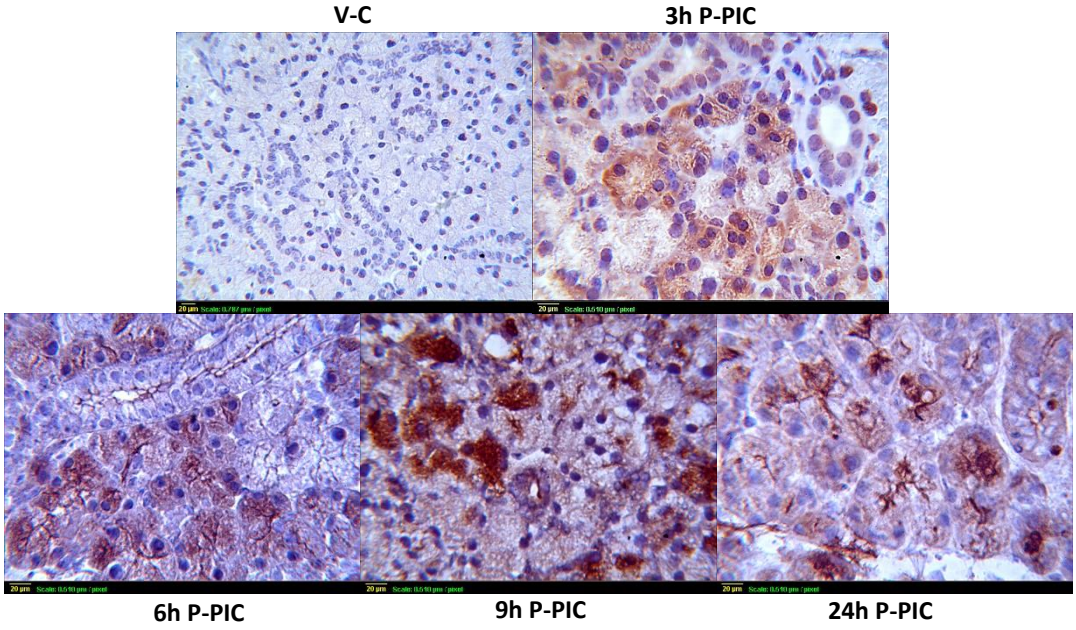

Figure 5.6 **iNOS immunoexpression in the SMGs**.
Photomicrographs showing the basal negative expression of iNOS, in the vehicle injected SMGs. **3hrs following poly (I:C) introduction**: moderate acinar immunolabelling of the acute inflammatory mediator was seen. **6h post poly (I:C):** increased acinar iNOS immunolabelling. **9hrs and 24 hrs after viral mimic injection**: iNOS was intensely expressed in focal acinar areas beside its extensive mild expression in all acinar cells. Original magnification: V-C=16x, all other images=40x.

5.3.2 Functional Recovery in Response to iNOS Inhibition

It was important subsequently to substantiate the injurious role that may have been played by iNOS in the acute SMG dysfunction. Short and long term inhibition of iNOS using AG, protected the SMG functions significantly despite harbouring a potent viral mimic, figure 5.7.

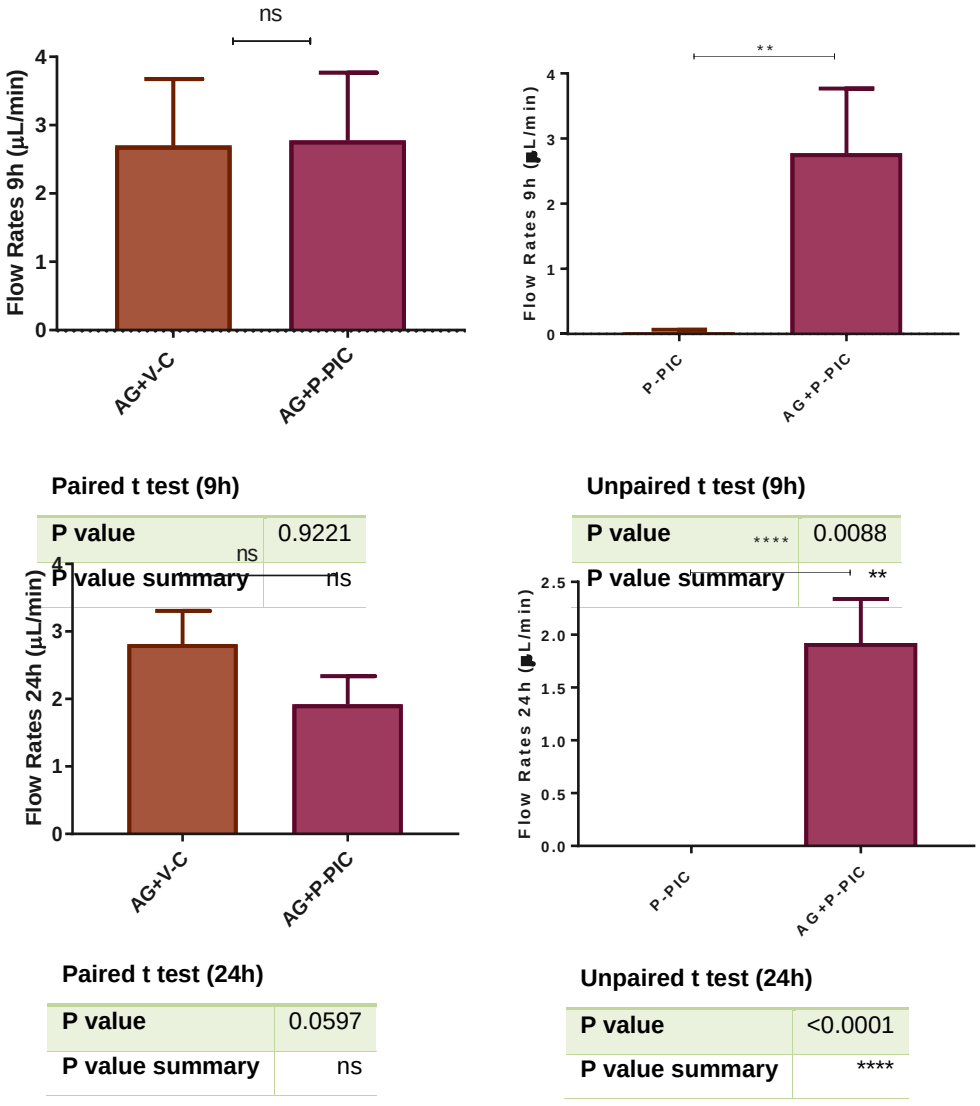

Figure 5.7 **Functional analysis following the selective iNOS inhibitor; aminoguanidine.** Enhancement of the SMGs' secretory function from mice treated with aminoguanidine compared to the glands from the untreated animals which received the viral mimic only. Summary of statistical analysis for the mean flow rates of the vehicle and poly (I:C) injected glands in both groups. ns: Non-significant, **p≤0.01, ****p≤0.0001.

To validate the inhibited production of nitric oxide in response to aminoguanidine treatment, tissue sections from AG-treated and non-treated SMGs were immunostained for peroxynitrite, using 3-Nitrotyrosine marker. Microscopic

examination of the stained sections showed that 3-nitrotyrosine is restricted to the SMG vasculature of the control groups. In the SMGs which received the viral mimic, 3-NT showed remarkable upregulation in the glandular parenchyma and stromal cells, in addition to the intense vascular immunoexpression. Conversely, AG reduced markedly the peroxynitrite marker to levels and profiles similar to the control glands, where 3-NT was seen exclusively in the abundant dilated blood vessels, which were not responsive to selective iNOS inhibition by AG, figure 5.8 A. Immunolabelling the SMGs with DAB peroxidase allowed a clear preview of the acinar expression of 3-NT induced by poly (I:C) in the AG-primed and non-primed SMGs. Importantly, the peroxynitrite marker intensely labelling acinar plasma membranes was markedly reduced in response to AG and limited only to the stromal blood vessels, figure 5.8 B.

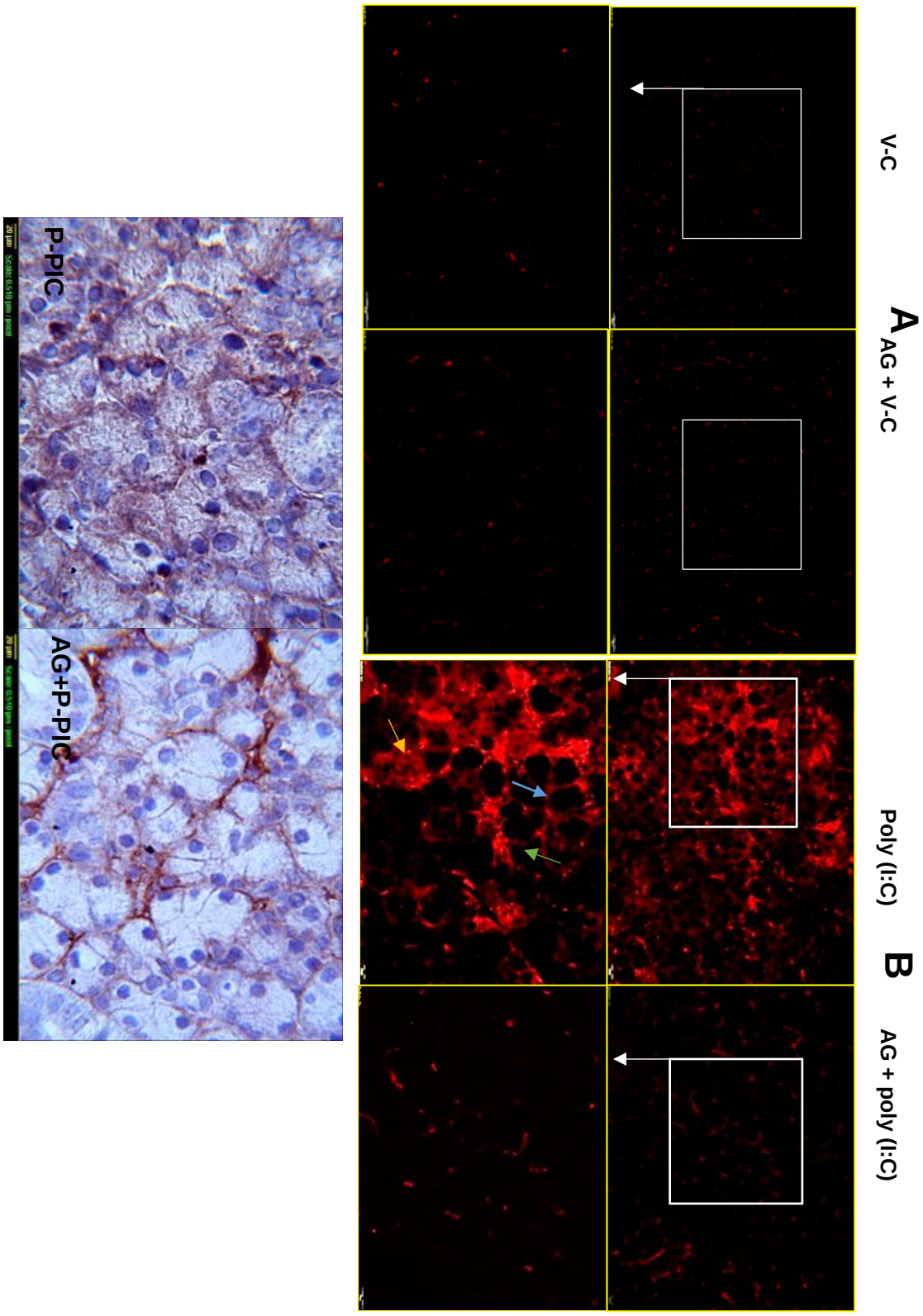

Figure 5.8 **Immunohistochemical staining of 3-nitrotyrosine**.
A: In the upper panel, basal immunoprofile of the peroxynitrite marker in the control SMGs of the AG treated and non-treated mice. Note the restricted immunoexpression of the gland vasculature in both groups. In the lower immunofluorescent images, poly (I:C) induced an extensive expression of the peroxynitrite marker in the ducts (yellow arrow), stroma (green arrow) as well as the basal surfaces of acinar cells (blue arrow), all obviously declined with AG treatment. **B:** DAB-labelled SMGs, demonstrating the strong and specific membranous nitrotyrosine expression in the acinar cells following poly (I:C) exposure, which was limited to the gland vasculature (showing intense nitrotyrosine positivity) in the AG treated animals. Original magnification of upper panels=20x, insets=40x, DAB labelled glands=40x.

5.3.3 Characterizing the Potential Injurious Contributions of iNOS in The Acute SMG Dysfunction Model

5.3.3.1 Peroxynitrite-Induced Nitration of Myriad of SMG Proteins.

To investigate the extent of SMG proteins' nitration with peroxynitrite, western blot analysis was conducted. Tissue extracts of glands injected with the vehicle and poly (I:C) in presence or absence of aminoguanidine were probed with 3-NT antibody. Figure 5.9 reveals the excessive nitration of the gland proteins upon single exposure to the viral mimic. In contrast, AG suppressed the nitrosative stress signal and 3-NT expression was retracted to the control level.

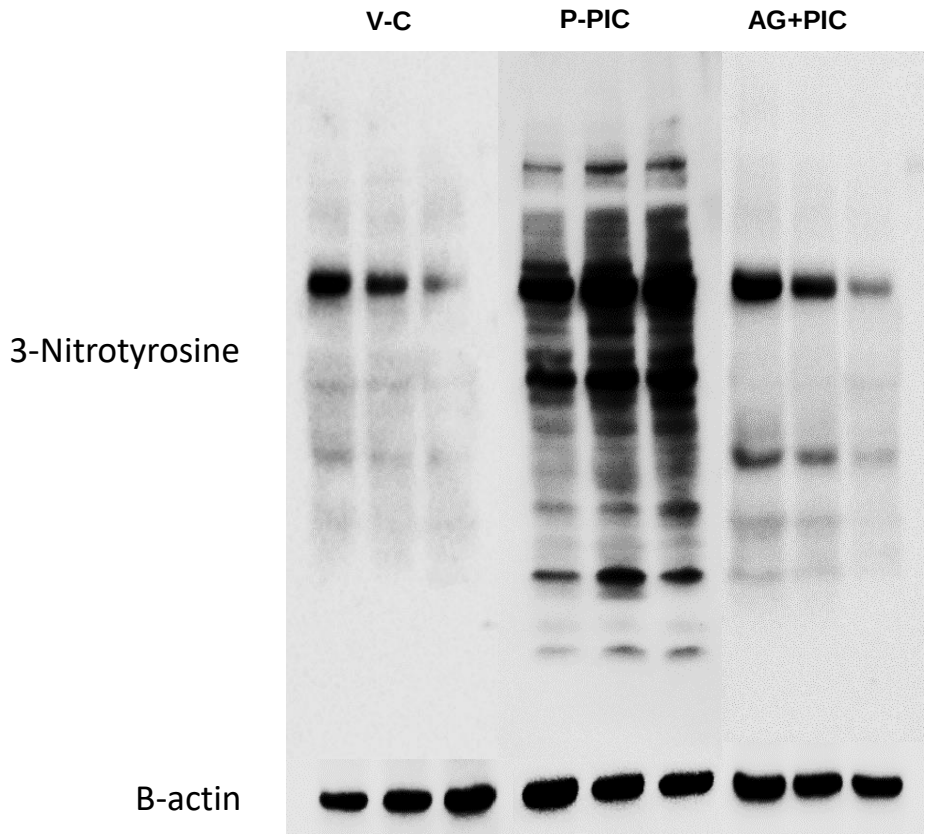

Figure 5.9 **Western blot representation of the peroxynitrite marker; 3-Nitrotyrosine.**
Induction of "nitroxidative stress" in the SMGs following poly (I:C) introduction (P-PIC), a plethora of SMG proteins exhibited tyrosine nitration which was markedly reduced upon aminoguanidine treatment.

5.3.3.2 SERCA2 ATPase Co-localization with 3-Nitrotyrosine

Western blot analysis of 3-Nitrotyrosine in the poly (I:C) injected SMGs revealed a noticeable band at the level of SERCA2 ATPase; 110 Kda, figure 5.9. To verify physical co-localization of 3-nitrotyrosine staining with SERCA2 ATPase, immunohistochemistry was performed to confirm the possibility of interaction between peroxynitrite and this key regulator of calcium transport (Periasamy and Kalyanasundaram, 2007).

Figure 5.10 A shows the normal distribution of the calcium pump in the vehicle injected SMGs. The fluorescence signal observed was arranged in dense peri-nuclear clusters in the cytosol of the acinar and duct cells coinciding with the normal ER distribution. Figure 5.10 B clearly displays co-localization between the 3-NT and SERCA-ATPase proteins after poly (I:C) retrograde injection. Following AG treatment, the iNOS inhibitor succeeded in blocking peroxynitrite formation, hence the subsequent, potentially injurious, co-localization with the calcium pump, figure 5.10 C.

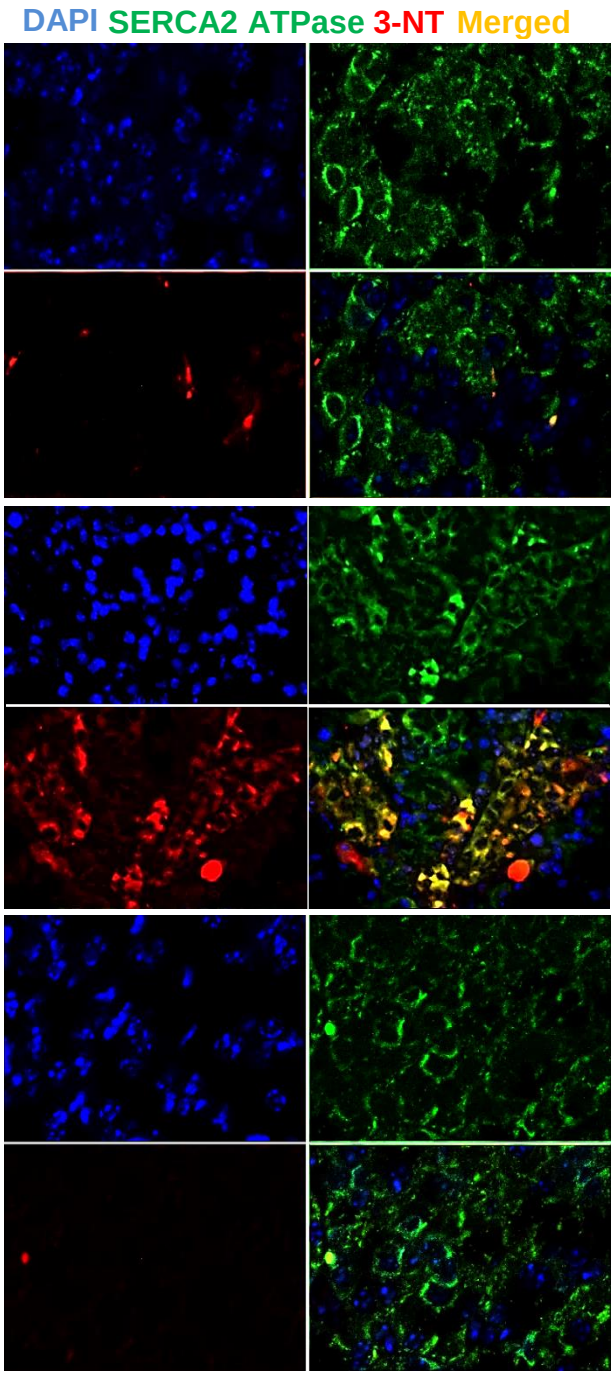

Figure 5. 5.10 **Co-localization of 3-NT and SERCA2 ATPase**.
A: immunofluorescence representation of the: negative NT expression in the normal SMGs. Note the clustered peri-nuclear SERCA2 ATPase immunolocalization.

B: Abundant co-localization of the upregulated 3-NT staining with SERCA2, 9hrs post infection with a viral mimetic.

C: AG-treated SMGs revealing the obvious decline of 3-NT expression and the regular SERCA2 labelling of the SMG cells.

5.3.3.3 Poly (I:C) Mediated-Disruption of Calcium Homeostasis

Co-localization of 3-NT and SERCA2 pump raised the possibility that the viral mimic may have mediated calcium disruption in the SMGs. Accordingly, a novel protocol was optimized and implemented to study poly (I:C)-induced changes of Ca^{2+} release from the ER, using a mAChRs agonist; carbachol. Fura-2 ratio (340/380) versus time was monitored for 2 minutes using Flexstatio 3. The preliminary experiments conducted revealed that in general, addition of variable concentrations of carbachol [5µM to 100µM] to the vehicle-injected SMG acinar units resulted in prompt $[Ca^{2+}]_i$ mobilization from intracellular ER stores, which was reflected as a sharp signal increase that peaked for 12 seconds after the secretagogue application. This peak was then followed by a plateau phase, whereby $[Ca^{2+}]_i$ oscillated in the form of elevated and depressed repetitive cycles. In the poly (I:C) treated gland, we noticed an overall decrease in the amplitude of $[Ca^{2+}]_i$ release from the ER upon carbachol addition, whereby drug concentrations [100µM-10µM] induced a minimally amplified $[Ca^{2+}]_i$ response, but at an extremely significant lower level ($p<0.0001$) compared to the vehicle injected control glands. On the contrary, when the poly (I:C) injected gland was stimulated with low agonist concentration [5µM], a sharp decrease in $[Ca^{2+}]_i$ mobilization was recorded, which barely reached above baseline, figure 5.11.

Two-way ANOVA

Source of Variation	P value	
Interaction	<0.0001	****
Carbachol Conc.	<0.0001	****
PIC Injection	<0.0001	****

Sidak's multiple comparisons test VC vs PIC	P Value	
100 uM	<0.0001	****
50 uM	<0.0001	****
20 uM	<0.0001	****
10 uM	<0.0001	****

Figure 5.11 **Fura-2-detected fluorescent signals in SMGs**.
Differential changes in $[Ca^{2+}]_i$ between Fura-2-loaded vehicle injected control glands (V-C) and those infused with poly (I:C) (P-PIC) after addition of different carbachol concentrations. Carbachol which was added after 20 seconds of baseline recording, induced a sharp increase in the fluorescence signal, which remained at an elevated level constantly up till 100 seconds following carbachol addition. Note the extremely significant reduction in calcium release in the poly (I:C)-treated group, in response to the high and low carbachol concentrations tested. All data is expressed as Δ340/380 (maximal $[Ca^{2+}]_i$ increase after carbachol minus its basal expression prior to stimulation). Bar chart represents the two-way ANOVA carried out to compare the mean ± SEM Δ 340/380 of various carbachol concentrations on ER calcium release in both groups. Statistical analysis revealed an extremely significant reduction in $[Ca^{2+}]_i$ in the glands which received poly (I:C) compared to the vehicle injected controls, a finding which was consistent with all carbachol concentrations tested, as shown by the Sidak's pairwise analysis, ****p≤0.0001. P-PIC: post poly (I:C).

The Flexstation 3 further permitted recording of the baseline calcium, prior to compound addition, which

surprisingly revealed an extremely significant increase in Fura-2 340/380 ratio, in the poly (I:C) injected glands, compared to the control group, figure 5.12.

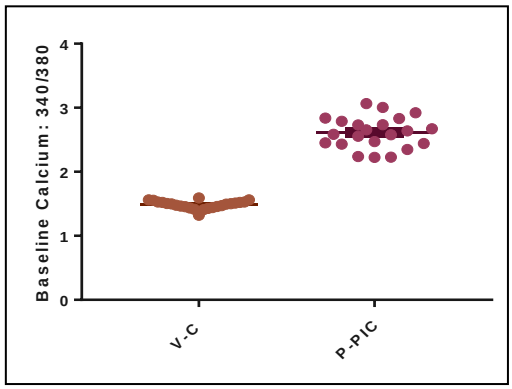

Unpaired t test	
P value	<0.0001
P value summary	****

Figure 5.12 **The baseline 340/380 ratio recorded prior to compound application.**
Unpaired t-test revealed that the acinar cells from poly (I:C) injected SMG had an extremely significant high basal Ca^{2+} compared to the vehicle injected control SMG. **** p≤0.0001.

Following these initial results, additional experiments were directed to detect the effect of AG treatment on the extremely disrupted calcium signalling. Acinar units from SMGs of AG treated and non-treated animals were prepared and for simplicity of analysis, these experiments were conducted using a single carbachol concentration (50µM). Figure 5.13 shows the extremely significant recovery conferred by AG treatment on the poly (I:C) injected glands and validates the detrimental consequences of extensive iNOS upregulation on acinar calcium homeostasis.

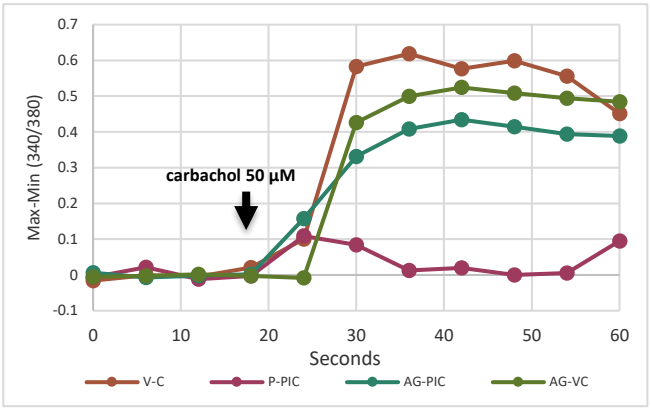

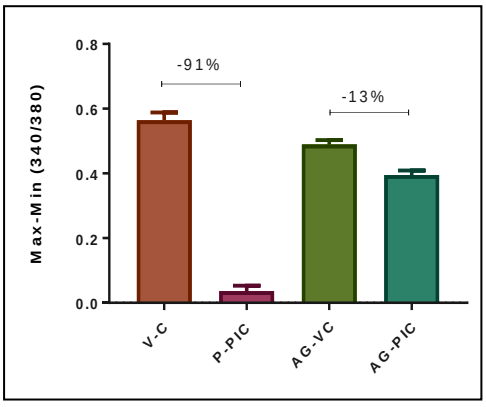

ANOVA	
P value	<0.0001
P value summary	****

Sidak's multiple comparisons test	Adjusted P Value	Summary	% Change
V-C vs. P-PIC	<0.0001	****	-91%
AG-PIC vs. AG-VC	0.0052	**	-13%
P-PIC vs. AG-PIC	<0.0001	****	
V-C vs. AG-VC	0.0306	*	

Figure 5.13 **Fura-2-detected fluorescent signals in SMGs in response to 50 µM carbachol stimulation.**
SMGs from mice treated or not treated with AG as well as the appropriate vehicle injected controls were used and carbachol was added to detect the $[Ca^{2+}]_i$ response in the acinar units. Stimulated Ca^{2+} response graph represents the Δ340/380 (maximal $[Ca^{2+}]_i$ increase after carbachol application minus its basal expression prior to stimulation). Sidak's pairwise comparison revealed the extremely significant recovery of the poly (I:C) injected glands when pre-treated with the selective iNOS inhibitor; AG. Data represents the mean ± SEM Δ 340/380 following carbachol addition, *p≤0.05, **p≤0.01 and ****p≤0.0001

To investigate whether iNOS mediated a reduced carbachol response via depleting ER stores, we assessed the amount of $[Ca^{2+}]_{ER}$ using ionomycin (an ionophore that, in the absence of external Ca^{2+}, releases Ca^{2+} from the intracellular stores in a receptor-independent manner (Albert and Tashjian, 1986). We found that Ca^{2+} liberation from internal stores induced by ionomycin was significantly decreased in the poly (I:C) injected glands when incubated in a calcium free buffer, and that the AG-mediated recovery of the carbachol-stimulated calcium release, demonstrated in figure 5.13, paralleled a relatively maintained $[Ca^{2+}]_{ER}$ level, figure 5.14.

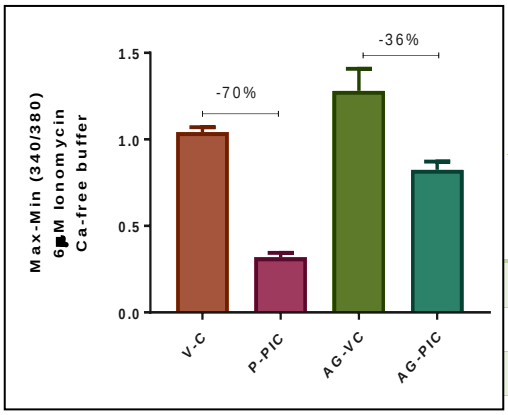

ANOVA summary	
P value	<0.0001
P value summary	****

Sidak's multiple comparisons test	P Value	Summary	% Change
V-C vs. P-PIC	<0.0001	****	-70%
AG-VC vs. AG-PIC	<0.0001	****	-36%
P-PIC vs. AG-PIC	<0.0001	****	
V-C vs. AG-VC	0.011	*	

Figure 5.14 **Ionomycin-induced Ca^{2+} release from the intracellular stores**.
Isolated acinar cells of vehicle and poly (I:C) injected SMGs from AG treated and non-treated animals were incubated in Ca-free medium. ANOVA followed by Sidak's pairwise comparison revealed that the viral mimic induced an extremely significant reduction in mean±SEM ionomycin-stimulated Ca^{2+} release from the internal stores and that AG mediated an extremely significant recovery in the ionomycin stimulated response of the poly (I:C) injected glands. *p≤0.05, **p≤0.01 and ****p≤0.0001

To dually assess the impact of extracellular calcium and iNOS inhibition on resting calcium levels in the control and poly (I:C) injected glands, the physiologic units were incubated in calcium free and calcium containing buffers and stimulated with the calcium ionophore; ionomycin. Recording of baseline calcium using the Flexstation 3 revealed some interesting findings that can be summarized as follows: (i) removal of calcium from the buffer and addition of a chelator, did not change baseline calcium levels in the **vehicle-injected control** glands of the tested groups. In the ***AG non-treated group*** (ii) the extremely significant increase (53%) in baseline calcium of the poly (I:C) injected glands, compared to the control glands, was extremely reduced when calcium was removed from the incubation buffer. (iii) Even in the absence of extracellular calcium, the physiologic clusters of the poly (I:C) injected glands showed an extremely significant increase (13%) in basal calcium compared to the vehicle

injected control, suggesting interplay of more than one mechanism in disrupting resting $[Ca^{2+}]_i$. In the ***AG-treated group***: (iv) poly (I:C) still induced 13% increase in basal calcium, and (v) it wasn't until the physiologic clusters of this group were incubated in a calcium-free buffer, when the resting $[Ca^{2+}]_i$ nearly paralleled the reference levels recorded in the control gland, figure 5.15.

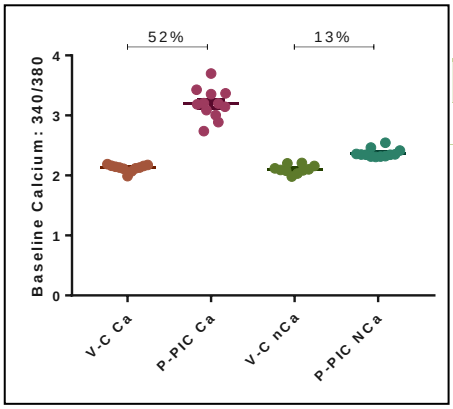

ANOVA AG Non-Treated Group

P value	<0.0001
P value summary	****

Sidak's multiple comparisons test	P Value	Summary	% Change
V-C Ca vs. V-C nCa	0.9962	ns	
P-PIC Ca vs. P-PIC NCa	<0.0001	****	
V-C Ca vs. P-PIC Ca	<0.0001	****	52%
V-C nCa vs. P-PIC NCa	0.0004	***	13%

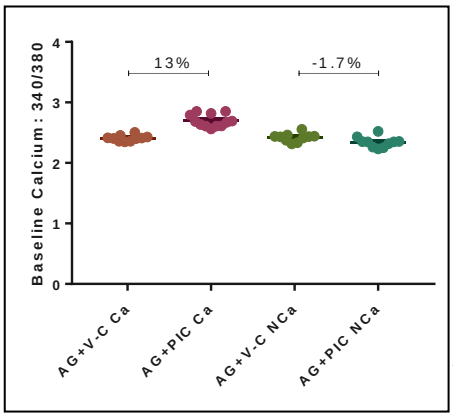

ANOVA summary AG-Treated Group

P value	<0.0001
P value summary	****

Sidak's multiple comparisons test	Summary	P Value	% Change
AG+V-C Ca vs. AG+V-C NCa	ns	0.9948	
AG+PIC Ca vs. AG+PIC NCa	****	<0.0001	
AG+V-C Ca vs. AG+PIC Ca	****	<0.0001	13%
AG+V-C NCa vs. AG+PIC NCa	ns	0.1361	-1.70%

Figure 5.15 **Baseline 340/380 ratio in the SMGs treated or not treated with AG.**
ANOVA followed by Sidak's multiple comparison analysis revealed the differential change in baseline calcium among the tested physiologic units as explained in the text above. Ns: Non-significant, ***p≤0.001, ****p≤0.0001. Ca: Calcium-containing buffer, NCa: Incubation buffer free of CaCl2 and containing 1M EGTA.

5.3.3.4 AG Inhibited Poly (I:C)-Induced Lysosomal Discharge

The finding that poly (I:C)-injected glands maintained a significantly high resting Ca^{2+} despite calcium chelation from the extracellular medium, directed us towards assuming leakage of an intracellular Ca^{2+}-rich organelle. Lysosomes contain up to 600 mM calcium (Christensen et al., 2002, Lloyd-Evans et al., 2008), nearly matching the concentration described for the classic calcium storage organelle; the ER (Bygrave and Benedetti, 1996). To assess whether poly (I:C) has induced lysosomal membrane breach and sequential release of the organelle contents, we assessed the basal immunoexpression of the lysosomal protease; cathepsin-B, in the control SMGs and following poly (I:C) injection in the AG-treated and non-treated mice. In the control vehicle injected glands, cathepsin B was widely localized in the SMG duct cells. Six hrs post its intraductal infusion, poly (I:C) induced extra-lysosomal cathepsin B immunolocalization, its widespread tissue distribution and its depletion by 9 hrs of ductal infusion. Surprisingly, AG priming of the SMGs resulted in efficient interference with cathepsin B release from their characteristic perinuclear lysosomal localization up till 24 hrs post poly (I:C) injection, compared to its complete depletion in the AG non-treated mice, figure 5.16.

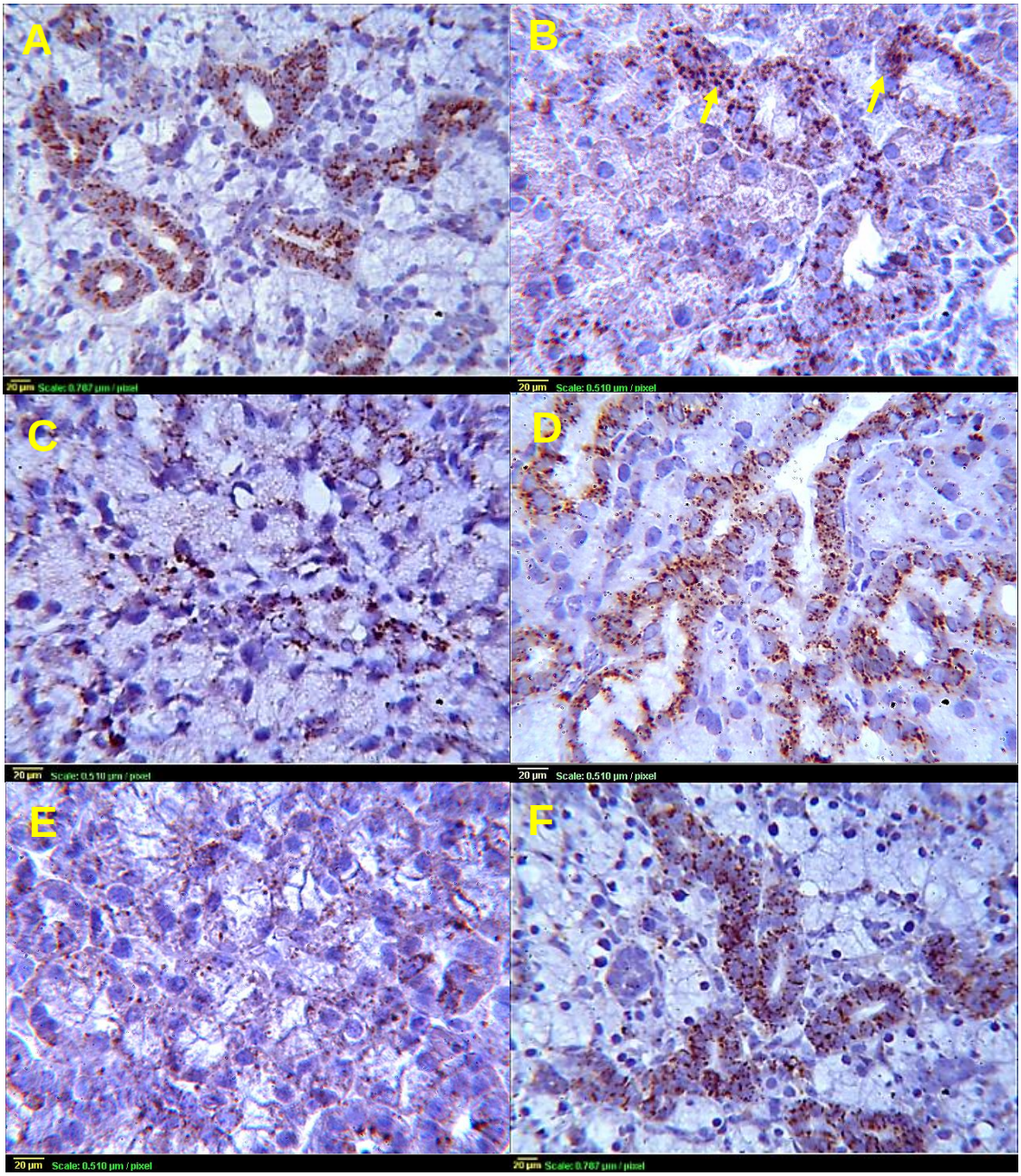

Figure 5.16 **Cathepsin B immunoexpression in the SMGs**.
Photomicrographs showing: **A** the characteristic fine perinuclear granules of cathepsin B consistent with its lysosomal localization in the vehicle injected control glands. **B: 6hrs post the viral mimic**: cathepsin B was extensively seen in the SMG tissues and not only restricted to their peri-nuclear ductal localization. In addition, the fine granular cathepsin B immunoreactivity was replaced by enlarged granules or diffused cytoplasmic staining (arrows), suggesting the leakage of the cathepsin B from the lysosomes into the cytosol. **C, E: 9hrs and 24 hrs respectively,** sporadic cathepsin B was seen in the ducts. **D, F:** AG treated SMGs after 9 hrs and 24 hrs respectively, revealed the efficient retention of the peri-nuclear lysosomal protease in the ducts of these glands. Original magnification: V-C, 9h P-PIC, AG+24h P-PIC= 25x and 6h P-PIC, AG+9h P-PIC, 24h P-PIC= 40x.

The cathepsin B extra-lysosomal discharge was further confirmed by its co-localization with the lysosomal marker; Lamp-1. The vehicle injected SMGs revealed constant ductal co-expression of cathepsin B and Lamp-1, figure 5.17 A. Upon poly (I:C) exposure, co-localization of the lysosomal markers was markedly lost and cathepsin B was seen within acinar cells in addition to their normal duct localization, figure 5.17 B. Conversely, AG treatment relatively maintained the perinuclear ductal cathepsin B expression as marked by physical co-localization with Lamp-1, figure 5.17 C.

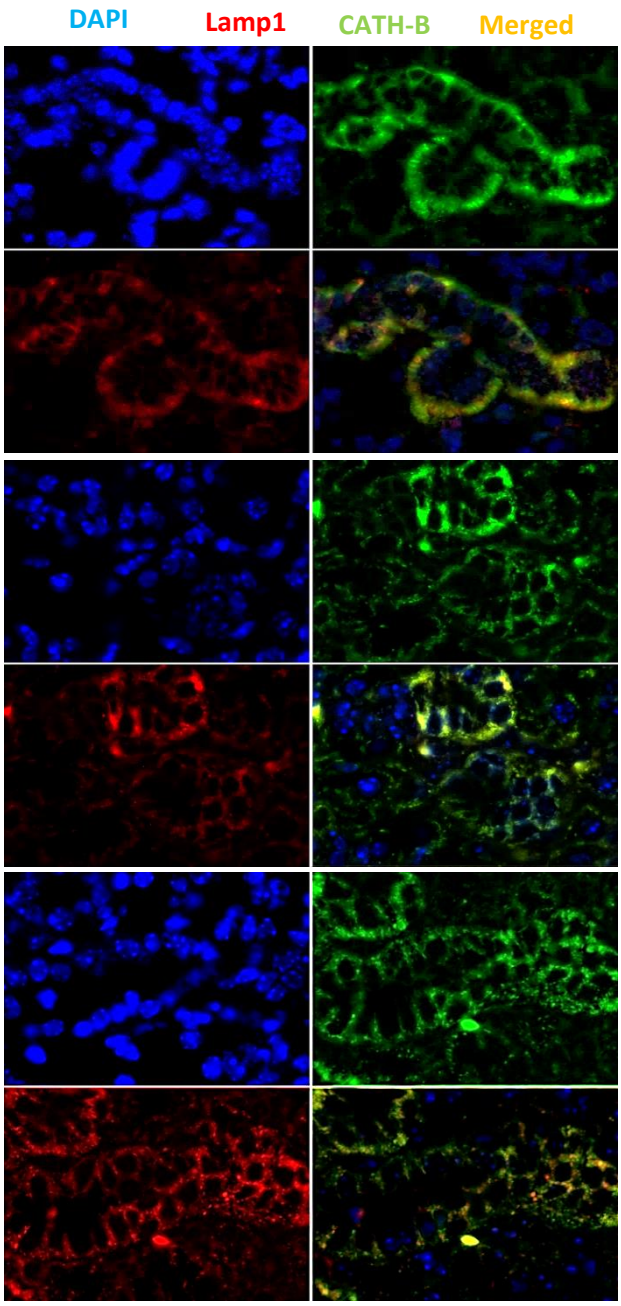

Figure 5.17 **Co-localization of Lamp1 and Cathepsin B**.
A: Double immunofluorescent staining of cathepsin B and Lamp-1 in the vehicle injected control glands. Note the co-localization of both lysosomal proteins in the SMG ducts.

B: 9hrs post poly (I:C), some preserved ductal co-localization of the lysosomal markers in addition to the extra-lysosomal cathepsin B in the duct cytoplasm as well as the surrounding acinar cells.

C: 9hrs post AG and poly (I:C), showing retention of peri-nuclear cathepsin B in lysosomes evidenced by the co-localization of both lysosomal markers in the duct cells.

5.3.3.5 AG Interfered with Induction of ER stress in the SMG Dysfunction Model

Since Ca^{2+} is central to the regulation of processing and targeted dispatch of proteins in the ER, including crucial SG receptors, channels and transporters, we hypothesized that Ca^{2+} dysregulation in the current model has induced an ER stress condition which may have interrupted the ER Ca^{2+}-dependent roles of protein synthesis and transport. ER-stress can induce the transcriptional activation of chaperones and protein folding-associated molecules to reduce the burden of protein synthesis in the ER (Zhang and Kaufman, 2006, Kimata and Kohno, 2011). Accordingly, to evaluate whether poly (I:C) has triggered ER stress, qRT-PCR analysis of ER-stress related genes; XBP1, GRP78 (Bip) and CHOP were performed. Poly (I:C)-injected SMGs displayed significant upregulation in the ER-stress related genes, an effect that was efficiently prevented by the iNOS selective inhibitor; AG, figure 5.18.

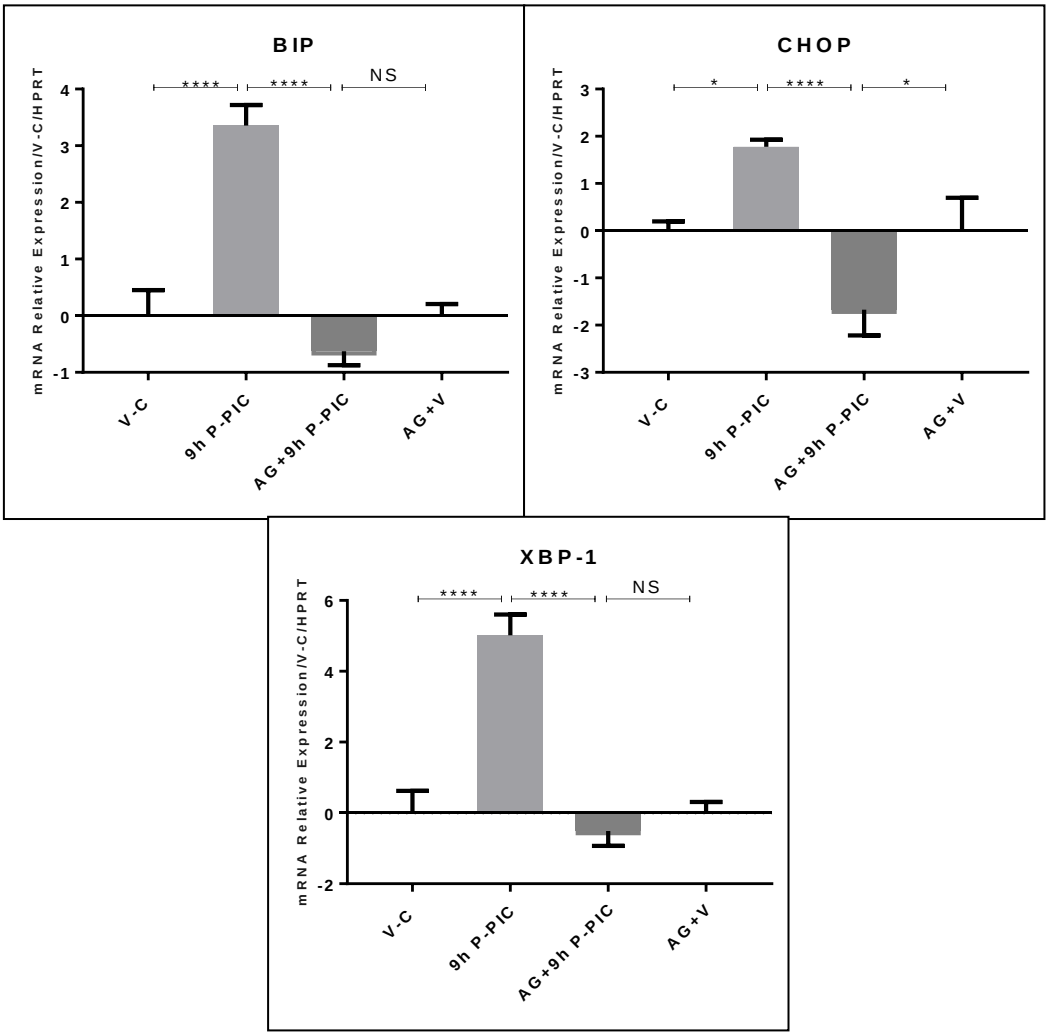

ANOVA	Bip	CHOP	XBP-1
P value	<0.0001	0.0001	<0.0001
P value summary	****	***	****

Sidak's multiple comparisons test

	Bip		CHOP		XBP-1	
V-C vs. 9h P-PIC	****	<0.0001	*	0.0301	****	<0.0001
9h P-PIC vs. AG+9h P-PIC	****	<0.0001	****	<0.0001	****	<0.0001
AG+9h P-PIC vs. AG+V	ns	0.4686	*	0.044	ns	0.8572

Figure 5.18 **mRNA expression of ER stress related genes; Bip, CHO and XBP-1**.
SMGs of mice treated or not-treated with AG were injected with the vehicle or poly (I:C). Tested genes were normalized to HPRT in both groups. A single aminoguanigine treatment restricted the significant acute upregulation of ER stress related genes, 9 hrs post poly (I:C) administration. Data represent means ± SEM (n=3). *p<0.01, ***p<0.001, ****P < 0.0001, ns: non-significant.

5.3.3.6 Downregulation of Water and Ion Transport Molecules

Following the substantiation of ER stress induction in the acute viral mimic model, we aimed to substantiate the UPR-triggered mRNA decay (Grootjans et al., 2016) of key water driving molecules in the viral mimic model. qRT-PCR revealed an extremely significant downregulation (approximately 80% of the baseline level) in the mRNA expression levels of all tested genes. Importantly, retrieval of the downregulated genes was perceived in all aminoguanidine treated animals, figure 5.19.

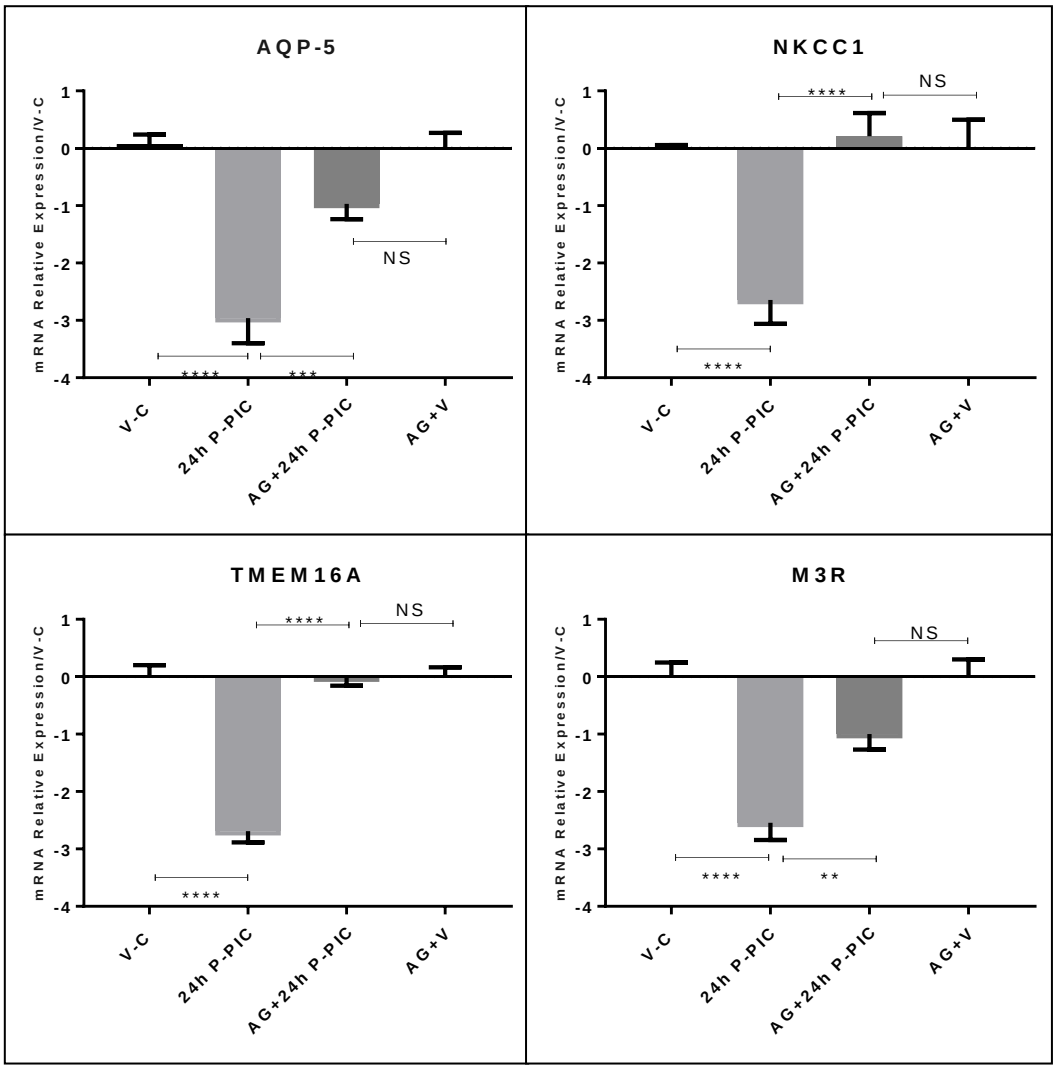

ANOVA	AQP-5	NKCC1	TMEM16A	M3R
P value	<0.0001	<0.0001	<0.0001	<0.0001
P value summary	****	****	****	****

Sidak's multiple comparisons test

	AQP5		NKCC1		TMEM16A		M3R	
V-C vs. 24h P-PIC	****	<0.0001	****	<0.0001	****	<0.0001	****	<0.0001
24h P-PIC vs. AG+24h P-PIC	***	0.001	****	<0.0001	****	<0.0001	**	0.0054
AG+24h P-PIC vs. AG+V	ns	0.3172	ns	0.9803	ns	>0.9999	ns	0.1954

Figure 5.19 **mRNA expression of genes encoding water driving molecules; AQP5, NKCC1, TMEM16A and M3R.**
SMGs of mice treated or not-treated with AG were injected with the vehicle or poly (I:C). SMGs were harvested 24 hrs post the local injections, and tested genes were normalized to HPRT in AG non-treated glands and B-actin in AG-treated groups. Long term inhibition of iNOS, by incorporating aminoguanidine in drinking water for seven days prevented the extremely significant downregulation of the mRNA of key water driving molecules. Data represent means ± SEM (n=3). **p≤0.01, ***p≤0.001, ****P < 0.0001, ns: non-significant.

5.3.3.7 Disrupted Subcellular Localization of Water and Ion Transport Proteins

Next, we used antibodies against M3R, AQP-5, NKCC1 and TMEM16A, to confirm the reduced expression of these water driving molecules at the protein level and assess their immunolocalization. Immunoperoxidase labelling of SMGs from AG treated and non-treated mice revealed the following expression patterns for the control vehicle injected glands: (i) **AQP-5** exhibited a strong, furrow-shaped expression on the apical domains of acinar cells. Similarly, (ii) **TMEM16A**, showed intense, trough-like immunoexpression on luminal surfaces of acinar cells. Interestingly, TMEM16A was frequently seen as a thick branch-like connector linking multiple acinar and ductal lumena together. Moreover, (iii) NKCC1 revealed intense positive basolateral immunostaining of acinar cells as well as specific cells of all types of ducts. Finally, (iv) the muscarinic receptor; M3R, revealed a punctate basolateral membranous immunolabelling of acinar cells. 24 hrs following poly (I:C) retrograde infusion, a remarkable reduction was seen in all key water driving molecules. In addition, a markedly disrupted and altered immunolocalization of these molecules was displayed in the form of punctate, beaded and shrunken acinar cytoplasmic granules and thick patches. Predominantly, AG maintained the normal immunolocalization patterns of the tested proteins at a level comparable to that seen in the control vehicle injected glands, figure 5.20.

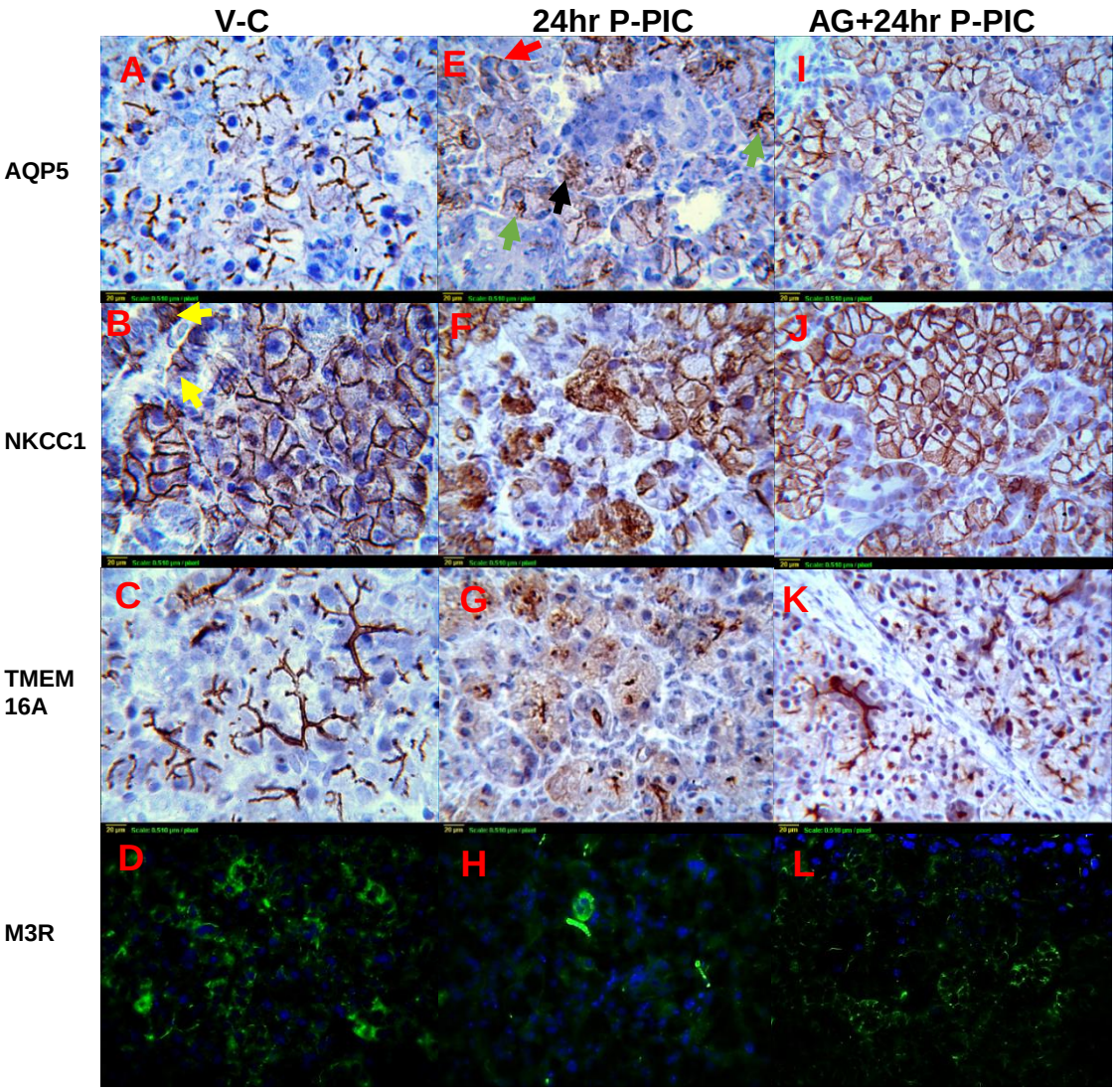

Figure 5.20 **Immunohistochemistry of key water driving molecules; AQP5, NKCC1, TMEM16A and M3R.**
Control SMG showed **A:** positive furrow-like AQP-5 immunostaining on the luminal membranes of acinar cells. **B:** strong basolateral and apical NKCC1 as well as specific duct cell positivity (yellow arrows). **C:** TMEM16A immunolabelling of acinar apical domains as well as acinar-ductal interconnecting branches. **D:** M3R visualized using fluorescently labelled secondary antibody. M3R displayed a punctate expression pattern in the basal membrane of acini and in the cytoplasm and membrane of epithelial cells lining the intercalated and striated ducts. 24 hrs post poly (I:C) **E:** thickened membrane patches of AQP-5 (green arrows), basolateral staining (red arrows), as well as granular cytoplasmic immunostaining (black arrows). **F:** NKCC1 revealed an irregular intense, granular cytoplasmic expression. **G:** TMEM16A expression showing reduced and altered positive cytoplasmic granularity. **H:** M3R staining was remarkably reduced compared to the control glands. **AG-treated glands; I, J, K and L**: Obvious recovery of the expression level and subcellular localization of all tested water and ion transport proteins in response to AG treatment. Original magnification=40x

5.4 Discussion

In the current chapter, we proposed an acute viral-mediated SG dysfunction mechanism, by which iNOS impaired saliva secretion via: dysregulating Ca^{2+} homeostasis, inducing ER stress and altering key water driving regulators at the gene and protein levels. Our results assigned iNOS upregulation as one of the earliest signals which takes place after acute infections of SGs. Moreover, we have shown the prompt parallel increase in peroxynitrite formation which culminated into nitrotyrosinilation of a plethora of SMG proteins.

To investigate the contribution of iNOS to the viral hypofunction perceived, we used systemic and local administrations of a selective iNOS inhibitor; aminoguanidine hydrochloride (Waz et al., 1997, Viaro et al., 2000). Since pilot experiments revealed that a single *i.p*. dose of AG was only sufficient to inhibit iNOS up till 9 hrs post poly (I:C) retrograde injection, we employed a longer-term inhibition protocol to acquire sufficient iNOS retraction 24 hrs post poly (I:C) (MacFarlane et al., 1999). Functional analysis of the AG-treatment model revealed an extremely significant recovery of the poly (I:C) injected glands at 9hrs and 24 hrs post infection.

Long-lasting and high levels of iNOS-derived NO has been hypothesized to directly nitrosylate functional proteins and disrupt essential cellular processes (Kimura-Shimmyo et al., 2002). In addition, peroxynitrite is believed to be responsible for the harmful effects of iNOS-derived NO during inflammation (Aydogan et al., 2006), via its rapid reaction with proteins to mediate radical tyrosine nitration and 3-nitrotyrosine production (Bigelow, 2009). In the present study, we were able to show that the AG-preserved saliva secretion paralleled decreased nitration of the SMG proteins and marked reduction of 3-nitrotyrosine

protein expression in the homogenates and tissue sections. Inhibition of the peroxynitrite marker in response to iNOS selective inhibition is in accordance with the previous demonstration that reactive nitrogen species production in mice is completely dependent upon the NO derived from iNOS (Koarai et al., 2002). Our results which verified the protective effects of AG on injured SGs, are in agreement with studies reporting the functional rescue afforded by: (i) selective iNOS inhibition in LPS-infected SMGs (Lomniczi et al., 2001) and (ii) peroxynitrite scavenging in irradiated SGs (Hanaue et al., 2007).

Immunofluorescence staining of the SMG tissue sections treated with AG demonstrated that 3-NT positivity was predominantly perceived in blood vessels. A similar phenomenon was seen in AG-treated, irradiated SGs (Hanaue et al., 2007), whereby AG, which extensively attenuated 3-NT, did not completely block its expression in the gland vasculature. These results may demonstrate that even though AG inhibited iNOS, which was the major source of NO-derived NT during the acute infection, eNOS which is responsible for most of the vascular NO produced and much less sensitive to AG (Alderton et al., 2001), may have given rise to the residual 3-NT in the AG treated glands.

The current acute viral mimic SMG model demonstrated excessive, iNOS-driven co-localization of the peroxynitrite marker and SERCA2 ATPase pump. As a rational outcome from vicinity with a potent oxidant, we assumed inhibition of SERCA2 ATPase activity, and loss of its tight control on the ER as well as cytosolic calcium levels. To assess our hypothesis, we intended to measure the carbachol induced Ca^{2+} release from the ER as well as the basal cytosolic calcium levels in the AG-treated and non-treated SMGs.

The novel protocol developed for assessment of calcium responses utilizes small clusters (5-20 cells) of parenchymal cells and represents a powerful tool to study the physiological and pathophysiological features of calcium homeostasis in vivo. Fura-2, is by far the most commonly used ratiometric dye for imaging Ca^{2+} signals in intact cells. It exhibits excitation spectrum changes upon Ca^{2+} binding such that the Ca^{2+}-free form is excited maximally at 380 nm while the Ca^{2+} bound form is excited maximally at 340 nm, figure 5.21. Both forms emit fluorescence with a peak at 510 nm, allowing for a simple excitation ratio (Marshall et al., 2006).

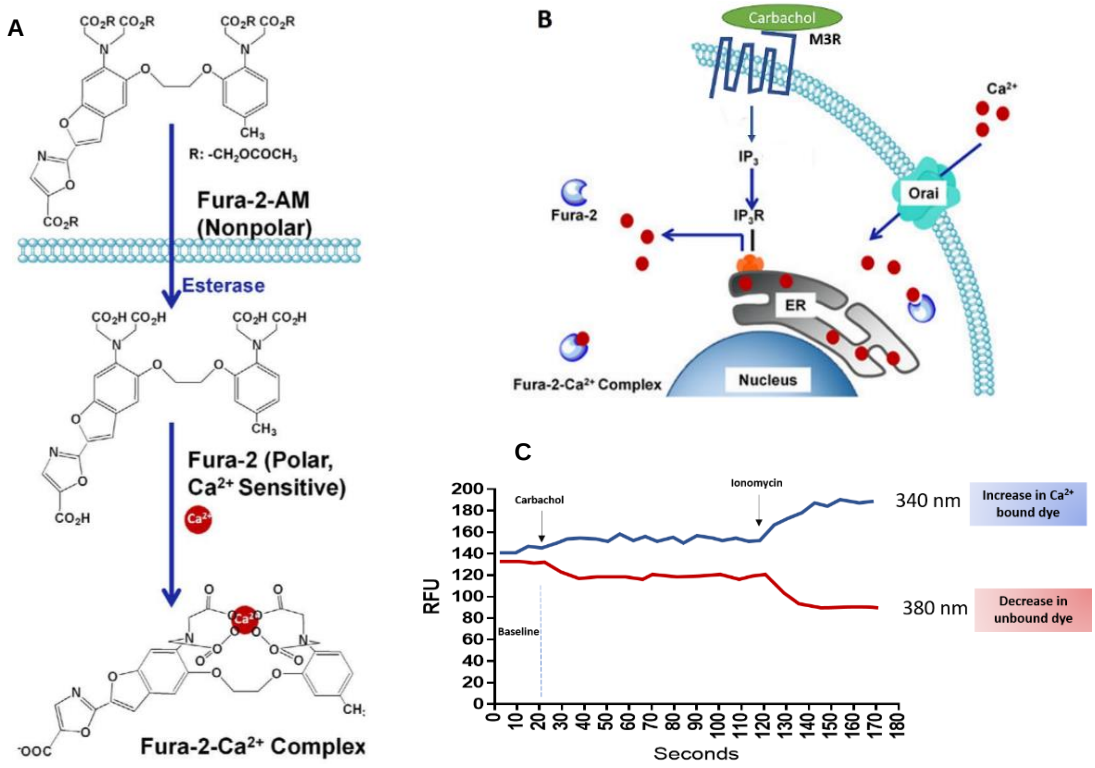

Figure 5.21 **FURA-2.**
A: Structural changes of Fura-2 by esterase activity and Ca^{2+} binding. Fura-2 AM ester is Ca^{2+} insensitive and nonpolar. Once inside the cell, esterase enzymes sequentially cleave the AM groups to leave Fura-2-free acid (Ca^{2+} sensitive, polar) trapped inside the cell, where it is able to bind Ca^{2+}. **B**: carbachol is a muscarinic receptor agonist that initiates a signalling pathway, resulting in the release of Ca^{2+} within seconds. Fura-2 exhibits a calcium dependent excitation spectral shift to report the 340/380 ratio (adapted from (Wang et al., 2015)). **C:** Schematic illustration of intracellular calcium changes as recorded by Flexstation 3. The raw data depicts the typical signals obtained from a fura-2-loaded cell when it is excited at 340 and 380 nm. Agonist stimulation will cause an increase in the 340nm signal and a decrease in the 380nm signal. Addition of an ionophore (Ionomycin) in the presence of Ca^{2+} will liberate Ca^{2+} from all intracellular stores and will result in the F_{340max} and F_{380min}.

Using a Flexstation 3 microplate fluorescent reader, baseline and variations of Fura-2 emission ratio were determined in the vehicle and poly (I:C) injected SMGs, from the AG treated and non-treated mice. We were able to record dramatic changes in Ca^{2+} homeostasis and signalling in the parenchymal clusters of mouse SMG, 24 hrs after poly (I:C) introduction. Disruption in stimulated $[Ca^{2+}]_i$ responses was observed in the form of reduced liberation of Ca^{2+} from the ER (evoked by either carbachol in Ca^{2+}-containing or ionomycin in Ca^{2+}-free medium). In addition, elevated resting $[Ca^{2+}]_i$ levels was recorded prior to compound applications. These results demonstrate the superimposition of several mechanisms implicated in the disruption of Ca^{2+} homeostasis.

The reduction in magnitude of Ca^{2+} release from the intracellular stores independent of activation of IP3R; i.e. with ionomycin, suggested the diminished $[Ca^{2+}]_{ER}$ content. This was expectedly reflected on the impairment of carbachol-stimulated Ca^{2+} release. SERCA2 isoform of the sarco/endoplasmic reticulum Ca^{2+}-ATPase is sensitive to cellular conditions of inflammation and oxidative stress as evidenced by the common appearance of 3-nitrotyrosine-modified forms of SERCA2 in diseases of human and rodent models (Bigelow, 2009). Since SERCA pump plays a major role in the rate-limiting replenishing of intracellular calcium stores after secretagouge-stimulated calcium release (Berridge et al., 2000, Bers, 2002, Vangheluwe et al., 2005, Homann et al., 2006), the physical co-localization of SERCA2 ATPase and peroxynitrite may explain the inability of the pump to replenish $[Ca^{2+}]_{ER}$, accounting for the reduced Ca^{2+} content in the intracellular store.

Importantly, AG which prevented ONOO- accumulation, induced an extremely significant recovery in the stimulated calcium response to carbachol and ionomycin, which further highlights the injurious contribution of the upregulated iNOS and it derivative; peroxynitrite in the impairment of salivary cells functioning following acute infections. Though, not comprehensively verified, it is worth noting that the extensively expressed acinar peroxynitrite may have similarly co-localized and disrupted other critical cytosolic and organellar Ca^{2+} regulators in the current model of acute SG dysfunction.

The novel protocol developed, further allowed the recording of resting $[Ca^{2+}]_i$, which showed extremely significant elevation in the poly (I:C) injected glands, prior to secretagogue additions. To investigate the basis of this finding, two buffers were formulated and used for preparation and incubations of the SMGs (Naftilan and Oparil, 1982, Pitelka et al., 1983). Our results demonstrated the overlap of more than one mechanism contributing to elevating baseline $[Ca^{2+}]_i$. Removal of calcium from the extracellular buffer as well as treatment of the mice with AG, remarkably retrieved the basal $[Ca^{2+}]_i$ levels, which denoted the likely breach of the plasma membranes in the poly (I:C) injected SMGs, mediated by iNOS or its derivative; peroxynitrite. The sites of peroxynitrite formation are assumed to be spatially associated with the sources of superoxide (such as the plasma membrane NADPH oxidases) (Szabo et al., 2007). In addition, a major aspect of peroxynitrite-dependent cytotoxicity relies on its ability to trigger lipid peroxidation in membranes, resulting in degeneration of membrane lipids (Hogg and Kalyanaraman, 1999, Radi et al., 1991) and changes in membrane permeability and fluidity, with significant biological consequences (Richter, 1987).

In the current model, immunohistochemical staining revealed the preferential localization of 3-NT in the acinar cell membranes, which may account for the unrestrained efflux of Ca^{2+} from the extracellular buffer, facilitated by the likely peroxynitrite-damaged plasma membranes.

Despite removal of Ca^{2+} from the prepared buffers, the baseline calcium level was not completely restored in the poly (I:C) injected glands, which indicated an intracellular leakage source, that may have contributed to the perceived increase in baseline Ca^{2+}. Lysosomes contain up to 600 mM calcium (Christensen et al., 2002, Lloyd-Evans et al., 2008), nearly matching the ER concentration (Bygrave and Benedetti, 1996). Immunostaining of the SMG tissue sections injected with the viral mimetic verified lysosomal membrane permeabilization (LMP) and the sequential release of the most abundant protease; cathepsin B (Rossi et al., 2004). These results were further validated by immunofluorescent dissociation of cathepsin B from lysosomal Lamp-1. Interestingly, cathepsin B may constitute an amplifying feedback loop, in which a small amount of released cathepsin B triggers more extensive LMP from outside the lysosome (Johansson et al., 2010, Liu et al., 2003). Several mechanisms can disrupt the integrity of the lysosomal membranes (Serrano-Puebla and Boya, 2016). Although the exact trigger for disruption of lysosomes in the current model has not been comprehensively investigated, we were able to verify the involvement of iNOS-dependent mechanisms. In fact, iNOS expression has been shown to evoke an increase in ROS production (Zhao et al., 2010), which can penetrate lysosomes and produce highly toxic intermediates that damage lysosomal membrane proteins, such as Hsp70 (Serrano-Puebla and Boya, 2016).

The ER is involved in folding, processing and trafficking of newly synthesised secretory and membrane proteins (Chan et al., 2011). The resting free Ca^{2+} concentration in the ER is three to four orders of magnitude higher than cytosolic Ca^{2+}. Disruption of ER homeostasis, as caused by alterations in $[Ca^{2+}]_{ER}$ concentration, leads to the accumulation of unfolded proteins and activation of a specific stress response (Rutkowski and Kaufman, 2004). In the current research, disruption of calcium homeostasis justified our rationale that exposure to excessive iNOS may have likewise driven the gland into an acute stressful condition, warranting UPR activation. To verify this hypothesis, we analysed the upregulation of genes encoding key chaperones and folding sensors as markers of UPR activation in the AG treated and non-treated glands. In the current model, we found that a single poly (I:C) dose induced iNOS-dependent UPR activation, after 9 hrs of its introduction, manifested by the increased transcriptional expression of XBP1, GRP78 (Bip), CHOP. Our results are in harmony with studies showing that pro-inflammatory cytokines could induce ER stress in cultured cells, possibly via the generation of nitric oxide (Oyadomari et al., 2001, Kharroubi et al., 2004). These studies demonstrated the role played by nitric oxide in: i) downregulation Serca2b expression, ii) depletion of ER calcium stores, and iii) induction of the ER stress pathway. Similarly, pancreatic studies reported NO-mediated induction of ER stress in rat pancreatic islets, a finding which was prevented by the iNOS blocker; N^{G}-methyl-$_{L}$-arginine (LMA) (Cardozo et al., 2005). In their study, they demonstrated that blocking NO production with LMA prevented cytokine-induced SERCA2b inhibition, ER Ca^{2+} depletion, xbp-1 mRNA processing, CHOP expression, and β-cell death.

The high demand for protein synthesis in specialized secretory SG cells requires an evolved mechanism to properly fold, process, and release proteins. This renders the SGs particularly sensitive to ER stress evolution.

With a conceptual identification of key mediators of the UPR in place, subsequent experiments turned towards investigating the relation between the verified SG stress, with its well documented negative impact on the mRNA and cellular protein realms and the compromised secretory machinery. Saliva secretion is predominantly initiated by the exciting effect of Acetylcholine on acinar M3 receptors (Proctor, 2006), followed by a multistage process which is coordinated through several ion channels and transporters, water channels, as well as polarized calcium signalling events. Therefore, we examined the mRNA expression of key water driving molecules; M3R, AQP5 water channel, as well as NKCC1 and TMEM16A ion transporters, 24 hrs following poly (I:C) injection in the AG-treated and non-treated glands. Our results revealed the global downregulation of the tested genes in the mouse SMGs following poly (I:C) administration. In a process known as regulated IRE1 dependent decay (RIDD), pIRE-1α degrades ER associated mRNAs encoding mostly secretory proteins as well as cytosolic mRNAs, to reduce protein synthesis and allow the endoplasmic reticulum (ER) to recover from the accumulation of misfolded proteins (Hollien and Weissman, 2006, Hollien et al., 2009). Our results can possibly signify the role played by the non-specific nuclease activity which may have been perceived subsequent to the acute evolution of ER stress.

Owing to the pivotal role played by the ER in calcium-activated protein folding and targeted transport (Tsai and Weissman, 2010), we presumed that iNOS-driven ER calcium depletion may have mediated defective protein folding as well as protein retention in the ER (figure 5.22).

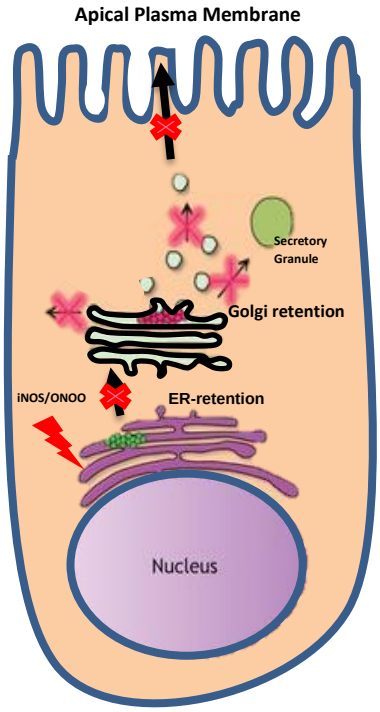

Figure 5.22 **Illustrated representation of iNOS-mediated disruption of membrane trafficking.**
Dysregulation of $[Ca^{2+}]_{ER}$ induced by iNOS or its oxidative derivative; peroxynitrite induced ER stress. Disruption of ER homeostasis may have caused misfolded proteins to be retained in the ER or in the Golgi, leading to loss-of-function.

To substantiate our hypothesis, immunohistochemical staining of the membranous water driving molecules was performed in the control and experimental glands from AG-treated and non-treated mice.

Immuno-analysis revealed that in the vehicle-injected control glands, AQP-5, TMEM16A were immunolocalized to the apical membranes of acinar cells. The furrow-shaped immunostaining pattern displayed by these molecules in normal glands represent the lateral intercellular canaliculi between neighbouring acinar cells, which are a specialized form of the lumen extending from the apical side towards the basal side between acinar cells (Pinkstaff, 1980, Segawa et al., 1998). In addition, the TMEM16A interconnecting branches seen represent the acinar-intercalated duct segments, where the ion channel is more frequently expressed in the distal portions of these ducts toward the acini (Chenevert et al., 2012). On the other hand, M3R and NKCC1 have predominantly immunolabelled the basolateral membranes of acinar cells and to a much lesser extent, NKCC1 was seen in duct cells, which may account for a functional role of Cl- uptake in these ducts. These results are in agreement with Walcott et al., who demonstrated the presence of NKCC1 in the basolateral membranes of duct and acinar cells of mice (Walcott et al., 2005). Conversely, SMGs which received the viral mimic exhibited aberrant immunoexpression after 24 hrs, with all membranous proteins displaying a granular cytoplasmic pattern. Similar accumulation of proteins in intracellular inclusion bodies has been reported in neurodegenerative disease featuring intracellular Ca^{2+} dysregulation with consecutive endoplasmic reticulum Ca^{2+} depletion (Grosskreutz et al., 2010). The preserved membranous localization of these proteins in the AG treated glands suggest that iNOS and its derivatives may have directly interfered with the SMG protein transport, presumably in an ER stress dependant manner.

Studies which deleted AQP5 (Ma et al., 1999, Krane et al., 2001), NKCC1 (Evans et al., 2000) and TMEM16A (Ousingsawat et al., 2009, Catalan et al., 2015) revealed vast reduction in saliva secretion. The present study demonstrates, for the first time, that loss of saliva secretion following acute SG infections and extensive iNOS upregulation, paralleled the ectopic cytoplasmic expression of membranous water and ion transport proteins.

The current SG dysfunction model develops rapidly, with clearly defined initial triggering and pathogenic processes. Accordingly, we were able to comprehensively characterize the signals which sequentially prompted loss of function. The perceived iNOS-driven **dysregulation of Ca^{2+}** homeostasis and the resultant ER stress-induced **aberrant expression** of key membranous water driving proteins, projected the dysfunction mechanisms by which acute infections can impair the salivary gland secretory machinery.

Chapter 6

General Discussion

Acute infections are often associated with SG pathology. To decipher the signal which triggers injury and dysfunction in the acutely infected SGs, it was essential to develop an *in vivo* model dually featuring functional compromise and innate immune exocrinopathy. Although viruses do not normally reach the SGs via a retrograde ductal route, we injected poly (I:C) locally into the SMGs to avoid systemic delivery, which is more likely to dilute the poly (I:C) and minimize the chance of its efficient exposure to the parenchymal cells. The cannulation technique established, allowed for the development of a reliable and reproducible mouse model, whereby intraductal conveyance of poly (I:C) pre-mixed with trypan blue fulfilled our aim in consistently ensuring successful infusion and delivering the same amount of the viral mimic into the SMGs (even when other drugs: TLR3/dsRNA inhibitor, RB6-8C5, z-VAD-fmk and AG, were systemically or locally used). In addition, this local innate immune activation protocol allowed us to rule out possible extraneous impacts that can arise from systemic delivery of the inflammagen. Another advantage of the current model was the possibility of temporally characterizing the innate immune events occurring in conjunction with the loss of function, this helped us during the quest for the signal which induced the early perceived dysfunction. For example, although it was completely surprising that the invasive MPO positive neutrophils/monocytes which infiltrated the gland 6hrs post poly (I:C) injection were bystanders in the current model (given their injurious roles during acute microbial infections), it became clear that extensive iNOS expression as early as 3hrs following delivery of the viral mimic has initialized the dysfunction signal even earlier than the immune cell infiltration. These results similarly, excluded any role played by potentially detrimental cytokines; like IL-1β, COX2 and IL-6, in the perceived loss of function.

To protect against viral infection, the host innate immune system has evolved sensors of nucleic acids. The same nucleic acid sensors that defend against viruses may also contribute to the SG pathogenesis (Holdgate and St Clair, 2016). In the current model of SG dysfunction, we have shown the indispensable injurious role played by TLR3. TLR3 activation must be strictly regulated; one mechanism by which this is achieved is its compartmentalization to intracellular locations where it is unlikely to encounter its ligand unless infection or tissue damage occurs (Oshiumi et al., 2003). Moreover, therapeutic modulation of TLR3 pathways has offered an attractive strategy to fight a variety of diseases. Cheng et al, successfully used specific small molecule agents to target the protein-RNA interface and disrupt dsRNA binding to TLR3 (Cheng et al., 2011). Interestingly, to evaluate the drug's inhibitory activity, they monitored the NO level as an indicator of poly (I:C)-induced TLR3 activation. In the current study, we used a thiophenecarboxamidopropionate compound that acts as a direct, competitive and high affinity inhibitor of dsRNA binding to TLR3 and selectively antagonizes stimulated TLR3 by blocking signalling at the receptor level. We showed for the first time that *in vivo* inhibition of TLR3 effectively rescues viral-induced secretory hypofunction and ameliorates injury-inducing downstream signals. Thus, our findings suggest blockade of TLR3 as a new therapeutic strategy for the treatment of SG or oral diseases with viral implications. Previous studies have shown that the TLR3/dsRNA complex inhibitor can be highly protective against TLR3-mediated tissue injury, even when administered after exposure to the damaging agent (Takemura et al., 2014).

Accordingly, the TLR3 inhibition mouse model presented in this study may be promising for assessment of the functional and pathologic consequences of restricting this PRR in mice with well-established chronic inflammation or autoimmune diseases.

One of the main and unexpected findings in the present study is the role played by the protease inhibitor; z-VAD-fmk in regulating the innate immune responses via controlling upregulation of TLR-3 and restricting its downstream signalling. The roles of endolysosomal proteases in innate immunity through the activation of TLRs has been previously highlighted. Endolysosomal TLRs are synthesized as quiescent pro-forms that have to be proteolytically activated to carry out their function (Bird et al., 2009). This has been shown for TLR9 (Ewald et al., 2008, Matsumoto et al., 2008, Park et al., 2008), TLR7 (Ewald et al., 2008) and TLR3 (Garcia-Cattaneo et al., 2012, Toscano et al., 2013). Interestingly, analyses of several protease-deficient cells and of the effects of protease inhibitors have concluded that no single protease is responsible for TLR7 or TLR9 processing, indicating that there is redundancy in this reaction (Ewald et al., 2008, Matsumoto et al., 2008, Park et al., 2008).

Previously, it has been shown that z-VAD-fmk inhibition of caspase 3 led to the down-regulation of JNK/SAPK and NF-kB, which were required for LPS-induced iNOS expression and NO production (Chakravortty et al., 2001). In the current model, we showed efficient control of TLR3 upregulation and abrogation of a wide array of cytokines in response to z-VAD-fmk, rendering this pan caspase inhibitor a promising immune-modulating drug that can restrict the tissue damaging effects of uncontrolled cytokine and signal propagation following acute viral infections.

Previous studies designed to investigate the role played by innate immunity in SG injury, considered type-I IFNs to be the chief contributors to dysfunction (Nandula et al., 2013). The outcome of our study, showing iNOS as the innate immune damaging signal may not be contradictory with these studies, since type-I interferons can promote upregulation of iNOS in various models (Zwaferink et al., 2008, Utaisincharoen et al., 2004, Bogdan et al., 2000). In addition, deletion of type-I IFN receptor; IFNAR-1, has substantially compromised iNOS induction (Huys et al., 2009).

This is due to the multiple binding sites for factors modulated by type-I IFNs recognized in the promoter region of the iNOS gene, including IFN-stimulated response element (ISRE), and IFN-regulatory factor element (IRF-E) (Xie et al., 1993). The scenario which may have taken place following introduction of poly (I:C) can be summarized in figure 6.1. TLR3 C-terminal which has been basally detected in the intercalated ducts may have initiated the entire response to poly (I:C) entry, inducing nuclear translocation of NF-κβ in these cells and upregulating IFN-β and IFN-γ. In turn, the released interferons may have signalled the neighbouring duct and acinar cells to: (i) enhance TLR3 mRNA synthesis (Miettinen et al., 2001), (ii) activate NF-κβ (Yang et al., 2005) and (iii) upregulate iNOS (Zwaferink et al., 2008, Utaisincharoen et al., 2004), which prompted the acinar cells into a state of injury and loss of function.

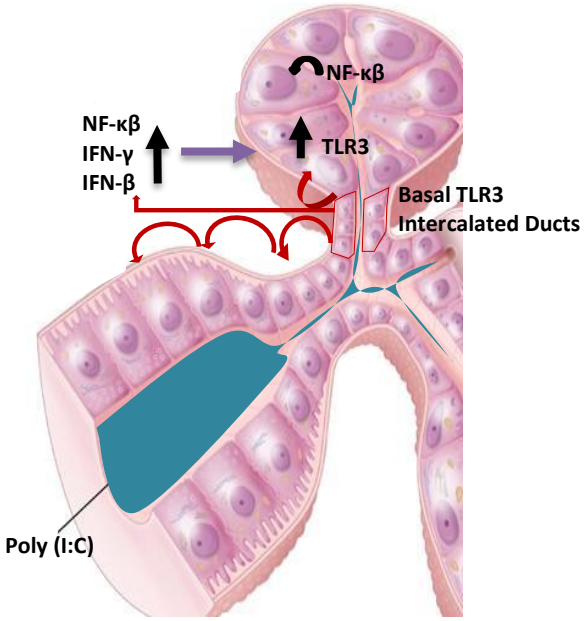

Figure 6.1 **Summary illustration depicting propagation of the immune signal initialized in TLR3 positive intercalated ducts to the neighbouring acinar and duct cells.**

Different studies have shown that acinar cells are able to activate signalling pathways involved in the expression of inflammatory mediators (Gukovsky et al., 1998, Ramudo et al., 2009, Ramnath et al., 2009, Dios, 2010). This changed the classically recognised theory that glandular injury would trigger a local and systemic inflammatory response, in which the immune cells play the central role. In addition, the exocrine acinar cells have displayed efficient ability to produce: (i) cytokines such as TNF-α, IL-6 and IL-1β (Gukovskaya et al., 1997, Blinman et al., 2000, Kim et al., 2000), (ii) chemokines such as CXCL1 (KC), monocyte chemoattractant protein-1 (MCP-1) or CCL2 and macrophage inflammatory protein 2 (MIP-2) or CXCL2 (Blinman et al., 2000) and (iii) adhesion molecules example intercellular adhesion molecule 1 (ICAM-1) (Zaninovic et al., 2000, Ramudo et al., 2007).

One of the interesting findings in the present study is the demonstrated ability of SG epithelial cells to overexpress different types of inflammatory mediators in response to innate immune activation. We have shown that during acute infection: (i) NF-κB was translocated to both ductal and acinar nuclei, (ii) SMG ducts displayed enhanced production of IFN-β, IFN-γ and Cox2 and (iii) acinar cells intensively expressed IFN-β, and iNOS. By showing that the exocrine parenchyma expresses these cytokines as early as 6 hrs after injection of an inflammagen, we clearly demonstrate the dominant role of these cells in releasing the first inflammatory signals in response to the injury initiated within them, independent of the bystander role assigned to the infiltrating immune cells.

The most important finding in the current study is the pattern of $[Ca^{2+}]_i$ disruption which was detected very early in the acinar cells upon their exposure to the viral mimic, TLR3 stimulation and iNOS overproduction. We have shown that this trilogy can trigger: (i) Ca^{2+} depletion from intracellular endoplasmic reticulum stores, (ii) increase Ca^{2+} entry through the plasma membrane, (iii) release Ca^{2+} from membrane-perturbed lysosomes and (iv) potentially affect Ca^{2+} pumps. Previous studies have allocated responses that can prevent Ca^{2+} mobilization as candidates for pathogenesis of SS (Caulfield et al., 2009) and radiation-induced SG damage (Coppes et al., 2005). In fact, these studies were based on earlier reports relating the pathological inhibition of salivary secretion to NO release (Konttinen et al., 1997). Alternatively, due to the increased occurrence of glandular destruction in SS (Duffy and O'Reilly, 2016) and following irradiation (Marino et al., 2014), release of DAMPs can represent a sustained endogenous source of TLR3 ligation, which can amplify the cycle of iNOS overexpression, NO production and Ca^{2+} signal disruption.

The present study may not only relate to the combination of events that drive glands from SS or irradiated patients to stop secretion but also outline the early time course of possible interaction between the immune system and interference with stimulus-secretion coupling.

In the final part of this study, it was revealed, for the first time, that one of the early acute events following exposure to a viral mimic and/or TLR3 stimulation is the activation of ER stress. In the current model, ER stress can be simply related to $[Ca^{2+}]_{ER}$ depletion, which may have culminated into loss of function by downregulating the mRNA machinery, protein translation or disrupted trafficking of key membranous water-driving molecules.

Interestingly, a mouse model of acute pancreatitis revealed that induction of ER stress provides acini an opportunity to suppress their secretory function and regenerate damaged cells, as evidenced by the acinar and centroacinar regenerative response which followed the exocrine disease (Hess et al., 2011). Indeed, ER stress is implicated in various inflammatory pathological conditions (Grootjans et al., 2016) and investigations have revealed a reciprocal regulation between ER stress and inflammation. ER stress can directly initiate inflammatory pathways and, in turn, pro-inflammatory stimuli such as ROS, TLR ligands and cytokines can trigger ER stress — such that the resulting UPR activation can further amplify inflammatory responses (Zhang et al., 2006). To what extent our results reproduce the chronic state that occurs in SG inflammation is an open question and ER stress may provide the link between chronic SG inflammation and loss of function. The scenario of acute viral SG injury and dysfunction generated by the present model can be summarized as in figure 6.2.

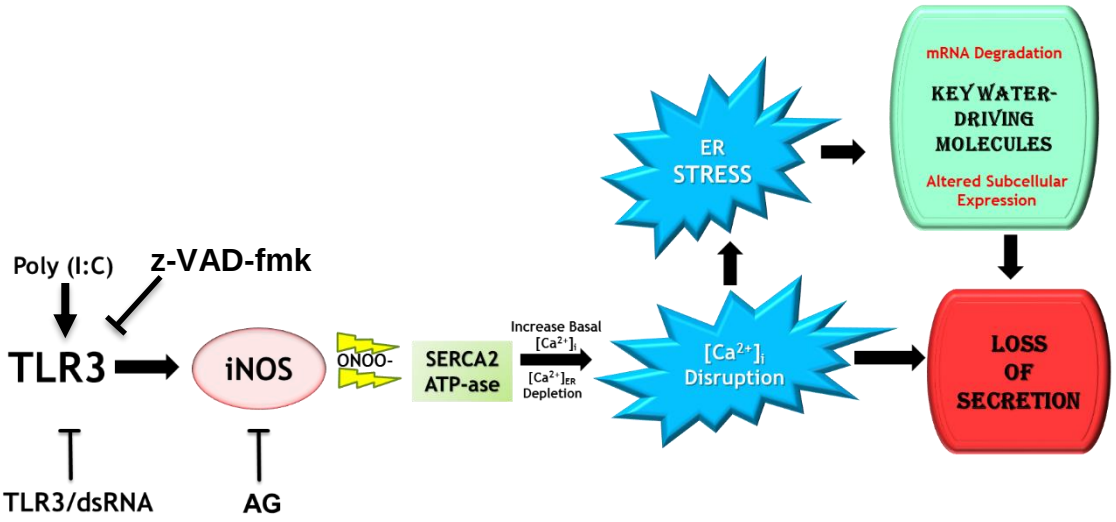

Figure 6.2 Summary illustration depicting the main TLR-3 mediated signalling events that induced SMG injury and loss of secretion and the drugs used to counteract the poly (I:C) injurious effects.

Chapter 7

Future Plans

The results presented in the current study have demonstrated clearly the mechanisms underlying loss of saliva secretion following exposure to primary viral infections. However, the mouse model developed herein outlines further aspects of research worthy of investigation.

- **Development of an SS Model Based Solely on Multiple Poly (I:C) Injections**

Initial independent experiments (not shown) provisionally showed that a total of four intraductal infusions of poly (I:C) (single injection/week for four consecutive weeks), resulted in loss of function, 24 hrs after the last injection received and infiltration of all SMG lobules with 1-3 peri-vascular immune cell clusters. Nevertheless, auto-antibody formation has not been verified, it may be promising to follow up with this protocol, towards: (i) possible development of an SS model, based uniquely on dynamic cycles of acute viral infections and (ii) verifying if the injurious mechanisms operating in the presented acute model are comparable to those perceived in the chronic autoimmune state.

- **Role Played by Cathepsins in SMG Injury and Dysfunction**

Primary experiments (two mice) utilizing the cathepsin B inhibitor; CA-074, revealed recovery of the poly (I:C) injected glands. Further reproducibility of these experiments added to the broadly verified z-VAD-fmk results provide a comprehensive foundation upon which further work can be executed to entirely confirm the beneficial role of cathepsin B inhibition in diseases featuring uncontrolled innate immune activation by endosomal TLRs (TLR3, 7, 8, 9 and 13 (O'Neill et al., 2013)).

- **Identification of the Mechanisms Involved in LMP**

In the present SMG mouse model, a single injection of poly (I:C) rapidly triggered global disruption of lysosomal membranes and release of the organelle contents, as early as 9 hrs post infection. Lysosomes form an ‘‘Achilles heel’’ for cancer cells by sensitizing them to death pathways through LMP, providing a potential new anti-cancer target. Through appropriate stimuli, the lysosome membrane is permeated to release lysosomal enzymes, especially cathepsin B, into the cytosol (Gao et al., 2014). Release of cathepsin B activates caspase-dependent death pathways, promoting cancer cell death even if those cancer cells are resistant to normal apoptotic pathways (Boya and Kroemer, 2008). Thus, many approaches have been developed to induce LMP, such as oxidation (Denamur et al., 2011) and cytotoxic cytokines (Erdal et al., 2005). Among these, reactive oxygen species (ROS)-associated oxidation has attracted much attention because it can cause rapid lysosomal leakage and dysfunction, causing cells to undergo apoptosis with high efficacy at low dose (Lin et al., 2010). However, ROS is generally cytotoxic and not cell specific, therefore, new strategies to selectively induce ROS-triggered LMP in cancer cells are needed for current anticancer therapy so as to prevent harmful side effects and increase treatment efficacy (Gao et al., 2014). The viral mimic provoked local LMP and cathepsin B release in the present mouse model. Thorough investigation of the mechanisms underlying poly (I:C)-triggered LMP may offer promising opportunities to limit this phenomenon to cancer cells, via driving them to express or signal in the same way which prompted the SMG duct cell lysosomes to disrupt and release their contents into the surrounding tissues.

- **TLR3 Modulation in Chronic Mucosal Inflammation and Autoimmunity**

The current study unravelled two mechanisms which efficiently controlled TLR3 upregulated expression and downstream inflammatory mediators in the SMGs, despite the presence of a potent stimulant; poly (I:C). The use of protease inhibitors in oral mucosal and SG diseases featuring chronically stimulated TLR3 receptors may act as brakes that can regulate and fine-tune the repeated cycles of mucosal damage by cytokines and apoptotic signals.

- **Regeneration of the mouse SMGs Following Activation of the Innate Immunity**

Stimulation of TLR3 causes rapid and global changes in the expression of epigenetic modifiers to enhance chromatin remodeling and nuclear reprogramming (Lee et al., 2012a). In the context of regenerative medicine, epigenetics is becoming a pivotal area of interest (Consalvi et al., 2016). The current model may be insightful for the study of regeneration following acute viral infections and the epigenetic events in SGs following injury, supported by the synchronized innate immune activation and TLR3 ligation. Moreover, owing to the resident stem or progenitor cell population harbored by SGs, which is capable of regenerating the parenchyme (Denny et al., 1993), stem cell-derived extracellular vesicles appear to be naturally equipped to mediate tissue regeneration (Ono et al., 2015) and recent evidence suggests their therapeutic potential for targeted delivery of exogenous miRNAs (Vlassov et al., 2012). Isolating and characterizing the exosomes secreted in the regeneration phase of this rapid-developing model can provide valuable information on the extracellular niches that can drive regeneration of injured SGs.

Chapter 8

References

ACAUAN, M. D., FIGUEIREDO, M. A. Z., CHERUBINI, K., GOMES, A. P. N. & SALUM, F. G. 2015. Radiotherapy-induced salivary dysfunction: Structural changes, pathogenetic mechanisms and therapies. *Archives of Oral Biology,* 60**,** 1802-1810.

AKIRA, S. & TAKEDA, K. 2004. Toll-like receptor signalling. *Nat Rev Immunol,* 4**,** 499-511.

ALBERT, P. R. & TASHJIAN, A. H., JR. 1986. Ionomycin acts as an ionophore to release TRH-regulated Ca2+ stores from GH4C1 cells. *Am J Physiol,* 251**,** C887-91.

ALDAPE, K., GINZINGER, D. G. & GODFREY, T. E. 2002. Real-time quantitative polymerase chain reaction: a potential tool for genetic analysis in neuropathology. *Brain Pathol,* 12**,** 54-66.

ALDERTON, W. K., COOPER, C. E. & KNOWLES, R. G. 2001. Nitric oxide synthases: structure, function and inhibition. *Biochem J,* 357**,** 593-615.

ALEXOPOULOU, L., HOLT, A. C., MEDZHITOV, R. & FLAVELL, R. A. 2001. Recognition of double-stranded RNA and activation of NF-kappaB by Toll-like receptor 3. *Nature,* 413**,** 732-8.

ALPER, S. L. 2009. Molecular physiology and genetics of Na+-independent SLC4 anion exchangers. *J Exp Biol,* 212**,** 1672-83.

AMANO, O. & ISEKI, S. 1993. Expression, localization and developmental regulation of insulin-like growth factor I mRNA in rat submandibular gland. *Archives of Oral Biology,* 38**,** 671-677.

AMANO, O. & ISEKI, S. 2001. [Expression and localization of cell growth factors in the salivary gland: a review]. *Kaibogaku Zasshi,* 76**,** 201-12.

AMANO, O., MATSUMOTO, K., NAKAMURA, T. & ISEKI, S. 1994. Expression and localization of hepatocyte growth factor in rat submandibular Gland. *Growth Factors,* 10**,** 145-151.

AMANO, O., MIZOBE, K., BANDO, Y. & SAKIYAMA, K. 2012. Anatomy and histology of rodent and human major salivary glands: -overview of the Japan salivary gland society-sponsored workshop. *Acta Histochem Cytochem,* 45**,** 241-50.

AMANO, O., TSUJI, T., NAKAMURA, T. & ISEKI, S. 1991. Expression of transforming growth factor beta 1 in the submandibular gland of the rat. *J Histochem Cytochem,* 39**,** 1707-11.

AMBUDKAR, I. S. 2014. Ca(2)(+) signaling and regulation of fluid secretion in salivary gland acinar cells. *Cell Calcium,* 55**,** 297-305.

AMBUDKAR, I. S. & MUALLEM, S. 2016. ROS and Ca2+—Partners in sickness and in health. *Cell Calcium,* 60**,** 51-54.

ANDERSON, L. C., GARRETT, J. R., ZHANG, X., PROCTOR, G. B. & SHORI, D. K. 1995. Differential secretion of proteins by rat submandibular acini and granular ducts on graded autonomic nerve stimulations. *J Physiol,* 485 (Pt 2)**,** 503-11.

ARREOLA, J., MELVIN, J. E. & BEGENISICH, T. 1996. Activation of calcium-dependent chloride channels in rat parotid acinar cells. *J Gen Physiol,* 108**,** 35-47.

ASKING, B. & GJORSTRUP, P. 1987. Synthesis and secretion of amylase in the rat parotid gland following autonomic nerve stimulation in vivo. *Acta Physiol Scand,* 130**,** 439-45.

AYDOGAN, S., YERER, M. B. & GOKTAS, A. 2006. Melatonin and nitric oxide. *J Endocrinol Invest,* 29**,** 281-7.

BALACHANDRAN, S., KIM, C. N., YEH, W. C., MAK, T. W., BHALLA, K. & BARBER, G. N. 1998. Activation of the dsRNA-dependent protein kinase, PKR, induces apoptosis through FADD-mediated death signaling. *Embo j,* 17**,** 6888-902.

BALASUBRAMANYAM, M., BALAJI, R. A., SUBASHINI, B. & MOHAN, V. 2001. Evidence for mechanistic alterations of Ca2+ homeostasis in Type 2 diabetes mellitus. *Int J Exp Diabetes Res,* 1**,** 275-87.

BANKS, P. 1968. Nonneoplastic parotid swellings: a review. *Oral Surg Oral Med Oral Pathol,* 25**,** 732-45.

BARTON, G. M. & KAGAN, J. C. 2009. A cell biological view of Toll-like receptor function: regulation through compartmentalization. *Nature reviews. Immunology,* 9**,** 535-542.

BARTON, G. M., KAGAN, J. C. & MEDZHITOV, R. 2006. Intracellular localization of Toll-like receptor 9 prevents recognition of self DNA but facilitates access to viral DNA. *Nat Immunol,* 7**,** 49-56.

BELL, J. K., BOTOS, I., HALL, P. R., ASKINS, J., SHILOACH, J., SEGAL, D. M. & DAVIES, D. R. 2005. The molecular structure of the Toll-like receptor 3 ligand-binding domain. *Proceedings of the National Academy of Sciences of the United States of America,* 102**,** 10976-10980.

BERRIDGE, M. J. 1993. Inositol trisphosphate and calcium signalling. *Nature,* 361**,** 315-25.

BERRIDGE, M. J., BOOTMAN, M. D. & RODERICK, H. L. 2003. Calcium signalling: dynamics, homeostasis and remodelling. *Nature Rev. Mol. Cell Biol.,* 4**,** 517-529.

BERRIDGE, M. J., LIPP, P. & BOOTMAN, M. D. 2000. The versatility and universality of calcium signalling. *Nat Rev Mol Cell Biol,* 1**,** 11-21.
BERS, D. M. 2002. Cardiac excitation-contraction coupling. *Nature,* 415**,** 198-205.
BETTIGOLE, S. E. & GLIMCHER, L. H. 2015. Endoplasmic reticulum stress in immunity. *Annu Rev Immunol,* 33**,** 107-38.
BIESSELS, G. J., TER LAAK, M. P., HAMERS, F. P. & GISPEN, W. H. 2002. Neuronal Ca2+ disregulation in diabetes mellitus. *Eur J Pharmacol,* 447**,** 201-9.
BIGELOW, D. J. 2009. Nitrotyrosine-modified SERCA2: a cellular sensor of reactive nitrogen species. *Pflugers Arch,* 457**,** 701-10.
BIRD, P. I., TRAPANI, J. A. & VILLADANGOS, J. A. 2009. Endolysosomal proteases and their inhibitors in immunity. *Nat Rev Immunol,* 9**,** 871-882.
BJ BAUM, W. R. 1999. *Receptors in salivary glands.*, Basel: Karger,.
BLASIUS, A. L. & BEUTLER, B. 2010. Intracellular toll-like receptors. *Immunity,* 32**,** 305-15.
BLINMAN, T. A., GUKOVSKY, I., MOURIA, M., ZANINOVIC, V., LIVINGSTON, E., PANDOL, S. J. & GUKOVSKAYA, A. S. 2000. Activation of pancreatic acinar cells on isolation from tissue: cytokine upregulation via p38 MAP kinase. *Am J Physiol Cell Physiol,* 279**,** C1993-2003.
BOGDAN, C., ROLLINGHOFF, M. & DIEFENBACH, A. 2000. Reactive oxygen and reactive nitrogen intermediates in innate and specific immunity. *Curr Opin Immunol,* 12**,** 64-76.
BOLOTINA, V. M. 2004. Store-operated channels: diversity and activation mechanisms. *Sci STKE,* 2004**,** pe34.
BOMBARDIERI, M., BARONE, F., LUCCHESI, D., NAYAR, S., VAN DEN BERG, W. B., PROCTOR, G., BUCKLEY, C. D. & PITZALIS, C. 2012. Inducible tertiary lymphoid structures, autoimmunity and exocrine dysfunction in a novel model of salivary gland inflammation in C57BL/6 mice(). *Journal of immunology (Baltimore, Md. : 1950),* 189**,** 3767-3776.
BOWZARD, J. B., DAVIS, W. G., JEISY-SCOTT, V., RANJAN, P., GANGAPPA, S., FUJITA, T. & SAMBHARA, S. 2011. PAMPer and tRIGer: ligand-induced activation of RIG-I. *Trends Biochem Sci,* 36**,** 314-9.
BOYA, P. & KROEMER, G. 2008. Lysosomal membrane permeabilization in cell death. *Oncogene,* 27**,** 6434-51.
BRAVO, R., PARRA, V., GATICA, D., RODRIGUEZ, A. E., TORREALBA, N., PAREDES, F., WANG, Z. V., ZORZANO, A., HILL, J. A., JAIMOVICH, E., QUEST, A. F. & LAVANDERO, S. 2013. Endoplasmic reticulum and the unfolded protein response: dynamics and metabolic integration. *Int Rev Cell Mol Biol,* 301**,** 215-90.
BRENCICOVA, E. & DIEBOLD, S. S. 2013. Nucleic acids and endosomal pattern recognition: how to tell friend from foe? *Frontiers in Cellular and Infection Microbiology,* 3**,** 37.
BROWN, J., WANG, H., HAJISHENGALLIS, G. N. & MARTIN, M. 2011. TLR-signaling networks: an integration of adaptor molecules, kinases, and cross-talk. *J Dent Res,* 90**,** 417-27.
BRUNO MIGUEL NEVES, M. C. L. A. M. T. C. 2012. Pathogen Strategies to Evade Innate Immune Response: A Signaling Point of View. *In:* XAVIER, G. D. S. (ed.) *Protein Kinases.*
BYGRAVE, F. L. & BENEDETTI, A. 1996. What is the concentration of calcium ions in the endoplasmic reticulum? *Cell Calcium,* 19**,** 547-51.
CAIN, C. C., SIPE, D. M. & MURPHY, R. F. 1989. Regulation of endocytic pH by the Na+,K+-ATPase in living cells. *Proc Natl Acad Sci U S A,* 86**,** 544-8.
CARDOZO, A. K., ORTIS, F., STORLING, J., FENG, Y. M., RASSCHAERT, J., TONNESEN, M., VAN EYLEN, F., MANDRUP-POULSEN, T., HERCHUELZ, A. & EIZIRIK, D. L. 2005. Cytokines downregulate the sarcoendoplasmic reticulum pump Ca2+ ATPase 2b and deplete endoplasmic reticulum Ca2+, leading to induction of endoplasmic reticulum stress in pancreatic beta-cells. *Diabetes,* 54**,** 452-61.
CARPENTER, G. H., PROCTOR, G. B., ANDERSON, L. C., ZHANG, X. S. & GARRETT, J. R. 2000. Immunoglobulin A secretion into saliva during dual sympathetic and parasympathetic nerve stimulation of rat submandibular glands. *Exp Physiol,* 85**,** 281-6.
CARROZZO, M. 2008. Oral diseases associated with hepatitis C virus infection. Part 1. sialadenitis and salivary glands lymphoma. *Oral Dis,* 14**,** 123-30.
CASKEY, M., LEFEBVRE, F., FILALI-MOUHIM, A., CAMERON, M. J., GOULET, J. P., HADDAD, E. K., BRETON, G., TRUMPFHELLER, C., POLLAK, S., SHIMELIOVICH, I., DUQUE-ALARCON, A., PAN, L., NELKENBAUM, A., SALAZAR, A. M., SCHLESINGER, S. J., STEINMAN, R. M. & SEKALY, R. P. 2011. Synthetic double-stranded RNA induces innate immune responses similar to a live viral vaccine in humans. *J Exp Med,* 208**,** 2357-66.

CATALAN, M. A., KONDO, Y., PENA-MUNZENMAYER, G., JARAMILLO, Y., LIU, F., CHOI, S., CRANDALL, E., BOROK, Z., FLODBY, P., SHULL, G. E. & MELVIN, J. E. 2015. A fluid secretion pathway unmasked by acinar-specific Tmem16A gene ablation in the adult mouse salivary gland. *Proc Natl Acad Sci U S A,* 112**,** 2263-8.

CATALÁN, M. A., KONDO, Y., PEÑA-MUNZENMAYER, G., JARAMILLO, Y., LIU, F., CHOI, S., CRANDALL, E., BOROK, Z., FLODBY, P., SHULL, G. E. & MELVIN, J. E. 2015. A fluid secretion pathway unmasked by acinar-specific Tmem16A gene ablation in the adult mouse salivary gland. *Proceedings of the National Academy of Sciences of the United States of America,* 112**,** 2263-2268.

CAULFIELD, V. L., BALMER, C., DAWSON, L. J. & SMITH, P. M. 2009. A role for nitric oxide-mediated glandular hypofunction in a non-apoptotic model for Sjogren's syndrome. *Rheumatology (Oxford),* 48**,** 727-33.

CHAI, Y., KLAUSER, D. K., DENNY, P. A. & DENNY, P. C. 1993. Proliferative and structural differences between male and female mouse submandibular glands. *Anat Rec,* 235**,** 303-11.

CHAKRAVORTTY, D., KATO, Y., SUGIYAMA, T., KOIDE, N., MU, M. M., YOSHIDA, T. & YOKOCHI, T. 2001. Inhibition of caspase 3 abrogates lipopolysaccharide-induced nitric oxide production by preventing activation of NF-kappaB and c-Jun NH2-terminal kinase/stress-activated protein kinase in RAW 264.7 murine macrophage cells. *Infect Immun,* 69**,** 1315-21.

CHAN, J. Y., COONEY, G. J., BIDEN, T. J. & LAYBUTT, D. R. 2011. Differential regulation of adaptive and apoptotic unfolded protein response signalling by cytokine-induced nitric oxide production in mouse pancreatic beta cells. *Diabetologia,* 54**,** 1766-76.

CHANDAK, R., DEGWEKAR, S., CHANDAK, M. & RAWLANI, S. 2012. Acute submandibular sialadenitis-a case report. *Case Rep Dent,* 2012**,** 615375.

CHANG, L. W., FU, A., WOZNIAK, E., CHOW, M., DUKE, D. G., GREEN, L., KELLEY, K., HERNANDEZ, J. A. & JACOBSON, E. R. 2013. Immunohistochemical detection of a unique protein within cells of snakes having inclusion body disease, a world-wide disease seen in members of the families Boidae and Pythonidae. *PLoS One,* 8**,** e82916.

CHANNON, K. M. & GUZIK, T. J. 2002. Mechanisms of superoxide production in human blood vessels: relationship to endothelial dysfunction, clinical and genetic risk factors. *J Physiol Pharmacol,* 53**,** 515-24.

CHATTOPADHYAY, S. & SEN, G. C. 2014. dsRNA-activation of TLR3 and RLR signaling: gene induction-dependent and independent effects. *J Interferon Cytokine Res,* 34**,** 427-36.

CHENEVERT, J., DUVVURI, U., CHIOSEA, S., DACIC, S., CIEPLY, K., KIM, J., SHIWARSKI, D. & SEETHALA, R. R. 2012. DOG1: a novel marker of salivary acinar and intercalated duct differentiation. *Mod Pathol,* 25**,** 919-29.

CHENG, K., WANG, X. & YIN, H. 2011. Small Molecule Inhibitors of the TLR3/dsRNA Complex. *Journal of the American Chemical Society,* 133**,** 3764-3767.

CHENG, K. T., ONG, H. L., LIU, X. & AMBUDKAR, I. S. 2013. Contribution and regulation of TRPC channels in store-operated Ca2+ entry. *Curr Top Membr,* 71**,** 149-79.

CHILDS, K. S., RANDALL, R. E. & GOODBOURN, S. 2013. LGP2 plays a critical role in sensitizing mda-5 to activation by double-stranded RNA. *PLoS One,* 8**,** e64202.

CHINTALA, S. K., PUTRIS, N. & GENO, M. 2015. Activation of TLR3 Promotes the Degeneration of Retinal Ganglion Cells by Upregulating the Protein Levels of JNK3. *Investigative Ophthalmology & Visual Science,* 56**,** 505-514.

CHOE, J., KELKER, M. S. & WILSON, I. A. 2005. Crystal structure of human toll-like receptor 3 (TLR3) ectodomain. *Science,* 309**,** 581-5.

CHOU, K. C., JONES, D. & HEINRIKSON, R. L. 1997. Prediction of the tertiary structure and substrate binding site of caspase-8. *FEBS Lett,* 419**,** 49-54.

CHRISTENSEN, K. A., MYERS, J. T. & SWANSON, J. A. 2002. pH-dependent regulation of lysosomal calcium in macrophages. *J Cell Sci,* 115**,** 599-607.

CLARKE, D. L., DAVIS, N. H., MAJITHIYA, J. B., PIPER, S. C., LEWIS, A., SLEEMAN, M. A., CORKILL, D. J. & MAY, R. D. 2014. Development of a mouse model mimicking key aspects of a viral asthma exacerbation. *Clin Sci (Lond),* 126**,** 567-80.

CLEMENS, M. J. 1997. PKR--a protein kinase regulated by double-stranded RNA. *Int J Biochem Cell Biol,* 29**,** 945-9.

CONSALVI, S., SANDONA, M. & SACCONE, V. 2016. Epigenetic Reprogramming of Muscle Progenitors: Inspiration for Clinical Therapies. *Stem Cells Int,* 2016**,** 6093601.

COOK, D. I., DINUDOM, A., KOMWATANA, P. & YOUNG, J. A. 1998. Control of Na+ transport in salivary duct epithelial cells by cytosolic Cl- and Na+. *Eur J Morphol,* 36 Suppl**,** 67-73.

COOK DI, V. L. E., ROBERTS ML, YOUNG J 1994. *Secretion by the major salivary glands.,* Raven, New York.

COPPES, R. P., METER, A., LATUMALEA, S. P., ROFFEL, A. F. & KAMPINGA, H. H. 2005. Defects in muscarinic receptor-coupled signal transduction in isolated parotid gland cells after in vivo irradiation: evidence for a non-DNA target of radiation. *Br J Cancer,* 92**,** 539-46.

CORREIA, P. N., CARPENTER, G. H., PATERSON, K. L. & PROCTOR, G. B. 2010. Inducible nitric oxide synthase increases secretion from inflamed salivary glands. *Rheumatology (Oxford),* 49**,** 48-56.

CUDDIHY, A. R., LI, S., TAM, N. W., WONG, A. H., TAYA, Y., ABRAHAM, N., BELL, J. C. & KOROMILAS, A. E. 1999. Double-stranded-RNA-activated protein kinase PKR enhances transcriptional activation by tumor suppressor p53. *Mol Cell Biol,* 19**,** 2475-84.

CUFI, P., DRAGIN, N., WEISS, J. M., MARTINEZ-MARTINEZ, P., DE BAETS, M. H., ROUSSIN, R., FADEL, E., BERRIH-AKNIN, S. & LE PANSE, R. 2013. Implication of double-stranded RNA signaling in the etiology of autoimmune myasthenia gravis. *Ann Neurol,* 73**,** 281-93.

CUNNINGHAM, P. N., WANG, Y., GUO, R., HE, G. & QUIGG, R. J. 2004. Role of Toll-like receptor 4 in endotoxin-induced acute renal failure. *J Immunol,* 172**,** 2629-35.

CUNNINGTON, P. G. & NAYSMITH, J. D. 1975. Naturally occurring double-stranded RNA and immune responses. Effects on plaque-forming cells and antibody formation. *Immunology,* 28**,** 451-68.

DALEY, J. M., THOMAY, A. A., CONNOLLY, M. D., REICHNER, J. S. & ALBINA, J. E. 2008. Use of Ly6G-specific monoclonal antibody to deplete neutrophils in mice. *J Leukoc Biol,* 83**,** 64-70.

DAWSON, L. J., FOX, P. C. & SMITH, P. M. 2006. Sjogrens syndrome--the non-apoptotic model of glandular hypofunction. *Rheumatology (Oxford),* 45**,** 792-8.

DE ALBA, J., OTAL, R., CALAMA, E., DOMENECH, A., PRATS, N., GOZZARD, N. & MIRALPEIX, M. 2015. Double-stranded RNA evokes exacerbation in a mouse model of corticosteroid refractory asthma. *Clin Sci (Lond),* 129**,** 973-87.

DE BOUTEILLER, O., MERCK, E., HASAN, U. A., HUBAC, S., BENGUIGUI, B., TRINCHIERI, G., BATES, E. E. & CAUX, C. 2005. Recognition of double-stranded RNA by human toll-like receptor 3 and downstream receptor signaling requires multimerization and an acidic pH. *J Biol Chem,* 280**,** 38133-45.

DE LA CAL, C., LOMNICZI, A., MOHN, C. E., DE LAURENTIIS, A., CASAL, M., CHIARENZA, A., PAZ, D., MCCANN, S. M., RETTORI, V. & ELVERDIN, J. C. 2006. Decrease in salivary secretion by radiation mediated by nitric oxide and prostaglandins. *Neuroimmunomodulation,* 13**,** 19-27.

DE VRIES, B., KOHL, J., LECLERCQ, W. K., WOLFS, T. G., VAN BIJNEN, A. A., HEERINGA, P. & BUURMAN, W. A. 2003. Complement factor C5a mediates renal ischemia-reperfusion injury independent from neutrophils. *J Immunol,* 170**,** 3883-9.

DENAMUR, S., TYTECA, D., MARCHAND-BRYNAERT, J., VAN BAMBEKE, F., TULKENS, P. M., COURTOY, P. J. & MINGEOT-LECLERCQ, M. P. 2011. Role of oxidative stress in lysosomal membrane permeabilization and apoptosis induced by gentamicin, an aminoglycoside antibiotic. *Free Radic Biol Med,* 51**,** 1656-65.

DENNY, P. C., BALL, W. D. & REDMAN, R. S. 1997. Salivary glands: a paradigm for diversity of gland development. *Crit Rev Oral Biol Med,* 8**,** 51-75.

DENNY, P. C., CHAI, Y., KLAUSER, D. K. & DENNY, P. A. 1993. Parenchymal cell proliferation and mechanisms for maintenance of granular duct and acinar cell populations in adult male mouse submandibular gland. *Anat Rec,* 235**,** 475-85.

DESHMUKH, U. S., NANDULA, S. R., THIMMALAPURA, P. R., SCINDIA, Y. M. & BAGAVANT, H. 2009. Activation of innate immune responses through Toll-like receptor 3 causes a rapid loss of salivary gland function. *J Oral Pathol Med,* 38**,** 42-7.

DEVRIES, M. E., HOSIAWA, K. A., CAMERON, C. M., BOSINGER, S. E., PERSAD, D., KELVIN, A. A., COOMBS, J. C., WANG, H., ZHONG, R., CAMERON, M. J. & KELVIN, D. J. 2003. The role of chemokines and chemokine receptors in alloantigen-independent and alloantigen-dependent transplantation injury. *Semin Immunol,* 15**,** 33-48.

DEWITTE-ORR, S. J., COLLINS, S. E., BAUER, C. M., BOWDISH, D. M. & MOSSMAN, K. L. 2010. An accessory to the 'Trinity': SR-As are essential pathogen sensors of extracellular dsRNA, mediating entry and leading to subsequent type I IFN responses. *PLoS Pathog,* 6**,** e1000829.

DEWITTE-ORR, S. J. & MOSSMAN, K. L. 2010. dsRNA and the innate antiviral immune response. *Future Virology,* 5**,** 325-341.

DI, A., GAO, X. P., QIAN, F., KAWAMURA, T., HAN, J., HECQUET, C., YE, R. D., VOGEL, S. M. & MALIK, A. B. 2012. The redox-sensitive cation channel TRPM2 modulates phagocyte ROS production and inflammation. *Nat Immunol,* 13**,** 29-34.

DIEBOLD, S. S., KAISHO, T., HEMMI, H., AKIRA, S. & REIS E SOUSA, C. 2004. Innate antiviral responses by means of TLR7-mediated recognition of single-stranded RNA. *Science,* 303**,** 1529-31.

DIOS, I. D. 2010. Inflammatory role of the acinar cells during acute pancreatitis. *World J Gastrointest Pharmacol Ther,* 1**,** 15-20.

DIXIT, E. & KAGAN, J. C. 2013. Intracellular pathogen detection by RIG-I-like receptors. *Adv Immunol,* 117**,** 99-125.

DONEPUDI, M., MAC SWEENEY, A., BRIAND, C. & GRUTTER, M. G. 2003. Insights into the regulatory mechanism for caspase-8 activation. *Mol Cell,* 11**,** 543-9.

DONZE, O., DOSTIE, J. & SONENBERG, N. 1999. Regulatable expression of the interferon-induced double-stranded RNA dependent protein kinase PKR induces apoptosis and fas receptor expression. *Virology,* 256**,** 322-9.

DRESCHER, B. & BAI, F. 2013. Neutrophil in viral infections, friend or foe? *Virus Res,* 171**,** 1-7.

DUFFY, L. & O'REILLY, S. C. 2016. Toll-like receptors in the pathogenesis of autoimmune diseases: recent and emerging translational developments. *ImmunoTargets and Therapy,* 5**,** 69-80.

EARNSHAW, W. C., MARTINS, L. M. & KAUFMANN, S. H. 1999. Mammalian caspases: structure, activation, substrates, and functions during apoptosis. *Annu Rev Biochem,* 68**,** 383-424.

EGGER, L., SCHNEIDER, J., RHEME, C., TAPERNOUX, M., HACKI, J. & BORNER, C. 2003. Serine proteases mediate apoptosis-like cell death and phagocytosis under caspase-inhibiting conditions. *Cell Death Differ,* 10**,** 1188-203.

EISERICH, J. P., BALDUS, S., BRENNAN, M. L., MA, W., ZHANG, C., TOUSSON, A., CASTRO, L., LUSIS, A. J., NAUSEEF, W. M., WHITE, C. R. & FREEMAN, B. A. 2002. Myeloperoxidase, a leukocyte-derived vascular NO oxidase. *Science,* 296**,** 2391-4.

EKSTRÖM J , *K. N., CASTAGNOLA M , MESSANA I* 2012. *Sa liva and the control of its secretion . In: EKBERG O* (ed.) *Dysphagia: diagnosis and treatment .* B*erlin Heidelberg* ,: *Springer-Verlag:*.

EPSTEIN, M. A., ACHONG, B. G. & BARR, Y. M. 1964. VIRUS PARTICLES IN CULTURED LYMPHOBLASTS FROM BURKITT'S LYMPHOMA. *Lancet,* 1**,** 702-3.

EQUILS, O., MOFFATT-BLUE, C., ISHIKAWA, T. O., SIMMONS, C. F., ILIEVSKI, V. & HIRSCH, E. 2009. Pretreatment with pancaspase inhibitor (Z-VAD-FMK) delays but does not prevent intraperitoneal heat-killed group B Streptococcus-induced preterm delivery in a pregnant mouse model. *Infect Dis Obstet Gynecol,* 2009**,** 749432.

EQUILS, O., SHAPIRO, A., MADAK, Z., LIU, C. & LU, D. 2004. Human immunodeficiency virus type 1 protease inhibitors block toll-like receptor 2 (TLR2)- and TLR4-Induced NF-kappaB activation. *Antimicrob Agents Chemother,* 48**,** 3905-11.

ERDAL, H., BERNDTSSON, M., CASTRO, J., BRUNK, U., SHOSHAN, M. C. & LINDER, S. 2005. Induction of lysosomal membrane permeabilization by compounds that activate p53-independent apoptosis. *Proc Natl Acad Sci U S A,* 102**,** 192-7.

EVANS, R. L., BELL, S. M., SCHULTHEIS, P. J., SHULL, G. E. & MELVIN, J. E. 1999. Targeted disruption of the Nhe1 gene prevents muscarinic agonist-induced up-regulation of Na(+)/H(+) exchange in mouse parotid acinar cells. *J Biol Chem,* 274**,** 29025-30.

EVANS, R. L., PARK, K., TURNER, R. J., WATSON, G. E., NGUYEN, H. V., DENNETT, M. R., HAND, A. R., FLAGELLA, M., SHULL, G. E. & MELVIN, J. E. 2000. Severe impairment of salivation in Na+/K+/2Cl- cotransporter (NKCC1)-deficient mice. *J Biol Chem,* 275**,** 26720-6.

EVCIMEN, N. D., PEKINER, B. D. & NEBIOGLU, S. 1999. Ca(2+)-ATPase activity in streptozotocin-induced diabetic rat kidneys. *Diabetes Metab,* 25**,** 399-403.

EWALD, S. E., ENGEL, A., LEE, J., WANG, M., BOGYO, M. & BARTON, G. M. 2011. Nucleic acid recognition by Toll-like receptors is coupled to stepwise processing by cathepsins and asparagine endopeptidase. *The Journal of Experimental Medicine,* 208**,** 643-651.

EWALD, S. E., LEE, B. L., LAU, L., WICKLIFFE, K. E., SHI, G. P., CHAPMAN, H. A. & BARTON, G. M. 2008. The ectodomain of Toll-like receptor 9 is cleaved to generate a functional receptor. *Nature,* 456**,** 658-62.

FEDIRKO, N. V., KRUGLIKOV, I. A., KOPACH, O. V., VATS, J. A., KOSTYUK, P. G. & VOITENKO, N. V. 2006. Changes in functioning of rat submandibular salivary gland

under streptozotocin-induced diabetes are associated with alterations of Ca2+ signaling and Ca2+ transporting pumps. *Biochim Biophys Acta,* 1762**,** 294-303.
FLAITZ, C. M., HICKS, M. J., CARTER, A. B., ROSSMANN, S. N., DEMMLER, G. J., SIMON, C. L., CRON, S. G., SHEARER, W. T. & KLINE, M. W. 1998. Saliva collection technique for cytologic, microbiologic and viral evaluation in pediatric HIV infection. *ASDC J Dent Child,* 65**,** 318-24, 355.
FOSKETT, J. K. 1990. [Ca2+]i modulation of Cl- content controls cell volume in single salivary acinar cells during fluid secretion. *Am J Physiol,* 259**,** C998-1004.
FRANCIS, L. & PERL, A. 2010. Infection in systemic lupus erythematosus: friend or foe? *Int J Clin Rheumtol,* 5**,** 59-74.
FUKUI, R., SAITOH, S., MATSUMOTO, F., KOZUKA-HATA, H., OYAMA, M., TABETA, K., BEUTLER, B. & MIYAKE, K. 2009. Unc93B1 biases Toll-like receptor responses to nucleic acid in dendritic cells toward DNA- but against RNA-sensing. *J Exp Med,* 206**,** 1339-50.
GABRIEL, C., HER, Z. & NG, L. F. 2013. Neutrophils: neglected players in viral diseases. *DNA Cell Biol,* 32**,** 665-75.
GANTIER, M. P. & WILLIAMS, B. R. G. 2007. The response of mammalian cells to double-stranded RNA. *Cytokine & growth factor reviews,* 18**,** 363-371.
GAO, W., CAO, W., ZHANG, H., LI, P., XU, K. & TANG, B. 2014. Targeting lysosomal membrane permeabilization to induce and image apoptosis in cancer cells by multifunctional Au-ZnO hybrid nanoparticles. *Chemical Communications,* 50**,** 8117-8120.
GARCIA-CATTANEO, A., GOBERT, F. X., MULLER, M., TOSCANO, F., FLORES, M., LESCURE, A., DEL NERY, E. & BENAROCH, P. 2012. Cleavage of Toll-like receptor 3 by cathepsins B and H is essential for signaling. *Proc Natl Acad Sci U S A,* 109**,** 9053-8.
GAUZZI, M. C., DEL CORNO, M. & GESSANI, S. 2010. Dissecting TLR3 signalling in dendritic cells. *Immunobiology,* 215**,** 713-23.
GERBER, P., LUCAS, S., NONOYAMA, M., PERLIN, E. & GOLDSTEIN, L. I. 1972. Oral excretion of Epstein-Barr virus by healthy subjects and patients with infectious mononucleosis. *Lancet,* 2**,** 988-9.
GIL, J. & ESTEBAN, M. 2000. Induction of apoptosis by the dsRNA-dependent protein kinase (PKR): mechanism of action. *Apoptosis,* 5**,** 107-14.
GIL, J., GARCIA, M. A. & ESTEBAN, M. 2002. Caspase 9 activation by the dsRNA-dependent protein kinase, PKR: molecular mechanism and relevance. *FEBS Lett,* 529**,** 249-55.
GORLACH, A., BERTRAM, K., HUDECOVA, S. & KRIZANOVA, O. 2015. Calcium and ROS: A mutual interplay. *Redox Biol,* 6**,** 260-71.
GREGOLI, P. A. & BONDURANT, M. C. 1999. Function of caspases in regulating apoptosis caused by erythropoietin deprivation in erythroid progenitors. *J Cell Physiol,* 178**,** 133-43.
GRESIK, E. W. 1994. The granular convoluted tubule (GCT) cell of rodent submandibular glands. *Microsc Res Tech,* 27**,** 1-24.
GRIMOUD, A.-M., ARNAUD, C., DELLAMONICA, P. & LODTER, J.-P. 1998. Salivary defence factor concentrations in relation to oral and general parameters in HIV positive patients. *European Journal of Oral Sciences,* 106**,** 979-985.
GROOTJANS, J., KASER, A., KAUFMAN, R. J. & BLUMBERG, R. S. 2016. The unfolded protein response in immunity and inflammation. *Nat Rev Immunol,* 16**,** 469-84.
GROSSKREUTZ, J., VAN DEN BOSCH, L. & KELLER, B. U. 2010. Calcium dysregulation in amyotrophic lateral sclerosis. *Cell Calcium,* 47**,** 165-74.
GUGGENHEIMER, J. & MOORE, P. A. 2003. Xerostomia: etiology, recognition and treatment. *J Am Dent Assoc,* 134**,** 61-9; quiz 118-9.
GUKOVSKAYA, A. S., GUKOVSKY, I., ZANINOVIC, V., SONG, M., SANDOVAL, D., GUKOVSKY, S. & PANDOL, S. J. 1997. Pancreatic acinar cells produce, release, and respond to tumor necrosis factor-alpha. Role in regulating cell death and pancreatitis. *J Clin Invest,* 100**,** 1853-62.
GUKOVSKY, I., GUKOVSKAYA, A. S., BLINMAN, T. A., ZANINOVIC, V. & PANDOL, S. J. 1998. Early NF-kappaB activation is associated with hormone-induced pancreatitis. *Am J Physiol,* 275**,** G1402-14.
GUZIK, T. J., KORBUT, R. & ADAMEK-GUZIK, T. 2003. Nitric oxide and superoxide in inflammation and immune regulation. *J Physiol Pharmacol,* 54**,** 469-87.
GUZIK, T. J., WEST, N. E., PILLAI, R., TAGGART, D. P. & CHANNON, K. M. 2002. Nitric oxide modulates superoxide release and peroxynitrite formation in human blood vessels. *Hypertension,* 39**,** 1088-94.

HAAS, M. 1989. Properties and diversity of (Na-K-Cl) cotransporters. *Annu Rev Physiol,* 51**,** 443-57.
HAAS, M. 1994. The Na-K-Cl cotransporters. *Am J Physiol,* 267**,** C869-85.
HAAS, M. & FORBUSH, B., 3RD 1998. The Na-K-Cl cotransporters. *J Bioenerg Biomembr,* 30**,** 161-72.
HALL, J. E. 2011. *The Autonomic Nervous System and the Adrenal Medulla*, Saunders, Elsevier.
HANAUE, N., TAKEDA, I., KIZU, Y., TONOGI, M. & YAMANE, G. Y. 2007. Peroxynitrite formation in radiation-induced salivary gland dysfunction in mice. *Biomed Res,* 28**,** 147-51.
HARRIS, P., SRIDHAR, S., PENG, R., PHILLIPS, J. E., COHN, R. G., BURNS, L., WOODS, J., RAMANUJAM, M., LOUBEAU, M., TYAGI, G., ALLARD, J., BURCZYNSKI, M., RAVINDRAN, P., CHENG, D., BITTER, H., FINE, J. S., BAUER, C. M. & STEVENSON, C. S. 2013. Double-stranded RNA induces molecular and inflammatory signatures that are directly relevant to COPD. *Mucosal Immunol,* 6**,** 474-84.
HATTON, O. L., HARRIS-ARNOLD, A., SCHAFFERT, S., KRAMS, S. M. & MARTINEZ, O. M. 2014. The interplay between Epstein–Barr virus and B lymphocytes: implications for infection, immunity, and disease. *Immunologic Research,* 58**,** 268-276.
HATTORI, T. & WANG, P. L. 2007. Calcium antagonists cause dry mouth by inhibiting resting saliva secretion. *Life Sci,* 81**,** 683-90.
HAYASHI, T. 2011. Dysfunction of lacrimal and salivary glands in Sjogren's syndrome: nonimmunologic injury in preinflammatory phase and mouse model. *J Biomed Biotechnol,* 2011**,** 407031.
HAYASHI, T., PORONNIK, P., YOUNG, J. A. & COOK, D. I. 1996. The ACh-evoked, Ca2+-activated whole-cell K+ current in mouse mandibular secretory cells. Whole-cell and fluorescence studies. *J Membr Biol,* 152**,** 253-9.
HEIL, F., HEMMI, H., HOCHREIN, H., AMPENBERGER, F., KIRSCHNING, C., AKIRA, S., LIPFORD, G., WAGNER, H. & BAUER, S. 2004. Species-specific recognition of single-stranded RNA via toll-like receptor 7 and 8. *Science,* 303**,** 1526-9.
HEMMERS, S., TEIJARO, J. R., ARANDJELOVIC, S. & MOWEN, K. A. 2011. PAD4-mediated neutrophil extracellular trap formation is not required for immunity against influenza infection. *PLoS One,* 6**,** e22043.
HEMMI, H., TAKEUCHI, O., KAWAI, T., KAISHO, T., SATO, S., SANJO, H., MATSUMOTO, M., HOSHINO, K., WAGNER, H., TAKEDA, K. & AKIRA, S. 2000. A Toll-like receptor recognizes bacterial DNA. *Nature,* 408**,** 740-5.
HESS, D. A., HUMPHREY, S. E., ISHIBASHI, J., DAMSZ, B., LEE, A.-H., GLIMCHER, L. H. & KONIECZNY, S. F. 2011. Extensive Pancreas Regeneration Following Acinar-Specific Disruption of Xbp1 in Mice. *Gastroenterology,* 141**,** 1463-1472.
HESTDAL, K., RUSCETTI, F. W., IHLE, J. N., JACOBSEN, S. E., DUBOIS, C. M., KOPP, W. C., LONGO, D. L. & KELLER, J. R. 1991. Characterization and regulation of RB6-8C5 antigen expression on murine bone marrow cells. *J Immunol,* 147**,** 22-8.
HICKEY, M. J. 2012. Has Ly6G finally found a job? *Blood,* 120**,** 1352-3.
HILGE, M. 2012. Ca2+ regulation of ion transport in the Na+/Ca2+ exchanger. *J Biol Chem,* 287**,** 31641-9.
HILTON, D. A., DAY, C., PRINGLE, J. H., FLETCHER, A. & CHAMBERS, S. 1992. Demonstration of the distribution of coxsackie virus RNA in neonatal mice by non-isotopic in situ hybridization. *J Virol Methods,* 40**,** 155-62.
HOGAN, P. G., LEWIS, R. S. & RAO, A. 2010. Molecular basis of calcium signaling in lymphocytes: STIM and ORAI. *Annu Rev Immunol,* 28**,** 491-533.
HOGG, N. & KALYANARAMAN, B. 1999. Nitric oxide and lipid peroxidation. *Biochim Biophys Acta,* 1411**,** 378-84.
HOLDGATE, N. & ST CLAIR, E. W. 2016. Recent advances in primary Sjogren's syndrome. *F1000Res,* 5.
HOLLIEN, J., LIN, J. H., LI, H., STEVENS, N., WALTER, P. & WEISSMAN, J. S. 2009. Regulated Ire1-dependent decay of messenger RNAs in mammalian cells. *J Cell Biol,* 186**,** 323-31.
HOLLIEN, J. & WEISSMAN, J. S. 2006. Decay of endoplasmic reticulum-localized mRNAs during the unfolded protein response. *Science,* 313**,** 104-7.
HOLMBERG, K. V. & HOFFMAN, M. P. 2014. Anatomy, biogenesis, and regeneration of salivary glands. *Monographs in oral science,* 24**,** 1-13.
HOMANN, V., KINNE-SAFFRAN, E., ARNOLD, W. H., GAENGLER, P. & KINNE, R. K. 2006. Calcium transport in human salivary glands: a proposed model of calcium secretion into saliva. *Histochem Cell Biol,* 125**,** 583-91.

HORAI, Y., NAKAMURA, H., NAKASHIMA, Y., HAYASHI, T. & KAWAKAMI, A. 2016. Analysis of the downstream mediators of toll-like receptor 3-induced apoptosis in labial salivary glands in patients with Sjogren's syndrome. *Mod Rheumatol,* 26**,** 99-104.

HORNUNG, V., HARTMANN, R., ABLASSER, A. & HOPFNER, K.-P. 2014. OAS proteins and cGAS: unifying concepts in sensing and responding to cytosolic nucleic acids. *Nat Rev Immunol,* 14**,** 521-528.

HOVANESSIAN, A. G. 1989. The double stranded RNA-activated protein kinase induced by interferon: dsRNA-PK. *J Interferon Res,* 9**,** 641-7.

HOVANESSIAN, A. G. 2007. On the discovery of interferon-inducible, double-stranded RNA activated enzymes: the 2'-5'oligoadenylate synthetases and the protein kinase PKR. *Cytokine Growth Factor Rev,* 18**,** 351-61.

HUYS, L., VAN HAUWERMEIREN, F., DEJAGER, L., DEJONCKHEERE, E., LIENENKLAUS, S., WEISS, S., LECLERCQ, G. & LIBERT, C. 2009. Type I interferon drives tumor necrosis factor-induced lethal shock. *J Exp Med,* 206**,** 1873-82.

ICHIKAWA, A., KUBA, K., MORITA, M., CHIDA, S., TEZUKA, H., HARA, H., SASAKI, T., OHTEKI, T., RANIERI, V. M., DOS SANTOS, C. C., KAWAOKA, Y., AKIRA, S., LUSTER, A. D., LU, B., PENNINGER, J. M., UHLIG, S., SLUTSKY, A. S. & IMAI, Y. 2013. CXCL10-CXCR3 enhances the development of neutrophil-mediated fulminant lung injury of viral and nonviral origin. *Am J Respir Crit Care Med,* 187**,** 65-77.

ICHIKAWA, T., SUGIURA, H., KOARAI, A., MINAKATA, Y., KIKUCHI, T., MORISHITA, Y., OKA, A., KANAI, K., KAWABATA, H., HIRAMATSU, M., AKAMATSU, K., HIRANO, T., NAKANISHI, M., MATSUNAGA, K., YAMAMOTO, N. & ICHINOSE, M. 2014. TLR3 activation augments matrix metalloproteinase production through reactive nitrogen species generation in human lung fibroblasts. *J Immunol,* 192**,** 4977-88.

IORDANOV, M. S., PARANJAPE, J. M., ZHOU, A., WONG, J., WILLIAMS, B. R., MEURS, E. F., SILVERMAN, R. H. & MAGUN, B. E. 2000. Activation of p38 mitogen-activated protein kinase and c-Jun NH(2)-terminal kinase by double-stranded RNA and encephalomyocarditis virus: involvement of RNase L, protein kinase R, and alternative pathways. *Mol Cell Biol,* 20**,** 617-27.

ISCHIROPOULOS, H. 1998. Biological tyrosine nitration: a pathophysiological function of nitric oxide and reactive oxygen species. *Arch Biochem Biophys,* 356**,** 1-11.

ISHIKAWA, Y., INOUE, N., ZHENFANG, Y. & NAKAE, Y. 2004. Molecular mechanisms and drug development in aquaporin water channel diseases: the translocation of aquaporin-5 from lipid rafts to the apical plasma membranes of parotid glands of normal rats and the impairment of it in diabetic or aged rats. *J Pharmacol Sci,* 96**,** 271-5.

ISLER, J. A., SKALET, A. H. & ALWINE, J. C. 2005. Human cytomegalovirus infection activates and regulates the unfolded protein response. *J Virol,* 79**,** 6890-9.

JACOBS, B. L. & LANGLAND, J. O. 1996. When two strands are better than one: the mediators and modulators of the cellular responses to double-stranded RNA. *Virology,* 219**,** 339-49.

JAYASINGHE, N. R., COPE, G. H. & JACOB, S. 1990. Morphometric studies on the development and sexual dimorphism of the submandibular gland of the mouse. *J Anat,* 172**,** 115-27.

JEFFERS, L. & WEBSTER-CYRIAQUE, J. Y. 2011. Viruses and salivary gland disease (SGD): lessons from HIV SGD. *Adv Dent Res,* 23**,** 79-83.

JENSEN, S. & THOMSEN, A. R. 2012. Sensing of RNA viruses: a review of innate immune receptors involved in recognizing RNA virus invasion. *J Virol,* 86**,** 2900-10.

JOHANSSON, A.-C., APPELQVIST, H., NILSSON, C., KÅGEDAL, K., ROBERG, K. & ÖLLINGER, K. 2010. Regulation of apoptosis-associated lysosomal membrane permeabilization. *Apoptosis,* 15**,** 527-540.

JONJIC, S., MUTTER, W., WEILAND, F., REDDEHASE, M. J. & KOSZINOWSKI, U. H. 1989. Site-restricted persistent cytomegalovirus infection after selective long-term depletion of CD4+ T lymphocytes. *J Exp Med,* 169**,** 1199-212.

JUTILA, D. B., KURK, S. & JUTILA, M. A. 1994. Differences in the expression of Ly-6C on neutrophils and monocytes following PI-PLC hydrolysis and cellular activation. *Immunol Lett,* 41**,** 49-57.

JUTILA, M. A., KROESE, F. G., JUTILA, K. L., STALL, A. M., FIERING, S., HERZENBERG, L. A., BERG, E. L. & BUTCHER, E. C. 1988. Ly-6C is a monocyte/macrophage and endothelial cell differentiation antigen regulated by interferon-gamma. *Eur J Immunol,* 18**,** 1819-26.

KAISER, W. J. & OFFERMANN, M. K. 2005. Apoptosis induced by the toll-like receptor adaptor TRIF is dependent on its receptor interacting protein homotypic interaction motif. *J Immunol,* 174**,** 4942-52.

KAISER, W. J., UPTON, J. W., LONG, A. B., LIVINGSTON-ROSANOFF, D., DALEY-BAUER, L. P., HAKEM, R., CASPARY, T. & MOCARSKI, E. S. 2011. RIP3 mediates the embryonic lethality of caspase-8-deficient mice. *Nature,* 471**,** 368-72.
KAISHO, T. & AKIRA, S. 2006. Toll-like receptor function and signaling. *J Allergy Clin Immunol,* 117**,** 979-87; quiz 988.
KANAYA, K., KONDO, K., SUZUKAWA, K., SAKAMOTO, T., KIKUTA, S., OKADA, K. & YAMASOBA, T. 2014. Innate immune responses and neuroepithelial degeneration and regeneration in the mouse olfactory mucosa induced by intranasal administration of Poly(I:C). *Cell Tissue Res,* 357**,** 279-99.
KATO, H., TAKEUCHI, O., MIKAMO-SATOH, E., HIRAI, R., KAWAI, T., MATSUSHITA, K., HIIRAGI, A., DERMODY, T. S., FUJITA, T. & AKIRA, S. 2008. Length-dependent recognition of double-stranded ribonucleic acids by retinoic acid-inducible gene-I and melanoma differentiation-associated gene 5. *J Exp Med,* 205**,** 1601-10.
KAWAI, T. & AKIRA, S. 2007. Antiviral signaling through pattern recognition receptors. *J Biochem,* 141**,** 137-45.
KAWAI, T. & AKIRA, S. 2008. Toll-like receptor and RIG-I-like receptor signaling. *Ann N Y Acad Sci,* 1143**,** 1-20.
KHARROUBI, I., LADRIERE, L., CARDOZO, A. K., DOGUSAN, Z., CNOP, M. & EIZIRIK, D. L. 2004. Free fatty acids and cytokines induce pancreatic beta-cell apoptosis by different mechanisms: role of nuclear factor-kappaB and endoplasmic reticulum stress. *Endocrinology,* 145**,** 5087-96.
KHURANA, I. 2009. *Textbook of Human Physiology for Dental Students*, Elsevier.
KIM, H., SEO, J. Y., ROH, K. H., LIM, J. W. & KIM, K. H. 2000. Suppression of NF-kappaB activation and cytokine production by N-acetylcysteine in pancreatic acinar cells. *Free Radic Biol Med,* 29**,** 674-83.
KIM, H. W., CH, Y. S., LEE, H. R., PARK, S. Y. & KIM, Y. H. 2001. Diabetic alterations in cardiac sarcoplasmic reticulum Ca2+-ATPase and phospholamban protein expression. *Life Sci,* 70**,** 367-79.
KIM, K. I., KIM, Y. S., KIM, H. K., CHAE, Y. S., YOEM, B. W. & KIM, I. 1999. The detection of Epstein-Barr virus in the lesions of salivary glands. *Pathol Res Pract,* 195**,** 407-12.
KIM, Y. M., BRINKMANN, M. M., PAQUET, M. E. & PLOEGH, H. L. 2008. UNC93B1 delivers nucleotide-sensing toll-like receptors to endolysosomes. *Nature,* 452**,** 234-8.
KIMATA, Y. & KOHNO, K. 2011. Endoplasmic reticulum stress-sensing mechanisms in yeast and mammalian cells. *Curr Opin Cell Biol,* 23**,** 135-42.
KIMURA-SHIMMYO, A., KASHIWAMURA, S., UEDA, H., IKEDA, T., KANNO, S., AKIRA, S., NAKANISHI, K., MIMURA, O. & OKAMURA, H. 2002. Cytokine-induced injury of the lacrimal and salivary glands. *J Immunother,* 25 Suppl 1**,** S42-51.
KLEBANOFF, S. J. 2005. Myeloperoxidase: friend and foe. *J Leukoc Biol,* 77**,** 598-625.
KLEBL, B. M., AYOUB, A. T. & PETTE, D. 1998. Protein oxidation, tyrosine nitration, and inactivation of sarcoplasmic reticulum Ca2+-ATPase in low-frequency stimulated rabbit muscle. *FEBS Lett,* 422**,** 381-4.
KNEPIL, G. J. & FABBRONI, G. 2008. A life-threatening complication of acute parotitis. *Br J Oral Maxillofac Surg,* 46**,** 328-9.
KNOWLES, R. G. & MONCADA, S. 1994. Nitric oxide synthases in mammals. *Biochem J,* 298 (Pt 2)**,** 249-58.
KOARAI, A., ICHINOSE, M., SUGIURA, H., TOMAKI, M., WATANABE, M., YAMAGATA, S., KOMAKI, Y., SHIRATO, K. & HATTORI, T. 2002. iNOS depletion completely diminishes reactive nitrogen-species formation after an allergic response. *Eur Respir J,* 20**,** 609-16.
KONDO, Y., NAKAMOTO, T., JARAMILLO, Y., CHOI, S., CATALAN, M. A. & MELVIN, J. E. 2015. Functional differences in the acinar cells of the murine major salivary glands. *J Dent Res,* 94**,** 715-21.
KONDO, Y., SARUTA, J., TO, M., SHIIKI, N., SATO, C. & TSUKINOKI, K. 2010. Expression and Role of the BDNF Receptor-TrkB in Rat Adrenal Gland under Acute Immobilization Stress. *Acta Histochem Cytochem,* 43**,** 139-47.
KONTTINEN, Y. T., PLATTS, L. A., TUOMINEN, S., EKLUND, K. K., SANTAVIRTA, N., TORNWALL, J., SORSA, T., HUKKANEN, M. & POLAK, J. M. 1997. Role of nitric oxide in Sjogren's syndrome. *Arthritis Rheum,* 40**,** 875-83.
KRAMMER, P. H. 2000. CD95's deadly mission in the immune system. *Nature,* 407**,** 789-95.
KRANE, C. M., MELVIN, J. E., NGUYEN, H. V., RICHARDSON, L., TOWNE, J. E., DOETSCHMAN, T. & MENON, A. G. 2001. Salivary acinar cells from aquaporin 5-

deficient mice have decreased membrane water permeability and altered cell volume regulation. *J Biol Chem,* 276**,** 23413-20.
KREBS, J., AGELLON, L. B. & MICHALAK, M. 2015. Ca2+ homeostasis and endoplasmic reticulum (ER) stress: An integrated view of calcium signaling. *Biochemical and Biophysical Research Communications,* 460**,** 114-121.
KREBS, J., GROENENDYK, J. & MICHALAK, M. 2011. Ca2+-signaling, alternative splicing and endoplasmic reticulum stress responses. *Neurochem Res,* 36**,** 1198-211.
KRUGLIKOV, I., GRYSHCHENKO, O., SHUTOV, L., KOSTYUK, E., KOSTYUK, P. & VOITENKO, N. 2004. Diabetes-induced abnormalities in ER calcium mobilization in primary and secondary nociceptive neurons. *Pflugers Arch,* 448**,** 395-401.
KUCHARZIK, T., WALSH, S. V., CHEN, J., PARKOS, C. A. & NUSRAT, A. 2001. Neutrophil Transmigration in Inflammatory Bowel Disease Is Associated with Differential Expression of Epithelial Intercellular Junction Proteins. *The American Journal of Pathology,* 159**,** 2001-2009.
KUNG, J. T., CASTILLO, M., HEARD, P., KERBACHER, K. & THOMAS, C. A., 3RD 1991. Subpopulations of CD8+ cytotoxic T cell precursors collaborate in the absence of conventional CD4+ helper T cells. *J Immunol,* 146**,** 1783-90.
LAGADIC-GOSSMANN, D., BUCKLER, K. J., LE PRIGENT, K. & FEUVRAY, D. 1996. Altered Ca2+ handling in ventricular myocytes isolated from diabetic rats. *Am J Physiol,* 270**,** H1529-37.
LEADBETTER, E. A., RIFKIN, I. R., HOHLBAUM, A. M., BEAUDETTE, B. C., SHLOMCHIK, M. J. & MARSHAK-ROTHSTEIN, A. 2002. Chromatin-IgG complexes activate B cells by dual engagement of IgM and Toll-like receptors. *Nature,* 416**,** 603-7.
LEE, H. K., DUNZENDORFER, S., SOLDAU, K. & TOBIAS, P. S. 2006. Double-stranded RNA-mediated TLR3 activation is enhanced by CD14. *Immunity,* 24**,** 153-63.
LEE, J., SAYED, N., HUNTER, A., AU, K. F., WONG, W. H., MOCARSKI, E. S., PERA, R. R., YAKUBOV, E. & COOKE, J. P. 2012a. Activation of innate immunity is required for efficient nuclear reprogramming. *Cell,* 151**,** 547-58.
LEE, M. G., OHANA, E., PARK, H. W., YANG, D. & MUALLEM, S. 2012b. Molecular mechanism of pancreatic and salivary gland fluid and HCO3 secretion. *Physiol Rev,* 92**,** 39-74.
LEE, M. G., SCHULTHEIS, P. J., YAN, M., SHULL, G. E., BOOKSTEIN, C., CHANG, E., TSE, M., DONOWITZ, M., PARK, K. & MUALLEM, S. 1998. Membrane-limited expression and regulation of Na+-H+ exchanger isoforms by P2 receptors in the rat submandibular gland duct. *J Physiol,* 513 (Pt 2)**,** 341-57.
LEIFER, C. A., KENNEDY, M. N., MAZZONI, A., LEE, C., KRUHLAK, M. J. & SEGAL, D. M. 2004. TLR9 is localized in the endoplasmic reticulum prior to stimulation. *J Immunol,* 173**,** 1179-83.
LEMAITRE, B., NICOLAS, E., MICHAUT, L., REICHHART, J. M. & HOFFMANN, J. A. 1996. The dorsoventral regulatory gene cassette spatzle/Toll/cactus controls the potent antifungal response in Drosophila adults. *Cell,* 86**,** 973-83.
LESTER, S. N. & LI, K. 2014. Toll-like receptors in antiviral innate immunity. *Journal of molecular biology,* 426**,** 1246-1264.
LEVER, A. R., PARK, H., MULHERN, T. J., JACKSON, G. R., COMOLLI, J. C., BORENSTEIN, J. T., HAYDEN, P. J. & PRANTIL-BAUN, R. 2015. Comprehensive evaluation of poly(I:C) induced inflammatory response in an airway epithelial model. *Physiol Rep,* 3.
LI, M., ONA, V. O., GUEGAN, C., CHEN, M., JACKSON-LEWIS, V., ANDREWS, L. J., OLSZEWSKI, A. J., STIEG, P. E., LEE, J. P., PRZEDBORSKI, S. & FRIEDLANDER, R. M. 2000. Functional role of caspase-1 and caspase-3 in an ALS transgenic mouse model. *Science,* 288**,** 335-9.
LI, X. L., BLACKFORD, J. A. & HASSEL, B. A. 1998. RNase L mediates the antiviral effect of interferon through a selective reduction in viral RNA during encephalomyocarditis virus infection. *J Virol,* 72**,** 2752-9.
LIMMON, G. V., ARREDOUANI, M., MCCANN, K. L., CORN MINOR, R. A., KOBZIK, L. & IMANI, F. 2008. Scavenger receptor class-A is a novel cell surface receptor for double-stranded RNA. *Faseb j,* 22**,** 159-67.
LIN, A. L., JOHNSON, D. A., STEPHAN, K. T. & YEH, C. K. 2003. Alteration in salivary function in early HIV infection. *J Dent Res,* 82**,** 719-24.
LIN, Q., FANG, D., FANG, J., REN, X., YANG, X., WEN, F. & SU, S. B. 2011. Impaired Wound Healing with Defective Expression of Chemokines and Recruitment of Myeloid Cells in TLR3-Deficient Mice. *The Journal of Immunology,* 186**,** 3710.

LIN, Y., EPSTEIN, D. L. & LITON, P. B. 2010. Intralysosomal iron induces lysosomal membrane permeabilization and cathepsin D-mediated cell death in trabecular meshwork cells exposed to oxidative stress. *Invest Ophthalmol Vis Sci,* 51**,** 6483-95.

LINDA H. KOOISTRA, D., PHD, DACVP & ABRAHAM NYSKA, D., DIPLOMATE ECVP, FELLOW IATP. *Nonneoplastic Lesion AtlasA guide for standardizing terminology in toxicologic pathology for rodents* [Online]. [Accessed].

LIOU, J., KIM, M. L., HEO, W. D., JONES, J. T., MYERS, J. W., FERRELL, J. E., JR. & MEYER, T. 2005. STIM is a Ca2+ sensor essential for Ca2+-store-depletion-triggered Ca2+ influx. *Curr Biol,* 15**,** 1235-41.

LIU, L., BOTOS, I., WANG, Y., LEONARD, J. N., SHILOACH, J., SEGAL, D. M. & DAVIES, D. R. 2008. Structural basis of toll-like receptor 3 signaling with double-stranded RNA. *Science,* 320**,** 379-81.

LIU, N., RAJA, S. M., ZAZZERONI, F., METKAR, S. S., SHAH, R., ZHANG, M., WANG, Y., BROMME, D., RUSSIN, W. A., LEE, J. C., PETER, M. E., FROELICH, C. J., FRANZOSO, G. & ASHTON-RICKARDT, P. G. 2003. NF-kappaB protects from the lysosomal pathway of cell death. *Embo j,* 22**,** 5313-22.

LIU, X., COTRIM, A., TEOS, L., ZHENG, C., SWAIM, W., MITCHELL, J., MORI, Y. & AMBUDKAR, I. 2013. Loss of TRPM2 function protects against irradiation-induced salivary gland dysfunction. *Nat Commun,* 4**,** 1515.

LLOYD-EVANS, E., MORGAN, A. J., HE, X., SMITH, D. A., ELLIOT-SMITH, E., SILLENCE, D. J., CHURCHILL, G. C., SCHUCHMAN, E. H., GALIONE, A. & PLATT, F. M. 2008. Niemann-Pick disease type C1 is a sphingosine storage disease that causes deregulation of lysosomal calcium. *Nat Med,* 14**,** 1247-55.

LOMNICZI, A., MOHN, C., FALETTI, A., FRANCHI, A., MCCANN, S. M., RETTORI, V. & ELVERDIN, J. C. 2001. Inhibition of salivary secretion by lipopolysaccharide: possible role of prostaglandins. *Am J Physiol Endocrinol Metab,* 281**,** E405-11.

LOO, Y. M. & GALE, M., JR. 2011. Immune signaling by RIG-I-like receptors. *Immunity,* 34**,** 680-92.

LU, F. X. & JACOBSON, R. S. 2007. Oral mucosal immunity and HIV/SIV infection. *J Dent Res,* 86**,** 216-26.

LUDVIKSDOTTIR, D., JANSON, C., HOGMAN, M., GUDBJORNSSON, B., BJORNSSON, E., VALTYSDOTTIR, S., HEDENSTROM, H., VENGE, P. & BOMAN, G. 1999. Increased nitric oxide in expired air in patients with Sjogren's syndrome. BHR study group. Bronchial hyperresponsiveness. *European Respiratory Journal,* 13**,** 739.

LUND, J. M., ALEXOPOULOU, L., SATO, A., KAROW, M., ADAMS, N. C., GALE, N. W., IWASAKI, A. & FLAVELL, R. A. 2004. Recognition of single-stranded RNA viruses by Toll-like receptor 7. *Proc Natl Acad Sci U S A,* 101**,** 5598-603.

LUO, X., CHOI, J. Y., KO, S. B., PUSHKIN, A., KURTZ, I., AHN, W., LEE, M. G. & MUALLEM, S. 2001. HCO3- salvage mechanisms in the submandibular gland acinar and duct cells. *J Biol Chem,* 276**,** 9808-16.

MA, T., SONG, Y., GILLESPIE, A., CARLSON, E. J., EPSTEIN, C. J. & VERKMAN, A. S. 1999. Defective secretion of saliva in transgenic mice lacking aquaporin-5 water channels. *J Biol Chem,* 274**,** 20071-4.

MACFARLANE, A. S., SCHWACHA, M. G. & EISENSTEIN, T. K. 1999. In vivo blockage of nitric oxide with aminoguanidine inhibits immunosuppression induced by an attenuated strain of Salmonella typhimurium, potentiates Salmonella infection, and inhibits macrophage and polymorphonuclear leukocyte influx into the spleen. *Infect Immun,* 67**,** 891-8.

MAHAY, S., PARIENTE, J. A., LAJAS, A. I., ADEGHATE, E., ROLPH, C. E. & SINGH, J. 2004. Effects of ageing on morphology, amylase release, cytosolic Ca2+ signals and acyl lipids in isolated rat parotid gland tissue. *Mol Cell Biochem,* 266**,** 199-208.

MAITLAND, N., FLINT, S., SCULLY, C. & CREAN, S. J. 1995. Detection of cytomegalovirus and Epstein-Barr virus in labial salivary glands in Sjogren's syndrome and non-specific sialadenitis. *J Oral Pathol Med,* 24**,** 293-8.

MAJDE, J. A. 2000. Viral double-stranded RNA, cytokines, and the flu. *J Interferon Cytokine Res,* 20**,** 259-72.

MAKI, T., KOWATCH, M. A., BAUM, B. J., AMBUDKAR, I. S. & ROTH, G. S. 1989. Evidence for an alteration in the microsomal Ca2+ release mechanism in senescent rat parotid acinar cells. *Biochim Biophys Acta,* 1014**,** 73-7.

MALLE, E., BUCH, T. & GRONE, H. J. 2003. Myeloperoxidase in kidney disease. *Kidney Int,* 64**,** 1956-67.

MANDEL, L. & SURATTANONT, F. 2002. Bilateral parotid swelling: a review. *Oral Surg Oral Med Oral Pathol Oral Radiol Endod,* 93**,** 221-37.
MARIETTE, X., GOZLAN, J., CLERC, D., BISSON, M. & MORINET, F. 1991. Detection of Epstein-Barr virus DNA by in situ hybridization and polymerase chain reaction in salivary gland biopsy specimens from patients with Sjogren's syndrome. *Am J Med,* 90**,** 286-94.
MARINO, G., NISO-SANTANO, M., BAEHRECKE, E. H. & KROEMER, G. 2014. Self-consumption: the interplay of autophagy and apoptosis. *Nat Rev Mol Cell Biol,* 15**,** 81-94.
MARSDEN, V. S., O'CONNOR, L., O'REILLY, L. A., SILKE, J., METCALF, D., EKERT, P. G., HUANG, D. C., CECCONI, F., KUIDA, K., TOMASELLI, K. J., ROY, S., NICHOLSON, D. W., VAUX, D. L., BOUILLET, P., ADAMS, J. M. & STRASSER, A. 2002. Apoptosis initiated by Bcl-2-regulated caspase activation independently of the cytochrome c/Apaf-1/caspase-9 apoptosome. *Nature,* 419**,** 634-7.
MARSHALL, I. C., BOYFIELD, I. & MCNULTY, S. 2005. Ratiometric Ca(2)+ measurements using the FlexStation(R) Scanning Fluorometer. *Methods Mol Biol,* 312**,** 119-24.
MARSHALL, I. C., BOYFIELD, I. & MCNULTY, S. 2006. Ratiometric Ca2+ measurements using the FlexStation scanning fluorometer. *Methods Mol Biol,* 312**,** 119-24.
MATSUMOTO, F., SAITOH, S., FUKUI, R., KOBAYASHI, T., TANIMURA, N., KONNO, K., KUSUMOTO, Y., AKASHI-TAKAMURA, S. & MIYAKE, K. 2008. Cathepsins are required for Toll-like receptor 9 responses. *Biochem Biophys Res Commun,* 367**,** 693-9.
MATSUMOTO, M., OSHIUMI, H. & SEYA, T. 2011. Antiviral responses induced by the TLR3 pathway. *Rev Med Virol,* 21**,** 67-77.
MATSUO, R., GARRETT, J. R., PROCTOR, G. B. & CARPENTER, G. H. 2000. Reflex secretion of proteins into submandibular saliva in conscious rats, before and after preganglionic sympathectomy. *J Physiol,* 527 Pt 1**,** 175-84.
MCARTHUR, C. P., AFRICA, C. W., CASTELLANI, W. J., LUANGJAMEKORN, N. J., MCLAUGHLIN, M., SUBTIL-DEOLIVEIRA, A., COBB, C., HOWARD, P., GUSTAFSON, S., PALMER, D. & MIRANDA, R. N. 2003. Salivary gland disease in HIV/AIDS and primary Sjogren's syndrome: analysis of collagen I distribution and histopathology in American and African patients. *J Oral Pathol Med,* 32**,** 544-51.
MCQUONE, S. J. 1999. Acute viral and bacterial infections of the salivary glands. *Otolaryngol Clin North Am,* 32**,** 793-811.
MEISEL, D. L., SKOBE, Z., PROSTAK, K. S. & SHKLAR, G. 1988. A light and electron microscope study of aging parotid and submandibular salivary glands of Swiss-Webster mice. *Exp Gerontol,* 23**,** 197-210.
MELCHJORSEN, J. 2013. Learning from the messengers: innate sensing of viruses and cytokine regulation of immunity - clues for treatments and vaccines. *Viruses,* 5**,** 470-527.
MELVIN, J. E., MORAN, A. & TURNER, R. J. 1988. The role of HCO3- and Na+/H+ exchange in the response of rat parotid acinar cells to muscarinic stimulation. *J Biol Chem,* 263**,** 19564-9.
MELVIN, J. E. & TURNER, R. J. 1992. Cl- fluxes related to fluid secretion by the rat parotid: involvement of Cl(-)-HCO3- exchange. *Am J Physiol,* 262**,** G393-8.
MELVIN, J. E., YULE, D., SHUTTLEWORTH, T. & BEGENISICH, T. 2005. Regulation of fluid and electrolyte secretion in salivary gland acinar cells. *Annu Rev Physiol,* 67**,** 445-69.
MEYLAN, E., BURNS, K., HOFMANN, K., BLANCHETEAU, V., MARTINON, F., KELLIHER, M. & TSCHOPP, J. 2004. RIP1 is an essential mediator of Toll-like receptor 3-induced NF-kappa B activation. *Nat Immunol,* 5**,** 503-7.
MICHALAK, M. & OPAS, M. 2009. Endoplasmic and sarcoplasmic reticulum in the heart. *Trends Cell Biol,* 19**,** 253-9.
MICHELSON, A. M., MASSOULIE, J. & GUSCHLBAUER, W. 1967. Synthetic polynucleotides. *Prog Nucleic Acid Res Mol Biol,* 6**,** 83-141.
MIETTINEN, M., SARENEVA, T., JULKUNEN, I. & MATIKAINEN, S. 2001. IFNs activate toll-like receptor gene expression in viral infections. *Genes Immun,* 2**,** 349-55.
MIKOSHIBA, K. 2007. The IP3 receptor/Ca2+ channel and its cellular function. *Biochem Soc Symp***,** 9-22.
MISAKO MATSUMOTO, M. T. 2016. Cell type-specific role of raftlin in the regulation of endosomal TLR signaling. Inflammation & Cell Signaling.
MOGENSEN, T. H. 2009. Pathogen Recognition and Inflammatory Signaling in Innate Immune Defenses. *Clinical Microbiology Reviews,* 22**,** 240-273.
MORESCO, E. M. & BEUTLER, B. 2010. LGP2: positive about viral sensing. *Proc Natl Acad Sci U S A,* 107**,** 1261-2.

MULLER, M., CARTER, S., HOFER, M. J. & CAMPBELL, I. L. 2010. Review: The chemokine receptor CXCR3 and its ligands CXCL9, CXCL10 and CXCL11 in neuroimmunity--a tale of conflict and conundrum. *Neuropathol Appl Neurobiol,* 36**,** 368-87.
MURAI, S., SAITO, H., MASUDA, Y., NAKAMURA, K., MICHIJIRI, S. & ITOH, T. 1996. Effects of short-term (2 weeks) streptozotocin-induced diabetes on acetylcholine and noradrenaline in the salivary glands and secretory responses to cholinergic and adrenergic sialogogues in mice. *Arch Oral Biol,* 41**,** 673-7.
MURAKAMI, Y., FUKUI, R., MOTOI, Y., KANNO, A., SHIBATA, T., TANIMURA, N., SAITOH, S. & MIYAKE, K. 2014. Roles of the cleaved N-terminal TLR3 fragment and cell surface TLR3 in double-stranded RNA sensing. *J Immunol,* 193**,** 5208-17.
MURIEL, P. & SANDOVAL, G. 2000. Nitric oxide and peroxynitrite anion modulate liver plasma membrane fluidity and Na(+)/K(+)-ATPase activity. *Nitric Oxide,* 4**,** 333-42.
N.S. MACCALLUM, G. J. Q., AND T.W. EVANS 2007. *The Role of Neutrophil-Derived Myeloperoxidase in Organ Dysfunction and Sepsis*, Springer.
NAFTILAN, A. J. & OPARIL, S. 1982. The role of calcium in the control of renin release. *Hypertension,* 4**,** 670-5.
NAGRA, R. M., BECHER, B., TOURTELLOTTE, W. W., ANTEL, J. P., GOLD, D., PALADINO, T., SMITH, R. A., NELSON, J. R. & REYNOLDS, W. F. 1997. Immunohistochemical and genetic evidence of myeloperoxidase involvement in multiple sclerosis. *J Neuroimmunol,* 78**,** 97-107.
NANDULA, S. R., DEY, P., CORBIN, K. L., NUNEMAKER, C. S., BAGAVANT, H. & DESHMUKH, U. S. 2013. Salivary gland hypofunction induced by activation of innate immunity is dependent on type I interferon signaling. *J Oral Pathol Med,* 42**,** 66-72.
NATHAN, C. & XIE, Q. W. 1994. Nitric oxide synthases: roles, tolls, and controls. *Cell,* 78**,** 915-8.
NAUNTOFTE, B. 1992. Regulation of electrolyte and fluid secretion in salivary acinar cells. *Am J Physiol,* 263**,** G823-37.
NAVONE, R., LUNARDI, C., GERLI, R., TINAZZI, E., PETERLANA, D., BASON, C., CORROCHER, R. & PUCCETTI, A. 2005. Identification of tear lipocalin as a novel autoantigen target in Sjogren's syndrome. *J Autoimmun,* 25**,** 229-34.
NELLIMARLA, S. & MOSSMAN, K. L. 2014. Extracellular dsRNA: its function and mechanism of cellular uptake. *J Interferon Cytokine Res,* 34**,** 419-26.
NGUYEN, H. V., STUART-TILLEY, A., ALPER, S. L. & MELVIN, J. E. 2004. Cl(-)/HCO(3)(-) exchange is acetazolamide sensitive and activated by a muscarinic receptor-induced [Ca(2+)](i) increase in salivary acinar cells. *Am J Physiol Gastrointest Liver Physiol,* 286**,** G312-20.
NIEDERMEIER, W., HUBER, M., FISCHER, D., BEIER, K., MULLER, N., SCHULER, R., BRINNINGER, A., FARTASCH, M., DIEPGEN, T., MATTHAEUS, C., MEYER, C. & HECTOR, M. P. 2000. Significance of saliva for the denture-wearing population. *Gerodontology,* 17**,** 104-18.
NIGGLI, V., SIGEL, E. & CARAFOLI, E. 1982. The purified Ca2+ pump of human erythrocyte membranes catalyzes an electroneutral Ca2+-H+ exchange in reconstituted liposomal systems. *J Biol Chem,* 257**,** 2350-6.
NIKOLOV, N. P. & ILLEI, G. G. 2009. Pathogenesis of Sjogren's syndrome. *Curr Opin Rheumatol,* 21**,** 465-70.
NONZEE, V., MANOPATANAKUL, S. & KHOVIDHUNKIT, S. O. 2012. Xerostomia, hyposalivation and oral microbiota in patients using antihypertensive medications. *J Med Assoc Thai,* 95**,** 96-104.
NOVAK, I. & YOUNG, J. A. 1986. Two independent anion transport systems in rabbit mandibular salivary glands. *Pflugers Arch,* 407**,** 649-56.
O'NEILL, L. A. & BOWIE, A. G. 2007. The family of five: TIR-domain-containing adaptors in Toll-like receptor signalling. *Nat Rev Immunol,* 7**,** 353-64.
O'NEILL, L. A. J., GOLENBOCK, D. & BOWIE, A. G. 2013. The history of Toll-like receptors [mdash] redefining innate immunity. *Nat Rev Immunol,* 13**,** 453-460.
OBBARD, D. J., GORDON, K. H., BUCK, A. H. & JIGGINS, F. M. 2009. The evolution of RNAi as a defence against viruses and transposable elements. *Philos Trans R Soc Lond B Biol Sci,* 364**,** 99-115.
OBERST, A., DILLON, C. P., WEINLICH, R., MCCORMICK, L. L., FITZGERALD, P., POP, C., HAKEM, R., SALVESEN, G. S. & GREEN, D. R. 2011. Catalytic activity of the caspase-8-FLIP(L) complex inhibits RIPK3-dependent necrosis. *Nature,* 471**,** 363-7.
OGAWA, N., PING, L., ZHENJUN, L., TAKADA, Y. & SUGAI, S. 2002. Involvement of the interferon-gamma-induced T cell-attracting chemokines, interferon-gamma-inducible 10-

kd protein (CXCL10) and monokine induced by interferon-gamma (CXCL9), in the salivary gland lesions of patients with Sjögren's syndrome. *Arthritis Rheum,* 46**,** 2730-41.
OKAHIRA, S., NISHIKAWA, F., NISHIKAWA, S., AKAZAWA, T., SEYA, T. & MATSUMOTO, M. 2005. Interferon-beta induction through toll-like receptor 3 depends on double-stranded RNA structure. *DNA Cell Biol,* 24**,** 614-23.
ONO, H., OBANA, A., USAMI, Y., SAKAI, M., NOHARA, K., EGUSA, H. & SAKAI, T. 2015. Regenerating Salivary Glands in the Microenvironment of Induced Pluripotent Stem Cells. *Biomed Res Int,* 2015**,** 293570.
OSHIUMI, H., MATSUMOTO, M., FUNAMI, K., AKAZAWA, T. & SEYA, T. 2003. TICAM-1, an adaptor molecule that participates in Toll-like receptor 3-mediated interferon-beta induction. *Nat Immunol,* 4**,** 161-7.
OTTOLIA, M. & PHILIPSON, K. D. 2013. NCX1: mechanism of transport. *Adv Exp Med Biol,* 961**,** 49-54.
OUSINGSAWAT, J., MARTINS, J. R., SCHREIBER, R., ROCK, J. R., HARFE, B. D. & KUNZELMANN, K. 2009. Loss of TMEM16A causes a defect in epithelial Ca2+-dependent chloride transport. *J Biol Chem,* 284**,** 28698-703.
OYADOMARI, S., ARAKI, E. & MORI, M. 2002. Endoplasmic reticulum stress-mediated apoptosis in pancreatic beta-cells. *Apoptosis,* 7**,** 335-45.
OYADOMARI, S., TAKEDA, K., TAKIGUCHI, M., GOTOH, T., MATSUMOTO, M., WADA, I., AKIRA, S., ARAKI, E. & MORI, M. 2001. Nitric oxide-induced apoptosis in pancreatic beta cells is mediated by the endoplasmic reticulum stress pathway. *Proc Natl Acad Sci U S A,* 98**,** 10845-50.
PACHER, P., BECKMAN, J. S. & LIAUDET, L. 2007. Nitric oxide and peroxynitrite in health and disease. *Physiol Rev,* 87**,** 315-424.
PARK, B., BRINKMANN, M. M., SPOONER, E., LEE, C. C., KIM, Y. M. & PLOEGH, H. L. 2008. Proteolytic cleavage in an endolysosomal compartment is required for activation of Toll-like receptor 9. *Nat Immunol,* 9**,** 1407-14.
PATEY, D. H. 1966. The clinical features and diagnosis of parotid calculi. *Practitioner,* 197**,** 67-9.
PAVIO, N., ROMANO, P. R., GRACZYK, T. M., FEINSTONE, S. M. & TAYLOR, D. R. 2003. Protein synthesis and endoplasmic reticulum stress can be modulated by the hepatitis C virus envelope protein E2 through the eukaryotic initiation factor 2alpha kinase PERK. *J Virol,* 77**,** 3578-85.
PEISLEY, A. & HUR, S. 2013. Multi-level regulation of cellular recognition of viral dsRNA. *Cell Mol Life Sci,* 70**,** 1949-63.
PERIASAMY, M. & KALYANASUNDARAM, A. 2007. SERCA pump isoforms: their role in calcium transport and disease. *Muscle Nerve,* 35**,** 430-42.
PERTOVAARA, M., ANTONEN, J. & HURME, M. 2007. Endothelial nitric oxide synthase +894 polymorphism is associated with recurrent salivary gland swelling and early onset in patients with primary Sjogren's syndrome. *Ann Rheum Dis.* England.
PETERSEN, O. H. & TEPIKIN, A. V. 2008. Polarized calcium signaling in exocrine gland cells. *Annu Rev Physiol,* 70**,** 273-99.
PINKSTAFF, C. A. 1980. The cytology of salivary glands. *Int Rev Cytol,* 63**,** 141-261.
PIPER M. TREUTING, S. M. D. 2012. *Comparative Anatomy and Histology: A Mouse and Human Atlas*, Elsevier.
PITELKA, D. R., TAGGART, B. N. & HAMAMOTO, S. T. 1983. Effects of extracellular calcium depletion on membrane topography and occluding junctions of mammary epithelial cells in culture. *J Cell Biol,* 96**,** 613-24.
PLATANIAS, L. C. 2005. Mechanisms of type-I- and type-II-interferon-mediated signalling. *Nat Rev Immunol,* 5**,** 375-86.
PODOBNIK, M., KUHELJ, R., TURK, V. & TURK, D. 1997. Crystal structure of the wild-type human procathepsin B at 2.5 A resolution reveals the native active site of a papain-like cysteine protease zymogen. *J Mol Biol,* 271**,** 774-88.
PRAKRIYA, M. 2013. Store-operated Orai channels: structure and function. *Curr Top Membr,* 71**,** 1-32.
PRINCE, L. R., WHYTE, M. K., SABROE, I. & PARKER, L. C. 2011. The role of TLRs in neutrophil activation. *Current Opinion in Pharmacology,* 11**,** 397-403.
PRINS, D. & MICHALAK, M. 2011. Organellar Calcium Buffers. *Cold Spring Harbor Perspectives in Biology,* 3**,** a004069.
PROCTOR, G. 1998. *Secretory protein synthesis and constitutive (vesicular) secretion by salivary glands.,* Basel: Karger.

PROCTOR, G. B. 2006. Muscarinic receptors and salivary secretion. *J Appl Physiol (1985).* United States.
PROCTOR, G. B. 2016. The physiology of salivary secretion. *Periodontol 2000,* 70**,** 11-25.
PROCTOR, G. B. & CARPENTER, G. H. 2007. Regulation of salivary gland function by autonomic nerves. *Auton Neurosci,* 133**,** 3-18.
PROCTOR, G. B. & CARPENTER, G. H. 2014. Salivary secretion: mechanism and neural regulation. *Monogr Oral Sci,* 24**,** 14-29.
PROUD, C. G. 1995. PKR: a new name and new roles. *Trends Biochem Sci,* 20**,** 241-6.
PUTNEY, J. W., JR. 1990. Capacitative calcium entry revisited. *Cell Calcium,* 11**,** 611-24.
PUZIANOWSKA-KUZNICKA, M. & KUZNICKI, J. 2009. The ER and ageing II: Calcium homeostasis. *Ageing Research Reviews,* 8**,** 160-172.
QI, R., SINGH, D. & KAO, C. C. 2012. Proteolytic processing regulates Toll-like receptor 3 stability and endosomal localization. *J Biol Chem,* 287**,** 32617-29.
QUISSELL, D. O., WATSON, E. & DOWD, F. J. 1992. Signal transduction mechanisms involved in salivary gland regulated exocytosis. *Crit Rev Oral Biol Med,* 3**,** 83-107.
RADI, R., BECKMAN, J. S., BUSH, K. M. & FREEMAN, B. A. 1991. Peroxynitrite-induced membrane lipid peroxidation: the cytotoxic potential of superoxide and nitric oxide. *Arch Biochem Biophys,* 288**,** 481-7.
RAEBURN, C. D., CALKINS, C. M., ZIMMERMAN, M. A., SONG, Y., AO, L., BANERJEE, A., HARKEN, A. H. & MENG, X. 2002. ICAM-1 and VCAM-1 mediate endotoxemic myocardial dysfunction independent of neutrophil accumulation. *Am J Physiol Regul Integr Comp Physiol,* 283**,** R477-86.
RAMNATH, D., POWELL, E. E., SCHOLZ, G. M. & SWEET, M. J. 2016. The toll-like receptor 3 pathway in homeostasis, responses to injury and wound repair. *Semin Cell Dev Biol*.
RAMNATH, D., POWELL, E. E., SCHOLZ, G. M. & SWEET, M. J. 2017. The toll-like receptor 3 pathway in homeostasis, responses to injury and wound repair. *Seminars in Cell & Developmental Biology,* 61**,** 22-30.
RAMNATH, R. D., SUN, J. & BHATIA, M. 2009. Involvement of SRC family kinases in substance P-induced chemokine production in mouse pancreatic acinar cells and its significance in acute pancreatitis. *J Pharmacol Exp Ther,* 329**,** 418-28.
RAMUDO, L., DE DIOS, I., YUBERO, S., VICENTE, S. & MANSO, M. A. 2007. ICAM-1 and CD11b/CD18 expression during acute pancreatitis induced by bile-pancreatic duct obstruction: effect of N-acetylcysteine. *Exp Biol Med (Maywood),* 232**,** 737-43.
RAMUDO, L., YUBERO, S., MANSO, M. A., VICENTE, S. & DE DIOS, I. 2009. Signal transduction of MCP-1 expression induced by pancreatitis-associated ascitic fluid in pancreatic acinar cells. *J Cell Mol Med,* 13**,** 1314-20.
RANA, T. M. 2007. Illuminating the silence: understanding the structure and function of small RNAs. *Nat Rev Mol Cell Biol,* 8**,** 23-36.
RAWLINGS, N. D., BARRETT, A. J. & BATEMAN, A. 2012. MEROPS: the database of proteolytic enzymes, their substrates and inhibitors. *Nucleic Acids Res,* 40**,** D343-50.
REN, X., ZHOU, H., LI, B. & SU, S. B. 2011. Toll-like receptor 3 ligand polyinosinic:polycytidylic acid enhances autoimmune disease in a retinal autoimmunity model. *Int Immunopharmacol,* 11**,** 769-73.
RICHARDSON, S. J., WILLCOX, A., HILTON, D. A., TAURIAINEN, S., HYOTY, H., BONE, A. J., FOULIS, A. K. & MORGAN, N. G. 2010. Use of antisera directed against dsRNA to detect viral infections in formalin-fixed paraffin-embedded tissue. *J Clin Virol,* 49**,** 180-5.
RICHTER, C. 1987. Biophysical consequences of lipid peroxidation in membranes. *Chem Phys Lipids,* 44**,** 175-89.
ROCHA, J. J., KOROLCHUK, V. I., ROBINSON, I. M. & O'KANE, C. J. 2011. A phagocytic route for uptake of double-stranded RNA in RNAi. *PLoS One,* 6**,** e19087.
ROMANENKO, V. G., CATALAN, M. A., BROWN, D. A., PUTZIER, I., HARTZELL, H. C., MARMORSTEIN, A. D., GONZALEZ-BEGNE, M., ROCK, J. R., HARFE, B. D. & MELVIN, J. E. 2010. Tmem16A encodes the Ca2+-activated Cl- channel in mouse submandibular salivary gland acinar cells. *J Biol Chem,* 285**,** 12990-3001.
ROSSI, A., DEVERAUX, Q., TURK, B. & SALI, A. 2004. Comprehensive search for cysteine cathepsins in the human genome. *Biol Chem,* 385**,** 363-72.
ROUSSA, E., ROMERO, M. F., SCHMITT, B. M., BORON, W. F., ALPER, S. L. & THEVENOD, F. 1999. Immunolocalization of anion exchanger AE2 and Na(+)-HCO(-)(3) cotransporter in rat parotid and submandibular glands. *Am J Physiol,* 277**,** G1288-96.
ROZMAN-PUNGERCAR, J., KOPITAR-JERALA, N., BOGYO, M., TURK, D., VASILJEVA, O., STEFE, I., VANDENABEELE, P., BROMME, D., PUIZDAR, V., FONOVIC, M.,

TRSTENJAK-PREBANDA, M., DOLENC, I., TURK, V. & TURK, B. 2003. Inhibition of papain-like cysteine proteases and legumain by caspase-specific inhibitors: when reaction mechanism is more important than specificity. *Cell Death Differ,* 10**,** 881-8.

RUTKOWSKI, D. T. & KAUFMAN, R. J. 2004. A trip to the ER: coping with stress. *Trends Cell Biol,* 14**,** 20-8.

SAITO, I., SERVENIUS, B., COMPTON, T. & FOX, R. I. 1989. Detection of Epstein-Barr virus DNA by polymerase chain reaction in blood and tissue biopsies from patients with Sjogren's syndrome. *J Exp Med,* 169**,** 2191-8.

SAKAI, H., SAGARA, A., MATSUMOTO, K., JO, A., HIROSAKI, A., TAKASE, K., SUGIYAMA, R., SATO, K., IKEGAMI, D., HORIE, S., MATOBA, M. & NARITA, M. 2014. Neutrophil recruitment is critical for 5-fluorouracil-induced diarrhea and the decrease in aquaporins in the colon. *Pharmacological Research,* 87**,** 71-79.

SALEH, M. C., TASSETTO, M., VAN RIJ, R. P., GOIC, B., GAUSSON, V., BERRY, B., JACQUIER, C., ANTONIEWSKI, C. & ANDINO, R. 2009. Antiviral immunity in Drosophila requires systemic RNA interference spread. *Nature,* 458**,** 346-50.

SALIH, M. A., KALU, D. N. & SMITH, T. C. 1997. Effects of age and food restriction on calcium signaling in parotid acinar cells of Fischer 344 rats. *Aging (Milano),* 9**,** 419-27.

SALVEMINI, D., ISCHIROPOULOS, H. & CUZZOCREA, S. 2003. Roles of nitric oxide and superoxide in inflammation. *Methods Mol Biol,* 225**,** 291-303.

SAMUEL, C. E. 1979. Mechanism of interferon action: phosphorylation of protein synthesis initiation factor eIF-2 in interferon-treated human cells by a ribosome-associated kinase processing site specificity similar to hemin-regulated rabbit reticulocyte kinase. *Proc Natl Acad Sci U S A,* 76**,** 600-4.

SAMUEL, C. E. 1991. Antiviral actions of interferon. Interferon-regulated cellular proteins and their surprisingly selective antiviral activities. *Virology,* 183**,** 1-11.

SAMUEL, C. E. 1993. The eIF-2 alpha protein kinases, regulators of translation in eukaryotes from yeasts to humans. *J Biol Chem,* 268**,** 7603-6.

SATO, S., SUGIYAMA, M., YAMAMOTO, M., WATANABE, Y., KAWAI, T., TAKEDA, K. & AKIRA, S. 2003. Toll/IL-1 receptor domain-containing adaptor inducing IFN-beta (TRIF) associates with TNF receptor-associated factor 6 and TANK-binding kinase 1, and activates two distinct transcription factors, NF-kappa B and IFN-regulatory factor-3, in the Toll-like receptor signaling. *J Immunol,* 171**,** 4304-10.

SATOH, T., KAMBE, N. & MATSUE, H. 2013. NLRP3 activation induces ASC-dependent programmed necrotic cell death, which leads to neutrophilic inflammation. *Cell Death Dis,* 4**,** e644.

SATOH, T., KATO, H., KUMAGAI, Y., YONEYAMA, M., SATO, S., MATSUSHITA, K., TSUJIMURA, T., FUJITA, T., AKIRA, S. & TAKEUCHI, O. 2010. LGP2 is a positive regulator of RIG-I- and MDA5-mediated antiviral responses. *Proc Natl Acad Sci U S A,* 107**,** 1512-7.

SAUNDERS, L. R. & BARBER, G. N. 2003. The dsRNA binding protein family: critical roles, diverse cellular functions. *Faseb j,* 17**,** 961-83.

SCHIODT, M., GREENSPAN, D., DANIELS, T. E., NELSON, J., LEGGOTT, P. J., WARA, D. W. & GREENSPAN, J. S. 1989. Parotid gland enlargement and xerostomia associated with labial sialadenitis in HIV-infected patients. *J Autoimmun,* 2**,** 415-25.

SCHONBORN, J., OBERSTRASS, J., BREYEL, E., TITTGEN, J., SCHUMACHER, J. & LUKACS, N. 1991. Monoclonal antibodies to double-stranded RNA as probes of RNA structure in crude nucleic acid extracts. *Nucleic Acids Res,* 19**,** 2993-3000.

SCHOTTE, P., DECLERCQ, W., VAN HUFFEL, S., VANDENABEELE, P. & BEYAERT, R. 1999. Non-specific effects of methyl ketone peptide inhibitors of caspases. *FEBS Lett,* 442**,** 117-21.

SCHWALLER, B. 2012. The regulation of a cell's Ca(2+) signaling toolkit: the Ca (2+) homeostasome. *Adv Exp Med Biol,* 740**,** 1-25.

SCOTLAND, R. S., STABLES, M. J., MADALLI, S., WATSON, P. & GILROY, D. W. 2011. Sex-differences in resident immune cell phenotype underlies more efficient acute inflammatory responses in female mice. *Blood,* 118**,** 5918-5927.

SCOTT, J. & BAUM, B. J. 1985. Involvement of cyclic AMP and calcium in exocrine protein secretion induced by vasoactive intestinal polypeptide in rat parotid cells. *Biochim Biophys Acta,* 847**,** 255-62.

SEGAWA, A., LOFFREDO, F., PUXEDDU, R., YAMASHINA, S., TESTA RIVA, F. & RIVA, A. 1998. Exocytosis in human salivary glands visualized by high-resolution scanning electron microscopy. *Cell Tissue Res,* 291**,** 325-36.

SEN, G. C. & SARKAR, S. N. 2005. Transcriptional signaling by double-stranded RNA: role of TLR3. *Cytokine Growth Factor Rev,* 16**,** 1-14.
SENANAYAKE, S. N. 2008. Mumps: a resurgent disease with protean manifestations. *Med J Aust,* 189**,** 456-9.
SEPULVEDA, F. E., MASCHALIDI, S., COLISSON, R., HESLOP, L., GHIRELLI, C., SAKKA, E., LENNON-DUMENIL, A. M., AMIGORENA, S., CABANIE, L. & MANOURY, B. 2009. Critical role for asparagine endopeptidase in endocytic Toll-like receptor signaling in dendritic cells. *Immunity,* 31**,** 737-48.
SERRANO-PUEBLA, A. & BOYA, P. 2016. Lysosomal membrane permeabilization in cell death: new evidence and implications for health and disease. *Ann N Y Acad Sci,* 1371**,** 30-44.
SHEN, L., SURESH, L., LI, H., ZHANG, C., KUMAR, V., PANKEWYCZ, O. & AMBRUS, J. L., JR. 2009. IL-14 alpha, the nexus for primary Sjogren's disease in mice and humans. *Clin Immunol,* 130**,** 304-12.
SHEN, L., SURESH, L., MALYAVANTHAM, K., KOWAL, P., XUAN, J., LINDEMANN, M. J. & AMBRUS, J. L., JR. 2013. Different stages of primary Sjogren's syndrome involving lymphotoxin and type 1 IFN. *J Immunol,* 191**,** 608-13.
SINGH, R., MOSTAFID, H. & HINDLEY, R. G. 2006. Measles, mumps and rubella -- the urologist's perspective. *Int J Clin Pract,* 60**,** 335-9.
SREEBNY, L. M. & SCHWARTZ, S. S. 1997. A reference guide to drugs and dry mouth--2nd edition. *Gerodontology,* 14**,** 33-47.
STAMLER, J. S., SIMON, D. I., JARAKI, O., OSBORNE, J. A., FRANCIS, S., MULLINS, M., SINGEL, D. & LOSCALZO, J. 1992a. S-nitrosylation of tissue-type plasminogen activator confers vasodilatory and antiplatelet properties on the enzyme. *Proc Natl Acad Sci U S A,* 89**,** 8087-91.
STAMLER, J. S., SIMON, D. I., OSBORNE, J. A., MULLINS, M. E., JARAKI, O., MICHEL, T., SINGEL, D. J. & LOSCALZO, J. 1992b. S-nitrosylation of proteins with nitric oxide: synthesis and characterization of biologically active compounds. *Proc Natl Acad Sci U S A,* 89**,** 444-8.
STODDART, C. A., CARDIN, R. D., BONAME, J. M., MANNING, W. C., ABENES, G. B. & MOCARSKI, E. S. 1994. Peripheral blood mononuclear phagocytes mediate dissemination of murine cytomegalovirus. *J Virol,* 68**,** 6243-53.
SUI, Y., POTULA, R., DHILLON, N., PINSON, D., LI, S., NATH, A., ANDERSON, C., TURCHAN, J., KOLSON, D., NARAYAN, O. & BUCH, S. 2004. Neuronal apoptosis is mediated by CXCL10 overexpression in simian human immunodeficiency virus encephalitis. *Am J Pathol,* 164**,** 1557-66.
SUI, Y., STEHNO-BITTEL, L., LI, S., LOGANATHAN, R., DHILLON, N. K., PINSON, D., NATH, A., KOLSON, D., NARAYAN, O. & BUCH, S. 2006. CXCL10-induced cell death in neurons: role of calcium dysregulation. *Eur J Neurosci,* 23**,** 957-64.
SUZUKI, C. K., BONIFACINO, J. S., LIN, A. Y., DAVIS, M. M. & KLAUSNER, R. D. 1991. Regulating the retention of T-cell receptor alpha chain variants within the endoplasmic reticulum: Ca(2+)-dependent association with BiP. *J Cell Biol,* 114**,** 189-205.
SZABO, C. 2003. Multiple pathways of peroxynitrite cytotoxicity. *Toxicol Lett,* 140-141**,** 105-12.
SZABO, C., ISCHIROPOULOS, H. & RADI, R. 2007. Peroxynitrite: biochemistry, pathophysiology and development of therapeutics. *Nat Rev Drug Discov,* 6**,** 662-80.
TABETA, K., HOEBE, K., JANSSEN, E. M., DU, X., GEORGEL, P., CROZAT, K., MUDD, S., MANN, N., SOVATH, S., GOODE, J., SHAMEL, L., HERSKOVITS, A. A., PORTNOY, D. A., COOKE, M., TARANTINO, L. M., WILTSHIRE, T., STEINBERG, B. E., GRINSTEIN, S. & BEUTLER, B. 2006. The Unc93b1 mutation 3d disrupts exogenous antigen presentation and signaling via Toll-like receptors 3, 7 and 9. *Nat Immunol,* 7**,** 156-64.
TAKAGI, K., YAMAGUCHI, K., SAKURAI, T., ASARI, T., HASHIMOTO, K. & TERAKAWA, S. 2003. Secretion of saliva in X-irradiated rat submandibular glands. *Radiat Res,* 159**,** 351-60.
TAKEDA, I., KIZU, Y., YOSHITAKA, O., SAITO, I. & YAMANE, G. Y. 2003a. Possible role of nitric oxide in radiation-induced salivary gland dysfunction. *Radiat Res,* 159**,** 465-70.
TAKEDA, K., KAISHO, T. & AKIRA, S. 2003b. Toll-like receptors. *Annu Rev Immunol,* 21**,** 335-76.
TAKEMURA, N., KAWASAKI, T., KUNISAWA, J., SATO, S., LAMICHHANE, A., KOBIYAMA, K., AOSHI, T., ITO, J., MIZUGUCHI, K., KARUPPUCHAMY, T., MATSUNAGA, K., MIYATAKE, S., MORI, N., TSUJIMURA, T., SATOH, T., KUMAGAI, Y., KAWAI, T., STANDLEY, D. M., ISHII, K. J., KIYONO, H., AKIRA, S. & UEMATSU, S. 2014. Blockade

of TLR3 protects mice from lethal radiation-induced gastrointestinal syndrome. *Nat Commun,* 5**,** 3492.

TANAKA, N., NAKANISHI, M., KUSAKABE, Y., GOTO, Y., KITADE, Y. & NAKAMURA, K. T. 2004. Structural basis for recognition of 2',5'-linked oligoadenylates by human ribonuclease L. *Embo j,* 23**,** 3929-38.

TARDIF, K. D., MORI, K. & SIDDIQUI, A. 2002. Hepatitis C virus subgenomic replicons induce endoplasmic reticulum stress activating an intracellular signaling pathway. *J Virol,* 76**,** 7453-9.

TEOS, L. Y., ZHANG, Y., COTRIM, A. P., SWAIM, W., WON, J. H., AMBRUS, J., SHEN, L., BEBRIS, L., GRISIUS, M., JANG, S. I., YULE, D. I., AMBUDKAR, I. S. & ALEVIZOS, I. 2015. IP3R deficit underlies loss of salivary fluid secretion in Sjogren's Syndrome. *Sci Rep,* 5**,** 13953.

THANOS, D. & MANIATIS, T. 1995. NF-kappa B: a lesson in family values. *Cell,* 80**,** 529-32.

TOSCANO, F., ESTORNES, Y., VIRARD, F., GARCIA-CATTANEO, A., PIERROT, A., VANBERVLIET, B., BONNIN, M., CIANCANELLI, M. J., ZHANG, S. Y., FUNAMI, K., SEYA, T., MATSUMOTO, M., PIN, J. J., CASANOVA, J. L., RENNO, T. & LEBECQUE, S. 2013. Cleaved/associated TLR3 represents the primary form of the signaling receptor. *J Immunol,* 190**,** 764-73.

TOYOSHIMA, C. 2009. How Ca2+-ATPase pumps ions across the sarcoplasmic reticulum membrane. *Biochim Biophys Acta,* 1793**,** 941-6.

TRIANTAFYLLOPOULOU, A., TAPINOS, N. & MOUTSOPOULOS, H. M. 2004. Evidence for coxsackievirus infection in primary Sjogren's syndrome. *Arthritis Rheum,* 50**,** 2897-902.

TRIPATHI, P., KASHYAP, L. & SINGH, V. 2007. The role of nitric oxide in inflammatory reactions. *FEMS Immunol Med Microbiol,* 51**,** 443-52.

TSAI, Y. C. & WEISSMAN, A. M. 2010. The Unfolded Protein Response, Degradation from Endoplasmic Reticulum and Cancer. *Genes Cancer,* 1**,** 764-778.

TSUKINOKI, K., SARUTA, J., SASAGURI, K., MIYOSHI, Y., JINBU, Y., KUSAMA, M., SATO, S. & WATANABE, Y. 2006. Immobilization stress induces BDNF in rat submandibular glands. *J Dent Res,* 85**,** 844-8.

TUNCTAN, B., ULUDAG, O., ALTUG, S. & ABACIOGLU, N. 1998. Effects of nitric oxide synthase inhibition in lipopolysaccharide-induced sepsis in mice. *Pharmacol Res,* 38**,** 405-11.

TURK, V., TURK, B. & TURK, D. 2001. Lysosomal cysteine proteases: facts and opportunities. *Embo j,* 20**,** 4629-33.

UEHARA, E. U., SHIDA BDE, S. & DE BRITO, C. A. 2015. Role of nitric oxide in immune responses against viruses: beyond microbicidal activity. *Inflamm Res,* 64**,** 845-52.

ULIRSCH, R. C. & JAFFE, E. S. 1987. Sjogren's syndrome-like illness associated with the acquired immunodeficiency syndrome-related complex. *Hum Pathol,* 18**,** 1063-8.

UTAISINCHAROEN, P., ANUNTAGOOL, N., ARJCHAROEN, S., LIMPOSUWAN, K., CHAISURIYA, P. & SIRISINHA, S. 2004. Induction of iNOS expression and antimicrobial activity by interferon (IFN)-β is distinct from IFN-γ in Burkholderia pseudomallei-infected mouse macrophages. *Clinical and Experimental Immunology,* 136**,** 277-283.

VANGHELUWE, P., RAEYMAEKERS, L., DODE, L. & WUYTACK, F. 2005. Modulating sarco(endo)plasmic reticulum Ca2+ ATPase 2 (SERCA2) activity: cell biological implications. *Cell Calcium,* 38**,** 291-302.

VAUX, D. L. & STRASSER, A. 1996. The molecular biology of apoptosis. *Proc Natl Acad Sci U S A,* 93**,** 2239-44.

VERSTAK, B., ARNOT, C. J. & GAY, N. J. 2013. An alanine-to-proline mutation in the BB-loop of TLR3 Toll/IL-1R domain switches signalling adaptor specificity from TRIF to MyD88. *J Immunol,* 191**,** 6101-9.

VETTER, R., REHFELD, U., REISSFELDER, C., WEISS, W., WAGNER, K. D., GUNTHER, J., HAMMES, A., TSCHOPE, C., DILLMANN, W. & PAUL, M. 2002. Transgenic overexpression of the sarcoplasmic reticulum Ca2+ATPase improves reticular Ca2+ handling in normal and diabetic rat hearts. *Faseb j,* 16**,** 1657-9.

VIARO, F., NOBRE, F. & EVORA, P. R. 2000. Expression of nitric oxide synthases in the pathophysiology of cardiovascular diseases. *Arq Bras Cardiol,* 74**,** 380-93.

VILLA, A., WOLFF, A., NARAYANA, N., DAWES, C., AFRAMIAN, D. J., LYNGE PEDERSEN, A. M., VISSINK, A., ALIKO, A., SIA, Y. W., JOSHI, R. K., MCGOWAN, R., JENSEN, S. B., KERR, A. R., EKSTROM, J. & PROCTOR, G. 2016. World Workshop on Oral Medicine VI: a systematic review of medication-induced salivary gland dysfunction. *Oral Dis,* 22**,** 365-82.

VINER, R. I., WILLIAMS, T. D. & SCHONEICH, C. 1999. Peroxynitrite modification of protein thiols: oxidation, nitrosylation, and S-glutathiolation of functionally important cysteine residue(s) in the sarcoplasmic reticulum Ca-ATPase. *Biochemistry,* 38**,** 12408-15.

VLASSOV, A. V., MAGDALENO, S., SETTERQUIST, R. & CONRAD, R. 2012. Exosomes: current knowledge of their composition, biological functions, and diagnostic and therapeutic potentials. *Biochim Biophys Acta,* 1820**,** 940-8.

WAITE, J. H. 1983. Evidence for a repeating 3,4-dihydroxyphenylalanine- and hydroxyproline-containing decapeptide in the adhesive protein of the mussel, Mytilus edulis L. *J Biol Chem,* 258**,** 2911-5.

WAITE, J. H. & TANZER, M. L. 1981. Polyphenolic Substance of Mytilus edulis: Novel Adhesive Containing L-Dopa and Hydroxyproline. *Science,* 212**,** 1038-40.

WALCOTT, B., BIRZGALIS, A., MOORE, L. C. & BRINK, P. R. 2005. Fluid secretion and the Na+-K+-2Cl- cotransporter in mouse exorbital lacrimal gland. *Am J Physiol Cell Physiol,* 289**,** C860-7.

WANCHU, A., KHULLAR, M., SUD, A. & BAMBERY, P. 2000. Elevated nitric oxide production in patients with primary Sjogren's syndrome. *Clin Rheumatol,* 19**,** 360-4.

WANG, J. X., BAIR, A. M., KING, S. L., SHNAYDER, R., HUANG, Y. F., SHIEH, C. C., SOBERMAN, R. J., FUHLBRIGGE, R. C. & NIGROVIC, P. A. 2012. Ly6G ligation blocks recruitment of neutrophils via a beta2-integrin-dependent mechanism. *Blood,* 120**,** 1489-98.

WANG, L., WANG, R., KONG, B. W., JIN, S., YE, K., FANG, W. & LI, Y. 2015. B cells Using Calcium Signaling for Specific and Rapid Detection of Escherichia coli O157:H7. *Sci Rep,* 5**,** 10598.

WANG, Q. & CARMICHAEL, G. G. 2004. Effects of Length and Location on the Cellular Response to Double-Stranded RNA. *Microbiology and Molecular Biology Reviews,* 68**,** 432-452.

WANG, X. 2001. The expanding role of mitochondria in apoptosis. *Genes Dev,* 15**,** 2922-33.

WANG, Y., LIU, L., DAVIES, D. R. & SEGAL, D. M. 2010. Dimerization of Toll-like receptor 3 (TLR3) is required for ligand binding. *J Biol Chem,* 285**,** 36836-41.

WATANABE, A., TATEMATSU, M., SAEKI, K., SHIBATA, S., SHIME, H., YOSHIMURA, A., OBUSE, C., SEYA, T. & MATSUMOTO, M. 2011. Raftlin is involved in the nucleocapture complex to induce poly(I:C)-mediated TLR3 activation. *J Biol Chem,* 286**,** 10702-11.

WATANABE, M., YAMAGISHI-WANG, H. & KAWAGUCHI, M. 2001. Lowered susceptibility of muscarinic receptor involved in salivary secretion of streptozotocin-induced diabetic rats. *Jpn J Pharmacol,* 87**,** 117-24.

WAZ, W. R., VAN LIEW, J. B. & FELD, L. G. 1997. Nitric oxide-inhibitory effect of aminoguanidine on renal function in rats. *Kidney Blood Press Res,* 20**,** 211-7.

WELLER, M. L., GARDENER, M. R., BOGUS, Z. C., SMITH, M. A., ASTORRI, E., MICHAEL, D. G., MICHAEL, D. A., ZHENG, C., BURBELO, P. D., LAI, Z., WILSON, P. A., SWAIM, W., HANDELMAN, B., AFIONE, S. A., BOMBARDIERI, M. & CHIORINI, J. A. 2016. Hepatitis Delta Virus Detected in Salivary Glands of Sjogren's Syndrome Patients and Recapitulates a Sjogren's Syndrome-Like Phenotype in Vivo. *Pathog Immun,* 1**,** 12-40.

WILLIAMS, B. R. 2001. Signal integration via PKR. *Sci STKE,* 2001**,** re2.

WINER, J., JUNG, C. K. S., SHACKEL, I. & WILLIAMS, P. M. 1999. Development and Validation of Real-Time Quantitative Reverse Transcriptase–Polymerase Chain Reaction for Monitoring Gene Expression in Cardiac Myocytesin Vitro. *Analytical Biochemistry,* 270**,** 41-49.

WU, H. H., KAWAMATA, H., WANG, D. D. & OYASU, R. 1993. Immunohistochemical localization of transforming growth factor alpha in the major salivary glands of male and female rats. *Histochem J,* 25**,** 613-8.

WU, Y. T., TAN, H. L., HUANG, Q., SUN, X. J., ZHU, X. & SHEN, H. M. 2011. zVAD-induced necroptosis in L929 cells depends on autocrine production of TNFalpha mediated by the PKC-MAPKs-AP-1 pathway. *Cell Death Differ,* 18**,** 26-37.

XIE, Q. W., WHISNANT, R. & NATHAN, C. 1993. Promoter of the mouse gene encoding calcium-independent nitric oxide synthase confers inducibility by interferon gamma and bacterial lipopolysaccharide. *J Exp Med,* 177**,** 1779-84.

XU, K. Y., HUSO, D. L., DAWSON, T. M., BREDT, D. S. & BECKER, L. C. 1999. Nitric oxide synthase in cardiac sarcoplasmic reticulum. *Proc Natl Acad Sci U S A,* 96**,** 657-62.

XU, L., EU, J. P., MEISSNER, G. & STAMLER, J. S. 1998. Activation of the cardiac calcium release channel (ryanodine receptor) by poly-S-nitrosylation. *Science,* 279**,** 234-7.

XU, W., LIU, L., CHARLES, I. G. & MONCADA, S. 2004. Nitric oxide induces coupling of mitochondrial signalling with the endoplasmic reticulum stress response. *Nat Cell Biol,* 6**,** 1129-34.

XUAN, J., SHEN, L., MALYAVANTHAM, K., PANKEWYCZ, O., AMBRUS, J. L., JR. & SURESH, L. 2013. Temporal histological changes in lacrimal and major salivary glands in mouse models of Sjogren's syndrome. *BMC Oral Health,* 13**,** 51.

YAMAMOTO, M., SATO, S., MORI, K., HOSHINO, K., TAKEUCHI, O., TAKEDA, K. & AKIRA, S. 2002. Cutting edge: a novel Toll/IL-1 receptor domain-containing adapter that preferentially activates the IFN-beta promoter in the Toll-like receptor signaling. *J Immunol,* 169**,** 6668-72.

YANG, C. H., MURTI, A. & PFEFFER, L. M. 2005. Interferon induces NF-kappa B-inducing kinase/tumor necrosis factor receptor-associated factor-dependent NF-kappa B activation to promote cell survival. *J Biol Chem,* 280**,** 31530-6.

YANG, Y. D., CHO, H., KOO, J. Y., TAK, M. H., CHO, Y., SHIM, W. S., PARK, S. P., LEE, J., LEE, B., KIM, B. M., RAOUF, R., SHIN, Y. K. & OH, U. 2008. TMEM16A confers receptor-activated calcium-dependent chloride conductance. *Nature,* 455**,** 1210-5.

YUAN, J. P., ZENG, W., DORWART, M. R., CHOI, Y. J., WORLEY, P. F. & MUALLEM, S. 2009. SOAR and the polybasic STIM1 domains gate and regulate Orai channels. *Nat Cell Biol,* 11**,** 337-43.

YULE, D. I. 2001. Subtype-specific regulation of inositol 1,4,5-trisphosphate receptors: controlling calcium signals in time and space. *J Gen Physiol,* 117**,** 431-4.

ZANINOVIC, V., GUKOVSKAYA, A. S., GUKOVSKY, I., MOURIA, M. & PANDOL, S. J. 2000. Cerulein upregulates ICAM-1 in pancreatic acinar cells, which mediates neutrophil adhesion to these cells. *Am J Physiol Gastrointest Liver Physiol,* 279**,** G666-76.

ZENG, W., LEE, M. G. & MUALLEM, S. 1997. Membrane-specific regulation of Cl- channels by purinergic receptors in rat submandibular gland acinar and duct cells. *J Biol Chem,* 272**,** 32956-65.

ZENG, W., YUAN, J. P., KIM, M. S., CHOI, Y. J., HUANG, G. N., WORLEY, P. F. & MUALLEM, S. 2008. STIM1 gates TRPC channels, but not Orai1, by electrostatic interaction. *Mol Cell,* 32**,** 439-48.

ZHANG, G. H., WU, L. L. & YU, G. Y. 2013. Tight junctions and paracellular fluid and ion transport in salivary glands. *Chin J Dent Res,* 16**,** 13-46.

ZHANG, K. & KAUFMAN, R. J. 2006. Protein folding in the endoplasmic reticulum and the unfolded protein response. *Handb Exp Pharmacol***,** 69-91.

ZHANG, K., SHEN, X., WU, J., SAKAKI, K., SAUNDERS, T., RUTKOWSKI, D. T., BACK, S. H. & KAUFMAN, R. J. 2006. Endoplasmic reticulum stress activates cleavage of CREBH to induce a systemic inflammatory response. *Cell,* 124**,** 587-99.

ZHANG, S. L., YU, Y., ROOS, J., KOZAK, J. A., DEERINCK, T. J., ELLISMAN, M. H., STAUDERMAN, K. A. & CAHALAN, M. D. 2005. STIM1 is a Ca2+ sensor that activates CRAC channels and migrates from the Ca2+ store to the plasma membrane. *Nature,* 437**,** 902-5.

ZHANG, X., WEN, J., BIDASEE, K. R., BESCH, H. R., JR., WOJCIKIEWICZ, R. J., LEE, B. & RUBIN, R. P. 1999. Ryanodine and inositol trisphosphate receptors are differentially distributed and expressed in rat parotid gland. *Biochem J,* 340 (Pt 2)**,** 519-27.

ZHAO, K., HUANG, Z., LU, H., ZHOU, J. & WEI, T. 2010. Induction of inducible nitric oxide synthase increases the production of reactive oxygen species in RAW264.7 macrophages. *Bioscience Reports,* 30**,** 233.

ZHAO, X., AI, M., GUO, Y., ZHOU, X., WANG, L., LI, X. & YAO, C. 2012. Poly I:C-induced tumor cell apoptosis mediated by pattern-recognition receptors. *Cancer Biother Radiopharm,* 27**,** 530-4.

ZHOU, H., LIAO, J., ALOOR, J., NIE, H., WILSON, B. C., FESSLER, M. B., GAO, H. M. & HONG, J. S. 2013. CD11b/CD18 (Mac-1) is a novel surface receptor for extracellular double-stranded RNA to mediate cellular inflammatory responses. *J Immunol,* 190**,** 115-25.

ZIGMOND, E., VAROL, C., FARACHE, J., ELMALIAH, E., SATPATHY, A. T., FRIEDLANDER, G., MACK, M., SHPIGEL, N., BONECA, I. G., MURPHY, K. M., SHAKHAR, G., HALPERN, Z. & JUNG, S. 2012. Ly6C hi monocytes in the inflamed colon give rise to proinflammatory effector cells and migratory antigen-presenting cells. *Immunity,* 37**,** 1076-90.

ZWAFERINK, H., STOCKINGER, S., REIPERT, S. & DECKER, T. 2008. Stimulation of Inducible Nitric Oxide Synthase Expression by Beta Interferon Increases Necrotic Death of

Macrophages upon Listeria monocytogenes Infection. *Infection and Immunity,* 76**,** 1649-1656.